

RUSSIAN ACADEMY OF SCIENCE
FEDERAL AGENCY ON EDUCATION OF RUSSIAN FEDERATION
RUSSIAN NATIONAL COMMISSION FOR UNESCO
COMMITTEE ON SCIENCE AND HIGHER EDUCATION OF THE GOVERNMENT OF SAINT-PETERSBURG
COUNCIL OF RECTORS OF SAINT-PETERSBURG HIGHER EDUCATION ESTABLISHMENTS
SAINT-PETERSBURG STATE UNIVERSITY OF AEROSPACE INSTRUMENTATION (SUAI)
UNESCO CHAIR "DISTANCE EDUCATION IN ENGINEERING" OF SUAI
RUSSIAN SECTION OF THE INTERNATIONAL SOCIETY OF AUTOMATION

**ИЗВЕСТИЯ КАФЕДРЫ UNESCO ГУАП
«ДИСТАНЦИОННОЕ ИНЖЕНЕРНОЕ ОБРАЗОВАНИЕ»**

Сборник статей

Выпуск 4

**BULLETIN OF THE UNESCO DEPARTMENT
«DISTANCE EDUCATION IN ENGINEERING» OF THE SUAI**

Collection of the papers

Issue 4

ББК 378.1
УДК 74.58
И33

И33 Bulletin of the UNESCO department “Distance education in engineering” of the SUAI: Collection of the papers. St. Petersburg, Issue 4. – SPb.: SUAI, 2019. – 123 p.

ISBN 978-5-8088-1345-8

ISA District 12 (The International Society of Automation) and SUAI (Saint-Petersburg State University of Aerospace Instrumentation) have organized the Fifteenth ISA European student paper competition (ESPC-2019). Papers of professors and the best students were included into this issue of the Bulletin of the UNESCO department “Distance education in engineering” of the SUAI. Papers can be interesting for students, post-graduated students, professors and specialists.

International editor’s committee:

Ovodenko Anatoly (Russia) – chairman,
Antokhina Yulia (Russia),
Bobovich Alexander (Russia) – secretary,
Cockrell Gerald (USA),
Collotta Mario (Italy),
Pau Giovanni (Italy)
Kryachko Alexander (Russia),
Mirabella Orazio (Italy),
Sergeev Anton (Russia),
Zamarreno Jesus (Spain).

ISBN 978-5-8088-1345-8



© Saint-Petersburg State University of
Aerospace Instrumentation, 2019



On behalf of ISA, I extend congratulations to the ISA Russia Section and the St. Petersburg State University of Aerospace Instrumentation (SUAI) on successfully completing the 15th ISA International Student Paper Competition.

The papers published in this volume have been selected by a review committee. Awards have been given at gold, silver and bronze levels. Winners have been asked to prepare presentations. The students from around the world who committed their time to prepare a paper should be very proud to be selected for this publication.

Students of today are the engineers of tomorrow. We are all excited about these talented individuals who will be instrumental in helping us achieve our vision of “creating a better world through automation”, and our mission of “advancing technical competence by connecting the automation community to achieve operational excellence”.

Whichever career path these students choose, we hope ISA will continue to play an important role in their continuing education and professional development.

May I extend my best wishes to all students and attendees in the 2019 ISA International Student Paper Competition.

Sincerely,

A handwritten signature in black ink that reads "Paul Gruhn". The signature is fluid and cursive.

Paul Gruhn
2019 ISA Society President

Standards
Certification
Education & Training
Publishing
Conferences & Exhibit

International Society of Automation
67 Alexander Drive
P.O. Box 12277
Research Triangle Park, NC 27709
PHONE (919) 549-8411
FAX (919) 549-8288
E-MAIL info@isa.org
www.isa.org



On behalf of ISA, I extend congratulations to the ISA Russia Section and the St. Petersburg State University of Aerospace Instrumentation (SUAI) on successfully completing the Fifteenth ISA European Student Paper Competition.

The papers published in this volume, selected by the advisory committee, represent the best contributions from among an excellent group of papers. The students who committed their time to prepare a paper should be very proud to be selected for this publication.

Students today are the engineers of tomorrow. We are excited about these talented individuals who will be instrumental in “setting the standard for automation” that will enhance our lifestyle into the future. To the lecturers and professors thank you for your development of today’s students.

ISA is focusing on Students Internationally to identify how ISA can develop career paths for students to choose. You will see these developments in late 2019. I hope ISA will continue to play an important role in your and other student’s continuing education and professional development.

I would like to extend my best wishes to all students, lecturers and attendees at the 2019 ISA European Student Paper Competition.

Sincerely,

A handwritten signature in black ink that reads "Brian J. Curtis". The signature is written in a cursive style and is placed on a light gray rectangular background.

Brian J. Curtis
ISA Society President 2018



I would like to extend congratulations to the ISA Russia Section, ISA District 12, and The Saint Petersburg State University of Aerospace Instrumentation (SUAI) for successfully organizing the Fifteenth ISA International Student Paper Competition.

As an educator and a member of ISA for over 33 years, I never tire of the opportunity to share with students the amazing challenges and personal rewards that a career in automation can bring. ISA is proud to have the opportunity to nurture the next generation of automation professionals.

We look forward to continuing the close relationship we have established between ISA, the Russia Section, District 12, and the SUAI. Through distance learning classes on project management and ongoing international online forums, we are developing new understandings in the technical, cultural, and personal arenas.

Congratulations to those who developed papers for this volume and to the advisory committee who had the difficult task of making paper selections.

Sincerely,

A handwritten signature in black ink that reads "Gerald W. Cockrell". The script is fluid and cursive.

Gerald W. Cockrell
ISA Former President

Standards
Certification
Education & Training
Publishing
Conferences & Exhibits

ISA
67 Alexander Drive
P.O. Box 12277
Research Triangle Park, NC 27709
PHONE (919) 549-8411
FAX (919) 549-8288
E-MAIL info@isa.org
www.isa.org

ACCOUNTING FOR ELECTROMAGNETIC WAVES SCATTERING IN THE ANGULAR AREAS DURING FORMATION OF THE MULTIPATH COMMUNICATION CHANNEL FREQUENCY CHARACTERISTICS

A. Kryachko, M. Kryachko,

Saint-Petersburg State University of Aerospace Instrumentation,
Saint-Petersburg State University of Aerospace Instrumentation
67, Bolshaya Morskaya str., Saint Petersburg, 190000, RUSSIA
alex_k34.ru@mail.ru
mike_kr@mail.ru

Abstract

Intensive development of radio technical equipment for transmitting discrete messages caused a spectral resources shortage, increasing of transmitted information volume, and the quality of message transmission requirements. In this regard, solving the problem of receiving signals with a high energy spectrum decline rate while ensuring the necessary reliability of receiving messages increases is very actual. Using atomic functions to build spectral-efficient signals makes it easy to form orthogonal sequences similar to Walsh functions. Energy concentration in the band and the out-of-band emissions rate decay can be easily defined with such functions. Inter-symbol interference injection leads to the peak-factor value decrease, that is very important in radio systems with limited energy resources. Orthogonal frequency-division multiplexing (OFDM) and spatial (MIMO) diversity, that are the most important directions in the development of new generation mobile communication technologies, potentially provides an approximation of their spectral efficiency to the Shannon limit. However, further evolutionary development of cellular systems with multiple antennas and OFDM is impossible without maximum utilization of all available resources like time, frequency spatiotemporal and polarization signal processing along with error-correcting coding. These steps necessary for a transmitted power minimization and, at the same time, increase the capacity of the communication system by adapting it to the state of the radio channel.

Keywords – OFDM, WiMAX, MIMO

Mobile communication technologies changes are the most evident in changes of radio interfaces, where fundamental differences are clearly seen.

Orthogonal frequency-division multiplexing (OFDM) and spatial (MIMO) diversity, that are the most important directions in the development of new generation mobile communication technologies, potentially provides an approximation of their spectral efficiency to the Shannon limit.

However, further evolutionary development of cellular systems with multiple antennas and OFDM is impossible without maximum utilization of all available resources like time, frequency spatiotemporal and polarization signal processing along with error-correcting coding. These steps necessary for a transmitted power minimization and, at the same time, increase the capacity of the communication system by adapting it to the state of the radio channel.

Currently, active-passive antenna modules have appeared on the market that combine passive and active phased antenna arrays.

The passive part replaces the existing 2g and 3g operator antennas, while the active part makes it possible to solve the task of adaptive space-time and polarization processing of 4g systems, significantly improving the SINR.

Using such antenna systems can be implemented adaptive antenna arrays for base stations of new generation communication systems.

Focusing on such antenna systems, it is necessary to develop algorithms for adaptive space-time and polarization signal processing, which ensure the formation of the maximum of the DP in the direction of the useful signal, the determination of the direction to interference and its deep suppression.

Thus, an actual scientific problem is to improve a quality of mobile communication based on the new adaptive modulation methods development and signal processing in the space-frequency and space-time channels of mobile communication systems of new generations from MIMO and OFDM.

FUNDAMENTALS OF THE ATOMIC FUNCTIONS THEORY USAGE FOR THE SPECTRAL-EFFECTIVE SIGNALS CONSTRUCTION

It is required to solve a problem of spectral-effective signals creation with a given rate of spectral decay outside the occupied band with a high concentration of energy within the occupied frequency band.

In general, it is necessary to select such time

functions $\varphi_k(t)$, that with expression $\sum_{k=1}^N C_k \varphi_k(t)$ it was possible to provide a given rate of decay of the spectrum outside the occupied band.

Linear combinations of $\varphi_k(t)$ functions should bring the synthesized signal spectrum to the required speed with the highest possible in theory speed, i.e. have the property of approximation universality. This imposes certain requirements on the choice of functions class.

The solution to this problem can be obtained on the basis R -mappings theory [1], that describes construction of local class functions C^∞ , possessing at the same time properties of polynomials and splines. Such functions are called atomic.

The rate of the out-of-band emission level decay for signals based on polynomials γ -degree of the final duration will decrease in proportion $C/\omega^{\gamma+1}$, if all derivatives of the signal envelope down to the derivative $(\gamma - 1)$ degree has no jumps, but γ -degree derivative is finite everywhere [2].

In turn, the degree splines γ - are functions, that are "piecewise" polynomials of degree γ , and in the nodes to pair till $(\gamma - 1)$ -degree derivatives.

Atomic functions are finite and represent a solution of a differential equation of the form:

$$y^{(n)}(t) + a_1 y^{(n-1)}(t) + \dots + a_{n-1} y'(t) + a_n y(t) = \sum_{k=1}^N C_k y(at - b_k) \quad (1)$$

The simplest and most important atomic functions are composed of infinite convolutions of rectangular pulses.

To research such convolutions, it is necessary to use the Fourier transform apparatus.

Using the Fourier transform, a rectangular pulse can be represented in the following form (as is well known, its spectrum has the form of $\sin x / x$)

$$\varphi(t) = \frac{1}{2\pi} \int_{-\infty}^{\infty} e^{jut} \frac{\sin(u/2)}{u/2} du.$$

N - multiple convolution of $(N + 1)$ identical square pulses $\varphi(t)$ is a finite spline $\theta_N(t)$.

In order to obtain a continuous finite function, the convolution of variable length pulses $\varphi_n(t)$ can be used (fig. 1):

$$\varphi_n(t) = \begin{cases} 2^{n-1}, & |t| \leq 2^{n-1} \\ 0, & |t| > 2^{n-1} \end{cases}$$

In order to obtain even smoother functions, this process can be repeated, and to obtain an infinite

smooth functions, it must be repeated an infinite number of times. The carrier of such an infinite convolution to be finite, we need to take convolutions of contractions of such functions $\varphi_1(t) * \varphi_2(t) * \dots * \varphi_n(t) * \dots$ so that to meet a series

$$\sum_{n=1}^{\infty} a_n < +\infty.$$

The simplest convergent series is the sum of an infinitely decreasing geometric progression with the denominator 2. Thus, the result of such an infinite convolution is a new finite function defined on the interval $[-1;1]$. It can be easy shown that it satisfies equation (0.1) in the simplest form

$$y'(t) = 2y(2t + 1) - 2y(2t - 1),$$

with conditions $\text{supp} = [-1,1]$, $y(-1) = y(1) = 0$, $y(0) = 1$. Consider the Fourier transform of both sides of the simplest equation:

$$\int_{-\infty}^{\infty} \exp[i\lambda t] y'(t) dt = a \left[\int_{-\infty}^{\infty} y(2t + 1) e^{i\lambda t} dt - \int_{-\infty}^{\infty} y(2t - 1) e^{i\lambda t} dt \right].$$

Then

$$-i\lambda \int_{-\infty}^{\infty} e^{i\lambda t} y(t) dt = \frac{a}{2} \left[\int_{-\infty}^{\infty} y(u) e^{\frac{i\lambda(u-1)}{2}} du - \int_{-\infty}^{\infty} y(u) e^{\frac{i\lambda(u+1)}{2}} du \right].$$

We can write that

$$F_y(\lambda) = a F_y\left(\frac{\lambda}{2}\right) \frac{\sin\left[\frac{\lambda}{2}\right]}{\lambda}, \quad (2)$$

where $F_y(\lambda)$ - is a entire function. Formula (2) was obtained in [3] (Theorem 6). By decomposing the right and left side of this expression into a power series and equating the coefficients at the same powers λ , we get $a = 2$. Then

$$F_y(0) = \int_{-1}^1 y(t) dt = y(0) = 1.$$

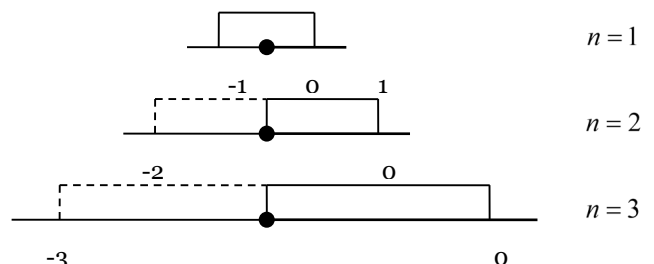


Figure 1 – Variable length pulse convolution

From here for $F_y^{(n)}(0)$ the recurrence formula is obtained

$$F_y^{(n)}(0) = \frac{n!}{2^n - 1} \sum_{k=1}^{[0.5n]} (-1)^k \frac{F_y^{(n-2k)}(0)}{(n-2k)!(2k+1)!}.$$

There is no more than one solution of equation (1) with the specified boundary conditions. In article [3], the existence of such solution was proved and it is defined as a function $up(t)$ and using a representation based on the Fourier transform –

$$F(up(t)) = \prod_{k=1}^{(n)} \frac{\sin \frac{u}{2^k}}{\frac{u}{2^k}}, \text{ we have}$$

$$up(t) = \frac{1}{2\pi} \int_{-\infty}^{\infty} e^{iut} \prod_{k=1}^{\infty} \frac{\sin(u2^{-k})}{u2^{-k}} du \quad (3)$$

Distinctive features of atomic functions are: analyticity; the combination of the finiteness of a function with a rapid decrease (faster than any degree) of its Fourier transform; an explicit connection of the derivatives with the function itself, as well as an explicit expression for the spectrum.

NUMERICAL METHOD FOR FINDING ATOMIC FUNCTIONS.

In the numerical solution of expression (3), it is necessary to determine the number n of the products that provides the specified standard deviation of the resulting function $a(t)$ from the true value obtained by the exact solution of the problem.

As an example, we consider the numerical solution of the problem to find the values of a function $up(t)$ for different values of n .

For $n = 3$:

$$up(t) = \frac{1}{2\pi} \int_{-\infty}^{\infty} e^{iut} \times \left(\frac{\sin(0.5u)}{0.5u} \cdot \frac{\sin(0.25u)}{0.25u} \cdot \frac{\sin(0.125u)}{0.125u} \right) du = \frac{1}{2\pi} \int_{-\infty}^{\infty} e^{iut} \frac{\sin(0.5u) \cdot \sin(0.25u) \cdot \sin(0.125u)}{0.015625u^3} du$$

For $n = 4$:

$$up(t) = \frac{1}{2\pi} \int_{-\infty}^{\infty} e^{iut} \left(\frac{\sin(0.5u)}{0.5u} \cdot \frac{\sin(0.25u)}{0.25u} \times \frac{\sin(0.125u)}{0.125u} \cdot \frac{\sin(0.0625u)}{0.0625u} \right) du = \frac{1}{2\pi} \int_{-\infty}^{\infty} e^{iut} \frac{\left(\sin(0.5u) \cdot \sin(0.25u) \times \sin(0.125u) \cdot \sin(0.0625u) \right)}{0.000976562u^4} du$$

and etc.

On fig. 2 are shown the values of the standard deviation of the function $up(t)$ depending on value of n . The values of the standard deviation for different n are conventionally connected by dotted lines. Forms of function $a(t)$ for $n=2, 3, 4, 5, 6, 8$ are shown on fig. 3.

$$\varepsilon(m) = \overline{|a_m(t) - a_{m-1}(t)|^2}$$

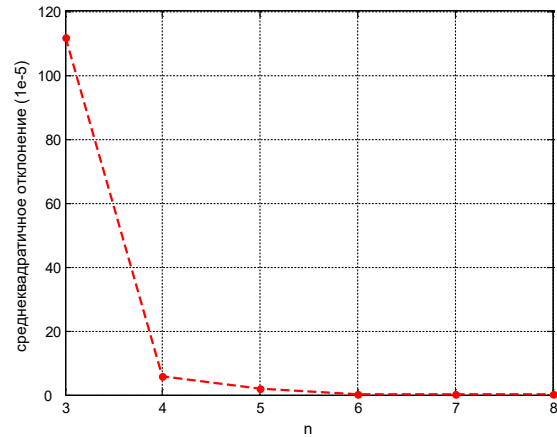


Figure 2 – The dependence of the standard deviation of the function $up(t)$, obtained by a numerical method for different values of n

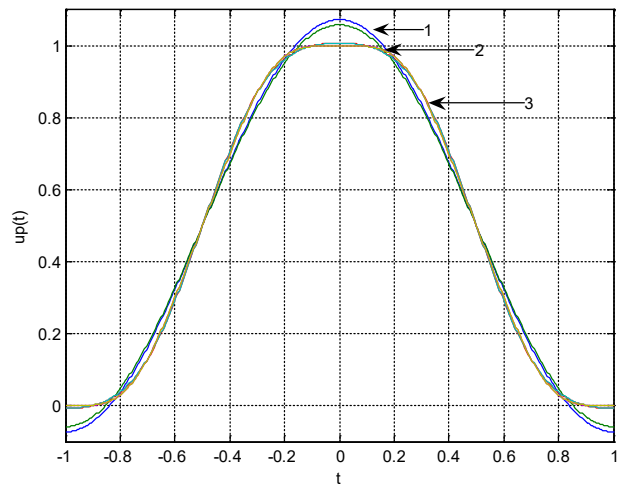


Figure 3 – View of function $up(t)$ with a numerical solution for $n = 2$ (line 1), $n = 3$ (line 2) and for $n = 4, 5, 6, 8$ (line 3)

It is advisable to use the method of determining the number n , which consists in the fact that the standard deviation is determined between two calculated functions $a(t)$, have an adjacent numbers n and $n+1$:

Selection of the standard deviation admissible value of the functions shape $up(t)$ defined, mainly, by the tolerance of the energy spectrum shape of a

synthesized signals random sequence. Indeed, when choosing a limited number n of multiplication members to build optimal signals the level of out-of-band emissions increases. In this regard, it is advisable to determine the allowable number n , starting with specifying the allowable increase in the level of the energy spectrum outside the occupied frequency band. This is the essence of the proposed numerical method for solving the problem of finding the envelope shape and assessing the accuracy of its solution.

The calculation results show that for $n \geq 6$ side-lobe attenuation level is about 50 dB. Starting from $n = 10$, the accuracy of the calculation compared with the theoretical results has an 10^{-30} error.

When calculating the real characteristics and parameters of mobile communication systems, it is necessary to take into account the spectral properties of signals.

For this purpose, the energy of an electromagnetic wave per unit flat surface located at the receiving point perpendicular to the direction of wave propagation is introduced into consideration [4].

$$W_2 = \int_{t_{mp1}}^{t_{mp2}} \Pi_2(t) dt = \int_{t_{mp1}}^{t_{mp2}} E_2(t) H_2(t) dt \quad (4)$$

Where t_{mp1} and t_{mp2} – are moments of time, corresponding to the appearance and disappearance of the signal at the point of reception; E_2, H_2 – are instantaneous values of the electric and magnetic field at the receive poin; Z_0 – is a propagation wave impedance.

Let's suppose the signal propagates in a vacuum. Then $Z = Z_0$. In turn, the instantaneous values of the electric and magnetic fields strengths can be represented as follows:

$$E_2(t) = f_2(t) E_{02} \quad (5)$$

$$H_2 = f_2(t) H_{02} = f_2(t) \frac{E_{02}}{Z_0} \quad (6)$$

where $f_2(t)$ – is a function that determines the law of change in signal at the point of reception. Its maximum value is one; E_{02}, H_{02} – maximum field strength.

Further written in the form of Fourier integrals:

$$E_2(t) = \frac{1}{2\pi} \int_{-\infty}^{+\infty} \dot{E}_2(i\omega) e^{i\omega t} d\omega \quad (7)$$

$$H_2(t) = \frac{1}{2\pi} \int_{-\infty}^{+\infty} \frac{\dot{E}_2(i\omega)}{Z_0} e^{i\omega t} d\omega \quad (8)$$

$\dot{E}_2(i\omega)$ – is spectral density of function $E_2(t)$.

Substituting the expression (7, 8) in (4) after simple transformations we obtain:

$$W_2 = \frac{1}{2\pi} \int_{-\infty}^{+\infty} \dot{E}_2(i\omega) \frac{\dot{E}_2(i\omega)}{Z_0} e^{i\omega t} d\omega$$

$$\frac{1}{2\pi Z_0} \int_{-\infty}^{+\infty} |\dot{E}_2(i\omega)|^2 d\omega \quad (9)$$

In accordance with the frequency method [5], the solution of the problem can be represented as

$$\dot{E}_2(i\omega) = \dot{E}_1(i\omega) K(i\omega) \quad (10)$$

where $\dot{E}_1(i\omega)$ – is a electric field spectral density at a point with the coordinates of the communication system; $K(i\omega)$ – is a frequency response of the current electrodynamic system.

Function $f_1(t)$ reflects the law of the electric field change with time (maximum value of $f_1(t)$ is 1). If the value of E_0 characterizes the amplitude of the electric field, then we can write the following equality:

$$E_1(t) = f_2(t) E_0 \quad (11)$$

Frequency response $K(i\omega)$ can be determined from the solution of diffraction problem of a flat electromagnetic wave with a complex amplitude of the electric field strength in a real communication channel in the steady-state harmonic mode. This solution is considered to be known.

Given the above expression (10) can be rewritten as follow:

$$\dot{E}_2(i\omega) = \dot{E}_1(i\omega) K(i\omega) = F_1 \times (i\omega) E_0 K(r, \theta, \varphi, i\omega) \quad (12)$$

Where

$$F_1(i\omega) = \int_{t_{ms1}}^{t_{ms2}} f_1(t) e^{-i\omega t} dt \quad (13)$$

$F_1(i\omega)$ – is a spectral density of function $f_1(t)$;

t_{ms1} and t_{ms2} – moments of time, corresponding to the beginning and end of the emitted signal.

Substituting the expression (12) in (9) we can write:

$$W_2 = \frac{1}{2\pi Z_0} \int_{-\infty}^{+\infty} |F_1(i\omega)|^2 |K(r, \theta, \varphi, i\omega)|^2 |\dot{E}_0|^2 d\omega = \frac{1}{2\pi} \int_{-\infty}^{+\infty} \dot{E}_2(i\omega) \frac{\dot{E}_2(i\omega)}{Z_0} e^{i\omega t} d\omega \quad (14)$$

It is easy to conclude that $E_0 K(r, \theta, \varphi, i\omega)$ represents a complex amplitude at the receiving point for harmonic mode.

In this case Π_1, Π_2 , can be rewritten as:

$$|F_1(i\omega)|^2 |K(r, \theta, \varphi, i\omega)|^2 |\dot{E}_0|^2 \quad (15)$$

$$\Pi_1 = \frac{1}{2Z_0} |\dot{E}_0|^2 \text{ и}$$

$$\Pi_2 = \frac{1}{2Z_0} |\dot{E}_0|^2 |K(r, \theta, \varphi, i\omega)|^2 \quad (16)$$

This shows that the flux density of electromagnetic energy at the point of reception depends both on the spectrum of the signal in the actual communication channel and on the magnitude

of the communication channel transfer characteristic at various frequencies within a given width of the spectrum.

Orthogonal frequency-division multiplexing (OFDM) and spatial (MIMO) diversity usage in modern and promising mobile communication systems potentially provides a significant improvement in their spectral efficiency to a value close to the Shannon limit. However, the implementation in practice of potentially high rates of communication quality in real conditions of a multipath broadband channel with variable parameters in the clock and frequency domains is not possible without adaptation to real conditions signal propagation [6]. Naturally, such an adaptation is possible only on the basis of properties and characteristics knowledge of the communication channel changes in the parameters in the clock and frequency domains, that is, its impulse and frequency characteristics, as well as their correlation properties.

In most cases, electromagnetic waves come to the receiving point as a result of multiple reflections from different scattering objects on the propagation path, which creates a complex multipath interference pattern at the receiving point. The multipath nature of radio wave propagation causes fluctuations of amplitude, initial phase and angle of signal arrival at the point of reception. In addition, the propagation paths can be non-stationary in nature, which is most often due to the mutual movement of the UE, or other objects relative to the BS (for example, people, cars, etc.). Even a small slow movement leads to a change in time of the multipath propagation conditions and, as a result, changes in signal parameters. As a result, the impulse response $h(\tau, t)$ multipath channel will experience significant changes (fig. 4).

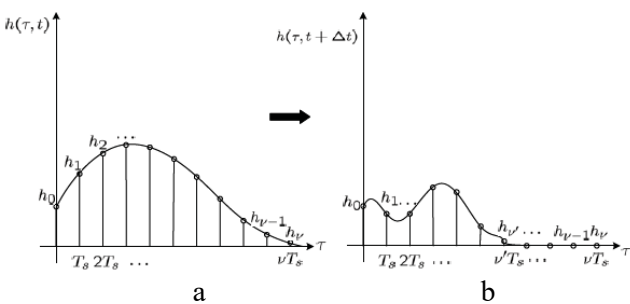


Figure 4 – Channel impulse response change

The model that quite sufficiently describes such a channel at discrete points in time is the delay line (DL) with taps and characteristics [6]:

$$\dot{h}(t) = \sum_{r=1}^R \dot{h}(r, t) = \sum_{r=1}^R \dot{h}_r(t) \delta(t - \tau_r(t)) + n(t) \quad (17)$$

where $\dot{h}_r(t)$ – is a complex attenuation coefficient in r ray; $\tau_r(t)$ – is a propagation delay задержка in

ray; $n(t)$ – is an additive white gaussian noise.

For stationary multipath channels, the parameters of which slowly vary over time, we can assume $\dot{h}_r(t) = \dot{h}_r$, $\tau_r(t) = \tau_r = r/c$. In this case, the signal $y(t)$ at the output of the multipath channel can be found as the convolution of the transmitted signal $x(t)$ with channel impulse response $\dot{h}(t)$.

$$y(t) = x(t) \sum_r \dot{h}_r x(t - \tau_r) + n(t) \quad (18)$$

The frequency response of a multipath channel can be determined based on the use of the Fourier transform of the impulse response (17):

$$H_k = \sum_r \dot{h}_r \exp\left(\frac{-j2\pi k \tau_r}{T_s N}\right) \quad (19)$$

where T_s – is a symbol duration.

In accordance with the frequency method [5], the solution of the determining frequency response in the communication channel in the presence of angular regions problem should be sought as the result of the inverse Fourier transform of the product of the propagating signal spectral density and the impedance wedge frequency response [7]:

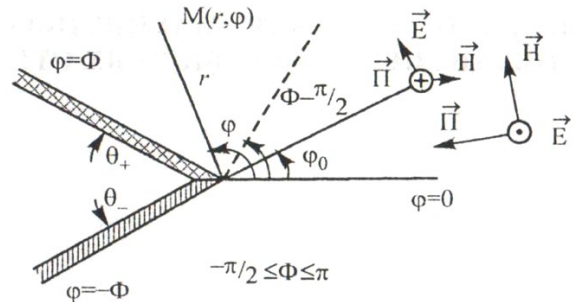


Figure 5 – Task geometry: Φ - angle of wedge opening, φ - angle of the incident wave arrival, M - observation point with polar coordinates (r, φ_0) .

$$\vec{H}(t) = \frac{1}{2\pi} \int_{-\infty}^{\infty} \dot{F}(i\omega) \dot{H}_z(\omega, \varphi, r) \exp[i\omega t] d\omega, \quad (20)$$

where

$$\dot{F}(i\omega) = \int_{-\infty}^{\infty} S(t) \exp[-i\omega t] dt \quad (21)$$

— is a incident signal spectral density, and $\dot{H}_z(\omega, \varphi, r)$ - is a solution to this problem for the case of harmonic oscillations [7].

For the case of E-polarization, the solution is written similarly:

$$\vec{E}(t) = \frac{1}{2\pi} \int_{-\infty}^{\infty} \dot{F}(i\omega) \dot{E}_z(\omega, \varphi, r) \exp[i\omega t] d\omega \quad (22)$$

where $\dot{E}_z(\omega, \varphi, r)$ - is a solution to this problem for the case of harmonic oscillations.

Considering the above, the solution for the case of diffraction of a non-harmonic pulse on an impedance wedge can be written as follows:

$$\dot{H}_z^{nl}(\varphi, r, t) = \frac{1}{2\pi} \int_{-\infty}^{\infty} \dot{F}(i\omega) \times \left[\begin{array}{l} \dot{H}_{z_{\text{ou}\phi}}^{uul.} + \dot{H}_{z_{\text{na}\delta}}^{nl} + \dot{H}_{z_{\text{omp}}}^{nl} + \\ \dot{H}_{z_{\text{omp}-}}^{nl} + \dot{H}_{z_{\text{nos}}}^{nl} + \dot{H}_{z_{\text{nos}-}}^{nl} \end{array} \right] \exp[i\omega t] d\omega. \quad (23)$$

Based on the integration properties (23) can be rewritten as:

$$\begin{aligned} \dot{H}_z^{nl}(\varphi, r, t) &\cong \frac{1}{2\pi} \int_{-\infty}^{\infty} \dot{F}(i\omega) \left[\dot{H}_{z_{\text{ou}\phi}}^{uul.} \right] d\omega + \\ &\frac{1}{2\pi} \int_{-\infty}^{\infty} \dot{F}(i\omega) \left[\dot{H}_{z_{\text{na}\delta}}^{nl} e^{i\omega t} \right] d\omega + \\ &\frac{1}{2\pi} \int_{-\infty}^{\infty} \dot{F}(i\omega) \left[\dot{H}_{z_{\text{omp}+}}^{nl} e^{i\omega t} \right] d\omega + \\ &\frac{1}{2\pi} \int_{-\infty}^{\infty} \dot{F}(i\omega) \left[\dot{H}_{z_{\text{omp}-}}^{nl} e^{i\omega t} \right] d\omega + \\ &\frac{1}{2\pi} \int_{-\infty}^{\infty} \dot{F}(i\omega) \left[\dot{H}_{z_{\text{nos}+}}^{nl} e^{i\omega t} \right] d\omega \\ &+ \frac{1}{2\pi} \int_{-\infty}^{\infty} \dot{F}(i\omega) \left[\dot{H}_{z_{\text{nos}-}}^{nl} e^{i\omega t} \right] d\omega \end{aligned} \quad (24)$$

For E polarization case:

$$\begin{aligned} \dot{E}_z^{nl}(\varphi, r, t) &\cong \frac{1}{2\pi} \int_{-\infty}^{\infty} \dot{F}(i\omega) \left[\dot{E}_{z_{\text{ou}\phi}}^{uul.} e^{i\omega t} \right] d\omega + \\ &\frac{1}{2\pi} \int_{-\infty}^{\infty} \dot{F}(i\omega) \left[\dot{E}_{z_{\text{na}\delta}}^{nl} e^{i\omega t} \right] d\omega + \\ &\frac{1}{2\pi} \int_{-\infty}^{\infty} \dot{F}(i\omega) \left[\dot{E}_{z_{\text{omp}+}}^{nl} e^{i\omega t} \right] d\omega + \\ &\frac{1}{2\pi} \int_{-\infty}^{\infty} \dot{F}(i\omega) \left[\dot{E}_{z_{\text{omp}-}}^{nl} e^{i\omega t} \right] d\omega + \\ &\frac{1}{2\pi} \int_{-\infty}^{\infty} \dot{F}(i\omega) \left[\dot{E}_{z_{\text{nos}+}}^{nl} e^{i\omega t} \right] d\omega \\ &+ \frac{1}{2\pi} \int_{-\infty}^{\infty} \dot{F}(i\omega) \left[\dot{E}_{z_{\text{nos}-}}^{nl} e^{i\omega t} \right] d\omega \end{aligned} \quad (25)$$

If the spectral width of the signal transmitted over the channel is less than the coherence band $B_s = |f_1 - f_2| \leq B_c$, then all spectral components of the signal vary approximately equally, and such fading is common.

Information on the dynamics of change in the transmission coefficient is provided by the correlation function or the nature of the change in the spectral power density fluctuations of this coefficient. This means that for analyze and synthesize of mobile communication systems adaptive signal processing, information is needed on the magnitude and nature of changes in the complex transmission coefficient $\dot{h}(\tau, t)$ or complex channel transfer function [6]:

$$\dot{H}(f, t) = \int_{-\infty}^{\infty} \dot{h}(\tau, t) \exp(-j2\pi f\tau) d\tau \quad (26)$$

and their correlation properties in the time and frequency-time domains:

$$R_h(\tau) = \lim_{T \rightarrow \infty} \frac{1}{T} \int_0^T h(t) h(t + \tau) dt \quad (27)$$

$$R_H(\Delta f, \Delta t) = \int_{-\infty}^{\infty} R_h(\tau, \Delta t) \exp(-j2\pi \Delta f \tau) d\tau \quad (28)$$

Naturally, when solving specific problems of transmitting digital information, it is necessary to use a device of discrete transformations

REFERENCES

1. Kravchenko V.F. Spectral properties of atomic functions in problems of digital signal processing. Radio engineering and electronics, 2001, v.46, #5, p.534-552.
2. S.H. Mezon. G. Cimmerman. Electronic circuits, signals and systems: Translation from English./M.: Foreign literature publisher. 1963.
3. Rvachev V.L. R-functions theory and some of its application. Kiev, 1982. – 552p.
4. Ufimtsev P.Y. Theory of diffraction edge waves in electrodynamics. M.: Binomial. Laboratory of Knowledge, 2007.
5. Zernov N.V. The solution of non-stationary boundary value problems of electrodynamics // Report Academy of Sciences of the USSR. 1951. V. 30, #1. p. 33.
6. Bestugin A.R., Kryachko A.F., Kryachko M.A. Methods to improve the spectral efficiency of telecommunication systems based on approximation of the signal envelope by atomic functions. // News of universities. Radio electronics. Vol. 59 No. 11 (629) p. 38-50, 2014
7. Kryachko A.F., Lihachev V.M., Smirnov S.N., Stashkevich A.I. The scattering of electromagnetic waves theory in angular structures. SPb .: Science, 2009.

MODELING OF AUTOMATED PROCESSES OF BUILDING A PHYSICAL MODEL OF AN OBJECT ON A 3D PRINTER

A. Chabanenko

Saint-Petersburg State University of Aerospace Instrumentation, Saint-Petersburg, Russia
E-mail Chabalexandr@gmail.com

Annotation

Modeling can be called the replacement of one object to another. The modeling process consists of three elements: the subject (the researcher), the object and the model, reflecting the connection between the object and the subject. The model should be to some extent similar to the object under study and take into account its features, which must be used in additive manufacturing. Simulation models are developed using special software that uses various modeling languages.

Additive technology today is one of the most dynamically developing types of "digital" production. They make it possible to accelerate the solution of the tasks of preparing and adjusting production and are already actively used to produce finished products.

Installations with several extruders make it possible to produce several identical objects using only one digital model, but at the same time allow the use of different materials and colors with different properties. The speed of printing and synthesis grows in proportion to the number of printheads. In addition, a certain saving of polymers and time resources is achieved by using a common working chamber, often requiring heating. Together, these two points reduce the cost of the printing process. But it requires ensuring control of temperature conditions of printing, which is advisable to implement through a system of tolerances, based on sensors additive installation.

To ensure the quality of the process of building a physical model of an object, it is necessary to build a model for the operation of a 3D printer in the system in the Abaqus Unified FEA system.

This is a simple simulator of a Cartesian robot with 3 degrees of freedom. This code basically displays the robot based on the technical specifications and updates the drawing based on the relationship between the links and the engines. The simulation results on physical models can be visualized using this model. The model can be used as an interface for a small prototype based on an Arduino microcontroller. Therefore, the engine parameters, thread, link, the size of the site are given to a single form. The types of additive plants used as a data set are presented in (Fig. 1).

- Picaso 3d Designer Pro 250.
- 3d printer Wanhao Duplicator i3.

The model of the automated installation of layer-by-layer synthesis is presented in (fig.2).

When designing the modules, the following work was done:

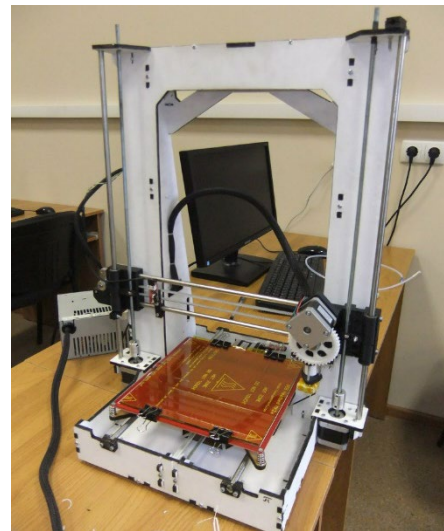


Figure 1. Additive installation using 3 degrees of freedom.

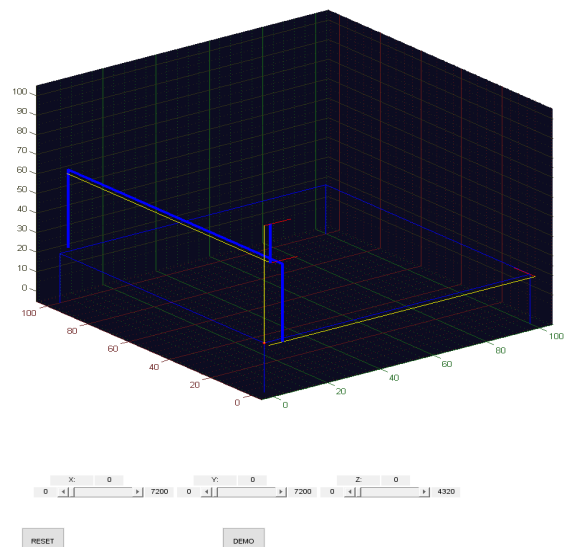


Figure 2. Model of automated installation of layer-by-layer synthesis

- study of functional diagrams in order to identify subschemas with the same purpose and unify their structure within a specific product;
- the choice of constructive;
- PCB design;
- the choice of ways to protect the module from overheating and external influences.

What was laid in the program model (fig. 3).

DRAW	51.0022	51.0022	51.0022
drawing	1000x3 double	1.5682...	89.9998
ee_motor_x	282.0574	282.05...	282.05...
ee_motor_y	2.8112e+03	2.8112...	2.8112...
ee_motor_z	2.5002e+03	2.5002...	2.5002...
ee_x	3.9175	3.9175	3.9175
ee_y	39.0442	39.0442	39.0442
ee_z	54.7256	54.7256	54.7256
fig	1	1	1
fr_height	20	20	20
fr_up2_x0	6.4175	6.4175	6.4175
fr_up2_x1	6.4175	6.4175	6.4175
fr_up2_y0	39.0442	39.0442	39.0442
fr_up2_y1	39.0442	39.0442	39.0442
fr_up2_z0	60	60	60
fr_up2_z1	80	80	80
fr_up_x0	8.9175	8.9175	8.9175
fr_up_x1	8.9175	8.9175	8.9175
fr_up_y0	-2.5000	-2.5000	-2.5000
fr_up_y1	102.5000	102.50...	102.50...

Figure 3. Program Fragment

The use of additive technologies makes it possible to incorporate qualitative characteristics into the design of a product, the screening of electromagnetic fields of radio electronic equipment units and their connections when using conductive materials.

When forming a product, it is necessary to consider those indicators that affect the production of body elements.

To maintain the required torque, a stepping motor is selected with a possibly large holding moment, which depends on the supply voltage. The fact is that the manufacturer indicates the minimum voltage for a stepper motor at which it begins to rotate without loads. The maximum allowable voltage can be calculated by the formula:

$$U_{\max} = 1000 \cdot \sqrt{L_{\text{III}}}$$

Where is L_{III} Inductance of one phase of the stepper motor.

Practice shows that the optimal voltage will be the value of ~ 80% of the received.

$$U_{\text{optim.}} = U_{\max} \cdot 0,8$$

In the process of designing a control scheme, it is necessary to clearly understand what tasks it should solve. In our case, the delta robot was chosen as the basis for the design. For the system to function successfully, it is necessary to solve two problems, namely, the inverse (inverse) and the direct problem

of kinematics. In the first case, the position to which the extruder of the 3D printer should be moved is known in advance. In the second case, the angles are known, on which the positioning mechanisms of the system are rotated, and it is necessary to find the position of the working platform in space.

The (fig. 4) shows the design stage of the body element for the subsequent layer-by-layer synthesis.

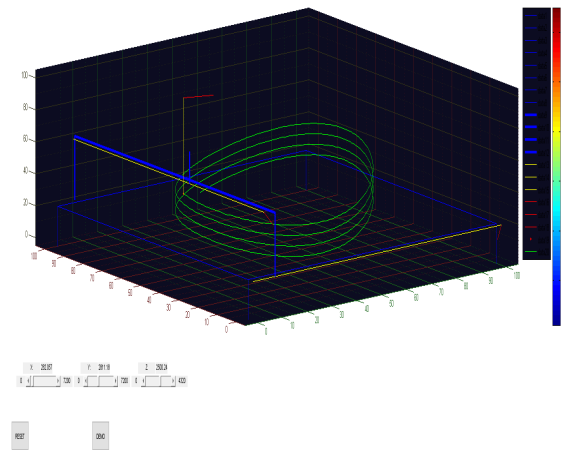


Figure 4. Model of automated installation at the stages of layer-by-layer synthesis

The signal from the control program goes to the controller (fig. 5), in which they are further converted and then transmitted to the drivers of stepping motors for each of the axes. The drivers convert the received signals for the subsequent switching of the motor windings, after that the engines make the necessary movements. After the engines have completed the necessary movement, the operation is repeated until the program is completed.

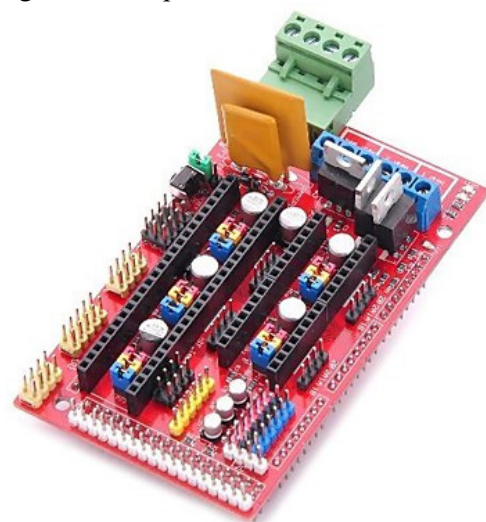


Figure 5. RAMPS expansion board

The type of production is determined from the analysis of the product design, the program of release and the actual annual fund of working time. For a certain type of production choose the best methods of assembly, the necessary equipment and equipment. The type of production is established using the

coefficient of seriality.

$$k_c = K_o \div n_p$$

Where is K_o – this is the number of assembly operations for the technological process.; n_p – the number of jobs required to complete the assembly process.

$$n_p = \frac{N_t \sum_{i=1}^{K_o} T_{um.i}}{60k\Phi_{\text{д}}}$$

Where is N_t is the annual volume of production Products, PCs.; $\sum_{i=1}^{K_o} T_{um.i}$ labor intensity of product assembly, min $T_{um.i}$ – standard time of the i-th assembly operation, Min; k – rate of compliance

during assembly; $\Phi_{\text{д}}$ – a valid annual time fund, h. values $k_c \leq 1$ corresponds to mass production, $k_c = 1$ – serial production, $k_c > 1$ – for small programs and single production. Additive manufacturing is applicable to the serial and single production of the product case elements.

Evaluation of the effectiveness of the additive production of body elements of the product.

The formula for the estimation of the efficiency of processes:

$$R = \sum B_i,$$

where: R – evaluation; B_i – number of points.

To control and improve the quality of the process of layer-by-layer synthesis of additive installation using additive technologies identified indicators that must be considered in the printing process (table. 1) and having the form (fig. 3).

Table 1 – Quality indicators in additive production

Quality indicator name	Quality designations	The name of the characterized properties
Softening temperature	°C	Temperature resistant
Shrinkage	%	Dimension
Duration of the plastic-viscous state	c	Print speed
Fluidity	Mm	Print accuracy

The analysis of individual elements of the production process, and then suggested ways to improve.

Proper understanding of the causes of non-performance of the organization at the level of individual operations eliminates or reduces the cost of operations that do not create added value in the process.

The cost of manufacturing the part is quite high, and depending on the complexity of the product, the question of the effectiveness of this method requires a separate study.

If the requirements are met, the polymers that are planned to be used in layer-by-layer synthesis and considering the moment of homogenization, which is achieved by observing the temperature regimes, will be able to achieve the quality requirements for products manufactured using additive manufacturing.

The use of additive technologies allows to include in the “Design” stage the “Model”, “Drawing” and “Equipping” stages. The stage “Tooling” is not required in the processes with the use of additive technologies, as the equipment does not require tooling. The stages “Designing” and “Printing” unite in themselves most of the processes of traditional technology. as in the “Design” stage, everything is considered in the 3D model and the equipment does not require a snap. The stages “Designing” and “Printing” unite in themselves most of the processes of traditional production technologies for body elements.

Conclusion

Thanks to the modeling of the layer-by-layer synthesis of 3D printing and considering the peculiarities of the technology and production stages, it turns out to ensure the quality of construction of the physical model of the object. Quality assurance in additive manufacturing makes it possible to achieve polymer savings and reduce the time of the preparatory stages of printing.

Reference

1. Quality Assurance of Hull Elements of Radio-Electronic Equipment by Means of Control System / Chabanenko, A.V., Anatoly P.Y. IEEE International Conference. 2018.
2. Quality management of REA case elements / A.V. Chabanenko // RIA: Magazine: “Standards and Quality”. 2018. №2. pp. 90-94.
3. An expert method for choosing a 3d-printer model suitable for pilot / small-scale production in instrument-making. Ya.A. Schenikov Radio industry. 2017. No. 2. pp. 107-112.
4. Identification of key indicators of the quality of the technological process of production of the case of electronic equipment based on FDM Semenova E. G., Chabanenko A. V., Nazarevich S. A. Radio industry, Issues of radio electronics. M. № 4. 2017. pp. 53-59.

AN EFFICIENCY ESTIMATION OF THE TRANSPORT CODING FOR PACKETS WITH AN EXPONENTIALLY DISTRIBUTED DELAY

M. Afanasev

Saint-Petersburg State University of Aerospace Instrumentation,
B.Morskaya 67, 190000, Saint-Petersburg, Russia
E-mail: af-mm@yandex.ru

Abstract

Recently, low message delay becomes more and more important. It allows an implementing of new applications and services interacting in almost real time that was impossible before. A requirement of low message delay now is a part of many communication standards such as 5G and recommendation papers of future standards such as Tactile Internet proposed by ITU-T. In this research, we perform an efficiency estimation of the transport coding for packets with an exponentially distributed delay. We consider a traffic model that is critical to message delay, and an influence of the transport coding on such traffic types and on the message delay jitter. Our research shows that the transport coding can be used not only for a decreasing of the average message delay but and for a decreasing of the message delay jitter.

Keywords: transport coding, latency, delay, latency critical applications, error correcting coding, network coding, Kleinrock's model

INTRODUCTION

There are types of applications and services that are critical to message delay. For instance, VoIP, remote control systems, spatially distributed security systems, etc. These systems use audio, video and control commands. When something happens these systems should response immediately in order to prevent possible consequences or support suitable quality of service. We can underline several parameters of such systems:

1. t_{max} is the maximum acceptable message delay (e.g. 250 ms for VoIP [1]);
2. Message delay jitter is a difference between average message delay and maximum and minimum message delay: $t'_{avg} - t'_{min}, t'_{max} - t'_{avg}$ [1].

Let us consider application, transport and network levels of OSI. Usual approaches to decrease message delay are:

1. Adjusting packet routing procedures in the network;
2. Adjusting a packet prioritization in the network (QoS);
3. Using buffers in order to fight with the message delay jitter;
4. etc.

An alternative approach is the transport coding first proposed by E.A. Krouk and G.A. Kabatiansky in [2][3]. The main purpose of the transport coding is a decreasing of the average message delay in the network. However, it also allows organizing a prioritization of urgent messages [4].

In initial research, the simplified Kleinrock's network model was considered. In subsequent

research, some simplified assumptions were dropped in order to consider more realistic cases, like non-exponential packet delay [5], different channel capacities [6], non-heterogeneous network structure [7], delivery of a message during limited time [8], application of the transport coding [9].

The difference of this research from others about the transport coding is that we add a new realistic assumption of the network model: maximum time limit of message delivery and the volume of messages that we can afford to lose. We perform an efficiency analysis of the transport coding for packets with exponentially distributed delay in the network with the added realistic assumption.

First, we need to consider a network model.

THE TRANSPORT CODING

The network model

In [2], Kleinrock's network model [10] is considered with additional assumptions. The network consists of M channels and N nodes. All channels are absolutely reliable and do not make errors. They have the same channel capacities C . Nodes perform a processing of received packets, including routing procedures, storing packets, controlling of packet queues. Nodes are absolutely reliable and do not make errors. The time of processing at nodes is performed instantly and is not taken into account in the consideration.

Packets arriving in the i th network node and moving towards to the j th network node form a Poisson process with the equal average value γ_{00} (packets per seconds) for every pair of i and j . The

value

$$\gamma_0 = N\gamma_{00}$$

is an external traffic of the i th node, and the value

$$\gamma = N\gamma_0 = N^2\gamma_{00}$$

is the total external traffic of the network.

The network has buffers for packets with infinite capacity. It means that packets in the network can never be lost because of buffer overflow.

All messages arriving in the network consist of k packets with length m . The length of packets inside the network satisfies an assumption of independence [10]: every time when a packet has been received at a node, a new length of this packet b' is chosen independently with PDF

$$P(b) = \mu e^{-\mu b}, b \geq 0,$$

where b (the size of a packet in bits) is a parameter of the pdf function.

The packet flow going through the channels is a Poisson process with the equal average value λ_0 (packets per a second) for every channel of the network. The total internal traffic in the network is

$$\lambda = M\lambda_0.$$

Let us denote ρ as the value of channel load in the network, and then the average packet delay is:

$$\bar{t}(\rho) = \frac{\lambda}{\mu C} \frac{1}{1 - \rho} \quad (1)$$

where ρ is

$$\rho = \frac{\lambda_0}{\mu C}$$

Let us make two additional assumptions that are not contained in the original Kleinrock's network model:

1. Packet delays in the network are random and independent values distributed according to an exponential distribution law with the average value $\bar{t}(\rho)$

$$F_\rho(t) = 1 - e^{-\frac{t}{\bar{t}(\rho)}}, t \geq 0, \quad (2)$$

where t (time units) is a parameter of the CDF function. An exponential distribution is used for describing of data flows in many researches, in particular in [11].

2. The routing procedure in the network is chosen in such a way that an increasing of an external traffic leads to the uniform increasing of an internal traffic of each channel.

The message encoding procedure

In [2], the following procedure named as the transport coding was proposed: Initially, original packets arriving in the network have the length m . Let us consider each character of a packet as an element of $GF(2^m)$. It allows us to encode each message by a 2^m MDS code (e.g. a Reed-Solomon code). Then each original message consisting of k packets maps to an encoded message consisting of n packets. After

encoding procedure, we will send the encoded message instead of the original message. It leads to an increasing of the network load ρ by a factor $\frac{n}{k} = \frac{1}{R}$ and the average packet delivery time becomes $\bar{t}(\rho/R)$.

It is well known that the word of MDS(n, k) code can be decoded by any k from n information characters. Hence, k first arrived encoded packets are enough to obtain our original message.

The message delay of original messages equals to the k th order statistic from $k - \bar{T}_{k:k}$. While the message delay of encoded messages equals to the k th order statistic from $n - \bar{T}_{k:n}$.

In the case of when m is too long, we need to deal with big fields GF, that is not desirable because of processing difficulty and it is unacceptable for low power devices like Internet Of Things. In [2], the solution of this case is described.

THE PROBLEM STATEMENT

Perform efficiency analysis of the transport coding for packets with an exponentially distributed packet delay (2) in the network model described above and traffic types that are critical to message delay.

Let us denote the problem statement: minimize the delivery time of packets arrived later than t_{max} ;

The traffic model that is critical to message delay

Network delay is one of the main factors, which can degrade the Quality of Experience (QoE) of network services [12]. Therefore, to prevent the degradation of the perceived quality of the services with delay constraints, a maximum limit is defined in the most of communication systems and protocols. This applies both real-time (VoIP, RDP, gaming, remote control, video [13] and audio [14] streaming) and non real-time services (instant messaging, M2M metering etc.). A guidelines for the maximum allowed latency and proposed multiplexing periods for different services/scenarios can be found for example in [15] and [16]. Now there are many research papers considering delay limit issues for video surveillance, real-time traffic over TCP [17] and other applications. Service latency limits are in the focus of 3GPP 5G recommendations. In particular 3GPP Technical specification "Mission Critical Video over LTE" [18] defines end-to-end maximum latency for different scenarios: urgent real time video transmissions, Robots video remote control etc.

We consider this fact in our research and network model and show that the transport coding can be used both for significant decreasing of the average message delay and jitter.

First, we start with a traffic model, which can be described by the following parameters:

1. t_{max} is the maximum acceptable packet

delivery time;

2. $p = \Pr\{\bar{T}_{k:n} > t_{max}\}$ is the volume of messages that have arrived later than t_{max} ;

3. k is the amount of packets of an uncoded message.

Taking into account the assumption (2) for considered network model, packet delivery time is a random variable distributed according to an exponential distribution law. For this traffic model, it is impossible to talk about methods that can guarantee that all messages will be delivered for the time less than t_{max} , but we can talk about a minimizing of the value p .

The average packet delivery time

The average packet delivery time of an individual packet (1) depends on many parameters, such as the total intensity of the internal traffic λ , the total intensity of the external traffic γ , μ , the capacity of all channels C . We can see that when $\rho = 0$ then $\frac{\lambda}{\mu C \gamma}$ is an initial packet delivery time in the empty network, and $\frac{1}{1-\rho}$ is the increasing coefficient depending only on ρ . Thus, absolute values of these parameters are not important. Only the initial packet delivery time in the empty network is of interest. Let us denote it as \bar{t}_s and rewrite (1) as

$$\bar{t}(\rho) = \bar{t}_s \frac{1}{1-\rho} \quad (3)$$

For all next calculations we consider $\bar{t}_s = 2$. This value was taken thus that for $t_{max} = 9$ the considered

network model will not be able to deliver messages for the average time less than t_{max} with the intensity of the channel traffic ρ . We need to note that using time units are abstract values and they can be expressed in needed units for a particular task.

The problem statement

Let us fix the value t_{max} , what is the probability $p(\rho)$ of that the message will be delivered later than t_{max} when ρ is known?

For the next calculations let us set $k = 8$.

$$\begin{aligned} \bar{t}\left(\frac{\rho}{R}\right) &= \bar{t}(\rho) \frac{1-\rho}{1-\rho/R} \\ p &= 1 - \Pr\{\bar{T}_{k:n} \leq t_{max}\} = \\ &= 1 - \sum_{i=k}^n C_n^i (1 - e^a)^i e^{a(n-k)}, \\ & \quad n = \frac{k}{R} \end{aligned}$$

where

$$a = -\frac{t_{max}}{\bar{t}\left(\frac{\rho}{R}\right)} = -\frac{t_{max}(1-\frac{\rho}{R})}{\bar{t}(\rho)(1-\rho)}$$

In Fig. 1, we can see the probability of message lost for different code rates for the case when $t_{max} = 9$ and the intensity of channel load $\rho = 0.6$:

1. In the case without the transport coding ($R = 1$) the probability of message lost is $p = 0.76$;
2. In the case $R = 0.89$, $p = 0.45$;
3. In the case $R = 0.80$, $p = 0.22$;
4. In the case $R = 0.67$, $p = 0.04$.

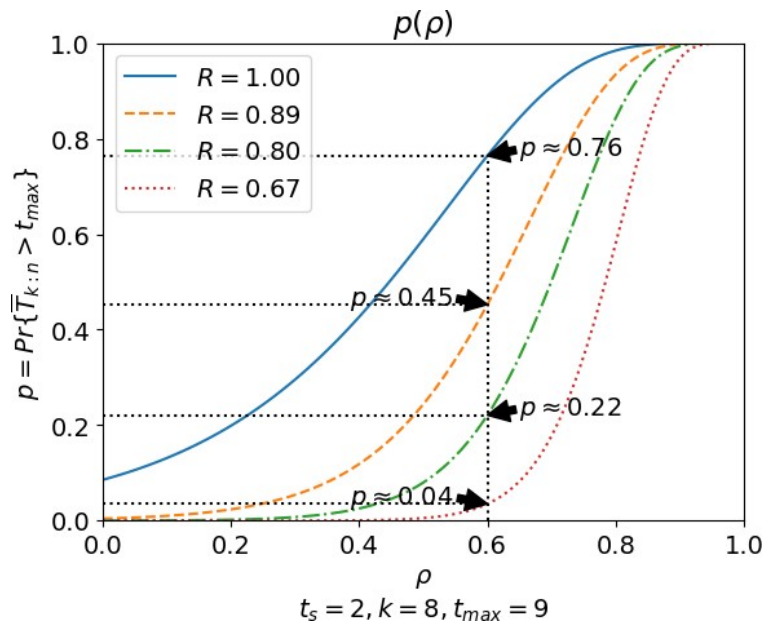


Figure 1. The direct problem statement when $t_{max} = 9$

When $p = 0.2$, without the transport coding the maximum channel load is $\rho_{max} \approx 0.2$, but in the case with transport coding and the code rate $R = 0.8$, the maximum channel load can be increased to $\rho_{max} \approx 0.6$.

The influence of the transport coding on the message delay jitter

First, we need to start with determining a dispersion and a standard deviation for the average message delay. Taking into account the assumption (2) about an exponential distribution law of packet delay, we can obtain:

$$\begin{aligned} M[T] &= \bar{t}(\rho) \\ D[T] &= \bar{t}(\rho)^2 \end{aligned}$$

The dispersion of the k th order static [19]:

$$D[T_{k:n}] = D[T] \sum_{i=n-k+1}^n i^{-2} =$$

$$= \bar{t} \left(\frac{\rho}{R} \right)^2 \sum_{i=n-k+1}^n i^{-2}$$

$$D[T_{k:k}] = D[T] \sum_{i=1}^k i^{-2} = \bar{t}(\rho)^2 \sum_{i=1}^k i^{-2}$$

The gain in the standard deviation is

$$\begin{aligned} f(R) &= \frac{\sigma[T_{k:k}]}{\sigma[T_{k:n}]} = \frac{\sqrt{D[T_{k:k}]}}{\sqrt{D[T_{k:n}]}} \\ &= \frac{\bar{t}(\rho) \sqrt{\sum_{i=1}^k i^{-2}}}{\bar{t}(\rho/R) \sqrt{\sum_{i=n-k+1}^n i^{-2}}} \\ &= \frac{(1 - \frac{\rho}{R}) \sqrt{\sum_{i=1}^k i^{-2}}}{(1 - \rho) \sqrt{\sum_{i=n-k+1}^n i^{-2}}} \end{aligned}$$

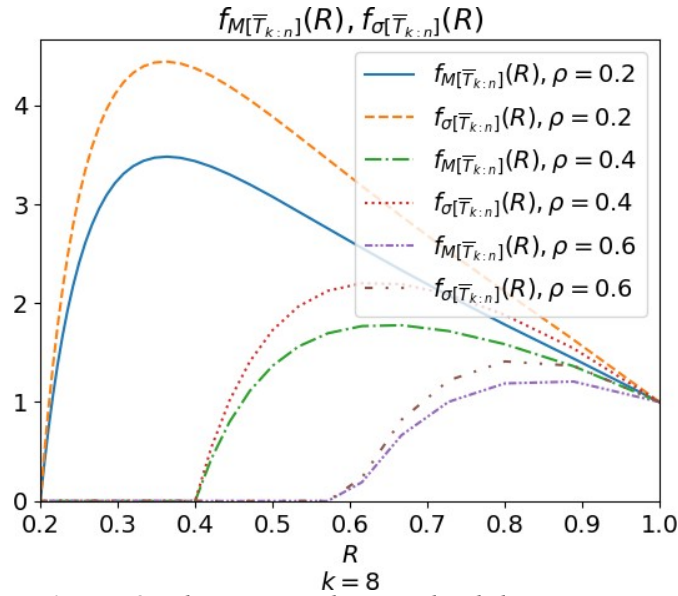


Figure 2. The gain in the standard deviation

In Fig. 2, we can see a curve line of the gain in the standard deviation depending on the intensity of channel load and the assessment of the gain in the standard deviation obtained in [2]. The following cases were depicted in that figure:

1. $\sigma[T_{k:n}]$ when $\rho = 0.2$;
2. $M[T_{k:n}]$ when $\rho = 0.2$;
3. $\sigma[T_{k:n}]$ when $\rho = 0.4$;
4. $M[T_{k:n}]$ when $\rho = 0.4$;
5. $\sigma[T_{k:n}]$ when $\rho = 0.6$;
6. $M[T_{k:n}]$ when $\rho = 0.6$.

We can conclude from obtained plots that the transport coding can decrease the standard deviation and it means that the transport coding can also

decrease jitter of message delay. In particular, in the case when $\rho = 0.2$ and $R = 0.36$, the gain of the standard deviation is ≈ 4.5 times, while the gain of the average message delay [2] is ≈ 3.5 times.

CONCLUSION

In this research we suggested new traffic model that is critical to the delay. The traffic model consists of the maximum acceptable message delay t_{max} and the probability that a message has been delivered later than t_{max} , $p = \Pr\{\bar{T}_{k:n} > t_{max}\}$. We performed efficiency analysis of the transport coding for considered traffic model.

For considered network model parameters ($\bar{t}_s = 2$) and the traffic model ($t_{max} = 9, k = 8, n_{max} = 100$), we concluded that the transport coding allows:

1. Decreasing of the message delay jitter. In the case of $\rho = 0.2$ and $R = 0.36$, the gain of the standard deviation is ≈ 4.5 times, while the gain of the average message delay [2] is ≈ 3.5 times;

2. Increasing of the maximum intensity of channel load ρ_{max} in order to maintain chosen parameters of traffic and network models. In the case of $p = 0.2$ and without transport coding, we can maintain chosen parameters of channel and network models with the maximum intensity of channel load is $\rho_{max} \approx 0.2$, while in the case with transport coding and the code rate $R = 0.8$, this parameter can be increased to $\rho_{max} \approx 0.6$;

Further possible research directions of the transport coding can include:

1. Efficiency analysis of the transport coding in more realistic cases including parameters such as: MTU size, packet's length in bytes, packet delay in milliseconds, etc.;

2. Considering of real protocols that are critical to the message delay.

REFERENCES

1. R.Swale: Voice over IP: systems and solutions. let (2001)
2. G.Kabatiansky, E.Krouk, S.Semenov: Error correcting coding and security for data networks: analysis of the superchannel concept. John Wiley & Sons (2005)
3. G.A.Kabatianskii, E.A.Krouk: Coding decreases delay of messages in networks. IEEE International Symposium on Information Theory. Proceedings (1993)
4. E.Krouk, S.Semenov: Transmission of priority messages with the help of transport coding. Telecommunications, 2003. ICT 2003. 10th International Conference on 2, 1273–1277 (2003)
5. D.Malichenko, E.Krouk: Estimation of the mean message delay for transport coding. Intelligent Interactive Multimedia Systems and Services pp. 239–249 (2015)
6. D.Malichenko: Efficiency of transport layer coding in networks with changing capacities. Problems of Redundancy in Information and Control Systems (REDUNDANCY), 2016 XV International Symposium pp. 82–86 (2016)
7. D.Malichenko: Transport layer coding with variable coding rate. Problems of Redundancy in Information and Control Systems (REDUNDANCY), 2014 XIV International Symposium on pp. 71–73 (2014)
8. E.Krouk, S.Semenov: Delivery of a message during limited time with the help of transport coding. Signal Processing Advances in Wireless Communications, 2004 IEEE 5th Workshop on pp. 1–5 (2004)
9. E.Krouk, S.Semenov: Application of coding at the network transport level to decrease the message delay. In Proceedings of Third International Symposium on Communication Systems Networks and Digital Signal Processing 15(17), 109–112 (2002)
10. L.Kleinrock: Queuing Systems. Theory, vol. 1. John Wiley & Sons (1975)
11. Sergeev, A., Shanyazov, R., Ilina, D., Bashun, V.: The evaluation of gain of statistical modulation method on the example of qam16 for input data with exponential distribution. In: 2018 Wave Electronics and its Application in Information and Telecommunication Systems (WECONF). pp. 1–5. IEEE (2018)
12. Internet Engineering Task Force (IETF): Guidelines for Considering New Performance Metric Development. <https://tools.ietf.org/html/rfc6390> (2011), Online; accessed 21-January-2019.
13. Ukhanova, A., Sergeev, A., Forchhammer, S.: Extending jpeg-ls for low-complexity scalable video coding. In: Image Processing: Algorithms and Systems (2011)
14. Sergeev, A.: Signal and code model for hidden data transmission over the voice channel. In: Control and Communications, 2003. SIBCON 2003. The IEEE-Siberian Conference on. pp. 123–126. IEEE (2003)
15. M.Suznjevic, J.Saldana: Delay limits for real-time services (2016)
16. ITU-T Technology: Watch Report. The Tactile Internet. https://www.itu.int/dms_pub/itu-t/opb/gen/T-GEN-TWATCH-2014-1-PDF-E.pdf (2014), Online; accessed 21-January-2019.
17. E.Brosh, S.Baset, V.D..H.: The delay-friendliness of tcp for real-time traffic. IEEE/ACM Transactions on Networking (TON) pp. 1478–1491 (2010)
18. ETSI: LTE; Mission Critical Video over LTE (3GPP TS 22.281 version 15.1.0 Release 15). https://www.etsi.org/deliver/etsi_ts/122200_122299/122281/15.01.00_60/ts_122281v150100p.pdf (2018), Online; accessed 21-January-2019.
19. H.A.David: Order statistics. John Wiley & Sons (1981)

DEVELOPMENT OF A MULTICHANNEL WIRELESS OPTICAL DIGITAL COMMUNICATION SYSTEM BASED ON FREQUENCY-DIVISION MULTIPLEXING

B. Akopyan

Saint-Petersburg State University of Aerospace Instrumentation,
Saint-Petersburg, Russia

E-mail: akopyan.bella@yandex.ru

Abstract

The article describes the development of the optical wireless digital communication system based on multichannel frequency-division multiplexing. The decision rule and processing algorithm are described. The results of experiments are given, the average error probability per bit is calculated.

Keywords: digital processing, digital communication, multichannel transmission, redundant encoding, frequency-division multiplexing, optoelectronics, ordinary least squares, average error probability per bit.

INTRODUCTION

Tests of the developed prototype of the optical wireless digital communication system [1] showed that the main disadvantage of the system is the sensitivity to the overall level of external illumination, which is accompanied by a distortion of the pulse shape; this leads to errors in signal reception. The improvement of quality of optical wireless digital transmission is possible not only through use of noise-resistant methods of signal processing on the receiving side [2], but also by multi-channel transmission. The task is to develop the optical wireless digital communication system based on multichannel transmission so that it significantly reduces the average error probability per bit.

REDUNDANT ENCODING

To reduce the negative impact of noise, developers of digital communication systems resort to excessive coding, which is characterized by high

resistance to various types of noise. It means that possible values of bits can be represented, for example, as opposite code combinations. The disadvantage of redundant encoding is that the bit transmission rate decreases in proportion to the increase in the duration of the signal.

FREQUENCY-DIVISION MULTIPLEXING

The method of additional improvement of communication quality is parallel communication, for which it is necessary to have several independent channels. One of the most common methods of organization of multichannel systems is frequency division multiplexing (FDM), in which each channel is allocated a certain frequency range [3, 4].

In application to optical transmission channels, the FDM can be converted into transmission of radiation with a wavelength λ for each channel. Figure 1 shows the functional diagram of a multichannel optical wireless digital communication system.

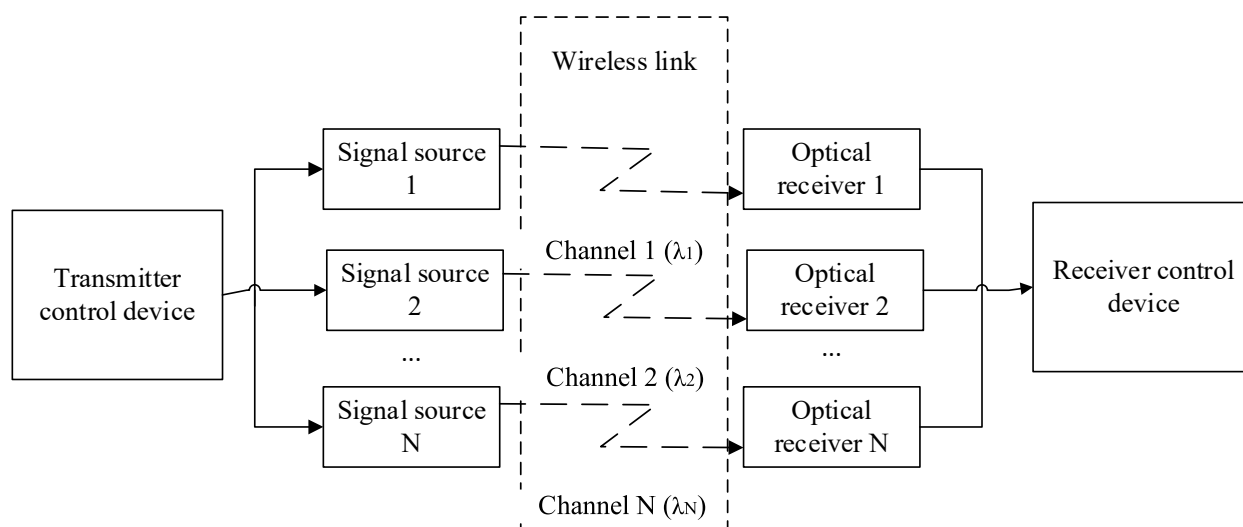


Figure 1. The functional diagram of a multichannel optical wireless digital communication system

Optoelectronics, depending on the wavelength, are divided into three categories: infrared (IR), visible and ultraviolet (UV), each of which corresponds to different wavelengths. The elements of these ranges are sensitive to various types of noise, due to which the noise on one channel will have minimal impact on the results of the rest, which will reduce the average probability of error per bit.

The prototype of developed system has two channels: one is IR and another is visible range

channel. The visible range channel is sensitive to light, but is indifferent to thermal radiation, and the quality of the IR channel is almost independent of the level of ambient light. In this case, an effective joint use of the capabilities of the element base of the IR and visible ranges is carried out. Figure 2 shows the electric circuit of the prototype's optical channels. The channel consists of the photodiode and emitting diode of the appropriate optical range. V_s is the supply voltage, equal to 5 volts.

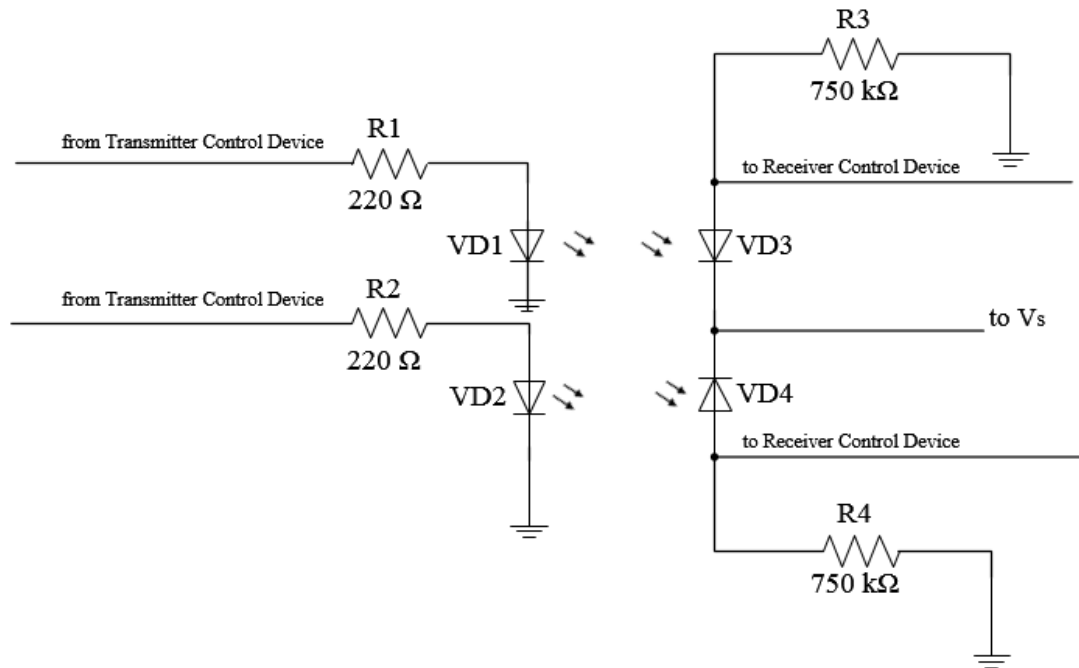


Figure 2. The electric circuit of the prototype's optical channels

DECISION RULE AND PROCESSING ALGORITHM

As described in [2], to compensate for the distortion of the pulse fronts, it is advisable to supplement the decision rule by processing an additional parameter that would characterize the shape of impulse. The proposed approach is to determine the slope coefficient of the regression line for the signal appropriate to each value of code combination's symbol (regression coefficient). The most common method of approximation due to computational simplicity is the method of the ordinary least squares (OLS).

The equation of the regression line equal to one code symbol of the i -th bit is:

$$y = K_i x + b_i.$$

The coefficients of this line a and b are defined as:

$$[K_i, b_i] = \arg \min \sum_{j=1}^n (K_i x_j + b_i - y_j)^2,$$

where x_j is the time instant corresponding to the j -th sample count. The defining parameters of this decision rule are the absolute value and sign of the slope coefficient K_i .

Moreover, it is also required to use the argument U_c which allows to take into account the intensity of noise in each channel; if impossible code combination was received, it makes possible to choose a channel in which information is more reliable. In the prototype the value of the correction term U_c was chosen equal to:

$$U_c = \frac{U_{in} - U_{out}}{6}.$$

The processing algorithm, as in the [2], is divided into two stages: calibration of threshold values and processing of the signal according to the decision rule. The difference is that since the transmission is carried out over two channels, the processing is carried out using two thresholds, one for each channel. Let K_{lim_c} be the threshold value of the regression coefficient of channel, then if the absolute value of the regression coefficient of the bit K_i exceeds K_{lim_c} , then the sign of

the regression coefficient is checked:

$$K_i > 0 \rightarrow "1", K_i < 0 \rightarrow "0".$$

After that, if a possible code combination is received, it is converted to the corresponding bit value. Otherwise, the symbol value is determined by a single-threshold processing [1] in channel, which has bigger U_c .

RESULTS

Figure 3 shows the results of processing. The time diagrams show that the impulses, despite the noise radiation, are processed correctly by switching the rules.

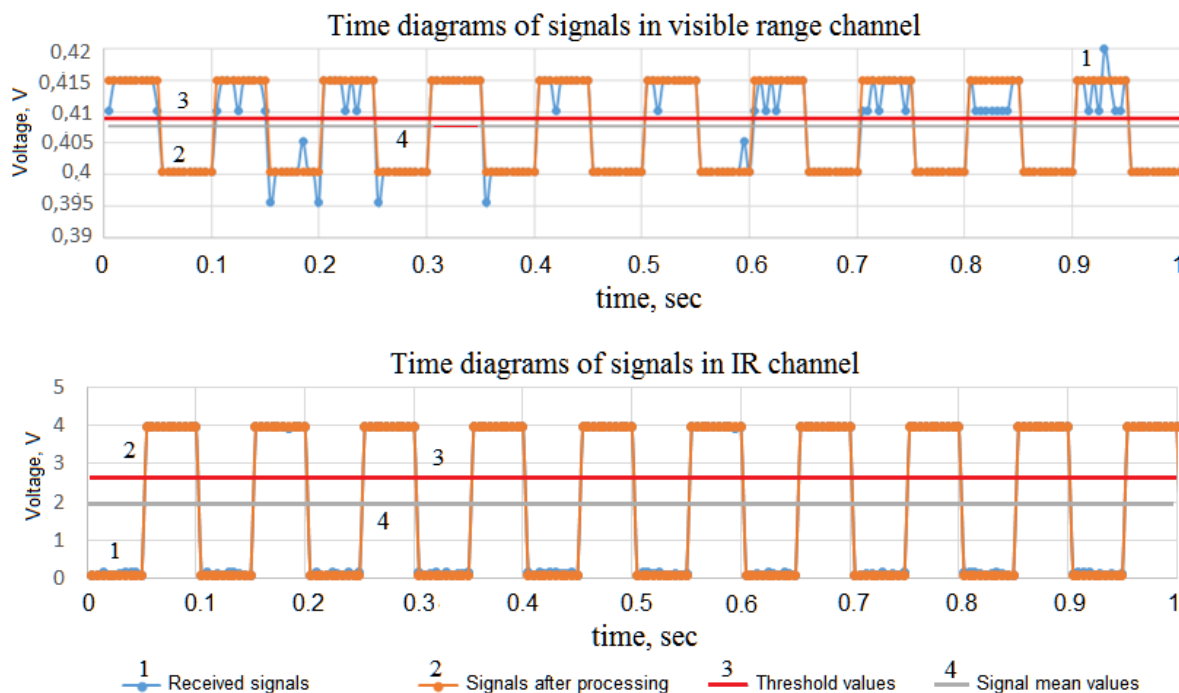


Figure 3. Time diagrams of the received and processed signals in each channel

CONCLUSION

According to results of the experiments, it was found that the average error probability per bit decreased from 0.0006 [2] to 10^{-5} . Thus, the combination of multichannel communication, frequency division multiplexing and redundant data encoding provides high resistance to interference without reducing the transmission speed in proportion to the increase in the signal duration corresponding to one bit. In the future, it is possible to develop a multichannel system based on optoelectronics of different wavelengths within the same optical radiation range.

REFERENCES

1. Akopyan B.K., Gorodetskaya A.V. Razrabotka maketnogo prototipa sistem tsifrovoy svyazi s peredachey po opticheskomu kanalu // Semidesyataya mezhdunarodnaya studencheskaya

nauchnaya konferentsiya GUAP / Development of a prototype of optical wireless digital communication system// The Seventieth International Student Scientific Conference of the SUAI. – SUAI, 2017. (in Russian)

2. Akopyan B. Research of data processing methods in an optical wireless digital communication system//Bulletin of the UNESCO department «Distance education in engineering» of the SUAI: Collection of the papers. St. Petersburg, Issue 3. – SPb.:SUAI, 2018.

3. Volkov V.G. Besprovodnyye opticheskiye sistemy svyazi // Zhurnal «Spetstekhnika i svyaz'». 2012. Wireless optical communication systems // Magazine "Special equipment and communications". 2012. № 3. p. 2-9.. (in Russian)

4. Vishnevskiy V.M., Lyakhov A.I., Portnoy S.L., Shakhnovich I.V.. Shirokopolosnyye besprovodnyye seti peredachi informatsii Broadband wireless information transfer networks / Moscow: Technosphere, 2005. 592 p.. (in Russian)

MODERN AUTOMATIC WAYS OF AIRCRAFT PRE-FLIGHT MANAGEMENT

N. Bogatov

Saint-Petersburg State University of Aerospace Instrumentation,
Saint-Petersburg, Russia
E-mail: nikita.bogatow@gmail.com

Abstract

Air transport is the fastest and most reliable way to deliver cargo, passengers on the basis of straightening routes. In connection with the decades in the field of air travel has undergone tremendous changes, both qualitative and quantitative. With the increase in the number of passengers and freight traffic, as well as the routes of the network of air carriers, which also require an increase of planes number. It has an influence on resources spending and requires some ways to optimize it.

With an increase in the number of routes and aircraft we can see the increase in costs of pre-flight management of air carriers. In connection with this, a key resource in air travel is the time that the air carrier spends on preparing the aircraft for a new flight or on troubleshooting.

One of the solutions to this task of reducing maintenance time is automation. One of the most illustrative examples of the application of this solution is the company Lufthansa Technic Logistic Services – a company belonging to the Lufthansa Group and providing timely delivery of spare parts for aircraft of Lufthansa and its partners around the world (Fig.1) [1].



Figure 1. Cargo terminal Lufthansa Technic Logistic Services in Munich airport.

The company is actively introducing automation into its processes, affecting a large part within the warehouse infrastructure and methods of delivering spare parts. The very first example shown in Figure 1 is the Agilox warehouse robot, represented working in the company's terminal at Munich Airport [2]. The tasks of the robot include the implementation within the warehouse flow of small and medium-sized cargo, from the place of reception and registration, to the place of storage or shipment to the aircraft. The robot works in its own software, using the Internet for

completely autonomous movements (Fig. 2) [3].

rients in space with a range of cameras and sensors. The second unique example of automation is its own automatic storage, which the company simply calls Autostore (Fig. 3) [4]. The task of this storage is to store medium and small cargo, parts of aircraft, as well as tools. The principle of operation of this storage, developed in the city of Hamburg, is a cell, located one above the other. Above the cells, autonomous robotic manipulators move along the rails, the task of which is to take the load into the storage and assign it a cell. The load is placed in a special container located in the system and having a bar code for recognition.

Access to the storage is carried out immediately by several operators through terminals (Fig. 4).

A feature of such a system is that, based on its own calculations about the frequency of accessing any cell with a load, the system itself sorts the containers according to their needs. Simply put, the containers that are constantly requested through the terminal are located in the maximum availability, which reduces the waiting time for accessing the system. Thus, such a storage at times reduces the time required to fulfill a request for the necessary part, and also, due to its structure, occupies minimal space.

The third example is the ProGlove system – an extremely practical and effective QR scanning system and barcode of cargo codes [5]. This system is a glove with a barcode reader and QR codes embedded in it. The operator, who enters the base of the newly arrived cargo scans with the help of such a glove all the information about the load, which through the transmitter immediately appears on his computer and is ready to be included in the base. In the absence of the need to read the documentation for the cargo, this greatly speeds up the maintenance time. In the future, the company plans to transfer all existing cargo to such a processing system.

In the shipping department, Lufthansa Technic Logistic Services has another automated storage

facility – Modula Lift [6]. Storage, which is developed in Italy, is a metal tower, in which pallets are placed at levels, each of which is assigned a number and a barcode in the system. The robotic elevator, having accepted the request from the terminal, rises to the desired level and collects the pallet with the cargo,

after that delivers it to the lower level of delivery. Such storage is used in the company mainly for packaging materials for shipment and office, but in the future it is planned to redistribute space in the storage for small cargoes.

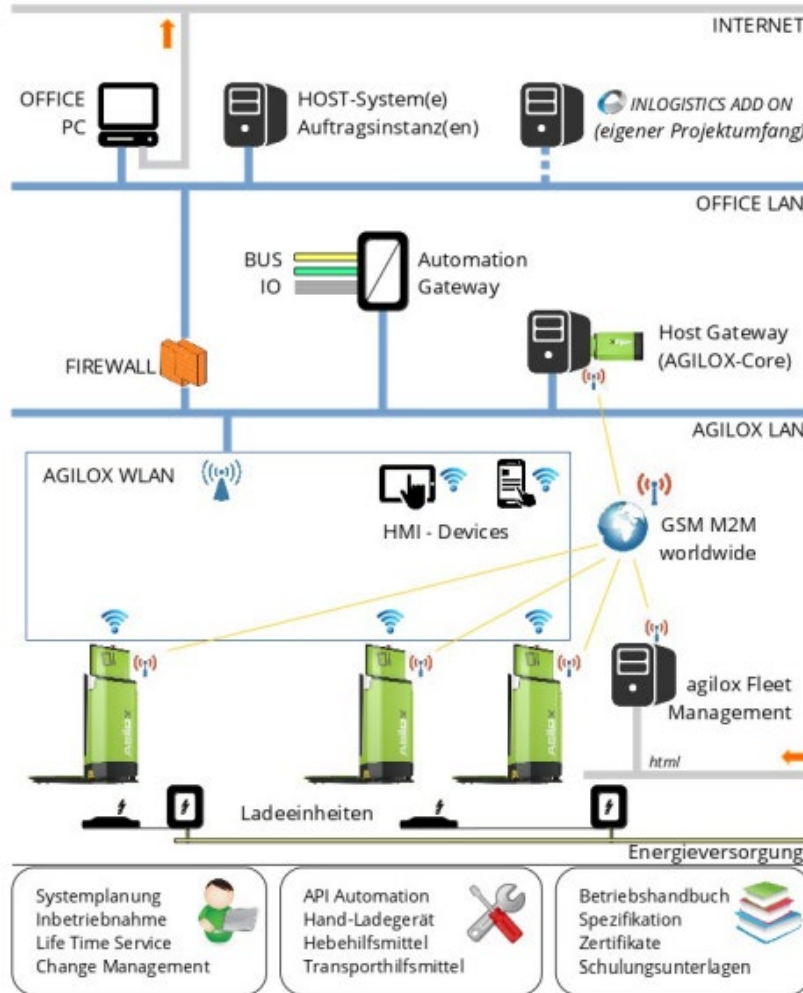


Figure 2. The way of work of Agilox



Figure 3. Autostore



Figure 4. Autostore terminals



Figure 5. Proglove



Figure 6. Modula Lift

The storage is able to independently assess the size of the cargo, thereby choosing the level to store the pallet. The disadvantage of such a system is the security measures under which the store does not accept cargoes and objects larger than

The advantages are the speed of access to pallets, as well as security, which is important.

The cargo terminal of the company has a direct connection with the repair hangars of Lufthansa Technic. When the aircraft maintenance engineer needs additional detail, he makes a request to the system, which is immediately received by the operator. If there is a spare part in stock, it is delivered to the hangar using an electric carrier (Fig 7).



Figure 7. Electric Carrier

However, in the future, the engineer will be able to make a request from a tablet on which special software is installed, and the cargo will be delivered to him not by an electric transport, but by an automated rail platform, somewhat reminiscent of a mini-train. Such a platform on rails will be able to instantly deliver the necessary parts and tools to the four main points of the hangar. The connection of this platform with the Autostore automatic storage will allow minimizing human participation, leaving behind only the introduction of goods into the system.

Conclusion

To sum it up, Lufthansa Technic Logistic Services is an excellent example of introducing automation to all types of cargo handling. The company has successfully implemented and plans to implement a huge number of projects aimed at automating processes and reducing cargo handling time, which will undoubtedly reduce the cost of air carriers for servicing aircraft. It shows, that the right usage of automation systems for the one goal – time, can effectively reduce costs for aircraft pre-flight management, because the air carrier will not pay the same money for the parking slot usage. Also, it makes possible to offer more routes and types of aircraft for air carriers, and makes a great goal for the future.

List of used literature:

1. Lufthansa Technic Logistic Services site [электронный ресурс] <https://www.ltls.aero> (11.03.2019)
2. Lufthansa digital warehouse gallery <https://www.mro-network.com/big-data/lufthansa-techniks-new-digital-warehouse-program/gallery?slide=1> [электронный ресурс] (11.03.2019)
3. Agilox [электронный ресурс] <https://agilox.net/?lang=en> (11.03.2019)
4. Autostore [электронный ресурс] <https://autostoresystem.com> (11.03.2019)
5. Система сканирования Pro Glove <https://www.proglove.com/de/> [электронный ресурс] (11.03.2019)
6. Система хранения Modula Luft <https://www.modula.ru>

PRACTICAL EXPERIENCE IN THE USE OF SIMULATION MODELING FOR PASSENGER TRANSPORTATION BY TAXI

A. Dobrovolskaya

Saint-Petersburg State University of Aerospace Instrumentation,
Saint-Petersburg, Russia
E-mail: angd999@gmail.com

Abstract

Currently in St. Petersburg 35689 valid permits for taxi transportation and only 33 official taxi parkings [5]. According to a large carrier, more than 50,000 trips are made every month in St. Petersburg [4], but if you consider the huge number of taxi services, there are much more trips. A huge number of rides is associated with the rapid development of taxi services: the cost of the ride is acceptable, you can order a taxi in any available way, and the time of car delivery is minimal.

Introduction

The main task of any urban passenger transport-delivery of the passenger to the necessary part of the city in the shortest time. In large cities, where the daily traffic load is estimated at millions of passengers, taxis are an important part of the transport system. The choice of mode of transport can be influenced by many factors: travel time, route, traffic congestion, convenience, etc. Public transport not always can provide high mobility: it is necessary to calculate the time with a margin, in some parts of the city can only be reached by taxi or by private transport, there may be difficulties for people with luggage. This is due to the fact that the public transport ride on a fixed route according to the current schedule. In turn, taxis are available around the clock and every day and also allows door-to-door travel. That is why a taxi should be one of the alternative ways to travel and an integral part of the developing metropolis.

There are different ways to order a taxi:

- By phone through the dispatcher;
- By the mobile application;
- Search for a free taxi on the street.

The last one is the least common in recent days, because quite often there are cases of drivers fraud, absence of licensing and lack of control of the drivers condition. When ordering through the application, you can see the plate number and the driver's name, the estimated cost and duration of the trip. These data allow passengers to calculate their time and money, as well as ensure safety. When making an order through the dispatcher, the passenger is also informed of the estimated cost and time of delivery of the car, which is also a more profitable option.

From the passenger's point of view, the taxi is a ride from point A to point B (Fig.1).

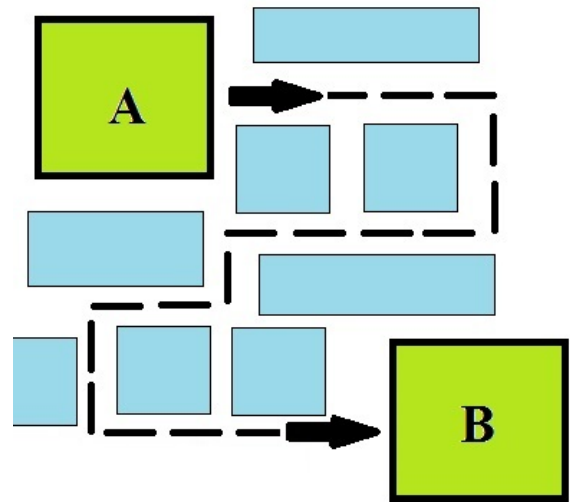


Figure 1 – movement of passenger

From the transportation management point of view, the scheme is a linear process aimed at meeting the needs of the passengers in taxi services.

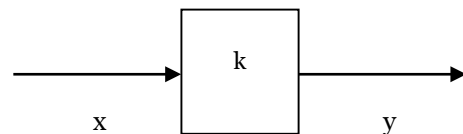


Figure 2 – Transportation management

On this figure x – single query on the trip unit k – the performance of the carriage, the output y meeting the demand for taxi services.

In General, the output stream y is the following expression:

$$y = x * k; \quad (1)$$

where k is the conversion factor of the application.

In the differentiation of the basic process of the carriage you can see the following components (Fig.3).

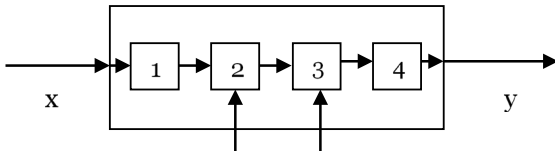


Figure 3-differentiated management scheme

In this scheme, 1-reception and processing of the received order; 2 – formation of the time of delivery of the car; 3 – calculation of the approximate cost and duration of the trip; 4 – recalculation taking into account real conditions.

Therefore, the output stream «y» has the form:

$$y = (k_1 + k_2 + k_3 + k_4) * x \quad (2)$$

The decisive factors for the passenger to travel by taxi are the cost of the trip and the time of submission. When calculating the time of delivery of the car, all taxis in the nearest radius are considered, and then individual requirements for the trip are taken into account.

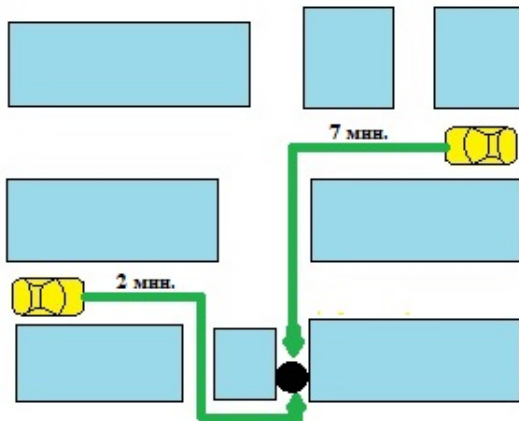


Figure 4-Selecting a suitable vehicle

Modern algorithms are able to calculate the time of car delivery when the user enters data about the trip. This takes into account the probability of making the received order.

To solve the problem of distribution of cars in the city, it is necessary to use transport zoning, in which the territory of the city is represented as a graph, with vertices at the points of gravity of the taxi. At the same time there is a macro – and micro-level in the conditional areas of movement.

At the micro-level, you can see the peaks in the number of orders, they will be the vertices of the graph (Fig. 5).

Since the time of delivery of the car is the main factor in making a decision about the trip – it should be minimal. At the micro level, a sufficient number of taxis are required to meet the need for transportation.

The task of finding a performer can be represented as a bipartite graph, where in one area there are many orders (P), and in the other there are many performers(A) (Fig.6).



Figure 5-micro level of taxi movement

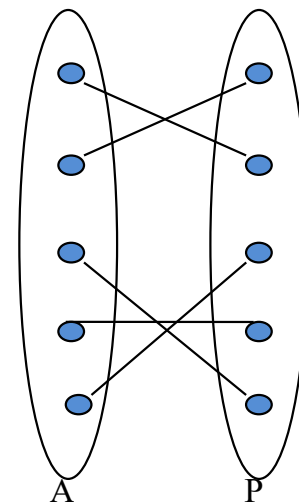


Figure 6-the task of selecting an executor

The matrix is a set of performers and orders and the cost of transportation, in this case time (t) (table 1):

Table 1 – of selecting an executor

	P1	P2	...	Pn
A1	t_{11}	t_{12}		t_{1n}
A2	t_{21}	t_{22}		t_{2n}
...				
An	t_{n1}	t_{n2}		t_{nn}

In General, selecting an executor is a task about assignments:

$$\sum_{i \in A} \sum_{j \in T} C(i, j) t_{ij} \rightarrow \min \quad (3)$$

where C is the target function of the destination, t is the vehicle delivery time.

To predict passenger transportation by taxi was selected transport hub of «Academicheskaya» metro

station, which was closed for major repairs for 11 months. The passenger flow of the station is 1,600,000 passengers per month[3], after the closure of the load passed to the nearest metro station «Polytechnicheskaya» and «Grazhdanskiy prospect», as well as changed the routes of land transport. However, transport is overloaded and passengers can choose an alternative to a taxi ride, therefore the number of applications may increase significantly. In this case, the matrix of distribution of applications will have the form:

When solving the problem, the waiting time of the car increases, and therefore the taxi service loses the possible profit from failures. The main task is to carry out an effective transfer of vehicles at the

macro-and micro-level to meet the demand for the trip.

Table 2 – matrix of distribution of applications when the number changes.

	P1	P2	...	Pm
A1	t_{11}	t_{12}		t_{1n}
A2	t_{21}	t_{22}		t_{2n}
...				
An	t_{n1}	t_{n2}		t_{nm}

To simulate the system with an increase in the number of taxi trips, the «AnyLogic» environment was chosen(Fig. 7).

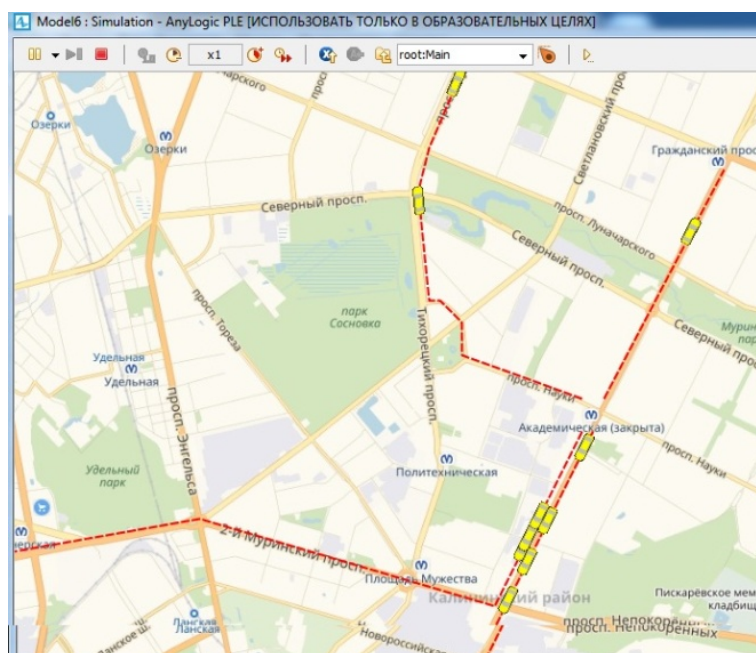


Figure 7-simulation model «AnyLogic»

Conclusion

The article deals with the ways of decision-making automation for taxi aggregators. Since taxi is a transport that provides high mobility, the transport organizer must respond quickly to changes in the current conditions. In St. Petersburg, not all areas have official city taxi stands, so it is necessary to develop a system that allows you to automate the process of distribution of cars in the city. Taxis should certainly be considered as part of the urban transport system, as they can affect the complete or partial abandonment of personal transport, which directly affects the improvement of environmental friendliness and unloading of the transport network.

List of used literature:

1. Fetisov V. A., Majorov N. N. Practical tasks in simulation of transport systems: proc. benefit. – SPb.: SUAI, 2012. – 185 p.
2. Majorov N. N. Modeling of transport processes / N. N. Majorov, V. A. Fetisov. — SPb.: Publishing house of SUAI, 2011. – 165 p.
3. Statistics. Passenger traffic in the subway [Electronic resource] – <http://www.metro-spb.ru/statisticheskie-dannye.htm> (6.03.2019)
4. Taxi in St. Petersburg [Electronic resource] <https://yandex.ru/company/researches/2015/spb/taxi> (6.03.2019)
5. Transportation of passengers and Luggage by taxi. Administration of St. Petersburg[Electronic resource] https://www.gov.spb.ru/gov/otrasl/c_transport/taxi/ (6.03.2019)

PIPELINE OF MOBILE SERVICE FOR GENERATING IMAGE DESCRIPTIONS

G. Emelyanov

Saint-Petersburg State University of Aerospace Instrumentation,
Saint-Petersburg, Russia
E-mail: porox9696@mail.ru

Abstract

This article explores pipeline of mobile service for automatic generating image descriptions using natural language. The goal of this service is help people with disabilities to get a positive user experience. Core steps are: image uploading, image processing using neural network and pronunciation of generated description using Accessibility.

Keywords: image descriptions, neural network, natural language, recurrent neural network, machine translation, accessibility, people with disabilities.

INTRODUCTION

By 2019-year mobile devices have become the major part of people's lives. According to a study by Counterpoint for 2017 year almost half of the smartphone users spend more than 5 hours a day on their mobile device [1]. But in the meantime, according to statistics by Apple, every seventh person has a disability [2]. It can be a visual impairment, hearing impairment, musculoskeletal disorders. If we take into account that more 1 billion Apple devices were sold, this value become significant.

At the same time a lot of producers of mobile devices and software support a development of Accessibility in order to give people with disabilities a positive user experience.

For example, mobile operation system iOS supports the following accessibility functions:

- VoiceOver – a gesture-based screen reader that lets user enjoys using iPhone even if it do not see the screen;
- Switch Control – let user moves on elements on screen coherently and performs different actions using third party I/O devices with Bluetooth;
- AssesstiveTouch – and accessibility feature that can help user with motor skill impairments get the most out of their device.
- Speak Screen, pronunciations, text pronunciation, predictive text with speech – all of these features let users get and assimilate information by acoustic meatus.

It's just small list of available features. Also, there are special commands for Siri, FaceTime communications using pantomimic speech and more [3].

Because all of this functionality is mainly a part of iOS, third-party developers can add these functions into their applications, adapting user experience for people with disabilities.

One on these applications can be service which will be transform a content from image into text format on natural language. And then it will pronounce text using Accessibility.

PIPELINE

The pipeline of the service is presented in Figure 1.

The user of the mobile device can perform one of three actions:

- take a photo;
- upload image from library;
- upload image from social network.

Then image is processed by neural network on the remote server. And as a result of processing will be a text description on natural language. Because all of open datasets for task of image annotation presented as sentences in English language, it is necessary add step which will be translate text from English into Russian language. And the text will be pass to Accessibility.

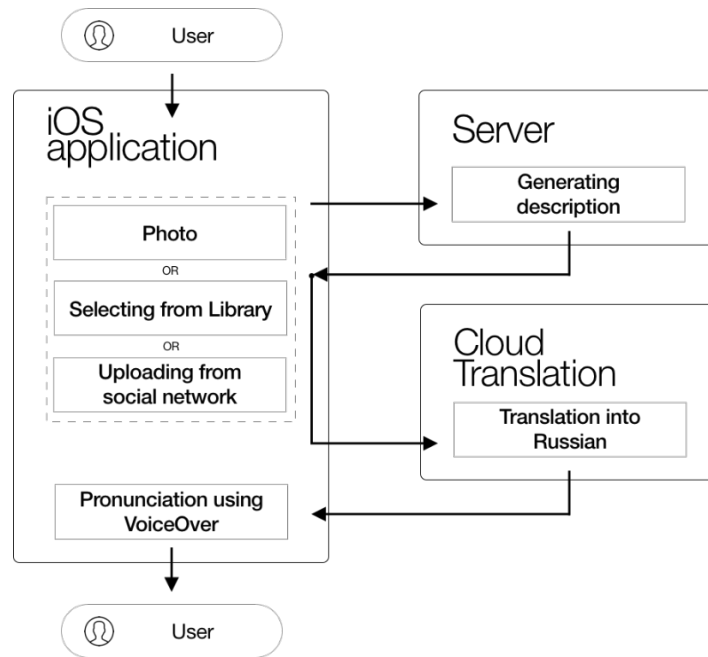


Figure 1. Service pipeline.

IMAGE PROCESSING

Humans find it easy to accomplish a wide variety of tasks that involve complex visual recognition and scene understanding, tasks that involve communication in natural language and tasks that combine translation between the two modalities. For

instance, a quick glance at an image is sufficient for a human to point out and describe an immense amount of details about the visual scene. Using the example in Figure 2, we can look at the image and immediately point out and describe the “red car Tesla”, the “undulating ground”, the “the car Tesla is riding on roadway”, “road marking double white lines”.

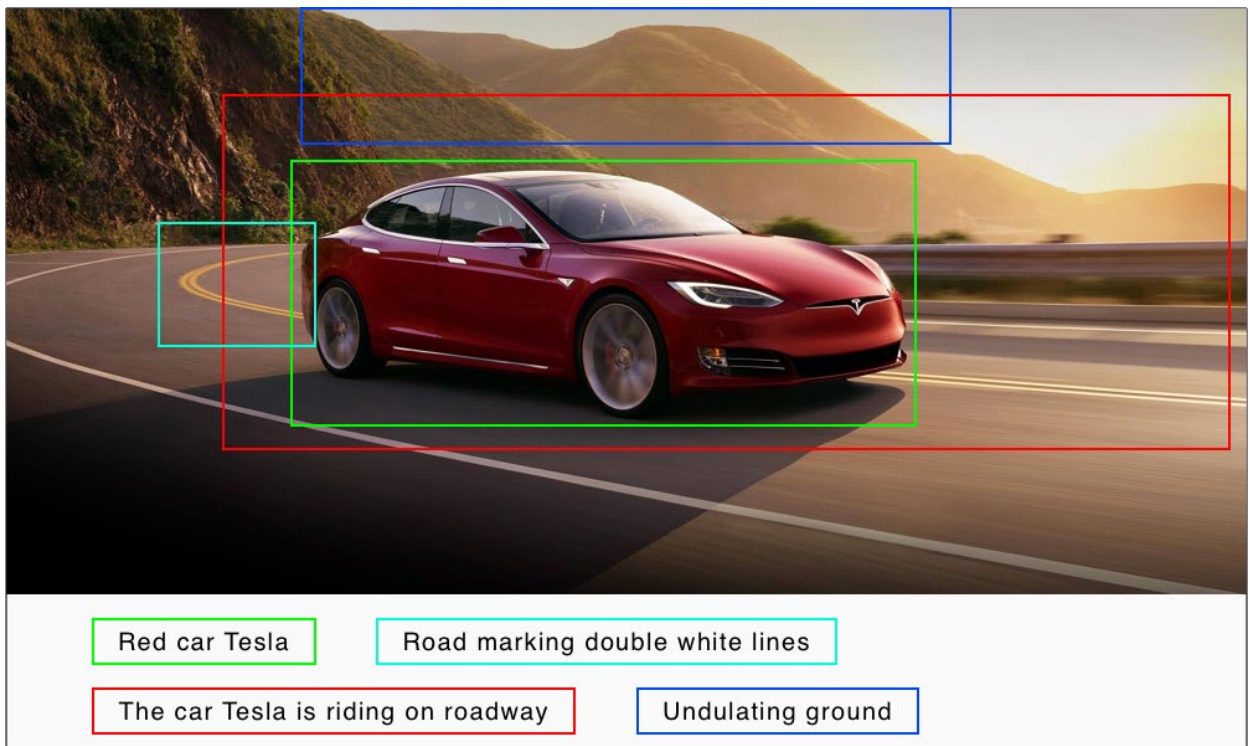


Рисунок 2. Example of parts descriptions of image.

However, this task is more difficult for computer. In a computer, this image is represented as one large array of numbers indicating the brightness at any position. An ordinary image might have a few millions of these pixels and a computer must transform these patterns of brightness values into high-level, semantic concepts such as a “car”. A natural language description such as “the car Tesla is riding on roadway” will be represented in the computer as a sequence of integers indicating the index of each word in a vocabulary (e.g. “the car Tesla is riding on roadway” might be {823, 300, 800, 400, 731, 534, 780}).

Therefore, the very natural task of pointing out and naming different parts of an image in fact involves a complex pattern recognition process of identifying salient subsets of a grid of a few million brightness values and annotating them with sequences of integers. Moreover, the image captions often require detecting and describing complex high-level concepts that are not only visual but require difficult inferences. For example, some images can be annotated by humans as “a traffic jam”, which requires the ability to detect multiple cars and analyze their quantity and spatial arrangements.

NEURAL NETWORK

There are a lot of different approaches that allow to transform images to texts [4]. Some of them use the estimating likelihood of data, some use common meaning space, others try to generate full sequences. Also, there are approaches with pretrained n-grams, building AND-OR graphs. But all of them are constrained by vocabulary size and quality [4].

Recent advances in statistical machine translation have shown that, given a powerful sequence model, it is possible to achieve state-of-the-art results by directly maximizing the probability of the correct translation given an input sentence in an “end-to-end” fashion – both for training and inference. These models make use of a recurrent neural network which encodes the variable length input into a fixed dimensional vector and uses this representation to “decode” it to the desired output sentence. Thus, it is natural to use the same approach where, given an image (instead of an input sentence in the source language), one applies the same principle of “translating” it into its description [5].

Oriol Vinyals suggested to directly maximize the probability of the correct description given the image by using the following formulation:

$$\theta^* = \arg \max_{\theta} \sum_{(I,S)} \log p(S|I; \theta), \quad (1)$$

where θ are the parameter of model, I is an input image, S its correct transcription. Since S represents any sentence, its length is unbounded. Thus, it is common to apply the chain rule to model the joint

probability over S_0, \dots, S_N , where N is the length of this particular example as:

$$\log p(S|I) = \sum_{t=0}^N \log p(S_t|I, S_0, \dots, S_{t-1}), \quad (2)$$

where θ was dropped for convenience. At training time (S, I) is a training example pair, and we optimize the sum of the log probabilities using stochastic gradient descent.

The using Recurrent Neural Network is a convenient way to model the probability $p(S_t|I, S_0, \dots, S_{t-1})$, where the variable number of words we condition upon up to $t - 1$, is expressed by a fixed length hidden state or memory h_t . This memory is updated after seeing a new input x_t , by using non-linear function f :

$$h_{t+1} = f(h_t, x_t). \quad (3)$$

To make the above RNN more concrete two crucial design choices are to be made: what is the exact form of f and how are the images and words fed as inputs x_t . For f we use a Long-Short Term Memory (LSTM) net, which has shown state-of-the-art performance on sequence tasks such as translation. For the representation of images, we use a Convolutional Neural Network (CNN). The architecture of LSTM memory block is presented on Figure 3.

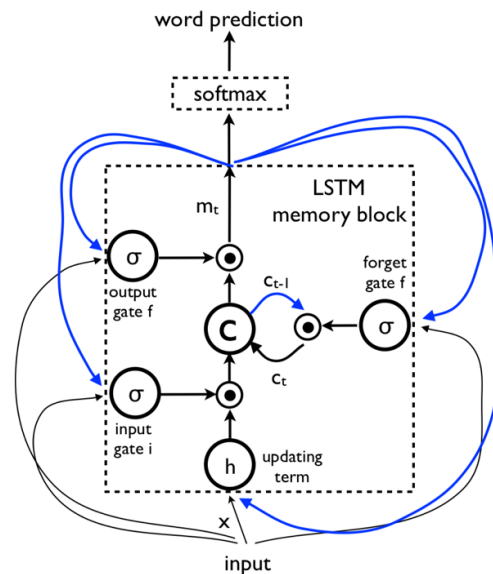


Figure 3. LSTM memory block.

The core of the LSTM model is a memory cell encoding knowledge at every time step of what inputs have been observed up to this step. The behavior of the cell is controlled by “gates” – layers which are applied multiplicatively and thus can either keep a value from the gated layer if the gate is 1 or zero this value if the gate is 0. In particular, three gates are being used which control whether to forget the current cell value (forget gate f), if it should read its input (input gate i) and whether to output the new cell value (output gate o).

The LSTM model is trained to predict each word of the sentence after it has seen the image as well as all preceding words as defined by $p(S_t|I, S_0, \dots, S_{t-1})$. For this purpose, it is instructive to think of the LSTM in unrolled form – a copy of the LSTM memory is created for the image and each sentence word such that all LSTMs share the same parameters and the output m_{t-1} of the LSTM at time $t - 1$ is fed to the LSTM at time t . All recurrent connections are transformed to feed-forward connections in the unrolled version. In more detail, if we denote by I the input image and by $S = (S_0, \dots, S_N)$, a true sentence describing this image, the unrolling procedure reads:

$$x_{-1} = CNN(I), \tag{4}$$

$$x_t = W_e S_t, t \in \{0 \dots N - 1\}, \tag{5}$$

$$p_{t+1} = LSTM(x_t), t \in \{0 \dots N - 1\}, \tag{6}$$

where each word is represented as one-hot vector S_t of dimension equal to the size of the dictionary. S_0 represents special start word and S_{N-1} is a special stop word which designates the start and end of the sentence.

Loss function is the sum of the negative log likelihood of the correct word at each step as follows:

$$L(I, S) = - \sum_{t=1}^N \log p_t(S_t). \tag{7}$$

MACHINE TRANSLATION

After server send text which describe image in English, service should translate it into Russian. For this task will be used Cloud Translation API by Google. For translation from one language into another Cloud Translation API uses Neural Machine Translation (NMT) by default. But is a requested pair of languages for translation is not supported by NMT will use Phrase-Based Machine Translation [6].

In 2016-year Google presented a new approach for solving task of machine translation which uses

neural networks [7]. This approach is named Google’s Neural Machine Translation (GNMT).

GNMT is an end-to-end learning approach for automated translation with two 8-layers recurrent neural networks LSTM and attention mechanism.

The first LSTM acts as an Encoder which transforms a source sentence into a list of vectors, one vector per input symbol. Given this list of vectors, the decoder produces one symbol at a time, until the special end-of-sentence symbol (EOS) is produced. The encoder and decoder are connected through an attention module which allows the decoder to focus on different regions of the source sentence during the course of decoding.

Let (X, Y) be a source and target sentence pair. Let $X = x_1, x_2, \dots, x_M$ be the sequence of M symbols in the source sentence; $Y = y_1, y_2, \dots, y_N$ be the sequence of N symbols in the target sentence. The encoder is simply a function of the following form:

$$x_1, x_2, \dots, x_M = EncoderRNN(x_1, x_2, \dots, x_M), \tag{8}$$

where x_1, x_2, \dots, x_M is a list of fixed size vectors. The number of members if the list is the same as the number of symbols in the source sentence. Using the chain rule the conditional probability of the sequence $P(Y | X)$ can be decomposed as:

$$P(Y | X) = P(Y | x_1, x_2, \dots, x_M) = \prod_{i=1}^N P(y_i | y_0, y_1, \dots, y_{i-1}; x_1, x_2, \dots, x_M), \tag{9}$$

where y_i is a special start symbol that is prepended to every target sentence.

During inference we calculate the probability of the next symbol given the source sentence encoding and the decoded target sequence so far:

$$P(y_i | y_0, y_1, \dots, y_{i-1}; x_1, x_2, \dots, x_M). \tag{10}$$

The full architecture of GNMT is presented in figure 4.

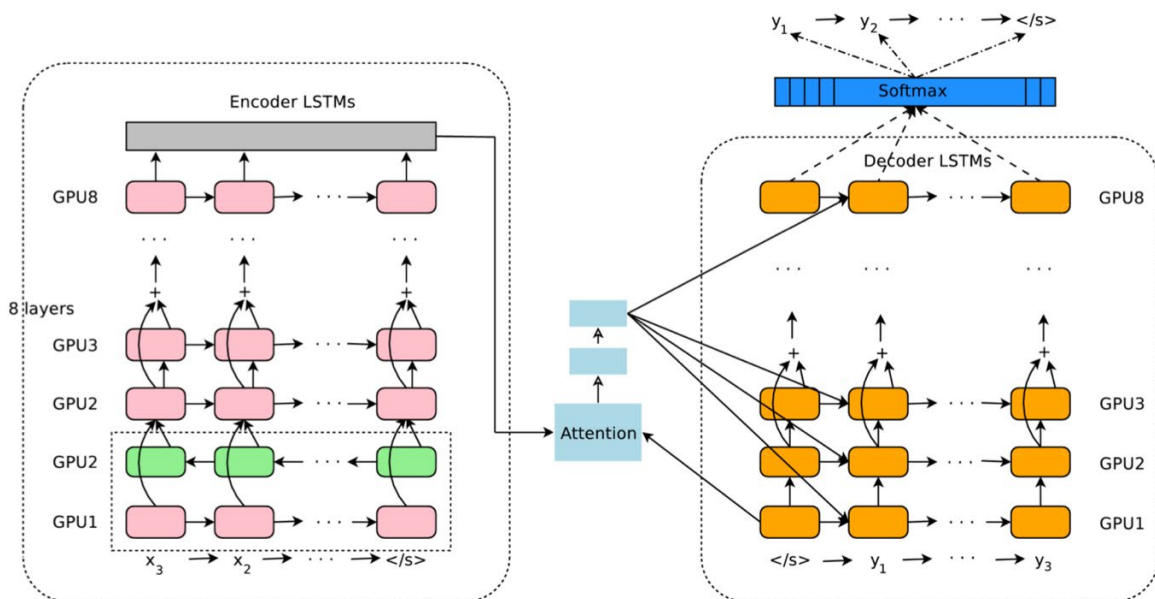


Figure 4. The architecture of GNMT.

Cloud Translation provide convenient API for translation performing: the request requires the sentence which will be translated, source language, target language, input text format (html or plain text) and translation method (by default – GNMT).

It should be noted, that required languages pair <English, Russian> is supported by GNMT.

VOICEOVER

The last core step of pipeline is pronunciation of translated text by one of Accessibility functions – VoiceOver. For this step must be configured instance of AVSpeechSynthesizer: should be configured target language of pronunciation, speed of pronunciation and text for pronunciation.

CONCLUSION

Presented mobile service consists of several independent modules: mobile application which allows to select and upload image from library or social network; remote server with neural network which processes image and generates text description in English language; Cloud Translation which perform sentence translation from English into Russian using Google Neural Machine Translation.

This service can be used by people with disabilities in order to assimilate information by acoustic meatus. This, in turn, will allow to improve user experience by closer integration Accessibility into mobile applications.

REFERENCES

[1] Almost Half Of Smartphone Users Spend More Than 5 Hours A Day on Their Mobile Device [electronic resource] URL:

<https://www.counterpointresearch.com/almost-half-of-smartphone-users-spend-more-than-5-hours-a-day-on-their-mobile-device/> (12.10.2017)

[2] Design for Everyone [electronic resource] URL:

<https://developer.apple.com/videos/play/wwdc2017/806/> (06.2017)

[3] As accessible as it is personal [electronic resource] URL:

<https://www.apple.com/accessibility/iphone/>

[4] *Emelyanov Georgij*. Techniques of image to text transformation // Bulletin of the UNESCO department «distance education in engineering» of the SUAI – 2018.

[5] *Oriol Vinyals*. Show and Tell: Lessons learned from the 2015 MSCOCO Image Captioning Challenge / Alexander Toshev, Samy Bengio, Dumitru Erhan // IEEE Transactions on Pattern Analysis and Machine Intelligence – 2016.

[6] Cloud Translation API [electronic resource] URL:

<https://cloud.google.com/translate/docs/translating-text>

[7] *Yonghui Wu*. Google’s Neural Machine Translation System: Bridging the Gap between Human and Machine Translation / Mike Schuster, Zhifeng Chen, Quoc V. Le, Mohammad Norouzi // arXiv – 2016.

RESEARCH OF METHODS FORMATION SAW TAGS FOR IDENTIFICATION SYSTEMS

I. Fedorov

Saint-Petersburg State University of Aerospace Instrumentation,
Saint-Petersburg, Russia
E-mail: iliagus2@gmail.com

Abstract

The technology of RFID objects based on tags with information contained on them is considered. This paper explores correlation properties of code sequences used in the construction of tags on surface acoustic wave (SAW).

Keywords: autocorrelation function (ACF), cross correlation function (CCF), frequency shift keying signals (FSK), impulse response, code sequence, coherence, signal properties, frequency modulation, phase modulation.

THE NOTION OF TAGS RFID SYSTEMS

Tag SAW device consisting of: interdigital transducer (IDT), based on the piezoelectric substrate

in the form of metal pin electrodes; reflective grooves located on both sides of the IDT; strip antenna, combined with the device on the surfactant. The tag is a passive device.

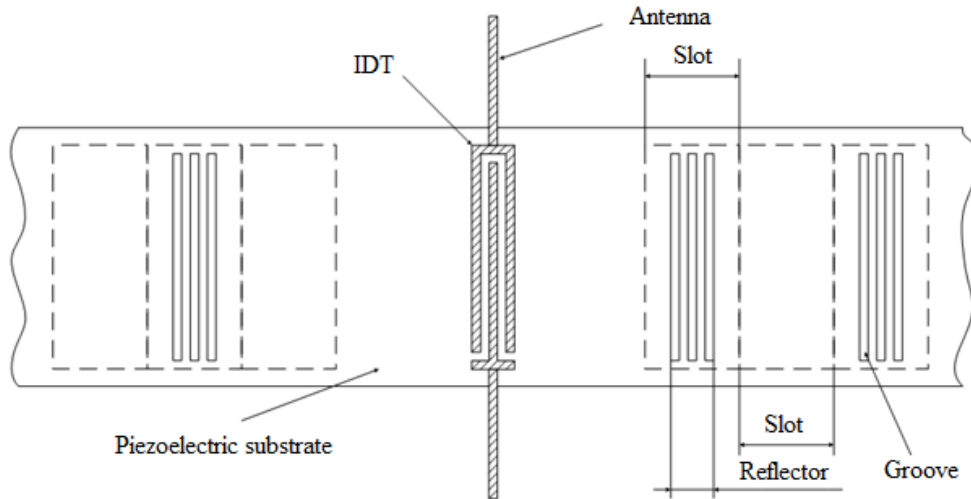


Figure 1. Topology of SAW tags

The tag topology allows forming the impulse response of the tag in the form of FSK signals. The width and distance between the grooves in the sections of the reflecting structure are determined by predetermined code frequencies. Each section of reflectors creates its own elementary radio pulse (symbol) in the impulse response of the tag. The total number of sections in the reflecting structure is determined by the number of symbols in the impulse response.

ANALYSIS OF THE CORRELATION BETWEEN FSK SIGNALS

The proposed identification system will use the correlation code distinction principle. The impulse responses of the tags are FSK signals, which consist of M symbols with rectangular envelopes, closely “docked” to each other in the time domain. The symbol frequencies are determined by $f_k =$

$=f_0 + \{Y_j\} * \Delta f$, where Δf – is the frequency jump between symbols, $\{Y_j\}$ – are integers characterizing the code sequence in the FSK signal. $\{Y_j\}$ can take values $0 \dots K-1$, where K is determined by the number of possible frequencies in the code $K = \Delta F / \Delta f$, and Δf is chosen from the condition

$$\Delta f = \frac{1}{t_c}, \tag{1}$$

where t_c – symbol duration.

The complex envelope of the FSK signal can be written

$$U(t) = \sum_{j=0}^{M-1} Y_j [t - jt_c] \exp [Y_j 2\pi \Delta f (t - jt_c)], \tag{2}$$

where j – symbol number in sequence, M – number of symbols in FSK signal.

With such a representation of the signal, the correlation relationship between the two impulse responses will be determined by CCF between the

code sequences of the frequencies of these impulse responses. We also assume that with this signal model, the symbols are orthogonal. Therefore, the CCF of a code sequence can be considered when the signals are shifted by $\Delta t = t_c$. We call such an estimate of the correlation properties of code sequences as “inexact”.

Elementary radio pulses in the impulse responses of a tag overlap in the frequency domain [1], since the amplitude spectra of symbols with a rectangular envelope are in the form of sinc. As it was shown in [2], the CCF of such symbols is 0.31. Therefore, the presence of a correlation coupling between symbols can lead to a deterioration of the correlation coupling between codes. With this calculation, the correlation connection between the Δt codes should be chosen in accordance with the Kotelnikov theorem ($\Delta t = 1/4F_h$). Such a calculation will be called “exact”. The differences of the normalized CCF’s between the “inexact” and “exact” calculations are on average approximately the value = 0.1[3].

RESEARCH OF CORRELATION BETWEEN FSK SIGNALS

The influence of coherent and incoherent construction of impulse responses on the CCF of codes was studied. An incoherent formation of FSK signals will be called such, where the duration of each symbol is constant and is chosen from equality (1). Coherent formation will be called such, where the duration of each symbol will contain an integer number of periods. A pair of code sequences was selected, which were forming using the algorithm described in [3] with a predetermined level of the CCF. On their basis, FSK signals were researched in order to achieve the minimum possible maximum value of the CCF between the codes.

A pair of 17-symbols FSK signals was selected. The codes and parameters of the signals ($F_0 = 1000$ MHz, $\Delta F = 340$ MHz) are known in advance, so we can calculate the CCF between the codes

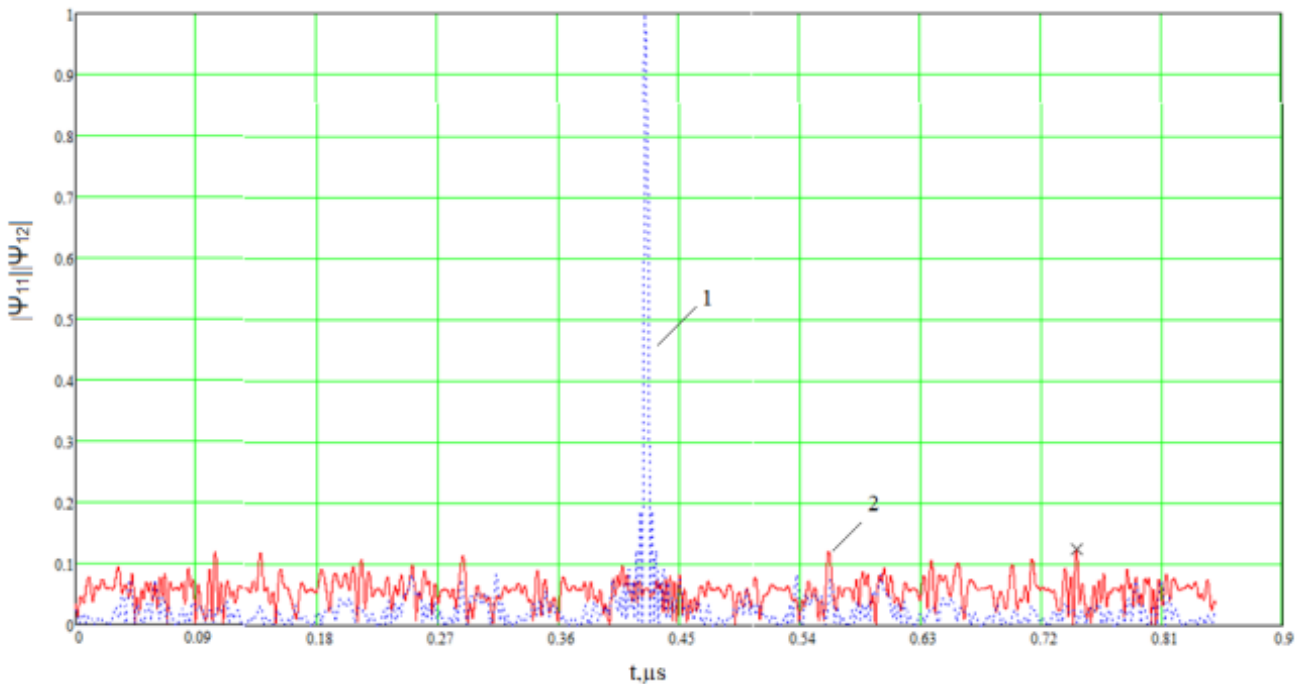


Figure 2. ACF – 1, CCF – 2. Normalized ACF and CCF of a 17-symbol signal with parameters $F_0 = 1000$ MHz, $\Delta f = 20$ MHz, $t_c = 50$ ns

In the place indicated by the cross, the CCF takes the maximum value of 0.12326. There was a research of how the change Δf affects the value of the CCF_{max} .

For this, we did not perform equality (1), leaving t_c the same. The number of symbols in the signal remained constant.

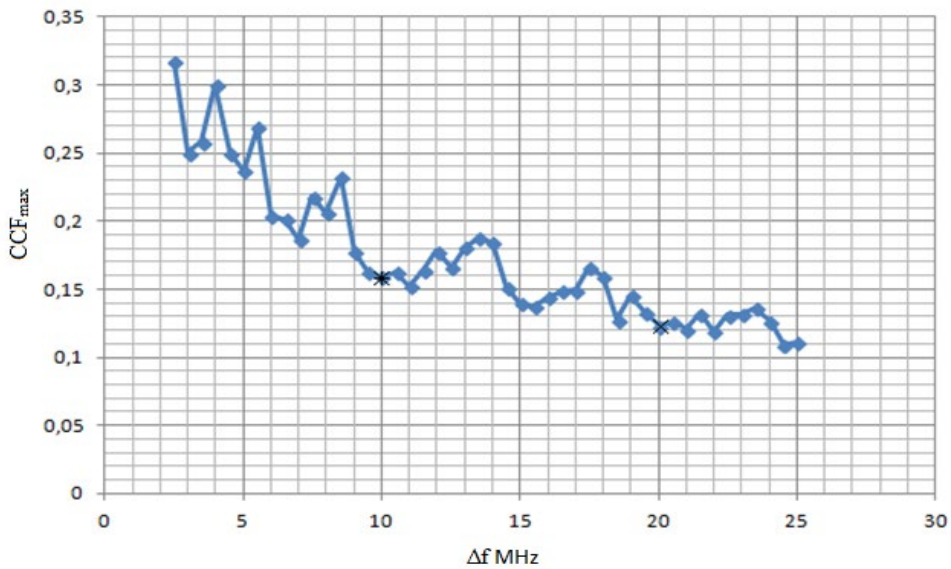


Figure 3. The influence of Δf on the CCF_{max} and ΔF at $F_0=1$ GHz

From the graph given above it is evident that with decreasing Δf , CCF_{max} value increases. However, the width of the amplitude spectrum decreases, which is good for devices based on SAW. By adopting $\Delta f=10$ MHz, while t_c the same, the equality $\Delta f = 1/t_c$

was broken. Because of this, an additional phase modulation appeared in the signal, that is, the synphase disappeared. The initial phase of each symbol is a random variable (Fig. 4).

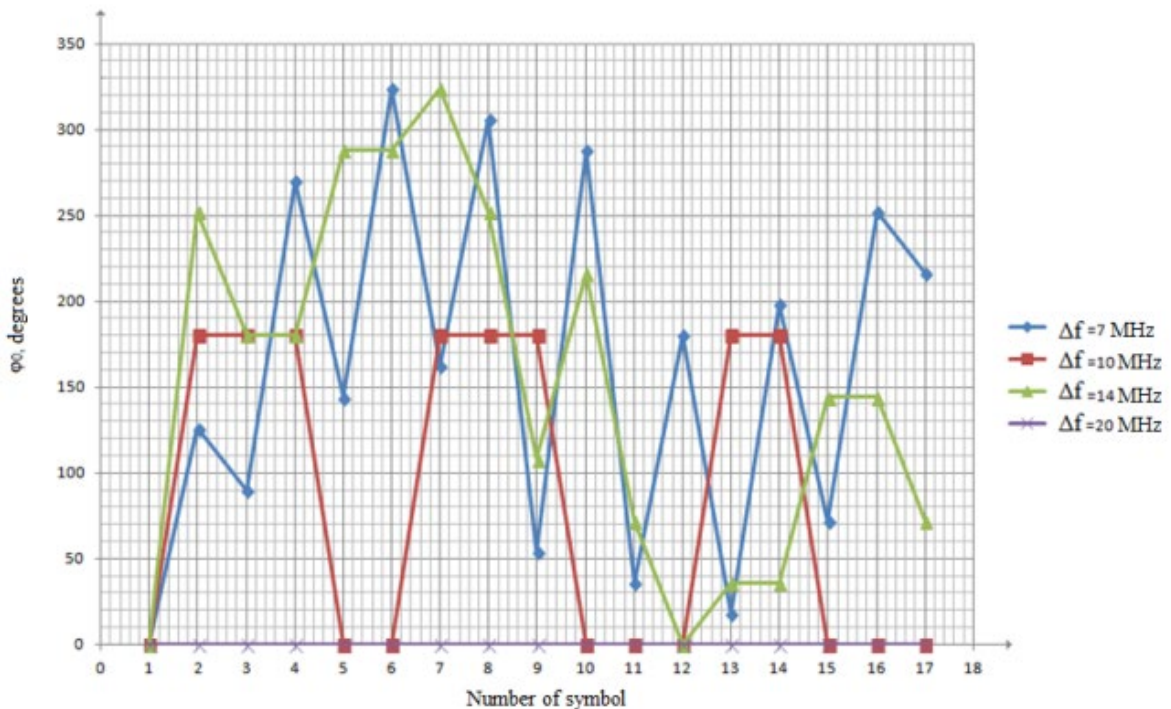


Figure 4. Dependence of φ_0 on Δf for the first code sequence

A method of reducing the CCF_{max} to the previous level was considered, while maintaining the same frequency band. Remove the phase shift and see how the CCF_{max} level changes. There are two ways to get rid of the phase shift. The first way is to select t_c based on (1). With this choice t_c φ_0 of each symbol is zero.

CCF_{max} of a signal with such parameters is equal to $CCF_{max} = 0,12403$ (Fig. 5)

The second way to remove the phase modulation is the choice of t_c , where each symbol contains an integer number of periods. It is impossible to remove phase modulation if we do not know in advance Δf

and the code that the signal is form from. CCF_{max} of a signal with such parameters is equal to $CCF_{max} = 0,1363$ (Fig. 6)

Calculations show that a further decrease Δf leads to a decrease ΔF (at a selected code length), but greatly increases the value of CCF_{max} . It is not rational when designing tags on SAW.

Thus, it can be seen that a significant decrease in ΔF (in the given example by a factor of 2) is possible with a relatively small increase in CCF_{max} in the considered code sequences. At the same time, the duration of the impulse response of the tag is preserved, which is a very positive moment when designing a device for SAW

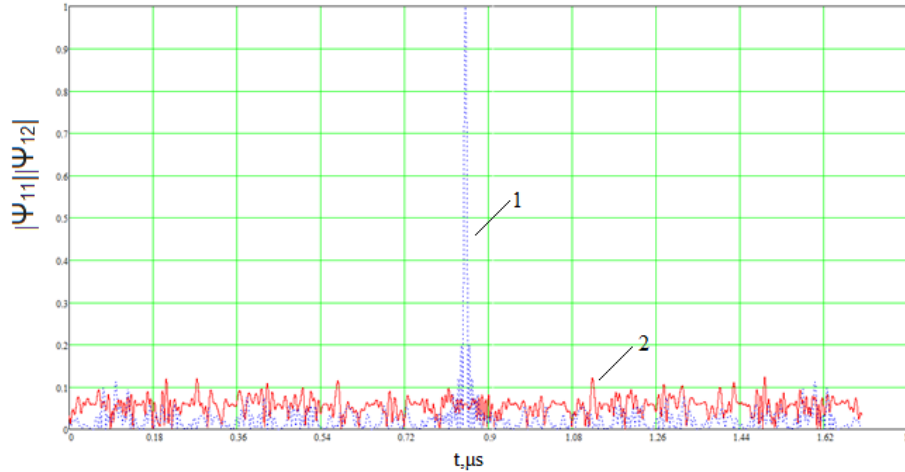


Figure 5. ACF – 1, CCF – 2. Normalized ACF and CCF of a 17-symbol signal with parameters $F_0 = 1000 \text{ MHz}$, $\Delta f = 10 \text{ MHz}$, $t_c = 100 \text{ ns}$

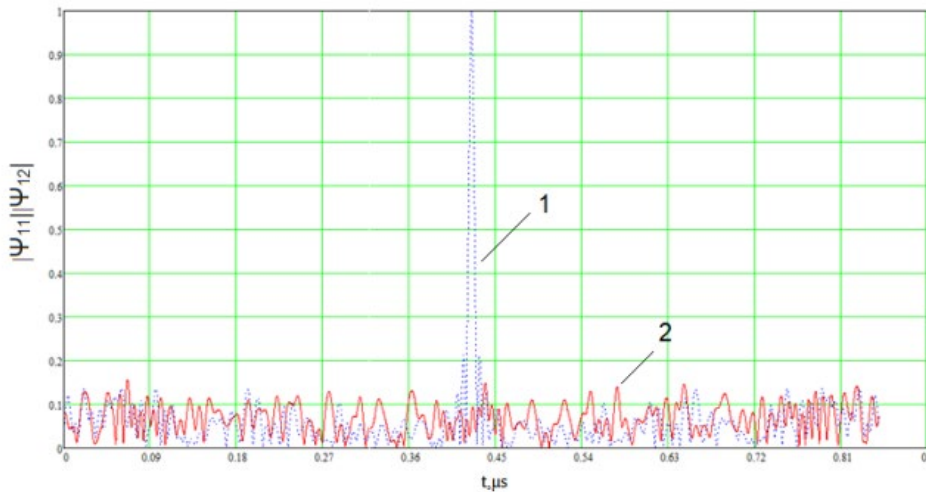


Figure 6. ACF – 1, CCF – 2. Normalized ACF and CCF of a 17-symbol signal with parameters $F_0 = 1000 \text{ MHz}$, $\Delta f = 10 \text{ MHz}$, $t_c \approx 50 \text{ ns}$

CONCLUSIONS

By arbitrarily choosing Δf (as opposed to the condition of formula (1)), we can reduce the width of the amplitude spectrum of the impulse response of the tag. But this will increase the value of CCF_{max} .

To reduce the value of CCF_{max} , one can use the incoherent construction, that is, choose t_c from (1). This will change the duration of the entire signal, which will lead to a change in the permissible dimensions of the tag, worsening the technical

characteristics of the tag.

Therefore, efficient use of the method of constructing a coherent tag, since with a permissible change in Δf , t_c can be left almost unchanged, and, therefore, the duration of the entire signal. In this case, it is necessary to correct the position of the grooves on the substrate of the device on the SAW in order to achieve the synphasic symbols in the signal. This method requires the complication of tag production technology.

REFERENCES

[1] B. Sklar, «Digital communications: fundamentals and application/ Bernard Sklar; 2007. c 227-231.

[2] Zhezherin A.,Petrov A., Chugunov A. «RESEARCH OF SAW TAGS FOR IDENTIFICATION SYSTEMS». XX International Conference for Young Researchers Wave Electronics and its applications in the Information and Telecommunication Systems. Scientific papers.

Saint-Petersburg. S-Pet SUAI. Saint-Pet.2017., 75-78

[3] – Zhezherin A.R., Chugunov A.A. Development And Research Of High-Volume Code Sequences For Identification Labels on Surfactants. Wave Electronics and its Applications in Information and Telecommunication Systems. XXI International Conference of the Suai, Coll., St. Petersburg, SUAI, 2018, 112-118.

[4] Rechitsky V.I. “Acoustoelectronic Radio Components. Elements and Devices on Surface Acoustic Waves.”Moscow, 1980.

AUTOMATIC HEADLIGHT DIMMING THROUGH SOFT COMPUTING TECHNIQUES

W. Forestiere, M. F. Turco

Computer Engineering and Networks Laboratory – Kore University of Enna – Italy
Email: {william.forestiere, mariafrancesca.turco}@unikorestudent.it

Abstract

This paper shows how it's possible to create an automatic headlight dimming system utilizing modern soft computing techniques such as the fuzzy logic.

INTRODUCTION

In the past there have been several attempts to improve the driving experience and reducing the amount of things the driver has to be aware of. One of them is the creation of a system for the automatic control of headlights in vehicles.

Around the 50s and 60s there have been different attempts to make such a system, but they had unconvincing results and had to be withdrawn from the market because of its unreliability. At last in 2008 Mercedes Benz put a new system of this kind in their newest car models. In the following pages we're going to give a personal solution to the problem of the automation of headlights management.

The first important choice which had to be done was the choice of network protocol to put in use. We had two main possibilities: a wireless network using Wi-Fi and a cabled Ethernet network. The cabled approach was chosen for the following reasons:

- Actual sensors utilized in modern vehicles are connected using a cabled structure. This means that there's no need to actually make space in the car to put our cables in because that space is already there. If this wasn't the case using a wireless network would have been much cheaper than a wired network.

- The high amount of metal and materials between the sensors and the other devices could cause a higher than normal loss rate for packets in the network, which means that transmission power would have to be increased to maintain normal working conditions. This leads to our next point.

- The constant transmission of packets at high power could be harmful to drivers and passengers in the vehicle. Future research may prove or disprove the dangers of constant electromagnetic transmissions to the human body.

- The most important characteristic of a wireless network, the mobility of its devices, would be meaningless because all the devices used in the proposed system are stationary in relation to each other.

In the related works section the past approaches to the problem will be described and then there will be a description of our take on this system of headlight automation. Afterwards the system is going to be put

to the test and we will show how it responds to different situations, and the related performance metrics are going to be calculated.

RELATED WORKS

There have been various tries to create an Automatic Headlight Dimming system, the first ones being the simplest and least performing, while the later ones considered several aspects. Starting from 1953 Jacob Rabinow patented various versions of this system, and its latest implementation [1] tried to solve one of the main problems of these kind of system: the constant flickering of the headlights caused by the reflection of the vehicle's lights onto reflecting road signals. To do so the headlights are first dimmed and if the light acquired by our system immediately goes down then this means that a reflective surface is present somewhere in front the vehicle. If this occurs the system will alternate between 1.5s of high beams and 0.2s of low-beams to keep determining if such a reflecting surface is present. Such a method was implemented in this implementation of the automatic headlight dimming system. In [2] the author explains that light from headlamps and taillamps contain a significant amount of information in the infrared region, while ambient light contains very little information in the infrared region. In his approach he put the light and infrared sensor right in the windshield and solved the problem of interrupted input caused by the windshield wipers. In our implementation we've decided to avoid using an infrared sensor because of a lack of information about the amount of infrared light emitted from various sources while some kind of approximation is possible when considering visible light. The problem of the windshield wipers is immediately solved in our system thanks to the MBSD control system.

THE PROPOSED APPROACH

The implemented network is made up of 6 devices:

1. A light sensor
2. A device to determine the current time
3. A device to determine the current location
4. A gateway

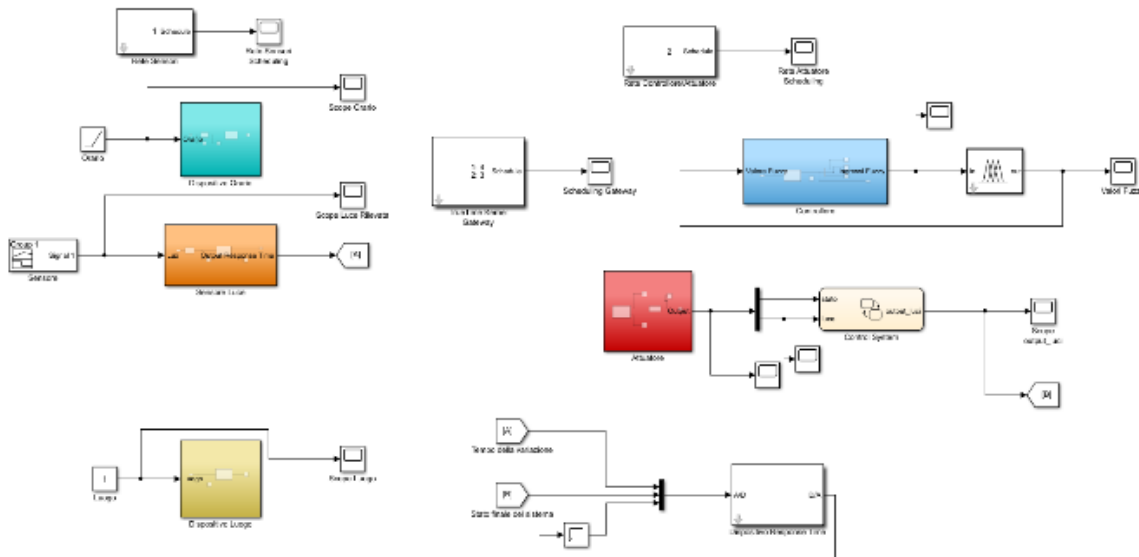


Figure 1: the proposed solution

5. A controller which receives the sensor's messages and pass them to the Fuzzy Control Block, which in turn gives the controller new value to be sent to the actuator.

6. An actuator which receives the value from the controller and it decides what action to perform and sends it to the MBSD anti-debounce control.

Through these six devices, we have a network with a tree topology, in which the root is the gateway while the remaining elements represent the leaves of the network. This topology has a high degree of reliability, in which the only weak point is the parent node whose failure would cause the breakdown of the entire network.

Analysis of the performance metrics

The only performance metric that's going to be measured is the response time. This performance metric has been chosen because it's necessary that excellent visibility is given to the user at all times, without being a potential danger to other drivers that come by our vehicle. Therefore the response time has to be less than a few seconds to actually comply with these characteristics.

The other performance metrics weren't taken into consideration for the following reasons:

- Throughput: it's irrelevant because the amount of data exchanged in the network is irrisory.
- Stretch factor: our network will always have the same amount of data circulating the network. That's because all of the operations made by devices are periodical, and the amount of data sent and receive will never increase or decrease.
- Nominal capacity: It's irrelevant because it's based on the throughput.

- Useful capacity: it's irrelevant because it's based on the throughput.
- Efficiency: it's irrelevant because it's based on the throughput
- Resource utilization: because our devices work periodically all our devices will always be occupied. This makes the performance metric irrelevant.
- Reliability: this is measurable as the probability of packets loss. Even if a packet is lost the network will use the previously received packet (which probably arrived in the 0.2 seconds before), which means that the system will not suffer any performance degradation. The reception of wrong data will not have a negative impact on the system thanks to the MBSD anti-debounce control. Anyway, for simplicity, because the parameter is controllable thanks to the Matlab environment, we have decided to set the probability of error equal to 0.
- Availability: it's irrelevant since the implemented system is completely automated and the interaction with the user is not foreseen (only for turning on the system itself, which we have decided not to consider, assuming to be immediately put in the different scenarios used).

Input devices in the first network

The first three devices of the first network (used for sensors) are: the device which determines the current time, the device that acts as a light sensor and the device that provides the current location.

The light sensor detects a quantity of Lux (intensity of the light that actually reaches the sensor),

whose range goes from 0 to 10001.

The device which determines the time, used to understand in which period of the day we are, and the time is represented by a value ranging from 0 to 86400 seconds. To simulate the passage from 11:59 p.m. to 00:00 a.m. a Matlab function was used that checks if the current time expressed in seconds is greater than 86400 seconds.

If the threshold is exceeded the time goes back to 0. To determine the location it's presupposed to have an external system that is able to determine at any time whether or not the vehicle is inside a city. In the first case the value sent by the device will be 0 otherwise in the second case the value sent will be 1.

The operation of these three devices is almost identical. Each of them receives the data related to its own function, and periodically sends a message (which can belong to the three types "time", "light" and "location") to the fourth device of the network, that is the gateway.

Gateway

The gateway device acts as a bridge between the sensors network and the one related to the management of the data detected by the sensors, and listens to all the messages coming from the first network.

Whenever the gateway receives a message, it checks the type of message received, which can belong to the three types listed above.

Subsequently it sends a message to the controller, through a mailbox dedicated to it, in which the data field of the message contains two subfields.

The first one is the raw data (amount of light, actual time and current location) while the second subfield is related to the type of data sent, which will also belong to one of the three categories and will be used by the controller to understand which type of data is been sent to the gateway.

Controller and Fuzzy Logic Control

The controller receives the gateway's messages, which can contain the three types of different contents.

Whenever a message is received, the message type is checked, and the data is placed in one of the controller's outputs that form the fuzzy logic control inputs.

The fuzzy logic control has three inputs: the value of the light captured by the sensor, the value of the time and the value of the current location.

The membership functions used are:

Input:

- time: night₁, day and night₂, night 1 and 2 are half triangles positioned at the ends of our range of possible simulation time while day is in the middle between the two.

- lux: low and high: "low" is a triangle placed at the left end of the graph while "high" is a triangle with a very wide base, placed at the right end of the graph.

- location: "city" and "notcity", these are trapezoidal shape and they are placed at the ends of the graph but their form are irrelevant, only the highest values of the membership functions are used, because the only values 0 and 1 are the only values that this input of the fuzzy logic control will assume.

Output:

- lights: it presents 3 triangles called noluci (no lights), anabbaglianti (low beam), and abbaglianti (high beam), positioned respectively to the left, in the center and to the right of the graph.

Implemented rules:

- if the captured light is low, it's daytime and the vehicle is in a city then the output is low-beams
- if the captured light is high, it's daytime and the vehicle is in a city then the output is no-lights
- if it's night and you the vehicle is in a city then the output is low-beams
- if it's daytime and the vehicle isn't in a city then the output is low-beams
- if the captured light is low, it's night and the vehicle isn't in a city then the output is high-beams.
- if the captured light is high, it's night and vehicle is in a city then the output is low-beams.

Actuator and MBSD

The actuator receives the messages from the controller and checks on the data that has just been received.

In particular if:

- received value < 0.3 : the output is no-lights
- $0.3 < \text{received value} < 0.7$: the output is low-beams
- received value > 0.7 : the output is high-beams.

The value 0 was associated with the no-light output, the value 1 was associated to the low-beams output and the value 2 was associated to the high-beams output. This output value represents the desired state of the system, before the application of the MBSD control system.

The control system uses the MBSD to manage the presence of alterations of data and/or real variations of the light detected by the sensor whose length is not sufficient duration to be significant.

The input of the MBSD is the value is the actuator's output.

¹ It has to be noted that these values are only indicative. They are not actual values taken from sensors.

The output of the MBSD system is “uscita_luci” (headlight output), which represents the final output of the system.

There are three stable states: “noluci” (no-lights), “anabaglianti” (low-beams) and “abbaglianti” (high-beams) and they interact as follows: whenever there’s a variation in the input if it doesn’t last for at least 0.2 seconds then the headlight’s state will not change. The most important part of the control system relates to the transition from high-beams to low-beams, because it takes into consideration if the light received is dependent on the headlight’s actual state, such as in the presence of a reflective road signal. If such a surface is “detected” then the high beams will be activated for 1.5 seconds. Afterwards low-beams will be activated for 0.3 seconds to determine if the reflective surface is still present. If in the 1.5 seconds of high beam a vehicle appears then the light received increases and goes over a certain threshold, and the headlights will be dimmed.

SCENARIO

In this section the Matlab TrueTime implementations of this system will be shown, followed by an example of how the system works when a vehicle is encountered.

Example of use: it’s night, outside of a city and a vehicle is coming towards us. When the light coming from said vehicle is strong enough the headlights are dimmed until the vehicle is passed at t=18s, after which the headlights go back to high-beams.

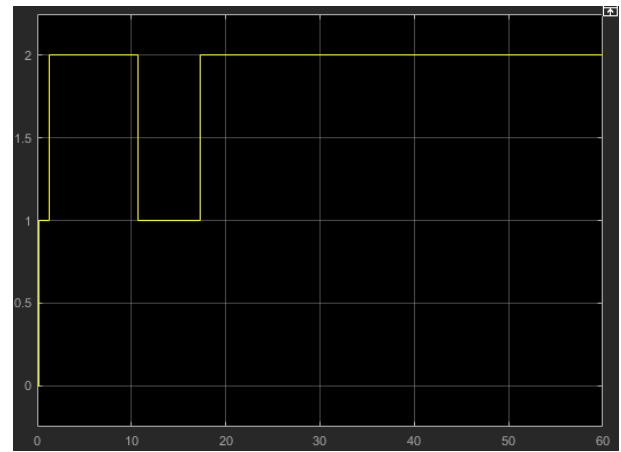


Figure 3: headlights dimming

PERFORMANCE EVALUATION

To calculate the response time the system was initially put in a stable condition and later given a sudden change in its input. We recorded the time of this change. Later we recorded the time in which the system adapted to the new condition, and calculated the reponse time as the difference between these two times. To do this a device has been introduced into the system and simulated through Matlab.

The calculated response time is approximately 0.3 seconds. About 2/3rd of this (0.2s) has been introduced by the anti-debounce control system, where we have made it so that the system will go to a new state only if a certain desired output has been maintained for at least 0.2 seconds.

A response time of 0.3 seconds is low enough, in accordance to the requirements of it's scenarios. This is because it's necessary that the response time doesn't go over the 4/5 seconds limit, after which this system would be a potential danger to other drivers.

CONCLUSIONS

The implemented system does improve the current state of headlight control, because in most vehicles such a system isn't even present. It's also been shown that the system works as expected in different scenarios. In the future it would be interesting to implement a variable intensity and height for the headlights, and to introduce a mechanism of vehicle-awareness through an external system of traffic analysis.

REFERENCES

[1] Jacob Rabinow. “Automatic headlight dimmer with antioscillation circuit”, Oct. 14, 1953.
 [2] Slotkowski et al. “Automatic headlamp dimmer having improved signal discrimination and signal processing”, Jul. 12 1994.

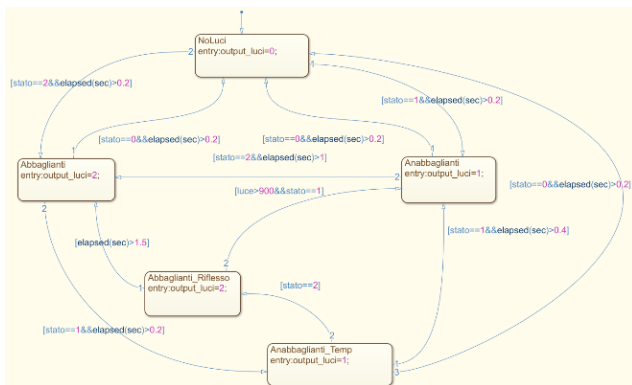


Figure 2: MBSD control system

COMPARATIVE ANALYSIS OF READY-MADE SOLUTIONS FOR IMPLEMENTATION OF VOICE CONTROL ON MICROCONTROLLERS

S. Gerasimov

Saint-Petersburg State University of Aerospace Instrumentation
 Saint-Petersburg, Russia
 E-mail: gerasimov310796@gmail.com

Abstract

The article presents an overview of ready-made solutions for speech recognition that are relevant today. As an example, the software and devices that were developed for the Arduino series platforms were given. These debugging boards are popular among amateur developments.

INTRODUCTION

Voice control devices are used in different spheres of human activity. They are used in "smart home" systems, in robotics, where they act as "hearing receptors" of robots, on-Board computers and even on smartphones, as a voice assistant. Basically, these devices are designed so that a person can interact with the equipment remotely without contacting them directly.

The main task in the implementation of such devices is to choose the method of voice control.

To solve this problem, it is necessary to analyze several methods to choose the most appropriate one.

Since this trend began to develop relatively recently, specific classifications for speech recognition devices have not yet been formulated. Therefore the conditional classification on three signs.

According to the type of processing of received information, there are two types of voice recognition devices: some are dependent and require the use of third – party computing devices/services for sound processing, others are independent, in which processing is carried out by the microcontroller or its modules.

According to the number of words used, the division occurs on devices with an unlimited and limited set of words. In the first case, voice libraries are used, in the second case, words are written manually in a limited number.

The last feature is the implementation of the processing mechanism. There are external and internal software implementations and hardware implementations.

This classification is shown in Figure 1.

COMPARATIVE ANALYSIS

Today there are many ready-made solutions for recognizing voice commands. This allows you to simplify the development of the device and to select methods based on the task.

Within the framework of this analysis, ready-

made solutions differing in the method of implementation of the processing mechanism will be considered.

Conditional classification

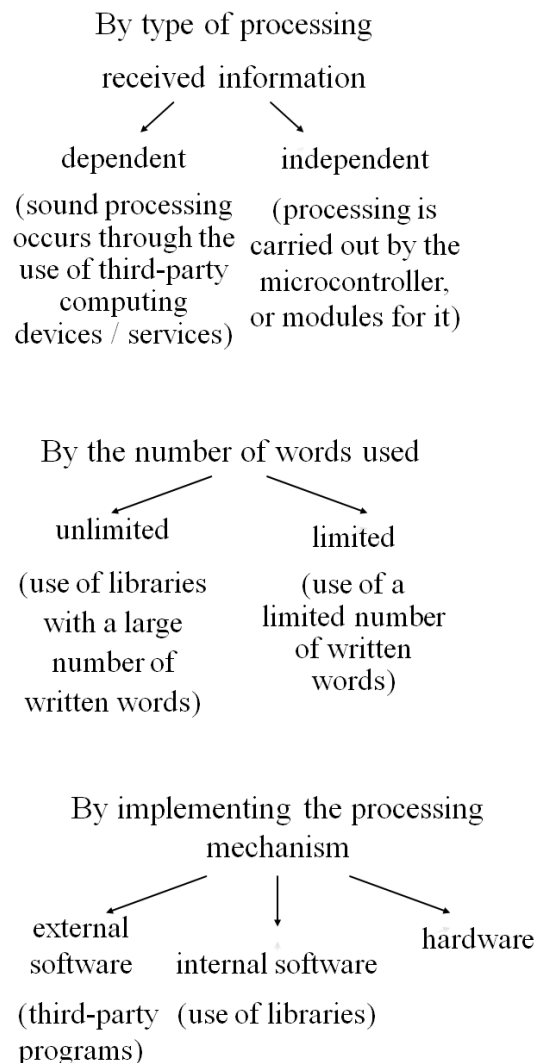


Figure 1. Conditional classification of voice recognition devices

scale.

In addition to the methods discussed, there are many approaches to voice recognition through devices, programs and libraries.

The choice of method depends primarily on the needs and resources. If the device does not have constant access to more powerful computing devices, such as a PC, it is advisable to use voice recognition modules. If you have a permanent Internet connection, as is usually implemented in "Smart home" systems, it makes sense to use libraries like speech-to-text libraries for Java/processing.

REFERENCES

1. Bitvoicer, URL: <http://www.bitsophia.com/en-US/BitVoicer/Overview.aspx> (date of the application: 09.02.2018)
2. VoiceRecognitionModule V3: data sheet, URL:https://www.elechouse.com/elechouse/images/product/VR3/VR3_manual.pdf (date of the application: 11.02.2018)
3. SpeechoTextLibraryforJava/Processing, URL: <http://florianschulz.info/stt/> (date of the application: 12.02.2018)

MODELING OF THE PROCESS OF ASSESSMENT OF COORDINATES OF OBJECTS IN THE TWO-POSITION RADAR SYSTEM

E. Grigoriev

Saint-Petersburg State University of Aerospace Instrumentation,
Saint-Petersburg, Russia
E-mail: ev.grig95@gmail.com

Annotation

The article discusses a simulation model of a two-position radar system. The formulas for calculating the coordinates of the observed object are given both from information about range and angular information. An algorithm for modeling the definition of the trajectory coordinates of the object is proposed.

Ключевые слова: Multistatic radar system, simulation modeling of technical systems, trajectory coordinates

INTRODUCTION

It is generally accepted that radars are useful sensors for detecting and classifying various objects in a densely populated coastal and urban environment. However, at present, with increasing capabilities of computing systems for processing information, the requirements for accuracy in determining the trajectory coordinates of ground-based, surface and air-based radar systems are growing. One of the ways to improve the accuracy of measurements of trajectory coordinates, resolution and noise immunity is the use of multi-position radar systems. Currently, multi-position systems are used in various areas of human life, such as monitoring near the airfield space, road safety, monitoring of coastal zones, in alarm systems, medicine, etc. [1-4]. In this regard, the search for new methods for processing information in these systems, as well as their modeling, is an urgent task.

The aim of the work is to simulate a two-position radar system and consider methods for determining the trajectory coordinates of a moving object based on angular and rangefinder information, conducting a comparative analysis of these methods to assess the accuracy in determining distance / azimuth coordinates, as well as comparing measurement results using single-position and multi-position Radar station

After analyzing the subject area [5-8], it was revealed that the process of combining radar information in a multi-position system into a single information field is a specific task that requires special in-depth analysis and research in designing such complexes in a specific field of application, which makes this article relevant.

TWO-POSITIONAL RADAR SYSTEM

Multi-location allows you to cope with the limitations of traditional single-station radars. For example, using a single-station radar station, it is difficult to determine the full velocity vector of the

observed object, and also these stations have a low accuracy in determining the angular coordinates.

One of the advantages of multi-station radars is the ability to determine the coordinates of moving objects, both in range and in the angular coordinate, and the accuracy of such radars in the angular coordinates is higher. [9-10]. It should also be noted the possibility of determining the full velocity vector of the observed object.

Consider a mathematical model of active two-position radar, in which at each transceiver position is measured the distance to the target only by the signal emitted from this position.

The geometry of determining the coordinates of an object using a two-position system is shown in Figure 1. Where are the two transceiver positions Radar 1 and Radar 2 distant from each other by a distance B , which observe the Obj object. R_1 and R_2 are the distances to the object of observation, β_1 , β_2 , ϵ_1 , ϵ_2 are the azimuths and elevation angles from Radar 1 and Radar 2, respectively. x_{Obj} , y_{Obj} , z_{Obj} – coordinates of the object in the Cartesian coordinate system.

The coordinates of an object in a rectangular coordinate system can be expressed in terms of the coordinates obtained with Radar 1 and Radar 2 in a spherical coordinate system:

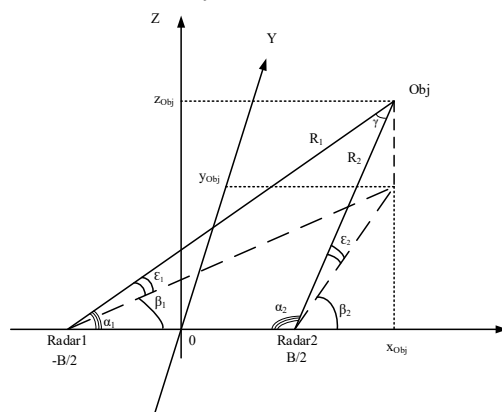


Fig. 1

$$x_{1Obj} = R_1 \sin\left(\frac{\pi}{2} - \varepsilon_1\right) \cos(\beta_1) - \frac{B}{2}$$

For Radar 1: $y_{1Obj} = R_1 \sin\left(\frac{\pi}{2} - \varepsilon_1\right) \sin(\beta_1)$

$$z_{1Obj} = R_1 \cos\left(\frac{\pi}{2} - \varepsilon_1\right)$$

$$x_{1Obj} = R_2 \sin\left(\frac{\pi}{2} - \varepsilon_2\right) \cos(\beta_2) + \frac{B}{2}$$

For Radar 2: $y_{1Obj} = R_2 \sin\left(\frac{\pi}{2} - \varepsilon_2\right) \sin(\beta_2)$

$$z_{1Obj} = R_2 \cos\left(\frac{\pi}{2} - \varepsilon_2\right)$$

The estimate of the speed of an object at any station can be calculated as follows:

$$V_{obj} = \frac{\sqrt{(x_{obj,n} - x_{obj,n-1})^2 + (y_{obj,n} - y_{obj,n-1})^2 + (z_{obj,n} - z_{obj,n-1})^2}}{\Delta t}$$

Where the indices n and n-1 indicate the time points at which the coordinates were estimated, and $\Delta t = t_n - t_{n-1}$.

Since the transceiver positions are fixed and their coordinates are known, the distance B between them is also known; Suppose that the angles α_1 and α_2 are known (for example, obtained from goniometric measurements); Radar 1 and Radar 2 use the same probing signals. The emission moments of the probing

signals in Radar 1 and Radar 2 are tied to a single time scale, but in the general case they differ from each other, i.e. ; for definiteness, let us establish where the known value, which is calculated in Radar 1 from the measured value and the value obtained from the communication channel from Radar 2. 2 will be measured distance corresponding to different points in time, which we denote by and. Since this article will examine the coordinates of the azimuth range, for their measurements carried out in Radar 1 and Radar 2, we write:

$$Z_{R1}(t_{r1,k}) = R_1(t_{r1,k}) + \eta_{mR1}(k)$$

$$Z_{R2}(t_{r2,k}) = R_2(t_{r2,k}) + \eta_{mR2}(k)$$

$$Z_{\beta1}(t_{r1,k}) = \beta_1(t_{r1,k}) + \eta_{m\beta1}(k)$$

$$Z_{\beta2}(t_{r2,k}) = \beta_2(t_{r2,k}) + \eta_{m\beta2}(k)$$

Where $Z_{R1}(t_{r1,k})$, $Z_{R2}(t_{r2,k})$, $Z_{\beta1}(t_{r1,k})$, $Z_{\beta2}(t_{r2,k})$ – range and azimuth measurements in Radar 1 and Radar 2 respectively, $R_1(t_{r1,k})$, $R_2(t_{r2,k})$, $\beta_1(t_{r1,k})$, $\beta_2(t_{r2,k})$ – true range and azimuth values for Radar 1 and Radar 2 respectively, $\eta_{mR1}(k)$, $\eta_{mR2}(k)$, $\eta_{m\beta1}(k)$, $\eta_{m\beta2}(k)$ – errors of measurements of distances and azimuths, which are considered independent discrete white Gaussian noise with zero expectation and variances D1, D2, D3, D4, respectively

The algorithm for modeling the process of estimating coordinates is presented in Figure 2.

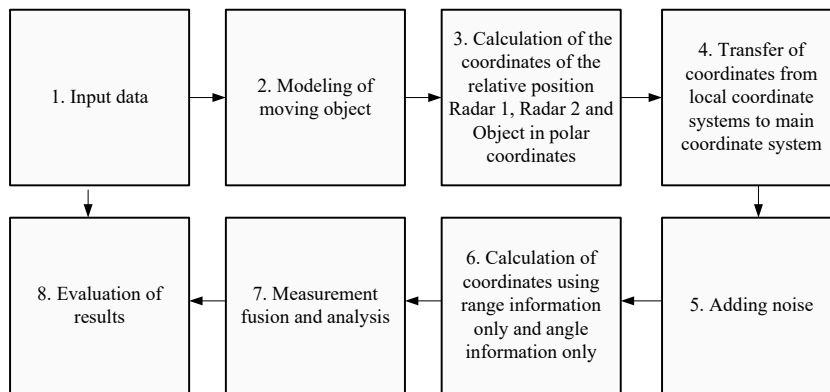


Fig. 2

In the course of joint processing of radar information, it is necessary to bring measurements to a single reference in space. This is achieved by converting the vectors of the measured parameters of the target from the local coordinate systems associated with the individual stations into a single coordinate system associated with the center of association. As a base, it is preferable to use a rectangular coordinate system, its main advantage is

that uniform linear motion of the target is described by linear differential or difference equations of the first order, while in other coordinate systems the equations of motion are nonlinear, which complicates the processing and can lead to additional methodological errors [9].

After measurements of parameters in a spherical coordinate system on each of the radars separately, information is collected in the control and processing

center, where the position of the object can be calculated both from purely angular information and from distance measuring [1 in this file], since the experiments will be carried out in the azimuth range coordinates, hereinafter we will only indicate the coordinates along the abscissa and ordinate axes:

$$x_{Obj} = \frac{B \sin(\alpha_1 + \alpha_2)}{2 \sin(\alpha_2 - \alpha_1)}$$

$$y_{Obj} = \frac{B \sin(\alpha_1) \sin(\alpha_2)}{\sin(\alpha_2 - \alpha_1)}$$

$$x_0 = \frac{R_1^2 - R_2^2}{2B} = \frac{(R_1 - R_2)(R_1 + R_2)}{2B}$$

$$y_0 = \frac{\sqrt{[B^2 - (R_1 - R_2)^2][(R_1 + R_2)^2 - B^2]}}{2B}$$

Simulation will be carried out in the MATLAB system. A model was implemented that allows one to obtain estimates of the range and velocity of the observed objects of two-position radar. For clarity, displays the mutual position of a moving object and both stations on 3-D and 2-D graphics. The model allows to obtain the coordinates of objects, both in the Cartesian coordinate system and the polar one [11]. After entering the source data, the object motion is simulated and the estimates of the relative position coordinates in the polar coordinate system Radar 1 and Radar 2 are calculated. The results of the work of blocks 2 and 3 of the algorithm are presented in Figures 3 and 4.

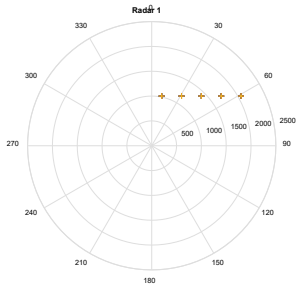


Fig. 3

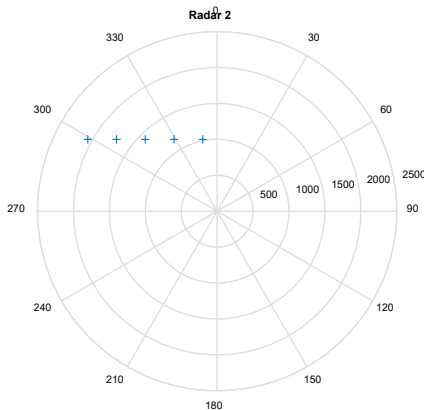


Fig. 4

Next, the data is transferred from the local coordinate systems to the base, in our case Cartesian, with the center at the point (0; 0) in Figure 5. Adding errors occurs in block 5, for clarity, the graph is shown in the 3-D plane, where the sign (+) shows the true position of the observed object, and the sign (O) shows the measured value of the position of the object.

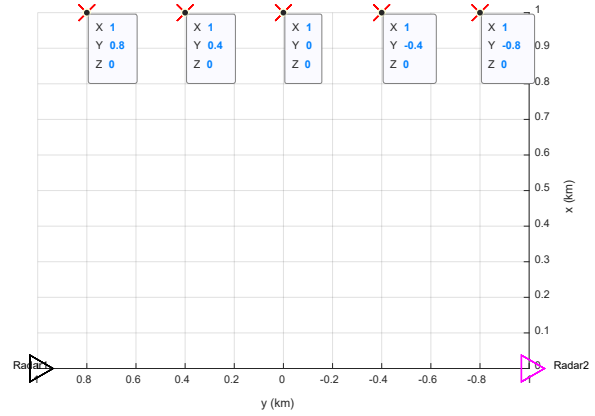


Fig. 5

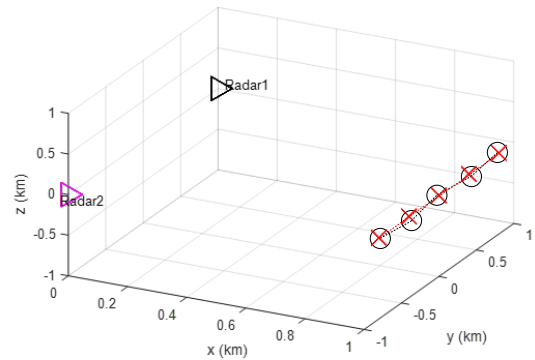


Fig. 6

Having made a simulation of determining the distances to an object from the available measured azimuths α_1 and α_2 in the case when the dispersions D_3 and D_4 were the same and changed in the interval from 1 to 100 meters with a step of 10, and with a fixed value of one dispersion D_3 and a gradually decreasing value of D_4 from 100 to 1 the results presented in figure. 7. From figure. 7, it can be seen that the distance estimates calculated from the angular information at $D_3 = 100$ and $D_4 = 50$ and at $D_3 = D_4 = 50$ differ slightly. The results obtained in the simulation of the definition of azimuth from the range information available from Radar 1 and Radar 2 are shown in figure. 8. Dispersions D_1 and D_2 changed in the same way as when calculating the MSE of the range in figure 7.

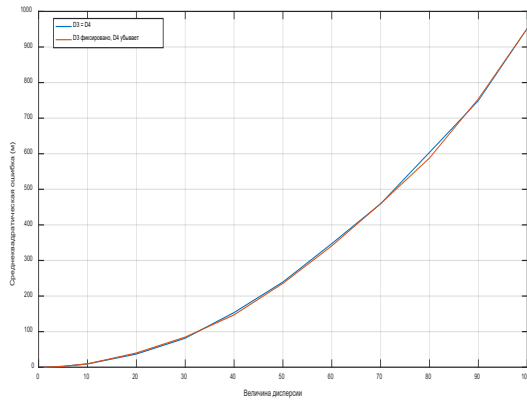


Fig. 7

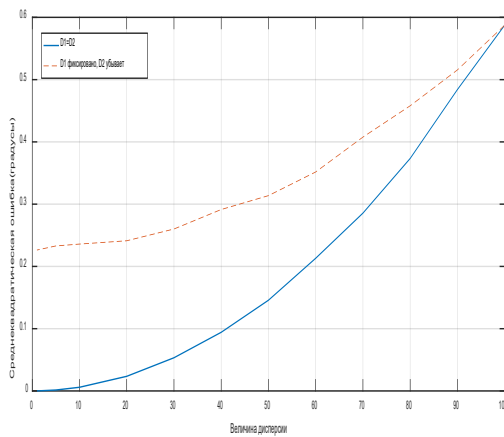


Fig. 8

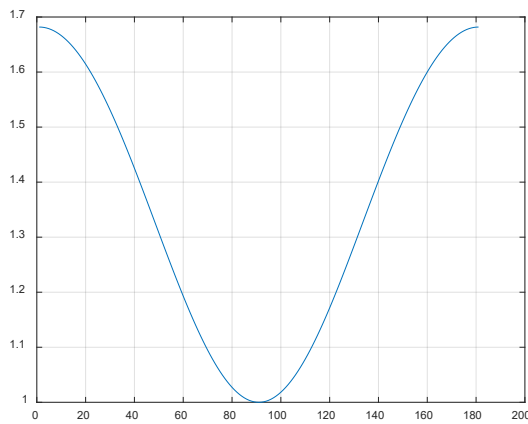


Fig. 9

In structural element 8, the data entered by the user are compared, without errors and data obtained during the measurement of the radar 1 and the jointly processed data. During the simulation of a two-position radar station, it has been established that it is possible to obtain a gain in estimating the range of the observed object, which depends on the angle γ . The dependence is shown in Fig. 9, where the angle γ is

plotted along the OX axis, and along the OY axis it is shown how many times it is possible to obtain a gain in the range estimate for a joint measurement compared to the measurement performed by a single-station station.

CONCLUSIONS

The software package MATLAB has developed a set of programs with a graphical user interface that allows you to simulate the movement of objects, determine their position in the Cartesian and polar coordinate systems, as well as carry out the process of joint processing of information from two different stations in the presence of measurement errors.

The simulation of the determination of the distance to the object on the basis of the available angular information and the simulation of the definition of azimuth on the available measurements of the range. The results are shown in figures 7 and 8.

In the course of the experiments, it was found that it is possible to obtain a gain in estimating the range measurement, which depends on the bistatic angle γ . The results are shown in Figure 9.

The two-position system makes it possible to achieve high measurement accuracy in comparison with a single-position radar station [9]. This makes it possible to improve the tactical characteristics of radar systems by complicating the algorithms for processing radar information without upgrading the equipment of these systems.

The expediency of using multi-station stations is shown. The developed simulation model is applicable to the study of tactical and technical characteristics at the design stage of these radar systems.

REFERENCES

1. Shishanov S.V., Myakinkov A.V. The system of the circular review for vehicles based on ultra-wideband sensors. Journal of the Russian Universities. Radioelectronics. 2015;(2):55-61. (In Russ.)
2. Almanah complex [Electronic resource] <http://www.nppcrts.ru/production/multilateratsiya/almanakh/> (10.03.2019)
3. Radeskan complex [Electronic resource] <http://www.umirs.ru/about/articles/263/> (10.03.2019)
4. Gimignani, Massimo & Paparo, Mario & Rossi, Domenico & Scaccianoce, Salvo. (2013). RF design and technology supporting Active Safety in automotive applications. 1-4. 10.1109/ASICON.2013.6811875.
5. Верба В.С. Оценивание дальности и скорости в радиолокационных системах. Часть 3. М.: Радиотехника 2010.
6. Zhengping Ji, Danil Prokhorov. Radar-Vision Fusion for Object Classification. Information Fusion, 2008 11th International Conference.

7. William L. Melvin, James A. Scheer. Principles of Modern Radar vol. II: Advanced Techniques. Scitech publishing, 2013.

8. Jitendra R. Raol. Multi-Sensor Data Fusion with Matlab. CRC Press, 2010

9. Зайцев, Д.В. Многопозиционные радиолокационные системы. Методы и алгоритмы обработки информации в условиях помех / Д.В. Зайцев. М.: Радиотехника, 2007. 96 с

10. Grigoriev Evgeniy Modeling the Algorithm for Integrating the Results of Independent Measurements. Bulletin of the UNESCO department «Distance education in engineering» of SUAI, Collection of the papers issue 2.Saint-Petersburh 2017.

11. Grigoriev Evgeniy. Moving Object Tracing Systems with Radar-Camera Fusion. Bulletin of the UNESCO department «Distance education in engineering» of SUAI, Collection of the papers issue 3.Saint-Petersburh 2018.

12. Шепета, А.П. Двухпозиционная модель формирования радиолокационного изображения высокого разрешения в передних зонах обзора бортовых РЛС / А.П. Шепета, В.А. Ненасhev, А.А. Сенцов // Роль и место информационных технологии в современной науке: сб. статей Международной научно-практической конференции (28 декабря 2017 г., г.

Магнитогорск). Уфа: ОМЕГА САЙНС, 2017. С. 118–123.

13. Nenashev V. A., Shepeta A. P., Grigoriev E. K., Spindzak I. I., Sentsov A. A., Kapranova E. A. The program for calculating the mutual position of the two-position radar and the observed objects in the polar and Cartesian coordinate systems // Certificate of state registration of computer programs № 2018661851 RF, publ. 09/20/2018. ROSPATENT

14. M. G. Wattimena, V. A. Nenashev, A. A. Sentsov and A. P. Shepeta, "On-Board Unlimited Aircraft Complex of Environmental Monitoring," 2018 Wave Electronics and its Application in Information and Telecommunication Systems (WECONF), St. Petersburg, 2018, pp. 1-5. doi: 10.1109/WECONF.2018.8604382

15. V. A. Nenashev, A. A. Sentsov and A. P. Shepeta, "The Problem of Determination of Coordinates of Unmanned Aerial Vehicles Using a Two-Position System Ground Radar," 2018 Wave Electronics and its Application in Information and Telecommunication Systems (WECONF), St. Petersburg, 2018, pp. 1-5. doi: 10.1109/WECONF.2018.8604329

16. Shepeta A. P., Nenashev V. A. Modeling Algorithm for SAR Image Based on Fluctuations of Echo Signal of the Earth's Surface. Proc. of SPIE Remote Sensing, Toulouse, France, 2015, vol. 9642, pp. 96420X-1-96420X-8.

DEVELOPMENT OF MOBILE APPLICATION BASED ON MACHINE LEARNING METHODS FOR SKIN CANCER SCREENING

A. Karataev

Saint-Petersburg State University of Aerospace Instrumentation,
Saint-Petersburg, Russia
E-mail: hol0d@me.com

Abstract

Skin cancer takes the third place among Russian men and the second place among Russian women in comparison with all cases of diagnosed cancer. Melanoma is one of the most aggressive types of skin cancer. Only half of the patients diagnosed with melanoma survive the threshold of five years. Therefore, early diagnosis of melanoma is the only way to achieve a favorable prognosis for a treatment. The solution to this problem can be a mobile application that will help make an early diagnosis of melanoma and get the necessary treatment on time. This article discusses the mobile training method for solving this problem. It also describes the practical experience obtained on the basis of a trained model as well.

Keywords: skin cancer screening, melanoma, mobile technology, machine learning, convolutional neural network, vgg16, transfer learning, fine tuning.

INTRODUCTION

An oncological disease is characterized by the appearance of a special cells that have the ability of uncontrolled division; due to this property, they invade the underlying tissues and metastasize to distant organs. The disease has been connected with damage of a cellular proliferation and a cellular differentiation owing to genetic disorders. Cutaneous carcinoma is the general name for a widespread malignant diseases. These diseases has been divided in two big groups: non-melanoma skin cancer and melanoma itself. The most widespread non-melanoma types of a skin cancer: squamous cell carcinomas and basal cell carcinoma also called basalioma.

Non-melanoma skin lesions tend to grow slowly and rarely metastasize. The melanoma is the most aggressive types of skin cancer, which usually develops from skin pigment cells. Long-term solar irradiation, chemical and thermal burns, as well as repeated damage of moles can cause the progression of a tumor growth.

According to the World Health Organization (2000) 200.000 cases of melanoma were diagnosed worldwide, with 65,000 deaths associated with it. Between 1998 and 2008, the increase in the incidence of melanoma in Russia was 38.17%; the standardized incidence rate increased from 4.04 to 5.46 per 100 thousand. Melanoma mortality rate in Russia was 3159 in 2008, and the standardized mortality indicator was 2.23 per one hundred thousand [1].

Early diagnosis of melanoma is carried out either by using a simple magnifying glass or by the dermatoscope, which makes the stratum corneum of

the epidermis look transparent. At the same time it is possible to determine with high probability whether the mole is dangerous or not based on the ABCDE system (Asymmetry, Border irregularity, Color, Diameter, Evolving). With the help of computer diagnostic systems one can also get a good results. Boldrick et al. compared results of diagnostics made by the expert and by the model of an artificial neural network during their research.

The results of the experiment were close to the results obtained by a specialist, where the indicators of sensitivity and specificity of the model were within 95% and 88%, respectively. At the same time expert's indicators of dermatological specificity and sensitivity were within 95% and 90% respectively [2].

There are ample opportunities for the implementation of a portable diagnostic system. The second part of the article deals with the development of a diagnostic model and a mobile application, by which is possible to make an early diagnostics and to address a necessary treatment in a right time.

METHODOLOGY

FORMULATION OF THE PROBLEM

Diagnosis of a melanoma is a problem of binary classification, therefore, function of a posteriori probability in this case takes a form of Kulbak—Leibler distance. This measure, describes the amount of information which is lost at approach of distribution of P by means of distribution of Q. Posterior probability is the conditional probability of random events, provided that there is a posteriori data, i.e. measurements after the experience.

$$KL(P||Q) = \sum_i p(x_i) \log \frac{p(x_i)}{q(x_i)}.$$

Optimizing the distance in its original form is not very convenient, so it must be reduced to a form called cross-entropy. For the binary classification problem, this objective function has the form of average cross entropy over all data points:

$$\begin{aligned} L(\theta) &= H(p_{data}, q(\theta)) = \\ &= -\frac{1}{N} \sum_{i=1}^N (y_i \log \hat{y}_i(\theta) + (1 - \hat{y}_i) * \\ &\quad * \log(1 - \hat{y}_i(\theta))). \end{aligned}$$

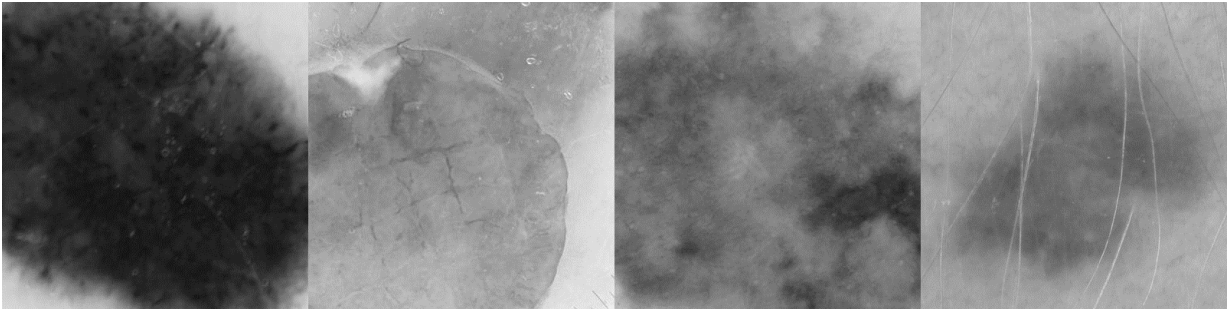


Fig. 1. Examples of cellular' growths from the Melanoma Project ISIC

Simple set of steps has been applied to pre-processing:

- Visual inspection.
- Cutting and turn of images.
- Removal of non-representative images.
- Augmentation for a data set balancing.

To combat retraining, it was decided to use an early stop strategy, so the main data set was divided into a training and validation subset. The strategy of an early stop means a training stop when the mistake on a validation set begins to grow. This method shows similar results with L2 regularization [4].

The training data set consisted of 3 thousand images; 1.5 thousand for each class, respectively. In turn, the validation collection consisted of a 1000 images, 500 for each class.

Data for test set, were taken from PH2Dataset. This set includes about 200 qualitative images with fields of damages and detail's masks [5].

Thus, mathematically, the problem is reduced to finding the vector of the maximum a posteriori hypothesis for the cross-entropy function:

$$\begin{aligned} \theta_{MAP} &= \arg \max_{\theta} p(\theta|D) = \\ &= \arg \max_{\theta} p(D|\theta)p(\theta) \end{aligned}$$

DATA SET AND PROCESSING

For model training the data set from International Skin Imaging Collaboration has been used: Melanoma Project ISIC. This partnership between academia and industry is designed to facilitate the use of digital skin imaging to reduce melanoma death rates [3]. Examples of cellular' growths from the Melanoma Project ISIC set are presented in Fig. 1.

DESIGN AND METHODS OF TRAINING

A pre-trained VGG16 model was selected for training in the generated data set. This model is a convolutional neural network that contains 13 convolutional and 3 fully connected layers [6]. The architecture of the convolutional layers of the model is presented in Fig. 2.

The first part of the network highlights the characteristic features in the image and consists of alternating stages of convolution and subsample. The size of the convolution kernel in all layers is 3 by 3. In a subsample, the maximum value is selected from a 2 by 2 square.

The second part is responsible for the classification of the object in the image according to the features that were highlighted in the previous step. This part contains 3 fully connected layers. In the first two layers are 4096 neurons, the number of neurons in the last layer depends on the number of classes of the problem being solved.

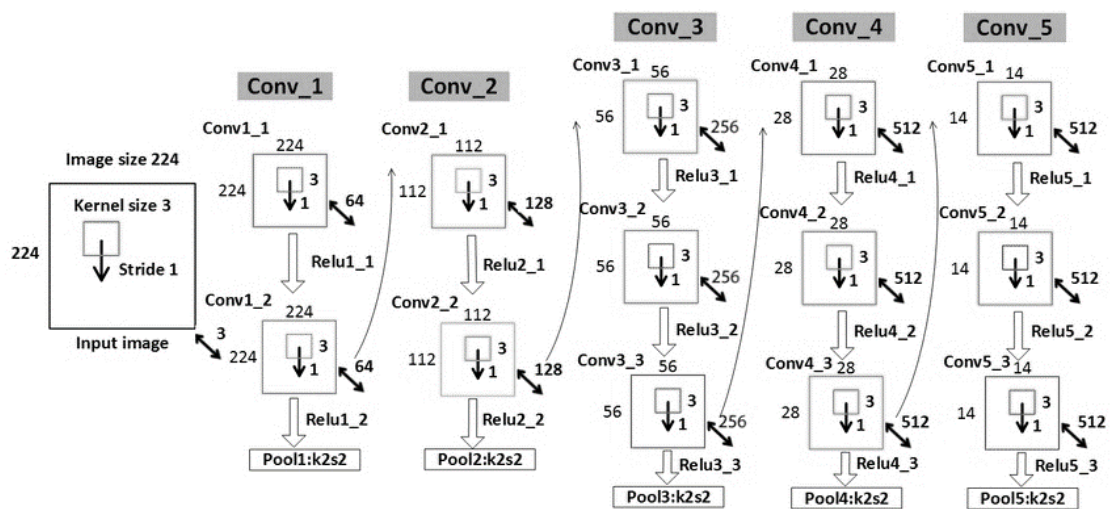


Figure 2. Convolution layers of VGG16 model

At the entrance, the VGG16 network receives an image of 224x224 pixels in size, 3 channels of color (red, green and blue). At the output, the network calculates the classification probabilities of an object in the one hot encoding format [6].

Since the size of the collected training sample does not allow to fully train a network of this size from scratch, it was decided to use such learning approaches as transfer learning and fine tuning.

Transfer learning allows you to use the weights of a pre-trained deep convolutional neural network, either as an initialization or as a distinction of distinctive features for the task. Thus, this ultimately allows the use of a much smaller data set for training, for a network of the required depth [7].

Fine tuning allows to adapt parameters of the pre-trained deep convolution neural network to objects of a solvable task, thereby reducing a final error of the posteriori probability's optimized function [8].

DEVELOPMENT OF APPLICATION

Treatment of melanoma in the early stages does

not pose a serious problem for modern medicine. However, timely treatment is possible only with an early diagnosis. Thus, the development of a mobile application for the early diagnosis of melanoma should reduce mortality rates from this type of disease. The application usage diagram is presented in Fig.3.

The mechanism of application's operation for the end user, is very simple:

- The user scans problem section of his skin by the device camera.
- The neural network algorithm analyzes the image.
- The user receives a diagnosis (classification result).

If the algorithm detects a high probability for the diagnosis of cancer, the application will select the nearest dermatological clinic and arrange an appointment for a consultation.

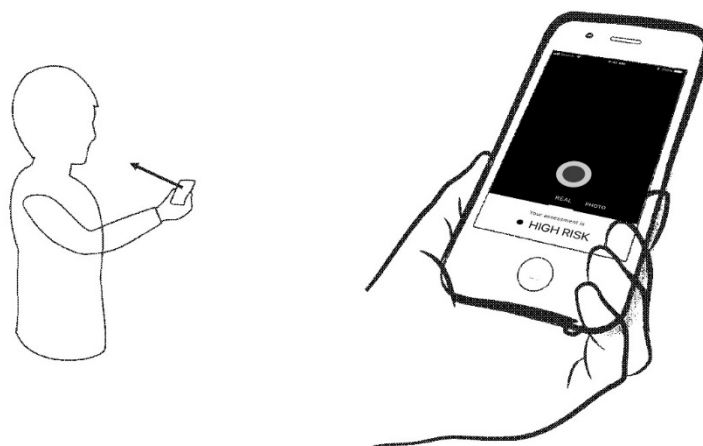


Figure 3. Screening by the mobile devices

RESULTS OF MODEL TRAINING

The chosen model studied 40 lessons which included 30 lessons of carrying out transfer learning and 10 lessons of fine tuning respectively. By results

of training the value of mistake function on a validation subset was about 0.2.; an accuracy indicator on the same subset was 0.9. Indicators of accuracy and error of model are presented in Fig. 4.

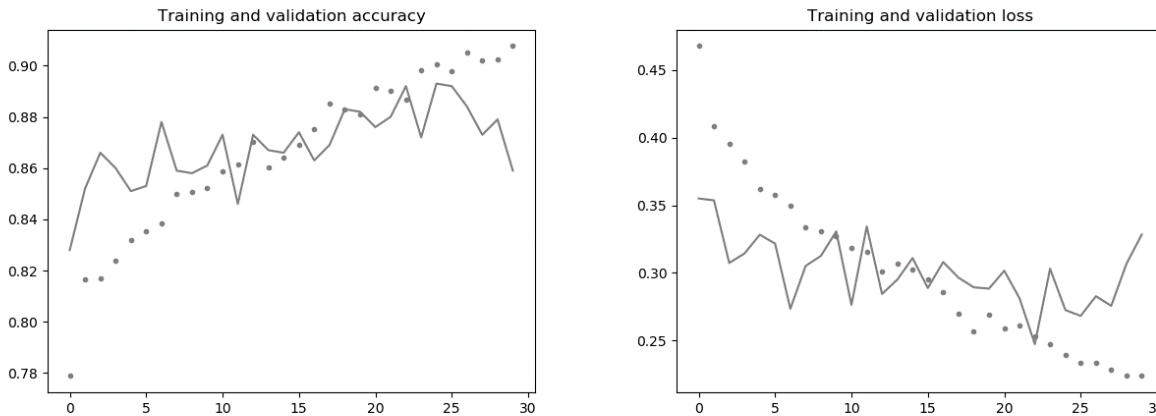


Figure 4. Indicators of accuracy and mistake for a training and validation subset

To analyze the errors of the first and second types, a ROC/AUC-graph was built, allowing to assess the quality of the binary classification. This graph displays the ratio between the share of objects in the total number of carriers of a trait, correctly

classified as bearing a trait, and the share of objects in the total number of objects that do not carry a trait, mistakenly classified as bearing a trait. The ROC/AUC graph is presented in Fig. 5.

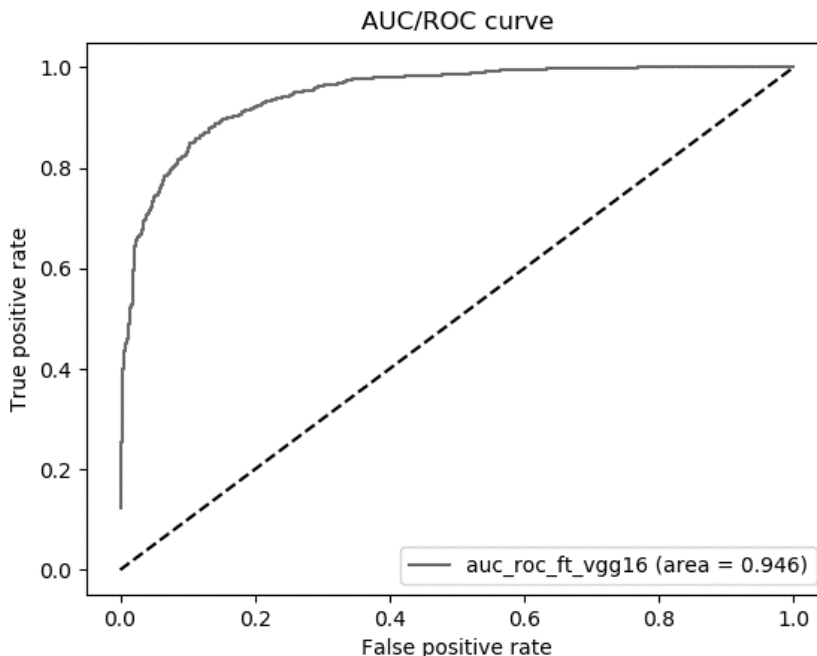


Figure 5. The ROC/AUC graph for the trained model

The quantitative interpretation of this graph is given by the AUC indicator – this is the area bounded by the ROC curve and the axis of the fraction of false

positive classifications. The higher the AUC, the better the classifier. The AUC index for the trained model of the classifier is presented in Fig. 5 and is

0.946. This indicator value indicates the possibility of using the classifier for diagnostic purposes.

RESULTS OF A RESEARCH

The study successfully developed a mobile application based on a trained model. You can learn more about the application source code or take part in an open source project by going to the github repository (<https://github.com/akarataev/gleam-ios>).

REFERENCES

[1] World Health Organization: Cancer Prevention [electronic resource] URL: <https://www.who.int/cancer/prevention/ru/> (15.10/2018).

[2] J. C. Boldrick, C. J. Layton, J. Nguyen, and S. M. Swetter, "Evaluation of digital dermoscopy in a pigmented lesion clinic: Clinician versus computer assessment of malignancy risk," *Journal of the*

[9] Yu, Y.: Borrowing Treasures from the Wealthy: Deep Transfer Learning through Selective Joint Fine-Tuning (2017).

American Academy of Dermatology, vol. 56, pp. 417-421, 2007/03/01/ 2007.

[3] International Skin Imaging Collaboration: Melanoma Project ISIC [electronic resource] URL: <https://www.isic-archive.com/> (15.10/2018).

[4] Collobert R., Bengio S. Links Between Perceptrons, MLPs and SVMs // Proc. 21st ICML, New York, NY, USA: ACM, 2004. — P. 23–.

[5] PH² Database – Universidade do Porto [electronic resource] URL: <http://www.fc.up.pt/addi/ph2%20database.html> (15.10/2018).

[6] Keras Application [electronic resource] URL: <https://keras.io/applications/> (15.10/2018).

[7] Liu, J., Wang, Y., Qiao, Y.: Sparse Deep Transfer Learning for Convolutional Neural Network. In: Association for the Advancement of Artificial Intelligence (2017).

[8] Ge, W.,

THE EFFECT OF OXYGEN INSTABILITY ON THE FORMATION OF AN INCOMMENSURATE PHASE IN LEAD HAFNATE

M. Kniazeva

Postgraduate student
Peter the Great Saint-Petersburg Polytechnic University,
Saint-Petersburg, Russia
kniazeva.maria225@yandex.ru

INTRODUCTION

Lead hafnate (PbHfO_3) attracts the interest of researchers both from the point of view of theoretical studies and from the point of view of practical application. Being an antiferroelectric, lead hafnate is a very promising material in many areas of production [1, 2]. At the same time, interest in the field of theoretical studies is dictated by one of the richest phase diagrams of lead hafnate among a group of simple lead-containing perovskites (ABO_3).

According to one of the first works on the description of this material [3, 4], at ambient pressure in lead hafnate there are three different phases [5]. In the temperature range from 163 °C and lower, the low-temperature antiferroelectric (AFE) phase is realized in lead hafnate. Rising the temperature above 163 °C leads to an incommensurate (IC) phase, which is also AFE [5]. At a temperature of 215 °C, lead hafnate passes into a paraelectric cubic phase. The low-temperature AFE phase is isostructural to the same phase in lead zirconate (PbZrO_3) and characterized by the two order parameters [6]. The first order parameter is associated with antiparallel displacements of Pb cations in the high-symmetry direction $[1\ 0\ 1]$. These displacements give rise to Σ -type superstructure reflections with coordinates $(h \pm \frac{1}{4}, k, l \pm \frac{1}{4})$ in the reciprocal space. The second order parameter is associated with rotations of oxygen octahedra O_6 ; this type of distortion leads to the appearance of an R -superstructure with reflections of the form $(h + \frac{1}{2}, k + \frac{1}{2}, l + \frac{1}{2})$ in the reciprocal space. During the phase transition to the IC phase, reflections of the type $(h \pm \xi, k \pm \xi, l)$, where $\xi = 0.15$, are added to the already existing superstructures, resulting from IC modulations of the lead subsystem [5].

Despite the still unabated interest of researchers in questions of the structure of lead hafnate phases [5,7-9], there is no unambiguous answer to the question about the mechanism of formation of the IC phase in this material. One of the possible explanations for the formation of an IC order in perovskite crystals of the type ABO_3 was given in [6]. In this paper, the authors put forward a version according to which the formation of IC phases in perovskites of the ABO_3 type (including lead hafnate) can be associated with rotations of oxygen octahedra.

In this work, the effect of the rotation of oxygen octahedra on the formation of an IC phase in lead hafnate is studied. During the study, lead hafnate single crystals are exposed to two thermodynamic effects — temperature and pressure. The change in temperature in the system is introduced to produce a phase transition from the low-temperature AFE phase to the IC phase. The role of external pressure applied to the sample is to enhance the contribution of the rotation of the oxygen octahedra in the crystal.

EXPERIMENTAL

For the analysis the results of two different experiments on the diffraction of synchrotron radiation on lead hafnate single crystals with simultaneous application of temperature and pressure were used. The difference between the experiments lies in the external pressure applied to the sample: for the first experiment from the series, measurements were carried out in the range of external pressures of 11.5 kbar, while data from the second experiment were obtained at an external pressure from 16 to 18 kbar. The measurements in the temperature range from 158 °C to 220 °C for each experiment were compared in order to capture the region of phases of interests.

The single crystals of PbHfO_3 for both experiments were synthesized by means of spontaneous crystallization from the high temperature solution in a $\text{Pb}_3\text{O}_4\text{-B}_2\text{O}_3$ solvent. The samples for the measurements were 30 by 30 by 30 micron size. Such small size was achieved by cutting the crystal of bigger size and then etching in hydrochloric acid.

Experiments were carried out at high-pressure beamline ID27 of the European Synchrotron Source (ESRF, Grenoble). The wavelength of synchrotron radiation was set to 0.3738 Å. For applying hydrostatic pressure and temperature to the samples we used resistively heated diamond anvil cell. The cell pressure was measured using the fluorescence of a ruby placed in a cell with samples of lead hafnate. For the first experiment of the series Ne was used as a pressure transmitting medium. Ar was used as a pressure transmitting medium for the second experiment of the series. The gasket, which limits the work area between the anvils, was made of Re. The experiments were conducted using diffractometer

equipped with Perkin Elmer Flat Panel position sensitive detector and PILATUS3 X 300K-W position sensitive detector. The angular step size during experiments was set at $\approx 0.5^\circ$ in ω with exposure time of 1 second per frame.

On the basis of the data obtained during each experiment, reciprocal space maps by the $(H\ 0\ L)$ plane for different external conditions were obtained. In order to exclude the intensity instabilities on different frames we have applied the normalization on the level of background intensity. For the analysis of the observed superstructures Intensity profile in $[1\ 0\ 1]$ direction with respect to the pseudocubic cell were also constructed. For processing and analysis we used a package of programs written specifically for these purposes in matlab / java environments.

RESULTS AND DISCUSSION

In the course of two experiments carried out with the application of external pressure $P=11.5$ kbar and 16-18 kbar respectively, diffraction data sets were obtained corresponding to different temperatures from the range 150 – 220 °C. Comparison of experimental data was carried out between experimental points belonging to the same phase.

Figure 1 shows fragments of the reciprocal space maps by $(H\ 0\ L)$ plane at temperatures corresponding to the low-temperature AFE phase for $P=11.5$ kbar (left) and $P=17.5$ (right). In both cases, lead hafnate demonstrated characteristic superstructures of the low-temperature AFE phase: Σ -superstructure and R -superstructure.

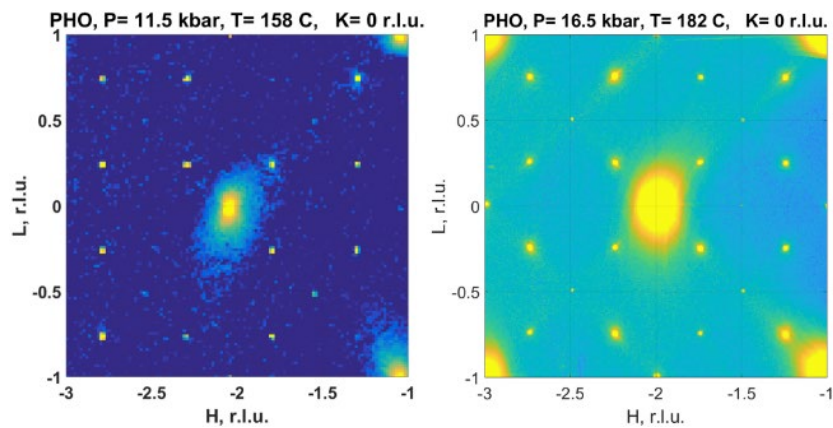


Fig. 1 Fragments of the reciprocal space maps by $(H\ 0\ L)$ plane at temperatures corresponding to the IC phase for $P=11.5$ kbar (left) and $P=17.5$ (right).

Presence of Σ -type can be seen more clear on fig.2. However, in addition to the declared superstructures, the presence of an M -superstructure with coordinates $(h + \frac{1}{2}, k, l + \frac{1}{2})$ in the reciprocal space, which is not typical for this phase, was also recorded during both experiments. The most likely

explanation for the presence of reflections in the M -positions of the reciprocal space may be distortions of the crystal lattice due to in-phase rotations of the oxygen octahedra [6] under pressure.

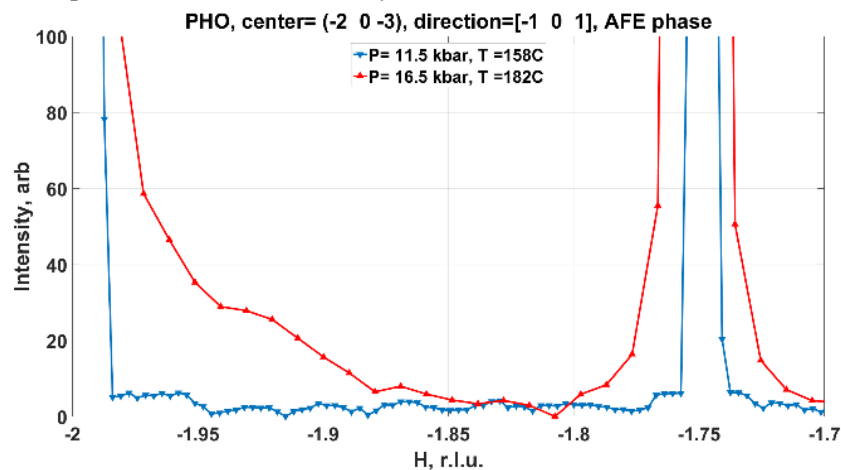


Fig. 2 Intensity profiles in the vicinity of the reflection $(-2\ 0\ -3)$ along the pseudocubic direction $[-1\ 0\ 1]$ for IC phase

Figure 3 shows fragments of the reciprocal space maps by $(H 0 L)$ plane at temperatures corresponding to the IC phase for $P= 11.5$ kbar (left) and $P= 17.5$ (right).

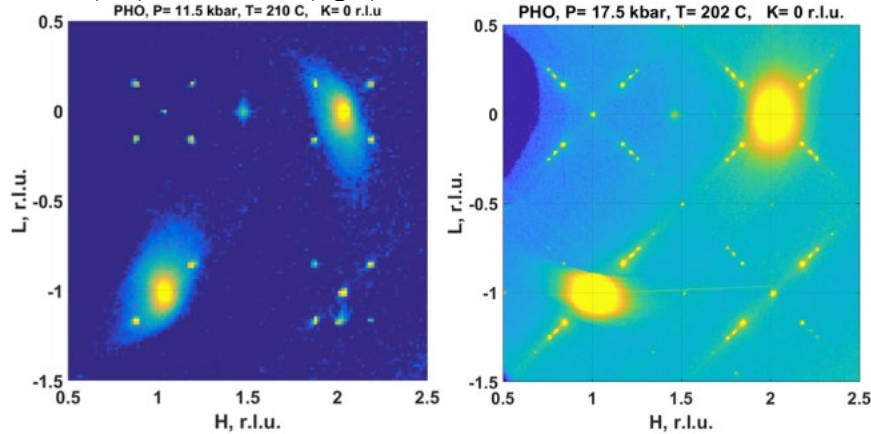


Fig. 3 Fragments of the reciprocal space maps by $(H 0 L)$ plane at temperatures corresponding to the IC phase for $P= 11.5$ kbar (left) and $P= 17.5$ (right).

The pressure has an obvious effect on the IC phase: with a higher level of external pressure applied to the crystal, the number of diffraction patterns increases. At $P = 11.5$ kbar along the $[1 0 1]$ and $[-1 0 1]$ directions, only one group of reflexes is observed in an IC position. Under conditions of higher external pressure, the coexistence of three different modulation patterns is observed on the reciprocal space map: one refers to the Σ -superstructure; the other two patterns refer to disproportionate

modulations of the lead subsystem. The coexistence of three different modulation patterns in the case of $P = 17.5$ kbar can be explained by the uneven distribution of pressure in the working chamber of a resistively heated cell with diamond anvils.

For both cases, one-dimensional intensity profiles in the vicinity of the reflection $(-2 0 -3)$ along the pseudocubic direction $[-1 0 1]$ help to determine the coordinates of the superstructural reflexes more precisely.

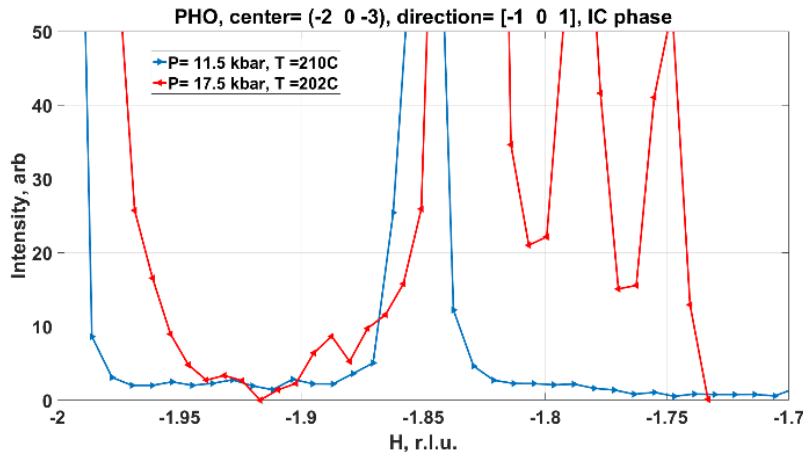


Fig. 4 Intensity profiles in the vicinity of the reflection $(-2 0 -3)$ along the pseudocubic direction $[-1 0 1]$ for IC phase

If at $P= 11.5$ kbar (blue curve on Fig. 4) the reduced wave vector of incommensurate modulations $\xi \approx 0.15$, which corresponds to the result obtained in [5], in the case of $P= 17.5$ kbar (red curve on Fig. 4) states in lead hafnate are realized with other modulation periods – $\xi_1 \approx 0.22$ and $\xi_2 \approx 0.17$, not previously observed.

Помимо If at $P= 11.5$ kbar (left on Fig. 4) M-superstructure is not presented, in the case of $P= 17.5$ kbar (right on Fig. 4) it appears. Furthermore, in case

of $P= 17.5$ kbar M-superstructure reflections are systematically absent for points of the form $(h + \frac{1}{2}, 0, h + \frac{1}{2})$. Such extinction in the M-position indicates that the appearance of the M-superstructure is due to the rotation of oxygen octahedra [8].

CONCLUSION

In the course of the work done, it was found that applying of pressure influences on both considered phases, both in terms of the behavior of the lead

subsystem and in terms of the behavior of oxygen octahedra. More research can contribute to a greater understanding of the processes occurring in lead hafnate with external pressure applied to it, as well as the combination of various measuring techniques, including inelastic scattering.

ASKNOLEGEMENTS

Author acknowledge the Russian Science Foundation for financial support (Grant No. 17-72-20083).

REFERENCES

1. Wei, Jing, Tongqing Yang, and Hongsheng Wang. "Excellent Energy Storage and Charge-discharge Performances in PbHfO₃ Antiferroelectric Ceramics." *Journal of the European Ceramic Society* 39.2-3 (2019): 624-630.
2. Waugh M. D. et al. STRUCTURE-PROPERTY INVESTIGATION OF A MODIFIED PbHfO₃ COMPOSITION FOR HIGH ENERGY STORAGE //Ceram. Trans. Vol. 90. – 1997. – C. 153-163.
3. Shirane G., Pepinsky R. Phase Transitions in Antiferroelectric PbHfO₃//Physical Review. – 1953. – T. 91. – №. 4. – C. 812.
4. G. A. Samara. Pressure and temperature dependence of the dielectric properties and phase transitions of the antiferroelectric perovskites: PbZrO₃ and PbHfO₃. Phys. Rev. B, 1:3777–3786, May 1970
5. Fujishita H. et al. Structural Modulations in the Intermediate Phase of Antiferroelectric PbHfO₃ //Journal of the Physical Society of Japan. – 2018. – T. 87. – №. 12. – C. 124603.
6. Glazer A. M. Simple ways of determining perovskite structures //Acta Crystallographica Section A: Crystal Physics, Diffraction, Theoretical and General Crystallography. – 1975. – T. 31. – №. 6. – C. 756-762.
7. Huband, S., et al. "Crystallographic and optical study of PbHfO₃ crystals." *Journal of applied crystallography* 50.2 (2017): 378-384.
8. Patel K. et al. Atomistic mechanism leading to complex antiferroelectric and incommensurate perovskites //Physical Review B. – 2016. – T. 94. – №. 5. – C. 054107.
9. Burkovsky R. G. Dipole-dipole interactions and incommensurate order in perovskite structures //Physical Review B. – 2018. – T. 97. – №. 18. – C. 184109.

SUSTENTION OF THE LIGHT FLOW FOR LED LIGHT SOURCES

V. Kuzmenko

Saint-Petersburg State University of Aerospace Instrumentation,
Saint-Petersburg, Russia
E-mail: mr.konnny@gmail.com

Abstract

It is difficult to accurately predict the service life or the deterioration of the light output of LED lamps. The article discusses the problems of testing and comparing the light characteristics of LED light sources. Specific failure criteria are proximately proposed. Offered more clear parameters for intercomparison of characteristics of LED lamps by a consumer. The idea of the sustention of the luminous flux of the LED lamp with a decrease in light output over time is formulated.

INTRODUCTION

To determine the service life of LED lamps the relative values of the total luminous flux at a given device operating time are widely used. This can mislead the consumer, due to the fact that the degradation of light output is only one of many reasons that affect the reliability of the lamp.

The main criterion for the failure of the LED lamp according to Russia's state standards GOST R 54815-2011 and GOST R IEC 60598-1-2011 accept a reduction of the luminous flux more than over from 20 to 30%. [1,2] However, in this paper, the degradation of the luminous flux was associated with a decrease in illumination from the LED lamp placed in a special black box. This assumption was made in view of the fact that expensive light equipment is necessary for measuring the luminous flux, as well as the fact that this concept is not understandable for the regular customer of LED lighting devices.

Figure 1 shows the experimentally obtained dependence of reducing illumination on the number of start-up cycles of an LED lamp in a black box.

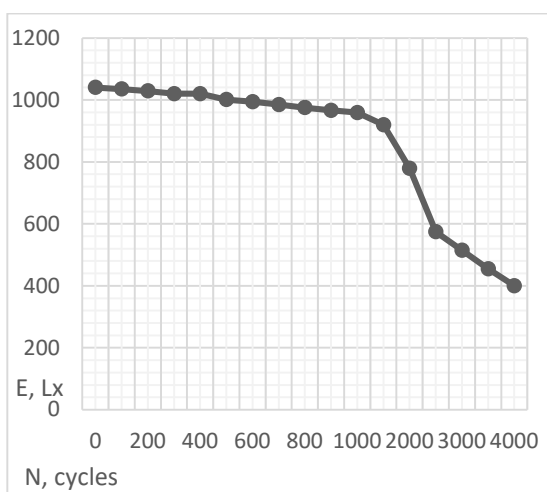


Fig. 1. The dependence of the decrease in the amount of illumination on the number of start-up cycles of the LED lamp in a black box.

Technical characteristics of the lamp are shown in table 1.

Table 1. Technical characteristics of the lamp

Power, W	5 w
Similar filament lamp power, W	35 w
Luminous flux, lm	400 lm
Color temperature, K	2700
Declared time to failure, hours	25000

Approximately the first 2000 cycles, the lamp showed excellent luminosity values, much higher than those declared in the product expected from the shown 400 lm in the technical documents of the lamp.

The claimed operating time of this LED lamp is 25000 hours. However, it is clear that after approximately 6000 lamp on / off cycles, the luminous flux will decrease by more than 15-30%. This means that the declared value of the lamp, indicated directly on the packaging, misleads the consumer in advance, including not complying with state standards GOST R 54815-2011 and GOST R IEC 60598-1-2011, since according to this document, the lamp reduced luminous flux of more than 30%.

Since the average consumer is rarely interested in complex concepts such as "luminous flux", it is possible that the concept of "dimming" will be much more practical for a completely dark room, with a single light source, along which measurements will be taken. This concept is optimal for ordinary consumers, since the main function of the lamp is to provide the required (stated) illumination, which will bring much greater practical clarity to the study of the shelf life parameters of LED lamps.

FORECASTING THE LIGHT FLUX

According to the TM-21-11 standard, values for at least 6000 hours of work are processed using an exponential regression, and then the illumination deterioration is statistically estimated six times during

this period.

Approximation by exponential regression is expressed by:

$$\Phi_t = B \cdot e^{-\alpha t},$$

Where:

t – work time (in hours);

Φ_t – the average normalized luminous flux at time t;

B – the initial constant obtained on the basis of the least square curve of the LM-80 standard data;

α – is the attenuation rate constant, derived from the least square curve of the LM-80 data.

To design the maintenance of the luminous flux after a test period (6000 hours), TM-21 will formulate the following equation:

$$L_{70} = \frac{\ln\left(\frac{B}{0,7}\right)}{\alpha}$$

In order to control the luminous flux, it is necessary to increase the amount of energy passing through the LEDs, by means of direct current, to achieve a certain level of illumination. Without using remote control, this simply means increasing the initial power to increase the light attenuation.

Another way is to depreciate the luminous flux with a fixed rate, for example, n-percent for every N-thousand hours of operation.

Significant disadvantages of these methods are that they do not account the type of light source, the LED technology, power supply source, as well as the gradual deterioration of the optical elements of the system (reflectors, diffusers, etc.) and environmental conditions.

DYNAMIC SUSTENTION OF THE LIGHT FLUX

In order to take into account the global degradation of light and the level of illumination over the entire lifetime of the LED lamp, it is necessary to use methods of balanced maintenance of luminous flux.

It is obvious that during operation, as a result of current surges in the network, disturbances in the operation of the luminaire driver, drying of the capacitor, the appearance of starting (pulse currents), the crystal lattice is damaged and the LED matrix luminous power decreases. An effect similar to the hole conduction effect occurs, and the electric current ceases to pass through portions of crystals that emit light, and because of the decrease in the voltage in current across the crystal, its power decreases.

It should also be remembered about the degradation of the luminophor, which occurs under the influence of high temperatures. When degradation of the luminophor in addition to reducing the brightness of the LED, a change in the colour of its glow occurs. It becomes colder, and its own radiation

of the crystal begins to predominate in the spectrum, in blue hues.

The human visual system is limited to a range from just below 400 nm to 700 nm. This visible radiation is commonly referred to as light, and the lighting industry mainly focuses on this range. This is characterized by the tendency to offer light sources that provide only the visible spectrum. This range of radiation, especially the high-energy blue range, is also related to photopic circadian signals and may cause damage to the organs of vision.

So in this way an increase in luminous flux is the result of an increase in the forward current through the LEDs, so it is necessary to strictly observe the precautions regarding temperature control. Therefore, the radiator must be designed to receive the maximum output power of the LED when it reaches its maximum light output to avoid overheating. For example, a 100 W LED luminaire must have a 120 W luminaire heat output, which is equivalent to the technical specifications of the L80 LED standard at the end of its service life.

To control the light flux, the IR sensor (consisting of a pair of emitter-receiver that detects the transmission of light through the diffuser) with a microprocessor, which ultimately controls the driver (power supply) can be used and the measurement of the light flux generated by the LEDs can be performed with a spectral sensor.

It is recommended that the power control should not exceed 20% of the nominal value, so that the action to increase the luminous flux does not affect the thermal control of the luminaire, if there is no thermal reserve. The suitable location of the sensor assembly depends on the mechanical characteristics of the luminaire, respectively, on the height of the LED emitters, on the availability of free space, and on the type and size of the optics.

The example of the location of the sensors in the LED lamp is shown on figure 2.

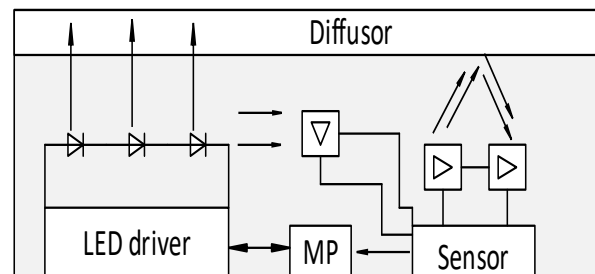


Fig. 2 block diagram of the use of IR sensor

When the diffuser material deteriorates, the light transmission decreases and is redirected inwards towards the IR receiver.

The VIS sensor, which indirectly faces the LED emitters, will perform the function of measuring the

equivalent value of the total luminous flux. The position of the sensor should only allow detection of light generated by LED emitters.

The photometric characteristics and maintenance of the light flux during the operation time are analyzed with respect to the recorded reference values through the microcontroller. Maintaining luminous flux is achieved by increasing or decreasing the forward current through the LEDs, referring to reference values.

CONCLUSION

It is practically impossible to reliably determine to what extent the change in the color of the lamp is due to the LED, and in which type of the lamp model or parameters of the electrical network it goes stronger. On this basis, the only way to determine the color change is to measure the parameters of the entire system, including the LEDs and all other elements of the electromechanical system of the lamp, as well as the environmental conditions. The stability of the parameters of the light flux and its color, as well as its degradation, is not determined only by the characteristics of the LED. This is due to the fact that as a result of differences in the designs of heat sinks, the LEDs and electronic circuits work in different conditions, despite the same operating time and operating temperature, and the different materials used in the device wear out differently.

Recent standards for testing LED luminaires do not apply to test times longer than 10,000 hours; further characterization is obtained by extrapolating the data using the least squares method (TM21-11 standard). [3] The factors complicating the extrapolation of color change data include differences in LED solutions, materials, manufacturing processes, optical systems, as well as in operating temperatures and times of operation of LEDs.

Unfortunately, regardless of the type of luminaire, at the moment there is no qualitative solution to the problem of degradation of the luminous flux, and the existing methods do not compensate for the real deterioration of the luminous efficiency of the luminaire.

A decrease in lumen output power is predicted with a certain tolerance of according to manufacturers of LED lamps, assembled from past products released on the market.

The term life does not include a change in color, even though in some applications this change may be considered by the user as a failure. The decision to consider the light output as the main priority in defining this concept reflects the fact that the stability of the luminous flux is related to the safety of life, whereas the stability of color is only with aesthetic perception. Many users regard a large color change as a failure, and the L80 and TM 21-11 standards recommend that this change be separately indicated in addition to the declared service life of the product.

The means of determining the service life is currently not fully standardized. Sampling and matching requirements are under development. Methods for measuring the luminous flux of the lamps are also under consideration. Measurement of the luminous flux according to ICE 84: 1989 according to the standard GOST R 54815-2011 is not optimized for LED lamps. [1,3] Additional service life definitions and methods for calculating it using short-term measurements are still under discussion.

A decrease in lumen output power is predicted with a certain tolerance in accordance with the information provided by the manufacturers of LED luminaires, collected from past products released to the market. Therefore it is worth considering the option where the driver controls the power supplied to the LEDs, providing the same intensity of illumination during the entire period of dimming.

REFERENCES

1. GOST R 54815-2011. Light-emitting diode lamps with built-in control device for general lighting for voltages above 50 V. Operational requirements.
2. State standard GOST R IEC 60598-1-2011 "Lamps. **Part 1.** General requirements and test methods"
3. IESNA LM-80-08 and TM-21-11.

STRAIN-DRIVEN MODIFICATION OF PHASE TRANSITION SEQUENCE IN EPITAXIAL ANTIFERROELECTRIC THIN FILMS

G. Lityagin

Postgraduate student
Peter the Great Saint-Petersburg Polytechnic University,
Saint-Petersburg, Russia
georgiy.lityagin@gmail.com

Abstract

Antiferroelectric thin film heterostructures are important in energy storage technology and have prospective applications in domain wall nanoelectronics. Controlling their functional properties requires detailed understanding of the relevant structural transformations under varying external conditions. This paper discusses the study of temperature-driven transitions in thin films of prototypical antiferroelectric PbZrO_3 . It was shown a dramatic change in the character of the antiferroelectric transition in comparison to the bulk case, manifesting itself in smearing of the onset of AFE order parameter on cooling and appearance of new superstructures. The X-ray diffraction profile with momentum transfer along the normal to the film surface have been investigated to clarify the possible reason for these features. The results suggest that the reasons for the phase transition sequence modification in thin films can be associated with inhomogeneous distribution of stress and defects in the near-interface area.

INTRODUCTION

Antiferroelectric (AFE) materials have attracted considerable research interest in the recent years due to their potential applications in sensors, actuators, charge storage devices and electrical refrigeration devices [1-3]. Characteristic useful properties of AFEs are connected to energetic proximity of competing low-symmetry phases (ferroelectric and AFE). It is known that this energy balance can be modified by going from the bulk to the thin film form, which can, in turn, enhance the characteristics that are relevant to energy storage applications and electrocaloric effect based cooling devices [4-7]. However, the full picture of how the particular factors are modifying the properties of AFE films is not yet fully explored and a range of related questions remain open. In particular, it is rather difficult to predict a priori the sequences of phase transitions and possible phase coexistence configurations in the film of particular thickness. Moreover, some of experimental results turn out to be controversial.

In particular, it is known that decreasing of the thickness of thin films made of prototypical antiferroelectric material PbZrO_3 tends to result in stabilizing FE phase [8,9]. However, the influence of temperature on the stability of different phases is established not fully unambiguously. According to the results of Refs. [10,11] the FE and AFE phases in films coexist in a broad temperature range below room temperature. On the other hand, there are results indicating FE phase also at high temperatures [12,13], in the intermediate region between the paraelectric and AFE phases. Therefore, the macroscopic

approaches, which have been used earlier, are insufficient to clarify the phase transition sequence unambiguously. Further studies based on alternative experimental techniques are on demand.

This paper reports on the results of X-ray scattering study of temperature-induced phase transitions in PbZrO_3 films grown epitaxially on SrTiO_3 substrate with the buffer layer of SrTiO_3 . X-ray scattering was used as the direct probe for order parameters associated with anti-polar patterns of ionic displacements and, on the other hand, as the means of studying the condition of near-interface layer of the film, which is expected to be strongly affected by epitaxial strain and dislocations [9] and influence the overall behavior of the film *via* these factors. The results indicate that the onset of anti-polar distortions are strongly smeared in the films, as contrasted to the sharp phase transitions in the bulk, and that this behavior is likely linked to the strong inhomogeneity of the near-interface layer of the film.

EXPERIMENTAL

PbZrO_3 thin film samples were grown using pulsed laser deposition technique at the University of California, Berkeley on the SrTiO_3 substrate with SrRuO_3 bottom electrode as buffer layer. The SrRuO_3 was grown at a heater temperature of 680 °C in a dynamic oxygen pressure of 100 mTorr and with a laser fluence and repetition rate of 1.0 J/cm² and 5 Hz, respectively. For the PbZrO_3 films, growth was completed at a heater temperature of 630 °C in a dynamic oxygen pressure of 80 mTorr and with a laser fluence and repetition rate of 1.8 J/cm² and 5 Hz, respectively. The thickness of the studied films was

50 nm and the thickness of the SrRuO₃ layer was 20 nm. The pseudocubic main axes of the film were coincident with the ones of the substrate, normal to which was oriented along the [001] direction.

The measurements of superstructure reflections intensity temperature dependence were performed at the ID03 beamline of European Synchrotron Radiation Facility (ESRF), which is dedicated for the surface X-ray diffraction (SXRD) experiments. The strain distribution along the film normal was analyzed on the basis of θ - 2θ scans. The experiments were conducted using a six-circle diffractometer. The temperature of the samples was controlled by resistive heating in vacuum chamber. The beam energy was set at 24 keV (corresponding to 0.517 Å), the measurements were conducted using grazing incidence scattering, with an incidence angle of 0.123°. This configuration enabled to maximize the signal from the film by probing its whole thickness and at the same time to limit the contribution of the substrate. The data were acquired using Maxipix 2D pixel area detector and treated using the BINoculars software [14] to obtain reciprocal space projections of the intensities. Temperature dependencies of the superstructure integral intensities were obtained using custom software based on Matlab platform.

RESULTS AND DISCUSSION

Synchrotron measurements revealed three types of superstructure reflections in PbZrO₃ film corresponding to the Σ , R and M points in pseudocubic Brillouin zone with coordinates of the form $(H+1/4, K+1/4, L)$, $(H+1/2, K+1/2, L+1/2)$ and $(H+1/2, K+1/2, L)$ respectively. Fig. 1 shows the temperature dependences for the six different Σ superstructure peaks that correspond to the six possible antiferroelectric (AFE) orientational domain states.

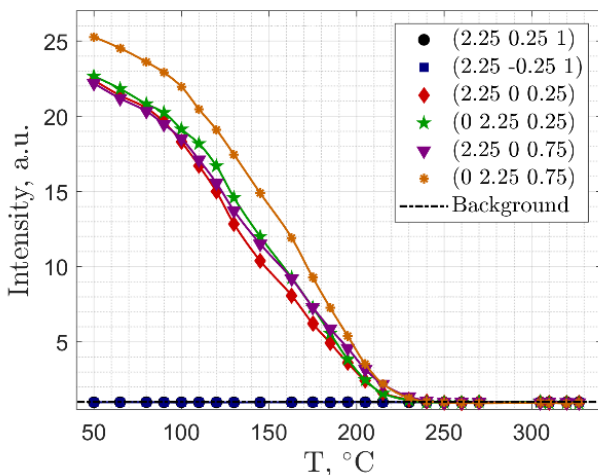


Fig. 1. Integrated intensities of Σ superstructures for the 50 nm thick PbZrO₃ film as a function of temperature. Lines are guides for the eye.

The intensities corresponding to the domains

with in-plane modulation wave vectors (superstructure reflections with integer L) are zero indicating the absence or negligible amount of such domains (c -domains). The smoothness of superstructure intensity evolution in the thin film has been also observed, which is in contrast with the sharp appearance of AFE superstructures in the bulk PbZrO₃ [14].

The next type of revealed superstructure reflections are M superstructures. In Fig. 2 temperature dependences of four non-equivalent M superstructure reflections are shown. Half of the M reflections correspond to the in-plane modulation vectors and half to the out-of-plane modulation vectors. The intensity of the in-plane reflections is much stronger than the intensity of the out-of-plane reflections. They differ further by the presence of a maximum in the in-plane case at about 150 °C. The starting formation temperature considerably differs for the in-plane and out-of-plane reflections. In the case of the in-plane M reflections it is close 300 °C, while the out-of-plane M reflections appear simultaneously with AFE phase formation. It can be suggested that the phase associated with M superstructures in thin films of PbZrO₃ is similar to the intermediate ferroelectric phase in bulk PbZrO₃ with small doping of titanate (PZT). The similarity manifests itself in the presence of intermediate phase associated with M superstructures between the paraelectric and AFE phases. By analogy with PZT, the intermediate phase in the PbZrO₃ film could also be assumed as ferroelectric.

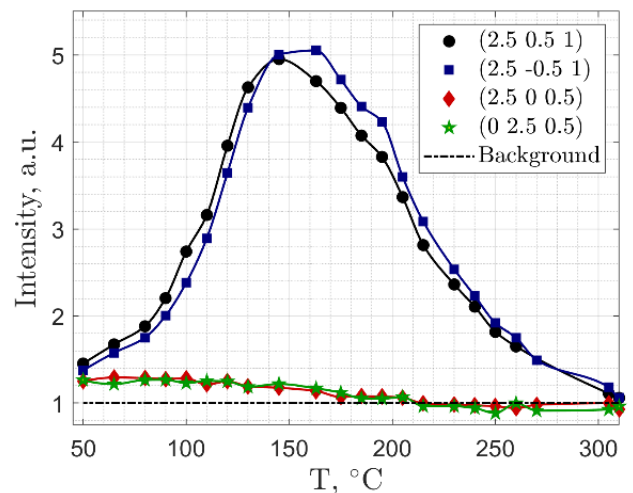


Fig. 2. Integrated intensities of M superstructures for the 50 nm thick PbZrO₃ film as a function of temperature. Lines are guides for the eye.

The nature of smoothness of AFE phase transition is sophisticated. It might be associated with the change of phase transition order from first to second, similarly to the situation discussed in the context of the ferroelectric thin films [15]. However,

we have observed that phase associated with the in-plane M reflections coexist with AFE phase associated with Σ reflections in the certain temperature region. Accordingly, we suspect that the smoothness can be linked to the continuous temperature evolution of the spatial distribution of different structures in the film volume. This assumption is supported by noting that the field and polarization in the film may be strongly inhomogeneous [16].

As shown above, we have observed considerable changes in PbZrO₃ thin film phase transition sequence compared with case of bulk sample. It is natural to suggest that these features are related to the specific condition of the near-interface layers, which are expected, in particular, to be strongly affected by strain and dislocations due to significant lattice mismatch between PbZrO₃ and SrRuO₃ layers (~6%). In order to obtain the information on the state of near-interface layer we have analyzed the diffraction profiles corresponding to wave vector transfer along the normal to the film. Fig. 3 shows the XRD profile obtained in θ - 2θ mode, which includes the (0 0 2) peaks corresponding to the film ($2\theta \approx 43.5^\circ$) and to the substrate ($2\theta \approx 46.5^\circ$). The main peak of the film is accompanied by the characteristic oscillations related to the finite thickness of the sample.

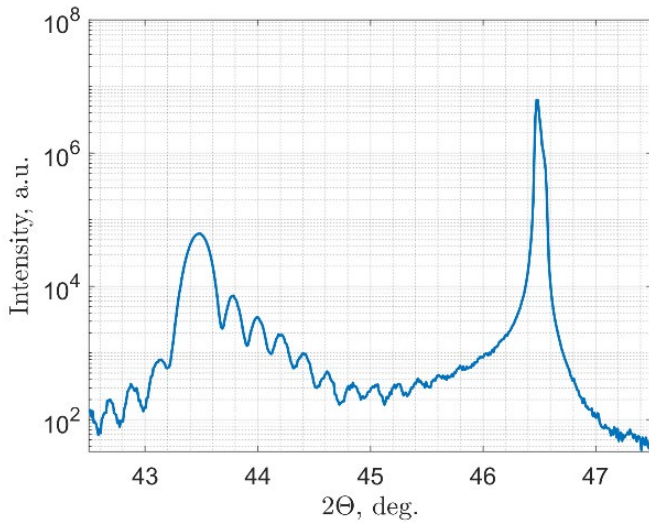


Fig. 3. XRD profile of the (0 0 2) reflection from the film (left peak) and substrate (right peak).

One can see that the oscillating intensity on the right of the main peak is about an order of magnitude stronger than it is on the left. Such asymmetry on XRD profile is caused by inhomogeneous strain in the film's volume. Modeling the inhomogeneously strained films has been performed in a number of studies [17,18], from which we largely derive our methodology. Within the kinematical scattering theory, the amplitude of the scattered wave distributed along surface normal is given by the equation [17]

$$E(q_z) = \int_0^\infty \left\{ F(z) \exp[-i\mathbf{h}\mathbf{u}(z)] \right\} \exp(-iq_z z) dz. \quad (1)$$

Here \mathbf{h} – reciprocal lattice point and $\mathbf{u}(z)$ – shift of the elementary unit cell as a whole at the height z . The intensity of X-ray scattering equals the square of (1)

$$I(q, t) = \left| F \int_0^\infty \Omega(z, t) \exp[-i\mathbf{h}\mathbf{u}(z)] \exp(-iq_z z) dz \right|^2. \quad (2)$$

$\Omega(z, t)$ is the shape factor of the layer. In the simplest case of a flat film with sharp surface and interface and thickness t , $\Omega(z, t) = 1$ if $z \in [0, t]$; otherwise, $\Omega(z, t) = 0$. The vertical strain profile follows from $\varepsilon_{zz} = \partial\mathbf{u}(z)/\partial z$.

Cubic B-spline functions have been considered to model vertical strain profile as it was regarded in Ref. [18]. Given a set of knots $x_i (i=1, 2, \dots, N)$, a spline function of degree m , $S_m(x)$, is such that $S_m(x)$ is a polynomial of degree m in each $\{x_i, x_{i+1}\}$ interval, and $m-1$ continuous derivatives over the whole x range. In the B-spline representation, any spline function can be written

$$S_m(x) = \sum_{i=1}^N w_i B_{i,m}(x), \quad (3)$$

where w_i is the weight of the i th B-spline of degree m , $B_{i,m}(x)$. Any spline function is therefore entirely determined by a set of N discrete weights. Some more information about B-spline functions and their properties can be found in Ref. [19]. We have used 13 knots to describe strain profile. Using this form of strain profile, we have performed a nonlinear least-square fit of measured profile with equation (2). A Levenberg–Marquardt minimization algorithm was used to refine the weights of spline function and thickness of the film. The result of fit with B-spline function presented in Fig. 4 by red dashed line. One can see that the modeled curve reproduces the experimental profile reasonably well. Therefore, the strain profile derived from this approach is close to the true vertical strain distribution in PbZrO₃ film.

The strain profile recalculated on the basis of fit parameters as $\partial\mathbf{u}(z)/\partial z$ is shown in Fig. 5. The strain magnitude is notably large in the direct vicinity of the interface. Its value of about 8 percent is comparable to the value of the lattice mismatch between PbZrO₃ and SrRuO₃ amounting to about 6 percent. An interesting question arises on the sign of the strain, which is negative, meaning that the PbZrO₃ lattice is compressed along the normal to the film. As long as the in-plane strain is expected to be compressive (ZrO₃ has larger lattice spacing), the simple elasticity theory would predict the out-of-plane strain to be

tensile according to the relation $\varepsilon_{\perp} = -2 \frac{c_{12}}{c_{11}} \varepsilon_{\parallel}$, where c_{12} and c_{11} are the elastic constants of the layer [17].

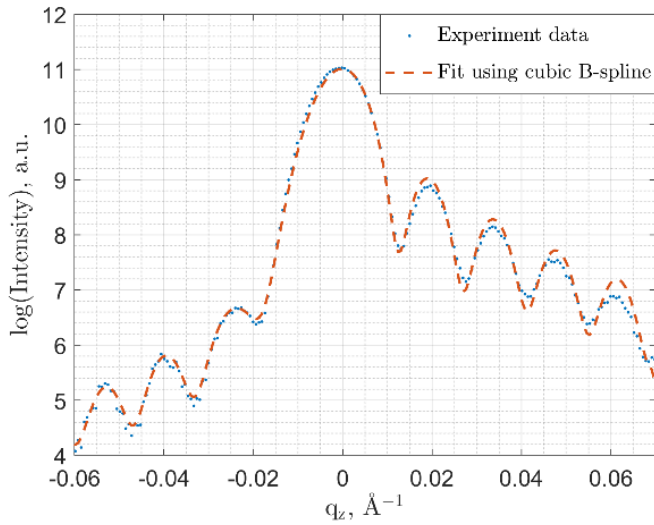


Fig. 4. X-ray diffraction pattern in θ - 2θ geometry. Blue dots correspond to the experimental data and red dashed line corresponds to the fitted profile. The origin of the wave vector axis is chosen to correspond to the scattering maximum.

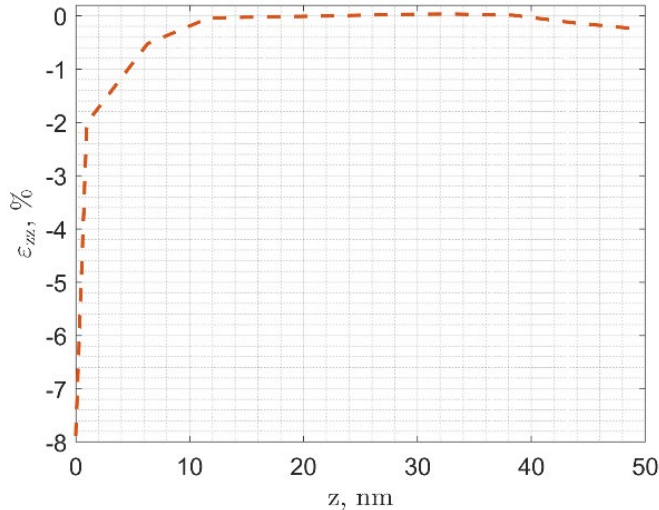


Fig.5. Strain profile determined from the fit.

On the other hand, we can expect that this situation can be changed qualitatively due to the presence of the near-interface dislocations that are going to inevitably accommodate the very large lattice parameter mismatch. In fact, such dislocations were observed in $\text{PbZrO}_3/\text{SrRuO}_3/\text{SrTiO}_3$ heterostructures by HRTEM [9], where the Burgers vectors were found pointing along $[1\ 1\ 0]$ pseudocubic directions. We suggest that the observed near-interface compressive strain in both the in-plane and out-of-

plane directions can be envisaged from the fact that the edge dislocations are expected to induce hydrostatic-like compression on the side of the “excess” half-plane [20], which in the case of the present heterostructure should be, and has been observed [9] on the side of the substrate.

CONCLUSION

We have identified strongly smeared phase transitions and revealed a new phase connected with M -type superstructure reflections, which is presumably ferroelectric, in PbZrO_3 thin films. The investigation of the effects associated with the lattice mismatch revealed that only the small near-interface part of PbZrO_3 film experiences significant strain along the normal to the surface, which decays very quickly on moving away from the interface. The out-of-plane strain is surprisingly of compressive character, which we attribute to the effects of hydrostatic-like compression associated with the presence of edge dislocations. The high inhomogeneity of the out-of-plane stress suggests that the smeared character of the observed phase transitions can be associated with the gradual expansion of the volume populated by the new phase on cooling, mediated by the inhomogeneous spatial distribution of the relevant critical temperatures. Our findings can be useful for tailoring the functional properties of thin film heterostructures for energy storage applications.

ACKNOWLEDGEMENT

The experimental research was carried out under the support of Russian Science Foundation (Grant № 17-72-20083). Thin films samples were synthesized in UC Berkeley.

REFERENCES

1. Singh K. Antiferroelectric lead zirconate, a material for energy storage //Ferroelectrics 94.1, 433-433, 1989.
2. Scott J.F. Applications of modern ferroelectrics //Science. 315(5814), 954-959, 2007.
3. Hao X. et al. A comprehensive review on the progress of lead zirconate-based antiferroelectric materials //Progress in materials science 63, 1-57, 2014.
4. Parui J., Krupanidhi S. B. Enhancement of charge and energy storage in sol-gel derived pure and La-modified PbZrO_3 thin films //Applied Physics Letters, 92.19, 192901, 2008.
5. Hao X., Zhai J., Yao X. Improved energy storage performance and fatigue endurance of Sr-doped PbZrO_3 antiferroelectric thin films //Journal of the American Ceramic Society, 92.5, 1133-1135, 2009.

6. *Mischenko A. S., et al.*, Giant electrocaloric effect in thin-film $\text{PbZr}_{0.95}\text{Ti}_{0.05}\text{O}_3$ //Science 311.5765, 1270-1271, 2006.
7. *Glazkova-Swedberg E. et al.*, Electrocaloric effect in PbZrO_3 thin films with antiferroelectric-ferroelectric phase competition //Computational Materials Science 129, 44-48, 2017.
8. *Boldyreva K., Pintilie L., Lotnyk A., Misirlioglu I. B., Alexe M., and Hesse D.* Thickness-driven antiferroelectric-to-ferroelectric phase transition of thin PbZrO_3 layers in epitaxial $\text{PbZrO}_3/\text{Pb}(\text{Zr}_{0.8}\text{Ti}_{0.2})\text{O}_3$ multilayers //Appl. Phys. Lett. 91(12), p.122915, 2007.
9. *Chaudhuri A. R., Arredondo M., Hähnel A., Morelli A., Becker M., Alexe M., and Vrejoiu I.*, Epitaxial strain stabilization of a ferroelectric phase in PbZrO_3 thin films //Phys. Rev. B. 84(5), p.054112, 2011.
10. *Asada T., Koyama Y.* Coexistence of ferroelectricity and antiferroelectricity in lead zirconate titanate //Physical Review B, 70.10, 104105, 2004.
11. *Pintilie L., Boldyreva K., Alexe M., and Hesse D.*, Coexistence of ferroelectricity and antiferroelectricity in epitaxial PbZrO_3 films with different orientations //J. Appl. Phys. 103(2), p.024101, 2008.
12. *Dobal P. S., Katiyar R. S., Bharadwaja S. S. N., and Krupanidhi S. B.*, Micro-Raman and dielectric phase transition studies in antiferroelectric PbZrO_3 thin films //Appl. Phys. Lett. 78(12), 1730-1732, 2001.
13. *Zhai J., and Chen H.* Direct current field and temperature dependent behaviors of antiferroelectric to ferroelectric switching in highly (100)-oriented PbZrO_3 thin films //Appl. Phys. Lett. 82(16), 2673-2675, 2003.
14. *Roobol, Sander, et al.* BINoculars: data reduction and analysis software for two-dimensional detectors in surface X-ray diffraction //Journal of applied crystallography 48.4, 1324-1329, 2015.
15. *Pertsev N. A., A. G. Zembilgotov, and A. K. Tagantsev.* Equilibrium states and phase transitions in epitaxial ferroelectric thin films //Ferroelectrics 223.1, 79-90, 1999.
16. *Bratkovsky A. M., Levanyuk A. P.* Smearing of phase transition due to a surface effect or a bulk inhomogeneity in ferroelectric nanostructures //Physical review letters, Physical review letters 94.10, 107601, 2005.
17. *Holy, Vaclav, Tilo Baumbach, and Ullrich Pietsch.* High-resolution X-ray scattering from thin films and multilayers. //Springer, 1999.
18. *Boulle, A. et al.* A new method for the determination of strain profiles in epitaxial thin films using X-ray diffraction //Journal of applied crystallography 36.6, 1424-1431, 2003.
19. *De Boor C. et al.* A practical guide to splines. Vol. 27. //New York: Springer-Verlag, 1978.
20. *Abbaschian, Reza, and Robert E. Reed-Hill.* Physical metallurgy principles //Cengage Learning, 2008.

AN OPTIMAL SHAPING FOR QAM MODULATION AND NON-UNIFORM DISTRIBUTION OF SOURCE DATA SYMBOLS

R. Shaniiazov

Department of Information Systems Security
SUAI
190000 Bolshaya Morskaya str., 67, St. Petersburg, Russia
Email: rost5000@vu.spb.ru

Abstract—This paper concerns new effective method of joint data coding/modulation which may improve energy-efficiency and energy savings of modern wireless transmission systems. The method require a priori knowledge of input data probability distribution to map them to the modulation symbols in the most efficient way.

Keywords — Quadrature amplitude modulation, Joint source-channel coding, QAM. SQAM, modulation, IoT.

INTRODUCTION

In this paper, we continue research in Statistical QAM (S-QAM) algorithm for messages which has non-uniform distribution of input symbols. The work is based on the ideas from the article of Anton Sergeev and Andrey Turlikov “JOINT SOURCE CODING AND MODULATION FOR LOW-COMPLEXITY VIDEO TRANSMISSION” [6] and corresponding patent of the same authors. The key research questions of this paper are “What is the maximum accessible BER-SNR gain for S-QAM approach considering distribution of the input symbols in comparison with typical QAM”?

The suggested solution is analyzed from the position of the Bit Error Rate, analyzing of energy signal, analyzing of noise, structure QAM constellation. All the explanations are shown for QAM system. Statistical QAM is based on the following two ideas. Firstly, the exponential

distribution is used to make a distribution of the image pixels closer to the non-uniform distribution. Secondly, the resultant values of the processed symbols are mapped into the constellation point according to their frequency.

The exponential distribution is the usual situation in real life and has a lot of in common with the output of real codecs or generators of values or sensors. This distribution is well-known and easy modulating in the different types of a programming environment.

In this work, let use the typical scheme of transfer data which consist:

1. Source of data symbols
2. Source coding to compress the alphabets.
3. Data modulation scheme. In this work, we will use Quadrature Amplitude Modulation (QAM).
4. Noisy communication channel.

Typical scheme of a data transfer is shown in figure 1.

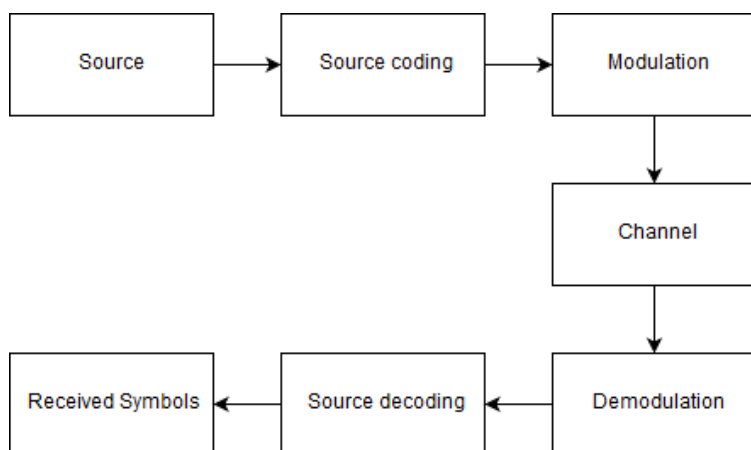


Fig. 1. Scheme of data transfer

Data transfer scheme

Due to the rapid growth of capacity demand in core networks and the advancement of digital

coherent detection technology, high-order M-ary quadrature amplitude modulation (QAM) formats such as square 16QAM and 64QAM have attracted significant attention due to their potential to realize

very high-speed transmission at high spectral efficiencies [4, 5].

Modulation

Modulation and demodulation QAM consist of the following main blocks:

1. Getting a value that is distributed according to the uniform continuous. Value are ranging from 0 to $M - 1$
2. Coding by Gray code [3].
3. A matching of the points to the constellation M-QAM and giving signal x which has two carriers shifted in phase by 90 degrees are modulated and the resultant output consists of both amplitude and phase variations.
4. Transmitting signal over the communication channel and adding a noise.
5. Receiving the signal and constellation decoding with the method neighbour [1] (Using midway point between 2 symbols as the detection threshold). If the noise was a huge the value of signal could move to another nearest point.

Average energy of QAM

Рассмотрим типичную схему модуляции 16-QAM, где алфавиты

$$\alpha_{QAM16} = \left\{ \begin{matrix} \pm 1 \pm i & \pm 1 \pm 3i \\ \pm 3 \pm i & \pm 3 \pm 3i \end{matrix} \right\} \quad (1)$$

For example, the average energy of QAM16 is $E_{QAM16} = 10$ [2].

Each point in constellation is symbol. QAM16 use 16 symbols. This value will be called $M = 16$.

The average power in general standard M-QAM in which probability distribution of input values is considered to be uniform is calculated as follows [6]:

$$E_s = \sum_{i=0}^{K-1} \sum_{j=0}^{K-1} p_{i,j} [(2i - K + 1)^2 + (2j - K + 1)^2] \quad (2)$$

p_i is probability of symbol, $K = \sqrt{M}$.

Noise Model

Let the received symbol is,

$$y = k\sqrt{E_s}s + n \quad (3)$$

Where $k = \sqrt{\frac{1}{\frac{2}{3}(M-1)}}$ is the normalizing factor. Value of k will be used $k = \frac{1}{\sqrt{10}}$ for $M = 16$ (QAM16). s is transmit symbol at the constellation and n is the noise. Assuming that the additive noise follows from the Gaussian probability distribution function,

$$p(x) = \frac{1}{\sqrt{2\pi\sigma^2}} e^{-\frac{(y-u)^2}{2\sigma^2}} \quad (4)$$

With $\mu = 0$ and $\sigma^2 = \frac{N_0}{2}$. If noise has huge

value, can go to another point and be decoded wrong.

Input distribution of a source

In this work, we want to use different types of distribution. In usual schemes of data transfer, we can see data compression block, as the result, the input symbols of modulation algorithms distributed uniformly because all redundancy was dropped. The probability of symbols is $p(r) = 1/M$.

However, if a compression block is not used, we can face non-uniform distribution. Distributions of data symbols which are similar to exponential we can find e.g. in lossless image and video coding and prediction. [6]

The second distribution will be an exponential distribution with probability with probability of symbols $p(r) = \exp(-\lambda * r) / Z(\lambda)$, where λ is regularization parameter of bit-rate. It is clear if $\lambda = 0$ we obtain a uniform distribution and $Z(\lambda) = \sum_{r \in \alpha_{QAM}} \exp(-\lambda * r)$ is normalization factor for distribution. The histogram of distribution are shown in figure 2.

When the criterion is one of minimizing the average transmitted energy for a given average bit rate, the best possible distribution with which to select constellation points is a Maxwell-Boltzmann distribution [7]. Let use the probability of symbol: $p(r) = \exp(-\lambda * ||r||^2) / Z(\lambda)$, where $||r||^2$ is an energy of symbol into constellation. The histogram are shown in figure 3.

Bit rate of a source

The average transmitted bits can be estimated. The Shannon proof that the average length of optimal code L can be estimated as $H \leq L \leq H + 1$

Where H is the entropy of a source. The formula:

$$H = - \sum_{r \in \alpha_{QAM}} p(r) \log p(r) \quad (5)$$

The maximum entropy $H = \log M$ can be obtained if uniform distribution is used. In this work we will use the entropy metric of a input symbols instead of the average length of code (bit rate).

Statistical QAM

The average energy is calculated as uniform distribution. If cryptography or data compression not included in the processing of symbol, there is used an exponential distribution in real systems. Every symbol has a different probability.

Main idea

The main idea of Statistical QAM (S-QAM) for exponential distribution is to map the most frequent input values to the QAM symbols with the lowest transmission energy. As the result, the average energy

consumption of the transmission system is seriously decreased because the low-energy modulation values are transmitted more common than the value with higher energy level.

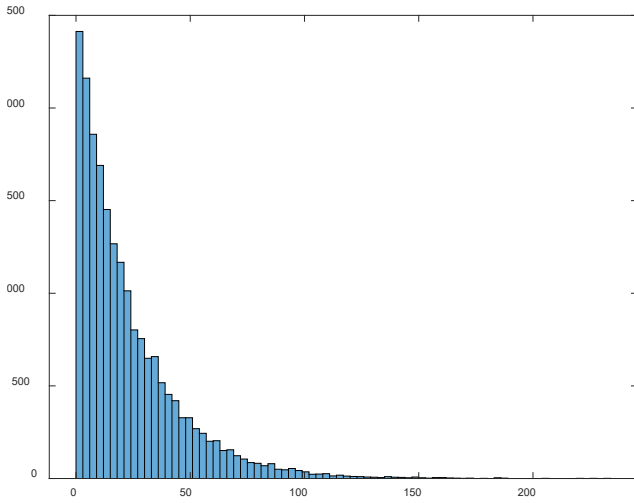


Fig. 2. Exponential distribution for $M = 256$ and entropy = 5.94

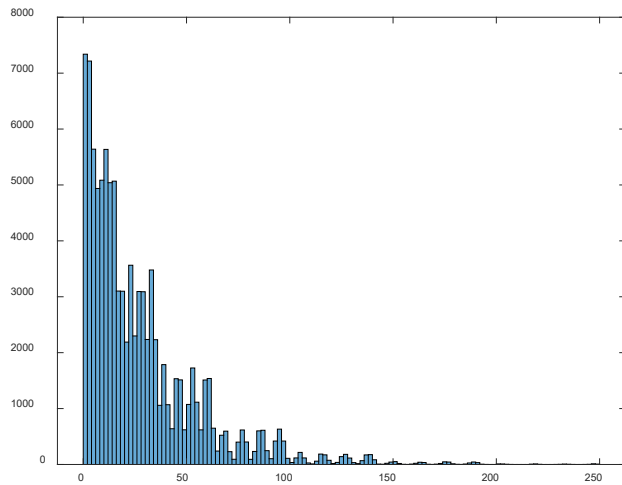


Fig. 3. Maxwell-Boltzmann distribution for $M = 256$ and with entropy = 5.949

Problem definition

The channel characteristics should not change in different schemes, however, the input distribution influences on the channel conditions. For example, the maximum capacity of input symbols can be achieved if and only if the source has the uniform distribution, otherwise channel is not used fully [7]. So, compare two signals with different energy and entropy is not correct enough because they have different statistic values.

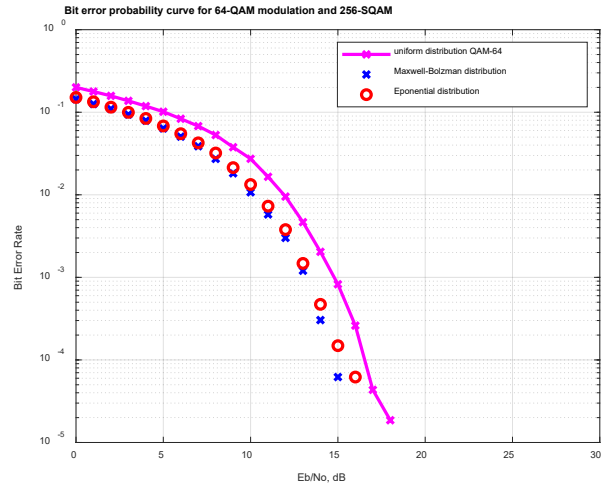


Fig. 4. BER-SNR curve for QAM and SQAM with entropy = 6

Let use the formula from section II-B for calculating of energy for a sprawling constellation and average energy. For example, the average energy for QAM16 is $E_{QAM16} = 10$:

$$10 = \sum_{i=0}^{K-1} \sum_{j=0}^{K-1} A^2 p_{i,j} \left[\begin{matrix} (2i - K + 1)^2 + \\ + (2j - K + 1)^2 \end{matrix} \right] \tag{6}$$

Where A is the coefficient of sprawling of the constellation. A can be gained

$$A^2 = \frac{10}{\sum_{i=0}^{K-1} \sum_{j=0}^{K-1} p_{i,j} \left[\begin{matrix} (2i - K + 1)^2 + \\ + (2j - K + 1)^2 \end{matrix} \right]} \tag{7}$$

This formula depends on a probability of each symbol, but the probability of symbols depends on exponential distribution, which has the features such as mathematical expectation or intensity of input inflow. If one of these characteristics could be gained, the A coefficient would be gained for SQAM.

Compare two signals with different energy is not correct enough because they have different energy level. QAM with exponential distribution can be comparable with usual QAM if they have the same average power. The average power of QAM can be increased by increasing distance between points in the constellation.

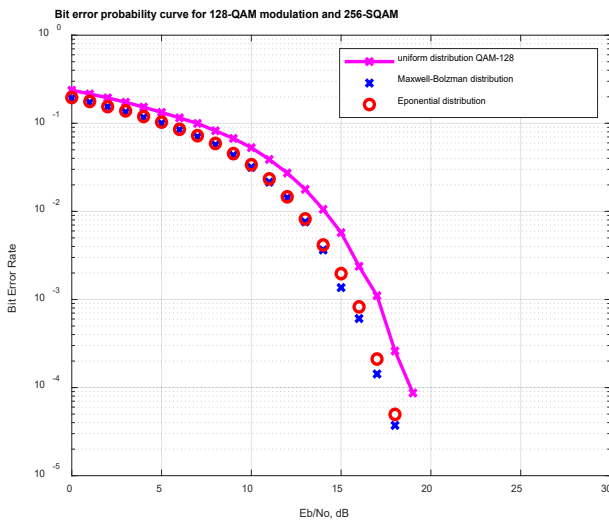


Fig. 5. BER-SNR curve for QAM and SQAM with entropy = 7

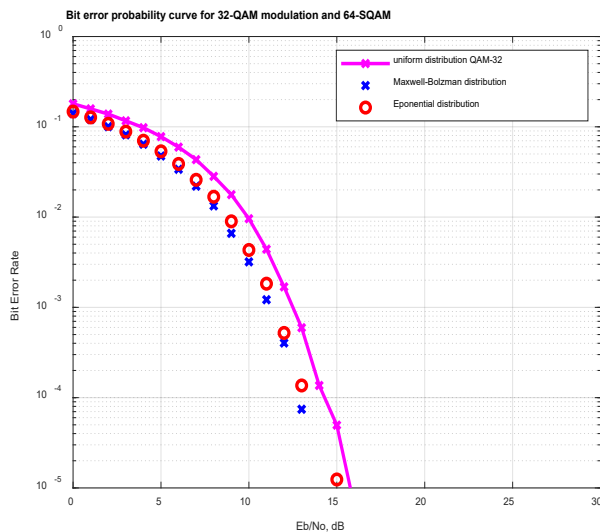


Fig. 6. BER-SNR curve for QAM and SQAM with entropy = 6

Consider if non-uniform distribution is used, the average bit rate is seriously decreasing, we should compensate also the average bit rate. The idea is simple if the maximum entropy of uniform distribution is $\log M$, that let use the QAM modulation with the smallest order in comparison with QAM with non-uniform distribution. For example, let use QAM64 with uniform distribution and QAM256 with non-uniform distribution, however, the entropy will be equal ($H = 6$).

Practical results

The Matlab codes used for generating signal QAM64/SQAM256 and QAM128/SQAM256 and transmission at a channel, pass it through additive white Gaussian noise and demodulation at the receiver will be useful for understanding the concept further. The results are shown in figure 4, 5 and 6. Meanwhile, if the value of the mathematical

expectation is large, when the distribution resembles a uniform one, the gain from the proposed modelling scheme will be minimal.

The results of gain for different dimensions of the constellation in QAM are shown in table 1. The symbol error rate plots obtained from simulations compare well with the theoretical formulas.

TABLE I. GAIN FOR DIFFERENT DIM.

QAM with uniform distribution	SQAM with non-uniform distribution	Gain (dB)	Entropy
32	64	1,5	4,9
64	256	2	5,9
128	256	1,5	6,9

Conclusion

The paper presents the results of gain of the so-called shaping constellation that takes into account the probability of the input flow symbol in comparison with the "traditional" scheme. The estimation was made for a quadrature-amplitude modulation scheme with 32/64/128/256 points in the constellation (QAM32/64/128/256) for uniformly and exponentially distributed input characters.

Evaluation of both methods (QAM + uniformly-distributed input symbols and SQAM + exponentially distributed entry) was made on the criterion of the BER-SNR for AWGN channel using simulation modeling. Experiments have shown that with equal average energy costs, the gain for SCAMS in bit error rate is up to 2 Db. The gain is achieved by more frequent transmission of symbols with low energy than symbols with high energy. At the same time, if the input signal is changed to uniform (while maintaining the display of SQAM points), the loss is also not observed.

References

1. A. Andoni and P. Indyk. Near-optimal hashing algorithms for approximate nearest neighbor in high dimensions. In *Foundations of Computer Science, 2006. FOCS'06. 47th Annual IEEE Symposium on*, pages 459–468. IEEE, 2006.
2. J. R. Barry, E. A. Lee, and D. G. Messerschmitt. *Digital communication*. Springer Science & Business Media, 2012.
3. A. P. Hiltgen, K. G. Paterson, and M. Brandestini. Single-track gray codes. *IEEE Transactions on information theory*, 42(5):1555–1561, 1996.
4. J. Hongo, K. Kasai, M. Yoshida, and M. Nakazawa. 1-gsymbol/s 64-qam coherent optical transmission over 150 km. *IEEE Photonics Technology Letters*, 19(9):638–640, 2007.

5. Y. Mori, C. Zhang, K. Igarashi, K. Katoh, and K. Kikuchi. Unrepeated 200-km transmission of 40-gbit/s 16-qam signals using digital coherent receiver. *Optics Express*, 17(3):1435–1441, 2009.

6. A. Sergeev, A. Turlikov, and A. Veselov. Joint source coding and modulation for low-complexity video transmission.

7. Shannon, C. E. (1948). A mathematical theory of communication. *Bell system technical journal*, 27(3), 379-423.

DEVELOPMENT OF AUTOMATED SYSTEM OF SITE SELECTION FOR EVENTS CONSIDERING QUALITY INDICATORS

D. Shchukina

Student Department Innovative and integrated quality systems
 Federal State Autonomous educational institution of higher Education St. Petersburg State University of
 Aerospace instrumentation
 Bodies: + 7-921-857-29-57
 E-mail shchukinad@icloud.com

Abstract

The difficulty of choosing a venue for events is due to the inability of choice according to the required criteria depending on the event and equipping the site. To solve this topical problem, it is necessary to create a site selection model for the event and establish a correlation relationship between the requirements of the consumer and the capabilities of the site (organizer) by creating a prototype Applications for automation of site selection for various events.

Keywords: evaluation of the quality, organization of events, automation.

According to the decision of administration of St. Petersburg in the Statute on the procedure for organizing holiday and other entertainment events, organizing and conducting entertainment events for the State University of aerospace Instrumentation (SUAE) is a current theme of the development models of automated site selection for activities for students and teachers. This is important in view of the fact that in a large number of students are studying SUAI and carried out many activities aimed at the development of education and Science (conferences, competitions, workshops), and organizing mass events University allocates a substantial budget to reduce the cost of quality parameters must be defined on the basis of which will be given a choice. But the search area (organizer) for scientific and educational activities to date is a problem.

Just as in the possibilities of automated selection of venues for events of various kinds needs not only of SUAI, this problem is topical and systems market selection of sites for holding mass events. Figure 1 shows the picture with the Organization of the all-Russia Forum Patriot III cosmonautics and aviation KosmoStart 2018 "

SUAI students took part in the Forum and appreciated the Organization of mass events. Were given all the quality parameters required for the event.

The set of quality traits should correspond to characteristics of the object of evaluation and provide the possibility of full information support of management decision processes at all levels of management.

For the ability to assess venues for the event and installation of correlation dependencies between consumer requirements and opportunities (organizer) needs to consider the tentative signs of various sites for determine whether they meet the requirements of the consumer. Identified indicators assess the quality sites:



Figure 1 example of activities within the framework of the III all-Russian patriotic Forum space and aviation KosmoStart 2018 "

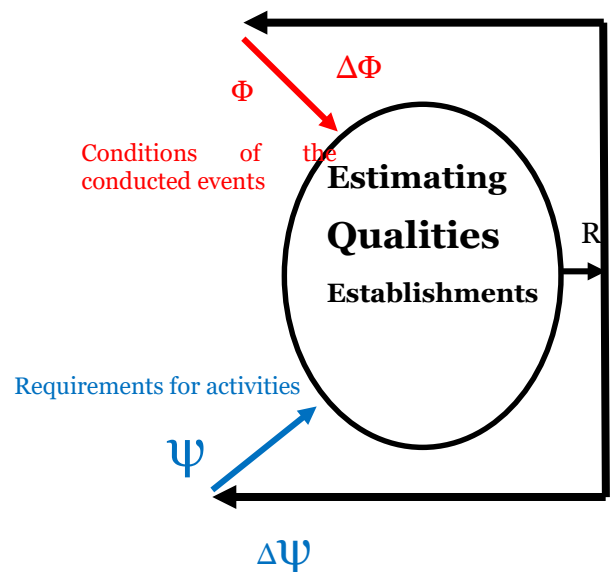


Figure 2. Typology of signs of quality assessment

- the presence of the event;
- the existence of an appropriate event software;
- fire safety;
- transport accessibility area (distance from Metro, transport congestion);
- size of the room;
- illumination of premises;
- relevant characteristics;
- relative humidity;
- air temperature;
- air pressure;
- the concentration of harmful substances in the air;
- the life cycle of the object;
- occupancy of the premises.

Each basis should be put in line measurement scale quantitative or qualitative parameters. This can be used the whole range of existing scales:

- nominal scale;
- ordinal scale;

- interval scale;
- scale relations.

The proposed procedure is based on building a comparative evaluation of the characteristics of an object composed of homogeneous systems.

- A set of signs that describe the State of each system must have a range of properties:
 - perfection of representation of each element of the system;
 - possibility of composition and decomposition of typological groups of signs;
 - izmerimostju each trait on quantitative or qualitative level;
- the possibility of the formation of integrated indicators.

Let the object of evaluation consists of n homogeneous systems $S_j(j \in \overline{1, n})$ each of which can be assessed the same set of m signs $P_i(i \in \overline{1, m})$. Then the results of the evaluation of all systems on each basis can be represented in matrix form:

Table 1 estimates of venues for events

Площадки мероприятий		Логистические																																																																																																																																																																																																																																																																																																																																																																																							
Наименование	Показатели	Относительная влажность, %	Освещенность, Лк	Возможность парковки, мест/чел.	Удаленность от метро, м	Площадь помещения, м ²	Высота потолков, м	N																																																																																																																																																																																																																																																																																																																																																																																	
									5	6	7	8	9	10	11	12	13	14	15	16	17	18	19	20	21	22	23	24	25	26	27	28	29	30	31	32																																																																																																																																																																																																																																																																																																																																																					
Евразия	→	51	→	141	→	9	→	889	→	181	↑	4,1	↓	ПетроКонгресс	→	49	→	125	→	8	↓	334	→	243	→	3,5	→	Олимпия	→	55	→	172	→	5	→	1529	→	173	→	3,8	→	Park Inn	→	49	→	163	→	8	→	684	→	120	→	3,9	↑	Мансарда	↑	60	↓	114	→	3	→	1073	↑	283	→	3,6	→	Палкин	→	46	→	162	→	3	→	1588	↓	87	↑	4,2	↓	Aglaya Hotel & Courtyard	→	55	→	155	→	3	→	1745	→	128	↓	3,0	→	Мука	→	54	↑	210	→	7	→	1327	→	228	→	3,5	→	Юникс Эдьюкейшн Центр	↑	60	→	181	→	7	→	1430	→	138	→	3,6	↓	Sreda project	↓	39	→	125	→	7	↑	1807	→	197	↓	3,1	↑	Ministerstvo	→	51	↓	112	→	6	↑	1888	→	237	→	4,0	→	Ординарная 16	→	52	→	137	↓	1	→	854	→	144	→	3,7	→	Место Роста	↓	38	↑	208	→	2	↑	1925	→	181	↑	4,1	↓	Grow Up	→	55	→	121	→	6	→	1617	→	115	→	3,4	→	Девять и три четверти	→	55	↓	114	→	3	↓	441	→	111	↓	3,1	→	Artplay Spb	→	55	→	186	→	9	→	560	↑	289	→	4,0	→	Эрарта	→	56	→	158	↑	10	↓	300	→	241	→	3,6	→	Манеж	→	51	↓	106	→	7	→	679	→	235	→	3,9	↓	Центральная библиотека им. М.Ю. Лермонтова	→	45	→	135	↓	1	↓	407	↑	280	↑	4,2	→	Ленэкспо	↑	60	→	165	↓	1	→	531	→	138	→	3,7	→	Экспофорум	→	42	→	174	→	7	→	568	→	197	→	3,4	→	АРТМУЗА	→	53	↓	107	→	5	→	1692	→	151	→	3,8	→	Буревестник	→	56	→	129	→	7	→	1519	↓	95	↑	4,1	→	Дом молодежи Санкт-Петербурга	→	42	→	162	→	3	→	1000	→	259	→	3,3	↑	ЕСОД	→	55	↓	113	→	9	→	1642	→	163	→	3,2	→	Флигель	↑	58	→	185	→	6	→	1628	→	196	→	4,0	↓	Julia Child Bistro	→	47	→	178	→	3	→	494	→	154	↑	4,1	→

$$P = \|p_{ij}\|, i = \overline{1, m}, j = \overline{1, n}$$

where the p_{ij} -nominal value (i)-the sign of j-assessment of the system. This matrix can contain data from different measurement systems, depending on the type of scales, and is starting to define the boundaries of situational rules and integral calculation of the relative quality of each system. When you use the percentilnogo approach bounds situational rules defined for each indicator statistics on the basis of the calculation of values of an arbitrary set of percentilej. In general terms, this set can be represented as a multitude of R_k ($k = 1, 2, 3, \dots, 100$). In practice, it is more convenient to use the percentile the following:

- $R_{min} = R_0$ – zero percentile;
- $R_{0,1} = R_{10}$ – the tenth percentile;
- $R_{0,25} = R_{25}$ – twenty-fifth percentile;
- $R_{0,75} = R_{75}$ – seventy-fifth percentile;
- $R_{0,9} = R_{90}$ – ninetieth percentile;
- $R_{max} = R_{100}$ – the 100th percentile.

The table 1 presents the results of the analysis. the most popular sites on the territory of Saint-Petersburg on the above grounds.

Next, on the basis of calculations carried out a comparative analysis of the different sites in the number 27 pieces of 15 indicators (figure. 4). After comparative analysis identified platforms meet the requirements of a specific customer.

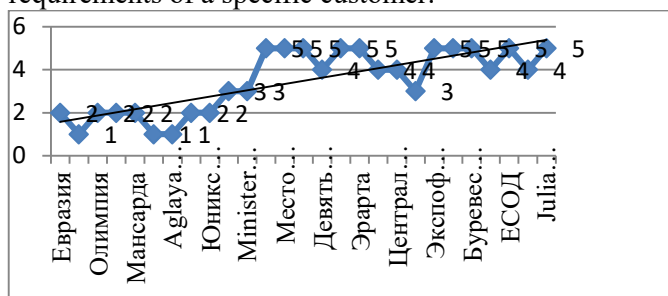


Figure 3. Generic quality assessment for Visual selection

Based on the developed technique built a mock-up of a mobile application for the service GOOGLEPLAY. Figure. 4 showingpage layouts.



Figure 4. Layout mobile application for automated searching sites for events on selected quality indicators and required criteria

Conclusion

Use the model selection of venues for events in the Organization of cultural events allows you to choose a venue for the activities corresponding to the selected quality indicators and the stated criteria. How to create a model for the selection of sites for certain events and mobile application allows you to not only improve the quality of the event itself, but also significantly reduce the time needed for the selection of the site and the amount of funds expended. This work describes the layout of the mobile application, identified indicators assess the quality of sites and comparative analysis of different sites located on the territory of St. Petersburg.

References

1. Chabanenko A.V., Semenova E. G. Nazarevich S.A., Diagnostic tools to improve the quality of the technical system. Selected scientific works of the sixteenth International Scientific and practical conference «quality management» M., 2018. 1 (444) pp. 280-288/

DEVELOPMENT OF AUTOMATED PRODUCTION PLANNING SYSTEM BASED ON LEAN PRINCIPLES

E. Skorniakova

Saint-Petersburg State University of Aerospace Instrumentation,
Saint-Petersburg, Russia
E-mail: elizavetasesina@mail.ru

Annotation

Methods and tools of lean manufacturing that must to be used in planning process of high-productivity plant are described. Necessity of it applying and benefits in case of correct usage is explained.

Keywords: lean manufacturing, production system, production planning, production plan, standardization, PDCA, tact time, Nemawashi, visualization.

A strategic management approach is imperative for the company's stable development. Strategic planning methods are rapidly spreading to all areas of industrial activity. This is related to unstable economic situation and efforts of companies to be prepared for any changes in environment.

Taking into account tight deadlines for reaction on changing conditions, companies are buying or developing integrated systems that takes into account various factors that affecting on efficiency of production processes, quality level and costs. At present, modern production planning methodologies are implemented by various classes of information systems. The most famous are MRP and ERP [1, 2] systems, as well as more modern systems CSRP, MES and APS. It should be noted that not all currently existing automated systems are based on globally recognized principles of "lean manufacturing" [3, 4]. That is why creation of systems that allow to take into account these principles remains actual to the present day.

Lean manufacturing principles are all-pervading and applicable to all processes of the company, but very often is situation when management applies them "pointwise", mainly in production processes, while losing sight of administrative and production processes, such as production planning, parts ordering and etc.

Production planning is one of the most strategic processes in any company and needs to be under special control. Automated planning system [5, 6] should create a plan that use company resources as efficient as it possible, especially when it used for high-productivity plant. Automation of the planning process is primarily intended to standardize this process, standardize the format of used data and constantly improve it in the future. The basic principles and tools that are must to be used in planning system are presented in Figure 1.

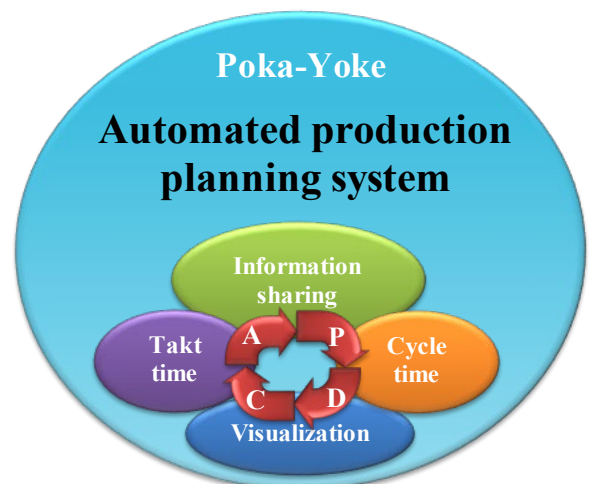


Fig. 1. Lean manufacturing principles in production planning

Automated planning system is a special case of Poka-Yoke – tool against unintentional mistakes. Process automation is intended to complete elimination of mistakes or “defects” in planning. Practice shows that during plan creation in Excel files in Microsoft Office, mistakes occurs frequently, even in conditional formatting and special macroses are used. Therefore, only process automation can completely eliminate the possibility of mistakes in the plan. In addition to errors elimination, standard format is defined, which also simplifies and speeds-up process of data gathering and handling. Standardization of processes is one of the main objectives of lean manufacturing principles applying.

Production planning process is cyclical and for high-productivity plants these cycles are repeated monthly due to receiving of more accurate forecasts from customers. For standardization and continuous improvement, planning process should be carried out according to the PDCA principle (Fig. 2), as well as its subprocesses [7].

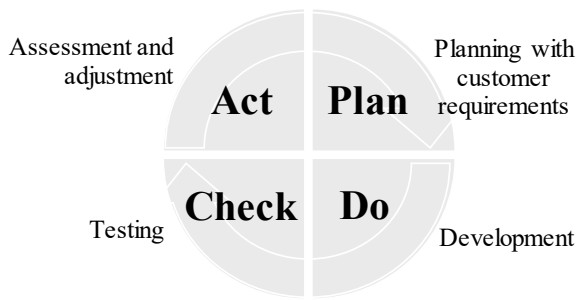


Fig. 2. PDCA cycle of production planning process

PDCA cycle is the basis of iterative approach applied for development of automated planning system.

The main goal to which any company should strive is just-in-time production of only the necessary quantity of high-quality products with minimal cost. The described production principle can be expressed as follows:

$$\Delta \rightarrow 0 \text{ where } \Delta = Q_{\text{production}} - Q_{\text{order}}$$

Production of only the required number of products included in the production plan in the form of “takt time” (BT) [8]. The takt time (TT) is a calculated value obtained by dividing of customer order by available production time. In essence, TT is the speed with which consumer wants to receive a unit of finished products. For high-productivity production TT measures in seconds. Depending on this time, each shop create design of its own processes. Change from one TT to another is a complex process and it needs to be included as a restriction from each shop or department involved in production process.

Taking into account TT and operational ratio (OPR), volume of production can be calculated by the following formula:

$$Q = \frac{t_{\text{avail.work.}} \cdot OPR}{TT}, \tag{1}$$

where Q- quantity of produced products, $t_{\text{avail.work.}}$ -available for production working time, TT – takt time, OPR – Operational Ratio.

OPR coefficient allows to input in plan risks related with unplanned stoppages due to possible defects, introduction of various projects into production, production of trial batches of products, testing of new equipment and etc.

It should also be noted that almost all shops/ departments of plant are involved in the production planning process, so “information sharing” (Nemawashi) is particularly important.

It should also be noted that almost all shops and departments of the plant are involved in the production planning process, so “information sharing” (Nemawashi) is very important. Creation of production plan starts with the process of information

exchanging (gathering of restrictions and information from shops and departments involved in planning process) and ends with it (evaluation of plan options). It is impossible to create correct and effective plan without Nemawashi. Planning and information sharing are processes that are related to each other. In order to maximize efficiency of information exchange, automated planning system need to be created in the form of a unified information environment. The interaction of plant shops and departments in the process of production planning through informational links is described using the Graph theory (Figure 3) [7, 9].

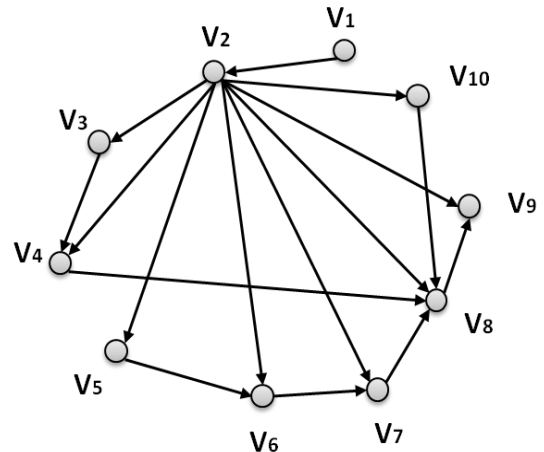


Fig. 3. Oriented graph that shows interaction of shops and departments in production planning process

In order to streamline the interaction of participants in the process (V_1, V_2, \dots, V_{10}) methods of separating internal stable subsets (the Malgrange method) and further topological sorting of the graph-separation into significance levels by the Demucron method (Figure 4) are used.

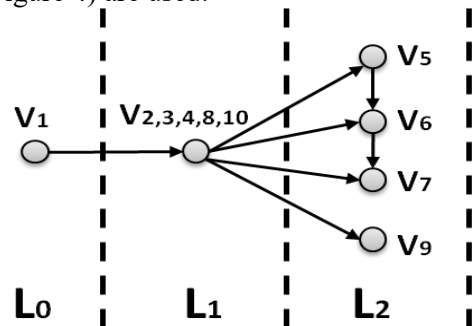


Fig. 4. Graph separated into significance levels

Application of such a method will allow to conduct workflow within any independent subset.

Particular attention should be paid to visualization in production planning process. Result of this process is created production plan – a plan with included assessment by all departments and shops that are involved in studied process. Since plan is a document that is submitted for approval by top

managers, it should be as informative and simple as possible. The most common mistake is "overloaded" or oversaturated documents, especially this is very often in planning, since the work is carried out with a large array of data.

All described elements were included in the created automated system. As a result, it was possible to significantly improve the effectiveness of the planning process, reduce time of plan creation and its assessment, standardize formats of data that used and make the process more "clear" for all participants.

REFERENCES

1. Gavrilov D. A. Production management based on MRP II standards. SPb.: Piter. 2005. 416 p.
2. Evgenev G.B. Fundamentals of automation of technological processes and production #01. Moscow State Technical University named after N.E. Bauman Publ. 2015. 441 p.
3. Varshapetian A., Semenova E. Aspects of integration management methods. International Journal for Quality Research. 2015. 9 (3). Pp. 481-494.
4. Grodzenskiy S.Y., Emanakov I.V., Ovchinnikov S.A. The concept of lean manufacturing and its application in the enterprise. Information Innovative Technologies. 2017. № 1. Pp. 227-229.
5. Skorniakova E.A. Model of quick response system for production planning. Quality and life. 2018. 2 (18). Pp. 39-41.
6. Sesina E. A. Model of risks movement during on-line data interchange in production planning process. Collected works of IX All- Russian research-to-practice conference «Innovatcionnie tehnologii i tehicheskie sredstva specialnogo naznacheniya» [«Innovation technology and technical means of special assignment»], book II. BALTIC STATE TECHNICAL UNIVERSITY «VOENMEH» named after D.F. Ustinov, Saint- Petersburg, Russia, 2017. Pp. 154-155.
7. Skorniakova E.A., Babaev S.A. Problems of prompt management decision making due to diviations in production planning process of high-productivity. Problems of endengineering and automation. 2018. 4. Pp. 36-39.
8. Liker J. The Toyota Way: 14 Management Principles from the World's Greatest Manufacturer. Moscow: Alpina Publisher. 2014. 400 p.
9. Kofman A. Introduction into Applied Combinatorial Analysis. Nauka, Moscow. 1975.

ANALYSIS OF COMPLEX FILTERS BASED ON TRANSITION CHARACTERISTICS

Yu. Sokolova

Student

Saint-Petersburg State University of Aerospace Instrumentation, Russia

E-mail: julia.12@mail.ru

Abstract

A method of research of complex filters with use of transition characteristics is developed. By the way of presenting complex input signal as sum of offsets of two stepped influences we have received a new form of complex integral of overlay, which allows, with pre-set complex input signal and known complex transition characteristic of a filter to find its output signal. We have showed that usage of complex filters allow to change frequency of setup easily and without changing amplitude and phase-frequency characteristics. We have introduced definitions of complex delta-function and complex transition characteristic, used for researching of dynamic properties of filters and analysis of transfer of various signals. In comparison to known methods of analysis of linear systems based on impulse characteristic, method proposed allows to synthesize complex discrete filters, dynamic properties of which is comparable to dynamic properties of uninterrupted filters. Proposed theoretical statements are proven by particular examples.

Keywords: complex signal, complex filter, complex impulse characteristic, complex transition characteristic, integral of overlay.

INTRODUCTION

In information processing most frequently being used procedure of filtering of signals with filters of hi and low frequencies., band and notch filters. in some cases, adaptive and complex filters are being used, parameters of which can be changed, depending on spectral characteristics of signals. In complex filters managing frequency of transfer function of a filter is easier than in actual filters.

In present moment, the theory of research of passing signal through various filters is well-developed [1—7].

Exhaustive characteristic of a filter is its frequency-transfer function. For filter analysis 2 methods are being used – frequency and time based. In case of frequency method of research of linear system with frequency bypass function $W(j\omega)$ complex output signal $z_{\text{BIX}}(t)$ with known spectral solidity $z_{\text{BX}}(j\omega)$ of complex input signal $z_{\text{BX}}(t)$ determined based on reverse Fourier transformation [1, 2]:

$$z_{\text{BIX}}(t) = \frac{1}{2\pi} \int_{-\infty}^{\infty} W(j\omega) z_{\text{BX}}(j\omega) e^{j\omega t} d\omega.$$

When using time method of analysis of complex filters with impulse characteristic $h^*(t)$ Duamel integral is applied [2, 3]:

$$z_{\text{BIX}}(t) = \int_0^{\infty} z_{\text{BX}}(t-\tau) h^*(\tau) d\tau, \quad (1)$$

where complex input $z_{\text{BX}}(t)$ and output $z_{\text{BIX}}(t)$ signals and also complex impulse characteristic $h^*(t)$ determined as

$$\begin{aligned} z_{\text{BX}}(t) &= x_{\text{BX}}(t) + jy_{\text{BX}}(t); \\ z_{\text{BIX}}(t) &= x_{\text{BIX}}(t) + jy_{\text{BIX}}(t), \\ h^*(t) &= h_x(t) + jh_y(t). \end{aligned} \quad (2)$$

In correlations (2) $x_{\text{BX}}(t)$ and $y_{\text{BX}}(t)$ – quadrature parts of input signal; $x_{\text{BIX}}(t)$ and $y_{\text{BIX}}(t)$ quadrature parts of output signal; $h_x(t)$ and $h_y(t)$ – quadrature parts of an impulse characteristic of a complex filter.

In works [4-6] is shown that when transitioning from uninterrupted filters to discrete present method of calculating coefficients of equations based on countdowns of impulse characteristics does not provide correct realization of transitioning processes. However, method of calculating coefficients using discrete filters, matching with dynamic properties of uninterrupted filters in transitioning as well as set regimes.

In these conditions appears actual problem of developing method of analysis of filters based on its transition characteristics. Solution to this problem takes main part of this article.

INTEGRAL OF OVERLAY WITH THE USE OF COMPLEX TRANSITION CHARACTERISTICS

For finding a solution of problem presented, parts $x_{\text{BX}}(t)$ and $y_{\text{BX}}(t)$ of complex input signal $z_{\text{BX}}(t)$ we

will present as sum of sequence step functions, beginning in the moments t_1, t_2, \dots, t_n :

$$\begin{aligned} x_{\text{BX}}(t) &= [x_{\text{BX}}(t-t_1) - x_{\text{BX}}(t-t_0)] + \\ &+ [x_{\text{BX}}(t-t_2) - x_{\text{BX}}(t-t_1)] + \dots \\ &[x_{\text{BX}}(t-t_i) - x_{\text{BX}}(t-t_{i-1})] \dots = \\ &= \Delta x_{\text{BX}}(t_1) + \Delta x_{\text{BX}}(t_2) + \dots + \Delta x_{\text{BX}}(t_i) + \dots; \\ y_{\text{BX}}(t) &= [y_{\text{BX}}(t-t_1) - y_{\text{BX}}(t-t_0)] + \\ &+ [y_{\text{BX}}(t-t_2) - y_{\text{BX}}(t-t_1)] + \dots \\ &[y_{\text{BX}}(t-t_i) - y_{\text{BX}}(t-t_{i-1})] \dots = \\ &= \Delta y_{\text{BX}}(t_1) + \Delta y_{\text{BX}}(t_2) + \dots + \Delta y_{\text{BX}}(t_i) + \dots, \end{aligned}$$

where $\Delta x_{\text{BX}}(t_i) = x_{\text{BX}}(t-t_i) - x_{\text{BX}}(t-t_{i-1})$, $\Delta y_{\text{BX}}(t_i) = y_{\text{BX}}(t-t_i) - y_{\text{BX}}(t-t_{i-1})$ – elementary step functions, appearing in moment $t = t_i$.

And complex input signal is determined by expression

$$z_{\text{BX}}(t) = \sum_{i=1}^{\infty} \Delta x_{\text{BX}}(t_i) + j \sum_{i=1}^{\infty} \Delta y_{\text{BX}}(t_i).$$

In result complex output signal of filter will be determined as equation

$$z_{\text{BBIX}}(t) = \begin{bmatrix} \sum_{i=1}^{\infty} \Delta x_{\text{BX}}(t_i) + \\ + j \sum_{i=1}^{\infty} \Delta y_{\text{BX}}(t_i) \end{bmatrix} g^*(t-t_i), \quad (3)$$

where $g^*(t)$ – complex transition characteristic, is a reaction of a filter on complex step input influence $\Delta z_{\text{BX}}(t) = \Delta x_{\text{BX}}(t) + j \Delta y_{\text{BX}}(t)$.

Transition characteristic of a complex filter is found from equation

$$g^*(t) = \int_0^t h^*(\tau) d\tau.$$

Considering fact that $h^*(t) = h_x(t) + j \Delta h_y(t)$, complex transition characteristic $g^*(t)$ is expressed through quadrature parts $g^*(t) = g_x(t) + j \Delta g_y(t)$, where

$$g_x(t) = \int_0^t h_x(\tau) d\tau, \quad g_y(t) = \int_0^t h_y(\tau) d\tau.$$

As result expression (3) is looking like this:

$$\begin{aligned} z_{\text{BBIX}}(t) &= \sum_{i=1}^{\infty} \Delta x_{\text{BX}}(t_i) g_x(t-t_i) - \\ &- \sum_{i=1}^{\infty} \Delta y_{\text{BX}}(t_i) g_y(t-t_i) + \end{aligned}$$

$$+ j \begin{bmatrix} \sum_{i=1}^{\infty} \Delta x_{\text{BX}}(t_i) g_y(t-t_i) - \\ - \sum_{i=1}^{\infty} \Delta y_{\text{BX}}(t_i) g_x(t-t_i) \end{bmatrix}. \quad (4)$$

Let's countdowns of quadrature parts of input signal $x_{\text{BX}}(t_i)$ and $y_{\text{BX}}(t_i)$ with forming of step functions is taken in same periods of time i.e. $t_i = iT$, where T – period of countdowns

Multiplying and dividing expression (4) by T , we got

$$\begin{aligned} z_{\text{BBIX}}(t) &= T \begin{bmatrix} \sum_{i=1}^{\infty} \Delta x_{\text{BX}}(t_i) g_x(t-t_i) / T - \\ - \sum_{i=1}^{\infty} \Delta y_{\text{BX}}(t_i) g_y(t-t_i) / T \end{bmatrix} + \\ &+ j T \begin{bmatrix} \sum_{i=1}^{\infty} \Delta x_{\text{BX}}(t_i) g_y(t-t_i) / T - \\ - \sum_{i=1}^{\infty} \Delta y_{\text{BX}}(t_i) g_x(t-t_i) / T \end{bmatrix}. \end{aligned}$$

In a limit transition with $T \rightarrow 0$ we can express:

$$\begin{aligned} z_{\text{BBIX}}(t) &= \int_0^t \frac{dx_{\text{BX}}(\tau)}{d\tau} g_x(t-\tau) d\tau - \\ &- \int_0^t \frac{dy_{\text{BX}}(\tau)}{d\tau} g_y(t-\tau) d\tau + \\ &+ j \begin{bmatrix} \int_0^t \frac{dx_{\text{BX}}(\tau)}{d\tau} g_y(t-\tau) d\tau - \\ - \int_0^t \frac{dy_{\text{BX}}(\tau)}{d\tau} g_x(t-\tau) d\tau \end{bmatrix}. \quad (5) \end{aligned}$$

The expression received (5) for output signal of complex filter is complex integral of overlay, tying derivations of quadrature parts of input signal and transition characteristic of filter.

It is known that [2, 7] impulse characteristic of linear system is derivative of transition characteristic $h^*(t) = \frac{dg^*(t)}{dt}$. In this case expression for output signal of filter looks like:

$$z_{\text{BBIX}}(t) = \int_0^t z_{\text{BX}}(t-\tau) \frac{dg^*(\tau)}{d\tau} d\tau. \quad (6)$$

In this manner, two equal transformations (5) and (6) allows to find output signal of complex filter with known complex input signal $z_{\text{BX}}(t)$ and transition characteristic $g^*(t)$.

To validate results we will review particular examples.

EXAMPLES

Example 1. Let input signal to be a complex step singular influence $z_{\text{BX}}(t) = 1(t)(\cos \varphi + j \sin \varphi)$, where angle φ can take any values and with $\varphi = 0$ signal becomes material.

For given signal $\frac{dz_{\text{BX}}(t)}{dt} = \delta^*[\cdot] =$
 $= \delta[\cdot](\cos \varphi + j \sin \varphi)$ – complex delta function, after using which in expression (5) we get

$$z_{\text{ВЫХ}}(t) = \int_0^t \delta^*[0] g^*(t - \tau) d\tau = g^*(t).$$

As result with complex singular set input influence, output signal of complex filter is its transition characteristic.

Example 2. Let's review complex band filter of first order with frequency transfer function like

$$W(j\omega) = \frac{1}{1 + j(\omega - \omega_0) / \omega_{\text{CP}}},$$

where ω_{CP} – frequency of filter cut, ω_0 – middle frequency.

On input complex harmonic fluctuation $z_{\text{BX}}(t) = [\cos(\omega t) + j \sin(\omega t)]$ with frequency ω is taking place.

For filter reviewed complex impulse and transition characteristics are [2]:

$$h^*(t) = \omega_{\text{CP}} e^{-\omega_{\text{CP}} t} [\cos(\omega_0 t) + j \sin(\omega_0 t)];$$

$$g^*(t) = \frac{\omega_{\text{CP}}}{\omega_0^2 + \omega_{\text{CP}}^2} \left\langle \begin{array}{l} e^{-\omega_{\text{CP}} t} \left[\begin{array}{l} \omega_0 \sin(\omega_0 t) + \\ \omega_{\text{CP}} \cos(\omega_0 t) \end{array} \right] - \\ + \omega_{\text{CP}} \end{array} \right\rangle -$$

$$- j \left\langle \begin{array}{l} e^{-\omega_{\text{CP}} t} \left[\begin{array}{l} \omega_{\text{CP}} \sin(\omega_0 t) + \\ \omega_0 \cos(\omega_0 t) \end{array} \right] + \omega_0 \end{array} \right\rangle. \quad (7)$$

And derivative of input signal is

$$\frac{dz_{\text{BX}}(t)}{dt} = \omega [\cos(\omega t) + j \sin(\omega t)].$$

After using derivative (5) with expression (7) we will get output signal of filter:

$$z_{\text{ВЫХ}}(t) = \int_0^t \omega [\cos(\omega \tau) + j \sin(\omega \tau)] \frac{\omega_{\text{CP}}}{\omega_0^2 + \omega_{\text{CP}}^2} \times$$

$$\left\langle \begin{array}{l} e^{-\omega_{\text{CP}}(t-\tau)} \left[\begin{array}{l} \omega_0 \sin(\omega_0(t-\tau)) + \\ \omega_{\text{CP}} \cos(\omega_0(t-\tau)) \end{array} \right] + \omega_{\text{CP}} \end{array} \right\rangle -$$

$$- j \left\langle \begin{array}{l} e^{-\omega_{\text{CP}}(t-\tau)} \left[\begin{array}{l} \omega_{\text{CP}} \sin(\omega_0(t-\tau)) + \\ \omega_0 \cos(\omega_0(t-\tau)) \end{array} \right] + \omega_0 \end{array} \right\rangle d\tau.$$

Integral in this formulae is table-like [7]. In final view for regime set we can express following codependencies of output signal of band filter:

$$x(t) = \frac{1}{\sqrt{1 + \left(\frac{\omega - \omega_0}{\omega_{\text{CP}}}\right)^2}} \cos \left(\omega t - \arctg \frac{\omega - \omega_0}{\omega_{\text{CP}}} \right);$$

$$y(t) = \frac{1}{\sqrt{1 + \left(\frac{\omega - \omega_0}{\omega_{\text{CP}}}\right)^2}} \sin \left(\omega t - \arctg \frac{\omega - \omega_0}{\omega_{\text{CP}}} \right).$$

These expressions determining output signal of complex band filter of first order with harmonical input signal.

Received in this work expressions (5) and (6) for complex integral of overlay completing method of analysis of linear systems

CONCLUSION

As a result of research performed, the theory of linear systems has got additional development. Presented form of integral of overlay allows with pre-set derivative of complex input signal and known complex transition characteristic of a filter with pre-set complex input signal, to find output signal of complex filter. Developed method can be used for synthesizing with pre-set transition characteristic of complex discrete of linear systems, dynamic properties of which are equal to dynamic properties of similar uninterrupted linear systems.

REFERENCES

- 1 Воробьев, С. Н. Цифровая обработка сигналов / С. Н. Воробьев М.: Академия, 2013. 318 с.
- 2 Гоноровский, И. С. Радиотехнические цепи и сигналы / И.С. Гоноровский М.: Радио и связь, 1986. 512 с.
- 3 Оппенгейм, А. Цифровая обработка сигналов / А. Оппенгейм, Р. Шафер М.: Техносфера, 2006. 855 с.
- 4 Голд, Б. Цифровая обработка сигналов / Б. Голд, Ч. Рэйдер. М.: Сов. радио, 1973. 367 с.
- 5 Зиатдинов, С.И. Синтез рекурсивных дискретных фильтров во временной области / С. И. Зиатдинов // Известия вузов. Радиоэлектроника. 2016. № 3. С. 3-6.
- 6 Зиатдинов, С.И. Анализ линейных систем на основе переходных характеристик / С. И. Зиатдинов // Информационно-управляющие системы. 2016. № 2. С. 104-106.
- 7 Сергиенко, А. Б. Цифровая обработка сигналов / А. Б. Сергиенко СПб.: БВХ-Петербург, 2015. 756 с.

ROLE OF AUTOMATION IN SAFE FUNCTIONING CROSSROADS

A. Svinina

Saint-Petersburg State University of Aerospace Instrumentation,
Saint-Petersburg, Russia
Email: nastas.97@mail.ru

Abstract: Consideration of the causes of traffic accidents at the intersection, ways of modeling intersections using automated systems. Cross-Bandwidth Analysis.

Keywords: Simulation, intersection, throughput, conflict points, traffic accidents.

CAUSES DANGEROUS SITUATIONS ON CROSSROADS

In recent years there has been a sharp increase in the number of vehicles on the roads, this is due to many factors, for example: the improvement of the economic situation and the general financial well-being of the population. In connection with this, the number of traffic accidents and related problems is growing. In this article we will focus on ensuring safe traffic at the intersection thanks to competent automated equipment.

Crossroads (hubs of the road network) are one of the most important components of the road network. According to the definition, a crossroads is a section of intersection of two or more roads between them. Particular attention to the monitoring of intersections and traffic on them should be given in large cities, where there is more intensive traffic and a high density of traffic congestion.

First of all, crossroads are divided into adjustable and unregulated, depending on whether traffic lights are present or not, as well as equivalent and unequal.

According to statistics, about 40% of all traffic accidents occur at intersections, so you need to pay special attention to monitoring and simulating traffic, figuring out conflict points and danger zones. In the beginning, you should understand the causes of dangerous traffic situations at intersections.

There are only four major factors affecting safety. These include:

1. Weather (Fog, heavy rainfall, complicating visibility, strong ice or rain, preventing timely braking of the vehicle);

2. The human factor (inattention, fatigue, poor health, deliberate violation of traffic rules, not knowing the rules of the road, drug or alcohol intoxication, and so on);

3. Problems with the correct functioning of the vehicle;

4. Poor infrastructure (road works, excessive congestion of the intersection, advertising or other banners that interfere with the review when making a maneuver, and so on)

Ensuring the correct and safe functioning of the entire intersection system is a top priority for transport specialists; for this, many intersections are equipped with cameras and radars that record the movement of vehicles and thus allow detecting "conflict points".

CONFLICT POINTS AND MODELING OF CROSSROADS

Conflict points are called the intersection of the trajectories of vehicles, pedestrians and equivalent participants in traffic, as well as places of confluence and deviation of traffic flows. The data points are clearly visible on the projected model of a particular intersection (fig. 1)

Various programs are used to determine the location of conflict points, such as Microsoft Visual C++.

For the design of the intersection and its proper functioning, it is necessary to calculate and simulate many parameters, such as:

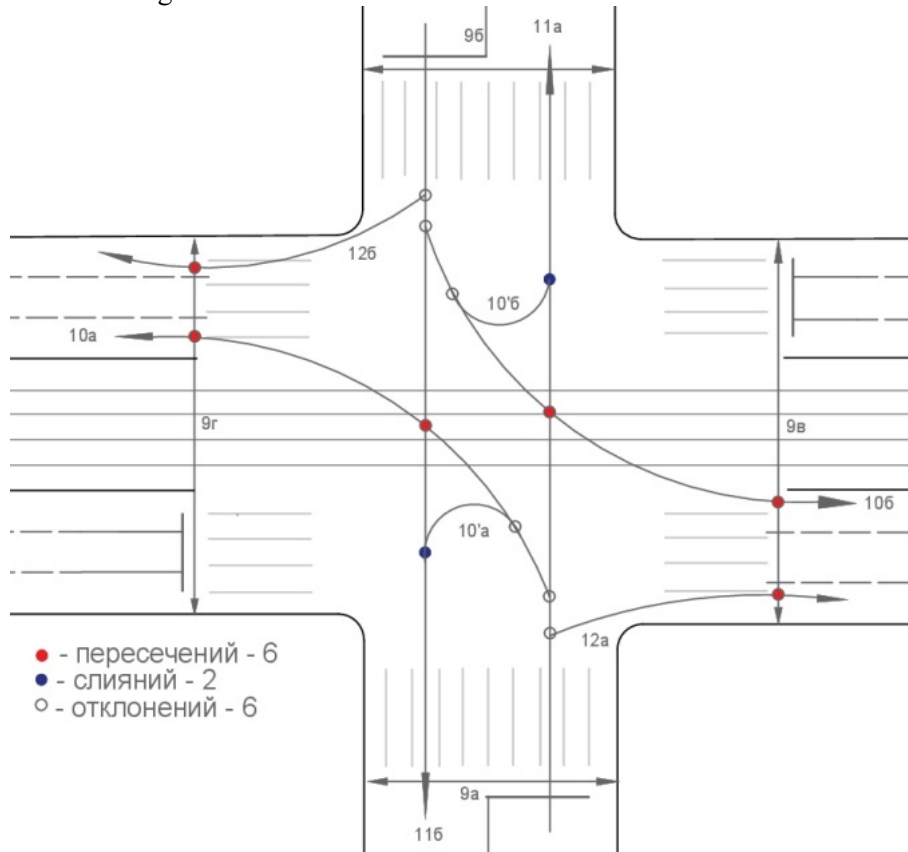
1. Transport and pedestrian flows;
2. Mode of operation of traffic lights;
3. Generation of the number of traffic lights at the intersection;
4. Calculate the time between the switching of traffic lights and time phases;
5. Simulation of driving directions at the intersection;
6. Take into account when calculating the intensity of pedestrian flows and in this regard, choose the most appropriate type of traffic light;
7. Calculation of traffic lights tact for pedestrians to walk to the end of the crossing or to the pedestrian island;
8. Determination of the bandwidth of the intersection.

All of the above for clarity, I would like to consider the example of a particular intersection.

At the intersection of Marshal Blucher Avenue and Kushelev road, horizontal road markings are used to separate traffic flows in opposite directions, designate lanes, pedestrian crossings, stopping points in front of a traffic light. At the approaches to the intersection, flows of opposite directions are

separated by a metal fence and an island. The quality of the markup is good, since it has been updated and brought into proper form due to recent road works. Below are photos confirming the formulation of

traffic signs, markings and showing the location of traffic lights.



Picture 1



CROSSING ABILITY OF CROSSROADS

Freight traffic is allowed in the section under consideration, but for the most part cars and public

transport are moving along the streets. The table below shows the intensity of movement of various vehicles on the intersection.

Traffic intensity studies are shown in the table below:

Entrance RP	№	Light car	Cargo		Bus	Minibus.	All		People
			До 2	2-6			FE	PE	
Entrance A	9	-	-	-	-	-			74
	10								
	10'	15					15	15	
	11	250			7	10	267	269,5	
	12	140	10	6		7	163	144,6	
Entrance B	9	-	-	-	-	-			
	10	300			10	6	316	318,5	
	10'	24					24	24	
	11	300			5	8	313	315,5	
	12								
Entrance C	9	-	-	-	-	-			200
	10	100					100	100	
	10'	30					30	30	
	11								
	12	137	6	3	4	10	160	166	

On Marshal Blucher Avenue (towards M. Lesnaya metro station)	Straight (1)	315	82%
	Left (2)	68	18%
On Marshal Blucher Avenue (in the direction of Laboratory Street)	Straight (3)	240	56%
	Left (4)	190	44%
Kushelev road (in the direction of M. Lesnaya) and in the direction of Laboratory Street	Right(5)	215	62%
	Left (6)	130	38%
Kushelev road (in the direction of the Unbowed Avenue)	Straight (7)	460	100%

From the above information it can be seen that the traffic at the intersection is quite lively, especially during peak hours. At this point in time, one of the lanes is under repair, which only complicates the passage, however, the intersection is competently equipped with traffic lights, which makes the level of its danger much lower.

Vissim/Visum was used in the process of creating this article and analyzing the data.

4. REFERENCES

1. Federal Law of December 10, 1995 N 196-FZ (as amended on 07/26/2017) "On Road Safety"

2. GOST R 50597-93 "Roads and streets. Requirements for the operational condition permissible under the conditions of road traffic safety". Approved and enacted by the Resolution of Gosstandart of Russia dated 10.10.93 No. 221.

3. Gorev A.E. Traffic Management / A.E. Gorev, L.B. Mirotin. – M.: "Academy", 2013. – 56s.

4. Federal target program "Improving road safety 2013-2020, dated October 8, 2013

5. Efremov A.Yu., Kuznetsov K.Yu. Simulation modeling of traffic flows at ring intersections of highways / Institute of Management. V.A. Trapeznikova RAS, 2012

SMART GARDEN: AUTOMATION APPLIED TO BOTANY

A. Tornabene

Computer Engineering and Networks Laboratory – Kore University of Enna – Italy
 Email: angelo.tornabene@unikorestudent.it

INTRODUCTION

This paper shows the simulative system of a greenhouse, offering automated and smart operations using a wireless sensor network (WSN) and Internet of Things solutions (IoT) to monitor and improve plant growth by simplifying daily operations in a small garden. Monitoring of the necessary parameters for plants is based on brightness, temperature and hydration soil sensors. All the sensors are part of a network to send and process the data adjusting appropriately irrigation pumps and lamps power.

In the following sections are examples of similar solutions already on the market, the results of the simulations, the evaluations of network performance and possible future developments.

RELATED WORKS

In the consumer market there are already smart greenhouse systems reproduced in scale that allow the hydration of the plants automatically, without needing exposure to natural light, with LEDs that simulate the natural cycle of the day and of the night. The model represented wants to expand the areas of use, going

beyond domestic boundaries to propose a greenhouse also suitable for a garden that has the possibility to use the network, as well as soft computing algorithms, to check and adjust accurately plant nutrients considering their needs.

THE PROPOSED APPROACH

A wireless network has been created that uses the IEEE 802.15.4 (ZigBee) standard in the communication between the sensors and the gateway; the latter has the task of forwarding the values received into the wired network to the two controllers of the irrigation pumps and the lamps, using CSMA/CD (Ethernet) protocol which guarantees a continuous and reliable transmission. The first controller has the function to regulate artificial light keeping the lighting directed to the plants constant, thus compensating for the variations of natural light, while the irrigation regulator manages the water flow thanks to a fuzzy logic in order to provide the right one hydration with temperature increase.

The network architecture is organized as follows (Figures 1, 2, and 3):

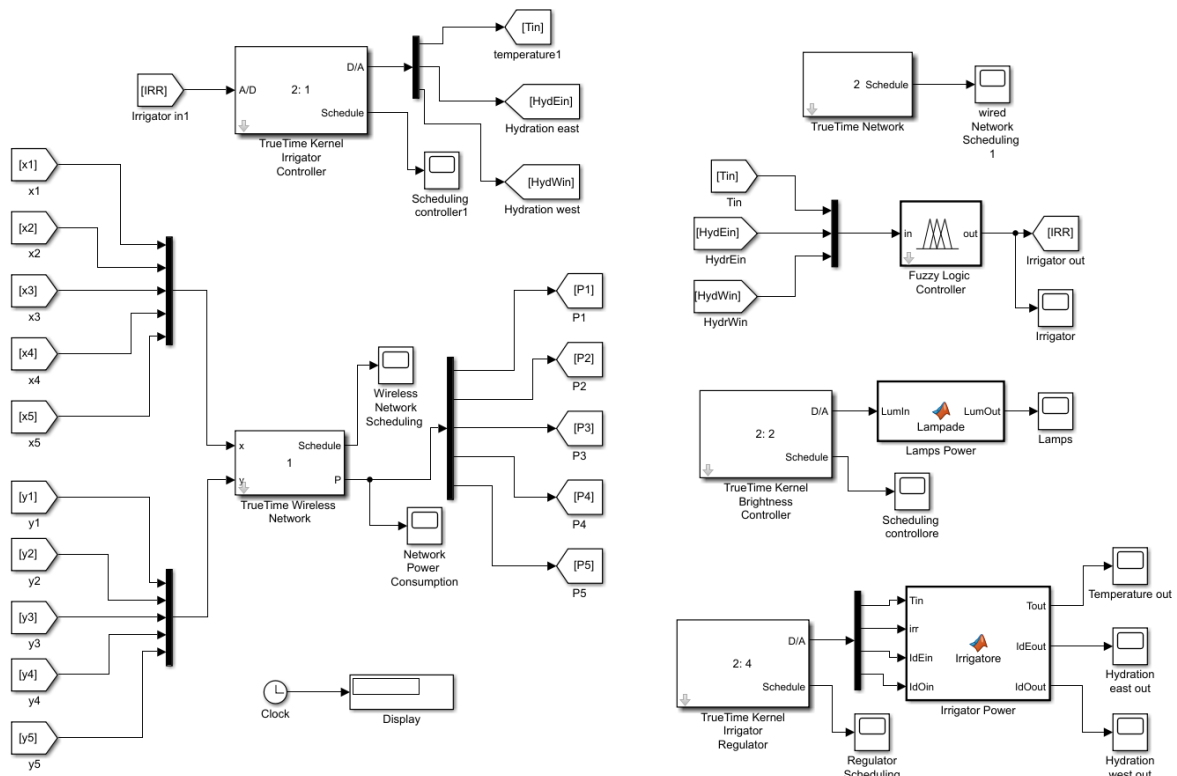


Figure 1: System architecture

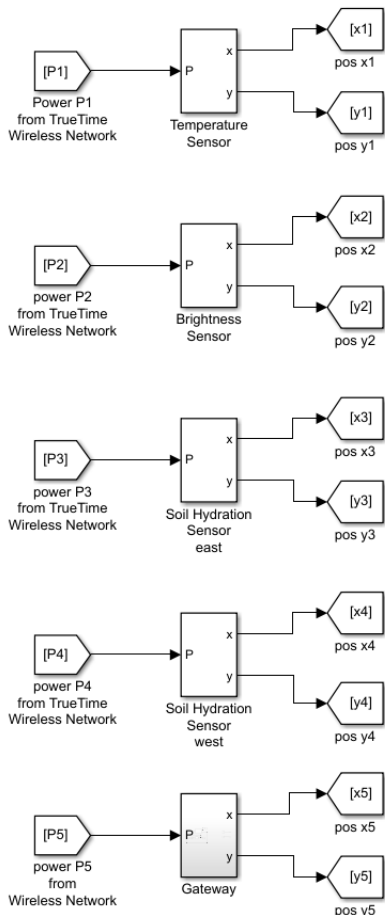


Figure 2: used sensors

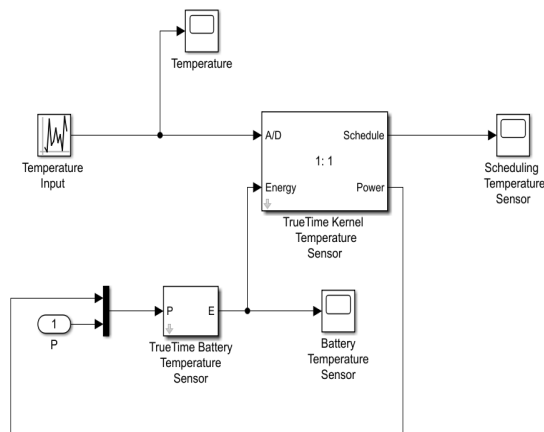


Figure 3: sensor architecture

- Brightness sensor;
- Temperature sensor;
- Soil Hydration Sensor (2x);
- Gateway;
- Irrigation controller;

- Irrigation regulator;
- Brightness controller/regulator.

SCENARIO

The scenario has been simulated with Matlab using Simulink and TrueTime tools. This is based on the input values to be processed, starting from the common scheme of the sensor that make up the network.

The fuzzy logic controller has determined the irrigation power (Figure 4).

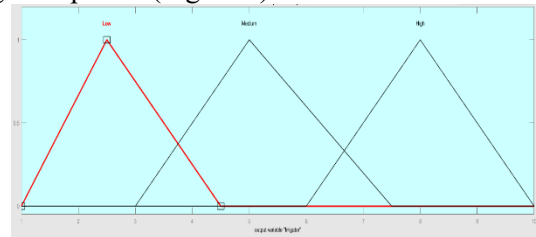


Figure 4. Membership functions of irrigation power

PERFORMANCE EVALUATION

To guarantee the correct functioning of the greenhouse it is not necessary to respect stringent time constraints but it is fundamental that requests to which the system is subjected are met, as the data processing by the regulators; a measure of network performance is therefore given by Availability, that is the fraction of time in which this system is available to process data.

From the results of the simulations it has been noted that the system, being composed of just four sensors, is efficient and rapid either in the processing of values and in the adjustments made by the actuators:

In particular, few tenths of a second pass, around 0.2 s, between the acquisition of the brightness value and its processing, with consequent adjustment of the lamps by the actuator, while it takes about 0.5 s to adjust the irrigation after the acquisition of hydration and temperature values.

In this way, with data rates of 0.8 Mbps and 10 Mbps respectively for the wireless network and the wired network, transmission does not suffer particular slowdowns and possible malfunctions can be determined just by the failure of a node of the network.

CONCLUSIONS

With the tools provided by TrueTime and Simulink it has been possible to simulate the functioning of this small greenhouse, taking inspiration from existing solutions and applying the concepts of automation and control to botany. The model built has been focused on the representation of an internet network and the continuous transmission of data. About the possible future developments it can

be think of expanding the scenarios managing large crops in the agricultural sector, increasing the number of sensors and parameters to monitor, defining different growth profile for each plant species, in

order to manage multiple crops simultaneously and provide the water and nutrients the crops need in an automated and diversified way.

DEVELOPMENT OF RECOGNITION SYSTEM OF HAND GESTURES

G. Tvardovsky

Saint-Petersburg University of Aerospace Instrumentation,
Saint-Petersburg, Russia
E-mail: gtvardovsky@gmail.com

Annotation

The paper describes the recognition system of human hand gestures using computer vision. The method of placing the hand on the image is segmentation, the process of "extracting" objects from the image that the system is interested in.

As a result, the recognition system of hand gestures gives a general idea of the possibilities of computer vision in a whole. As well as of the development and further, useful for society, of the use of the developed algorithm for recognizing hand gestures (without participation of a human)

Key words: computer vision, recognition of gestures.

Introduction

One of the important trends in the development of artificial intelligence is computer (machine) vision. It allows you solving a huge number of tasks, such as object recognition, identification, detection, text recognition, motion estimation, image restoration, etc.

The use of machine vision can improve the safety of human life, save a huge amount of time and money. For example, in the United States a grocery store without cashiers was launched and successfully operates, in which all the goods placed by the buyer in the basket, are captured by a special system with a camera. The funds are automatically debited from the customer's banking card based on the products recognized by the system. Thus, using computer vision in the store, the developers have achieved a lack of queues and a minimum percentage of thefts.

This paper will focus on the recognition of the hand and its fingers. A successful result will give great opportunities for gesture control of any modern device, such as TV, computer, cash registers in stores, phones and many others. This trend is very actual [1-8], as gesture control will simplify the use of modern technology and make life easier for users (for example, there will be no need to look for a remote control from the TV).

Stages of algorithm operation by hand gestures recognition

In general, the algorithm of the developed system can be represented in the form of stages, which are shown on figure 1. To find the hand on the image, segmentation is used – the process of "extracting" the objects of interest from the image. There are many ways to solve this problem, each of which has a different degree of complexity. The method that will be discussed in this article is based on fixing the background image.

Thus, the stages of the system operation, which are shown on figure 1, starting with the background

fixation by binarization, are segmentation of the input image. It removes unnecessary details from the image, leaving only the binarized image of the hand.

Next stages of the system operation are contour analysis and subsequent calculation of the data obtained after it to display information about the gesture recorded by the camera.

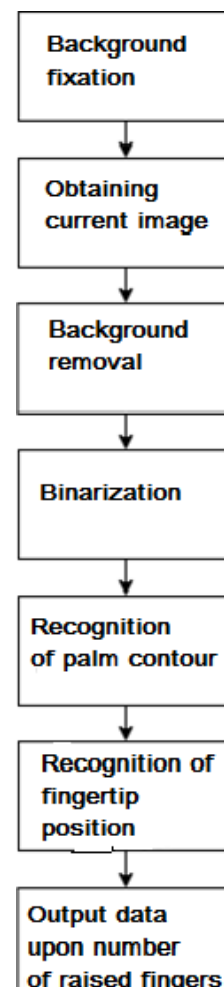


Figure 1. Consequence of actions when recognizing hand gestures

Used stack of technologies by system development

By development of this application the following stack of technologies was used:

1. Programming language – Python;
2. Computer vision library – OpenCV;
3. IDE – PyCharm CE.

Python – interpreted, object-oriented programming language, including the modules, dynamic data types and classes [9].

OpenCV – library of computer vision algorithms with open initial code [10], developed by Itseez, Intel and Google corporations.

PyCharm CE – integrated design medium for Python programming language, which represents devices to analyze the code, graphic adjustment and launch of unit-tests [11].

Background fixation

The method using background fixation has an advantage against most other methods, such as segmenting the hand by skin color, trying to determine the distance to objects in the image, and others. The advantage is that the user does not need to look for the perfect background and light, because after fixation (figure 2a), the final image will be obtained by subtracting the previously fixed background (figure 2b) from the current image.

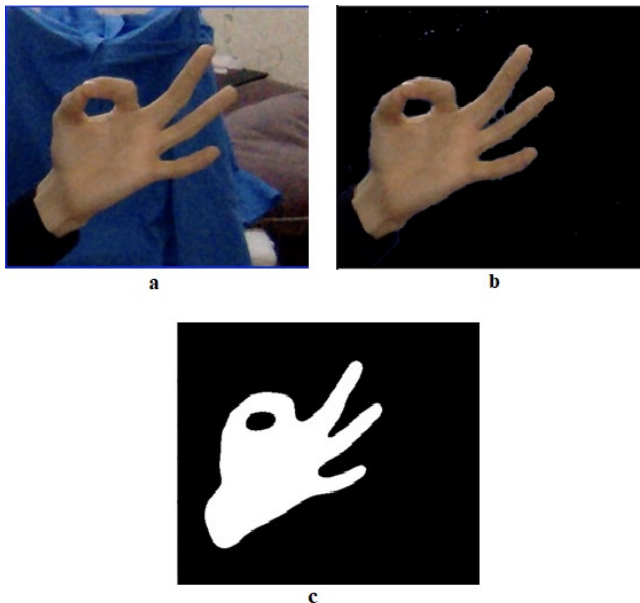


Figure 2 – Background removal and hand binarization (a – current image, b – image after background removal, c – binarized image b)

Binarization

The image binarization is executed by means of the computer vision library method OpenCV – cv2.threshold. The binarization formula of this method is represented in the following way [12]:

$$dst(x, y) = \begin{cases} maxVal, & \text{if } src(x, y) > thresh \\ 0, & \text{otherwise} \end{cases}$$

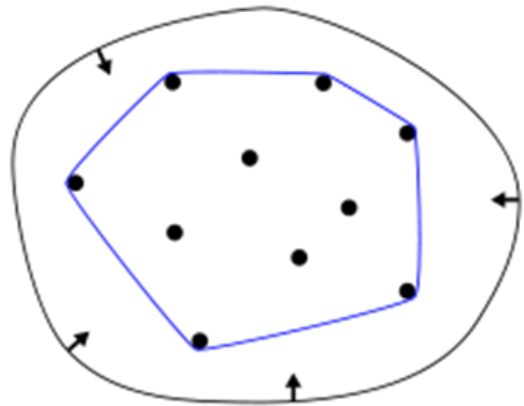


Figure 3 – Convex hull

This functions as follows: if a pixel value is bigger than the threshold value, it is assigned one value (white), otherwise it is assigned a different value (black). The result of hand binarization from figure 2b is shown on figure 2c:

Detection of palm contour and allocation of fingers on the input image

Next step of the algorithm is to find the contour of the hand from the binary image, which we got at the stage of binarization, after which the fingers will be searched on the image. For this purpose the computer vision library method OpenCV findContours is used, which finds all contours on the binarized image. Upon results of this method operation, one chooses a contour with the largest area and executes its delineation using drawContours method (figure 4a).

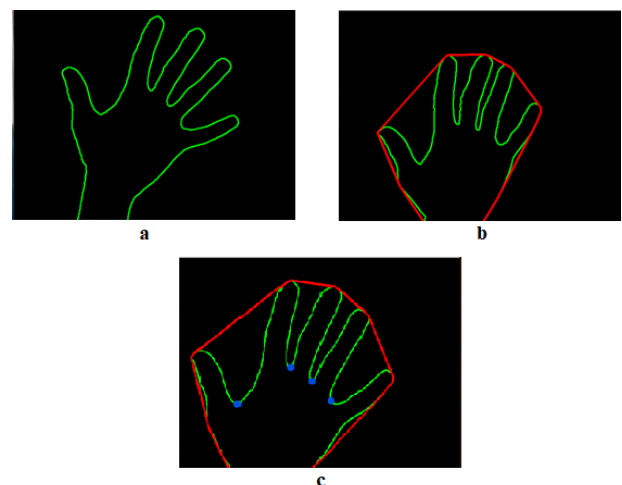


Figure 4 – Outlining hand contour on the image (a – delineation of the found hand contour, b – result of processing with convex Hull method, c – result of search for hand fingers)

To determine the number of raised up fingers, the convex hull method (Convex Hull) is used. In mathematics, the convex hull is the smallest set containing a set of points (figure 5). Moreover, a convex set is such a set of points that if you draw a straight line through any pair of points in the set, that line must also be inside the area. Thus, after using the convexHull method, a smoother area is obtained than the contour that was found earlier (figure 4b).

Now finding the location of the fingertips is a fairly simple task. Their location coincides with the corners of the convex hull polygon. To find them one uses the convxtDefects method. Such approach has the following problem: it is not always that the

number of polygon corners coincides with the number of the raised up fingers, sometimes there are more corners.

At next stage, only those angles that will form an angle with an adjacent angle of less than 90° are searched. The result of such search of hand fingers is given in the figure 4c:

Knowing the number of points visible at the moment, you can find the number of fingers raised at this moment. But there is a problem associated with the fact that when one finger is raised, there are no points, which means that we can not say exactly if one finger was raised or no fingers at all were raised, as shown in figure 5.

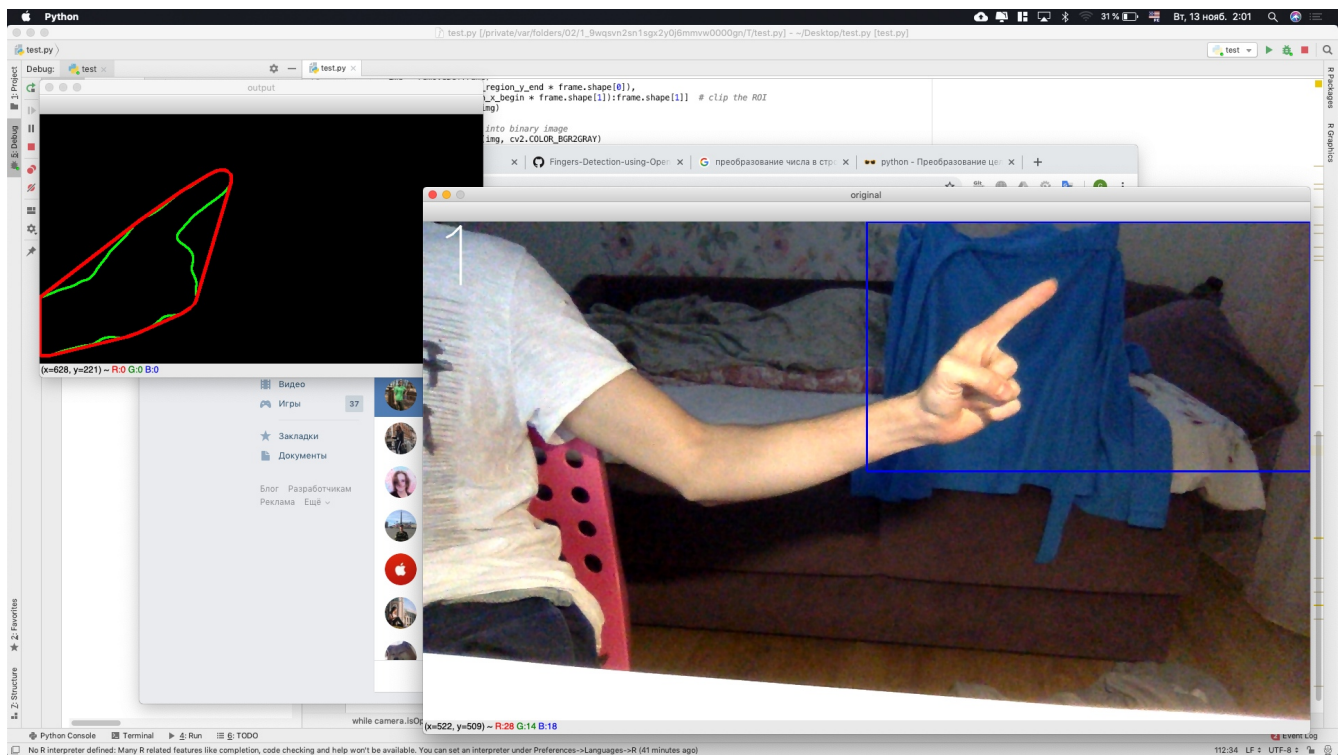


Figure 5 – shows the problem of one finger recognition

To solve the problem, one simply finds the ratio of the areas of the convex region and the contour, and in the case where the value found is approximately 0, it is assumed that no fingers are in the image. In the same way it turned out to learn how to identify some gestures, though not accurately enough. (Figures 6-10)

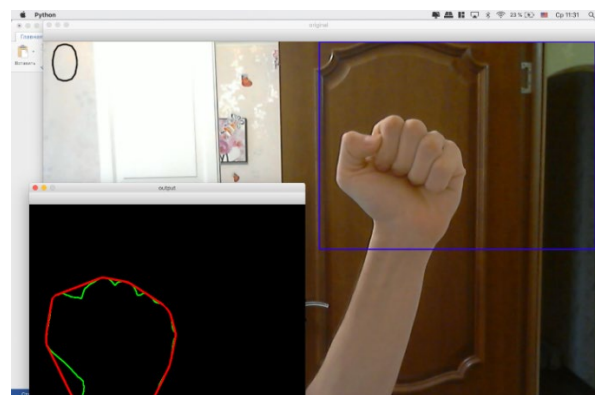


Figure 6 – Shows program operation (0 fingers)

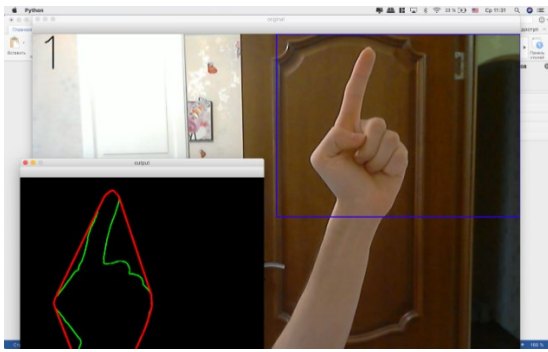


Figure 7 – Shows program operation (1 finger)

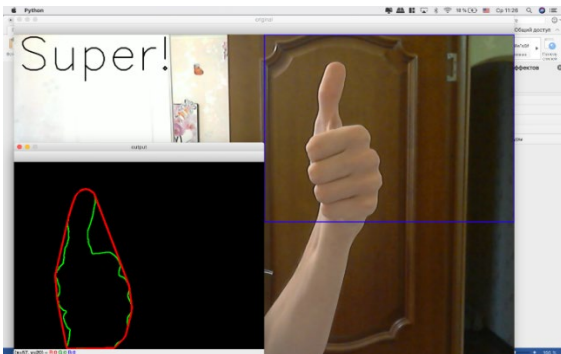


Figure 8 – Shows program operation (sign “super”)

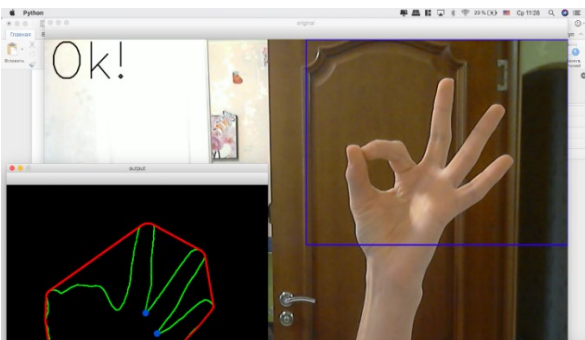


Figure 9 – Shows program operation (sign “ok”)

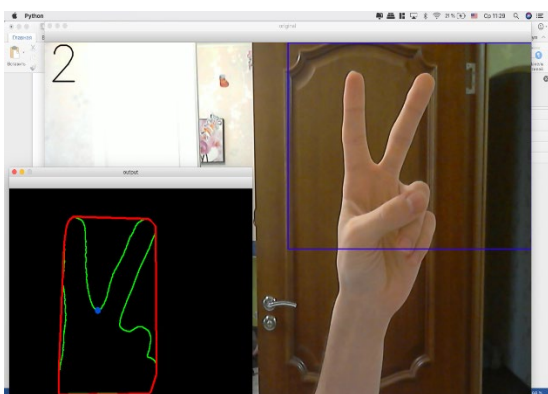


Figure 10 – shows program operation (2 figures)

Conclusion

The described hand gesture recognition system gives an idea of the possibilities of computer vision

and, specifically, the OpenCV library.

The algorithm used for recognition is not ideal and will be improved. Despite the existing problems, the described approach can already be used to control the operation modes of some equipment (switching from 0 to 5, start, stop, etc.).

To increase the number of gestures recognized by the system, and in the future to reach a level that allows recognizing the sign language in sign language translation, will allow using the deep learning with the preparation of the appropriate training sample and training of the neural network.

BIBLIOGRAPHY

1. Finger Detection and Tracking using OpenCV and Python [Electronic resource] – Access mode – <https://dev.to/amarlearning/finger-detection-and-tracking-using-opencv-and-python-586m>
2. Fingertip Detection in OpenCV [Electronic resource] – Access mode – <https://picoledelimao.github.io/blog/2015/11/15/fingertip-detection-on-opencv/>
3. Handy, hand detection with OpenCV Python [Electronic resource] – Access mode – <https://medium.com/@soffritti.pierfrancesco/handy-hands-detection-with-opencv-ac6e9fb3cec1>
4. Hand Keypoint Detection using Deep Learning and OpenCV [Electronic resource] – Access mode – <https://www.learnopencv.com/hand-keypoint-detection-using-deep-learning-and-opencv/>
5. Nosov A.V. Hand gesture recognition algorithm based on skeleton hand model /A.V.Nosov//Siberian magazine of science and technologies. — 2014. — no.2. — P.62-67.
6. Nagapetyan V.E. Recognition of hand alphabet gestures ASL/B.Э. Nagapetyan// Bulletin of the peoples' friendship University of Russia. Series: Mathematics, informatics, physics. — 2013. — no.2. — P.105-113.
7. Nosov A.V. Localization of key hand points on the image based on the uninterrupted skeleton /A.V.Nosov/Reshetnev reading. — 2015.— P.77-79.
8. Nagapetyan V.E. Non-contact control of robotized hand by means of human gestures/V.E. Nagapetyan. F. Tolmachyov I.L. // Bulletin of the peoples' friendship University of Russia.— 2014.— no. 2. — P. 157-163.
9. Python Software Foundation [Electronic resource] – Access mode – <https://www.python.org/>
10. Open Source Computer Vision Library [Electronic resource] – Access mode – <https://opencv.org>
11. JetBrains s.r.o. Developed [Electronic resource] – Access mode – <https://www.jetbrains.com/pycharm/>
12. Open Source Computer Vision Library – Access mode – <https://docs.opencv.org/2.4/doc/tutorials/imgproc/threshold/threshold.html>

METHODS OF VISUALIZATION OF ANTIPHASE POLAR DOMAIN WALLS IN A SOLID SOLUTION OF LEAD ZIRCONATE-TITANATE BY MEANS OF SYNCHROTRON RADIATION SCATTERING

S. Udovenko

Postgraduate student
Peter the Great Saint-Petersburg Polytechnic University,
Saint-Petersburg, Russia
kniazeva.maria225@yandex.ru

Abstract

The temperature and field dependences of the distribution of diffuse scattering in a solid solution of lead zirconate titanate ($\text{Pb} [\text{Zr}_x\text{Ti}_{(1-x)}] \text{O}_3$), (PZT) were analyzed. Small volumes of reciprocal space were reconstructed in the vicinity of Bragg reflections to establish the shape of the spatial distribution of diffuse scattering at different temperatures. When an electric field is applied in the orthorhombic phase, the existence of diffuse scattering in the form of narrow rods is shown. Rod direction was determined by the direction of the applied electric field.

Introduction

The research of antiferroelectric materials originates in the late 1950s. The first antiferroelectric materials to be developed were lead zirconate and tungsten trioxide [1, 2]. In the paraelectric phase the dielectric constant behaves similarly for antiferroelectric and ferroelectric materials. For both material the dielectric constant shows a large increase as it approaches the phase transition temperature. [3]. Uniquely high values of the dielectric constant of antiferroelectric materials allow the production of high-capacity capacitors using these materials.[4]. However, a significant difference between antiferroelectric and ferroelectric materials is the fact that the low-temperature phase in antiferroelectrics is not polar. Another distinctive feature of antiferroelectrics is the dependence of polarization on the polarizing field in the form of a double hysteresis loop.

In view of the structural similarity of antiferroelectrics and ferroelectrics, efforts were made to create a solid solution composed of antiferroelectric and ferroelectric materials for example lead zirconate-titanate. Lead zirconate titanate solid solution has a complex phase diagram (Fig. 1).

The nearly vertical border between the rhombohedral and tetragonal phases, corresponding to a concentration of titanium near 50% is called the morphotropic phase boundary. The PZT solid solution at this composition has a giant piezoelectric response, which makes this material an excellent substrate for the manufacture of efficient electro-mechanical and mechano-electric transducers [6] As a result all practical applications of PZT are related to its behavior in electric fields.

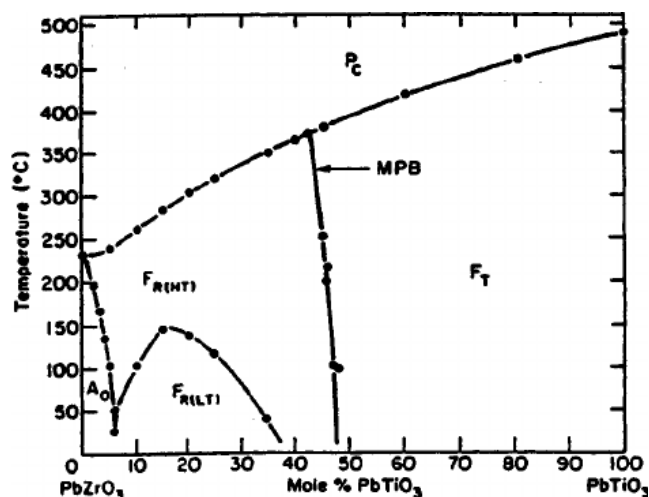


Fig.1 PZT phase diagram

While PZT with titanium concentrations near the morphotropic phase boundary has been studied in details, PZT with a titanium concentration of just a few percent has not been adequately investigated. Our desire is to understand the phase transitions of low titanium concentration PZT when an electric field is applied. The most natural method for studying the dynamics of phase transitions and the structural rearrangements that accompany them is the diffraction of synchrotron (X-ray radiation).

Experimental

Data was taken at the European Synchrotron radiation facility (ESRF). Samples were PZT single crystals with a titanium content of 1.1%. Samples were tested in the temperature range of 170–350 °C with and without an applied electric field of 5 kV / cm. Diffraction patterns were compared for test samples, with and without the electric field applied, and the difference in patterns analyzed to understand the

influence of the electric field on the dynamic of phase transition of the crystal. The experimental setup is shown schematically in Fig.2.

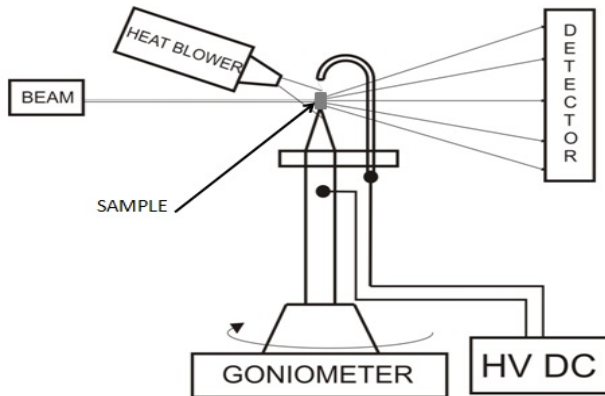


Fig. 2 Experimental arrangement

The sample (SAMPLE) was a PZT single crystal plate with dimensions of 1000 * 60 * 60 microns. The sample was mounted on a holder that allowed the sample to be subjected to an electric field. The sample

temperature was controlled by blowing the sample with a nitrogen jet of a given temperature (HEAT BLOWER). A collimated and monochromatic beam of synchrotron radiation (BEAM) was scattered by the sample and the results captured by a two-dimensional position-sensitive detector (DETECTOR). The data generated by the diffractometer was automatically stored on a computer. The sample was scanned at an angle using a high precision stepper motor. High voltage was applied to the sample from a high-voltage source (HV DC).

Results

Data processing was performed using software developed in Matlab software [7]. Two-dimensional cuts of the reciprocal space were constructed by the H0L planes. Figure 3 shows slices of the reciprocal space with of the sample at three different temperatures, with and without applied electric field. Results on the left are without an applied field, results on the right are with the applied field. The field direction is indicated by the blue arrow.

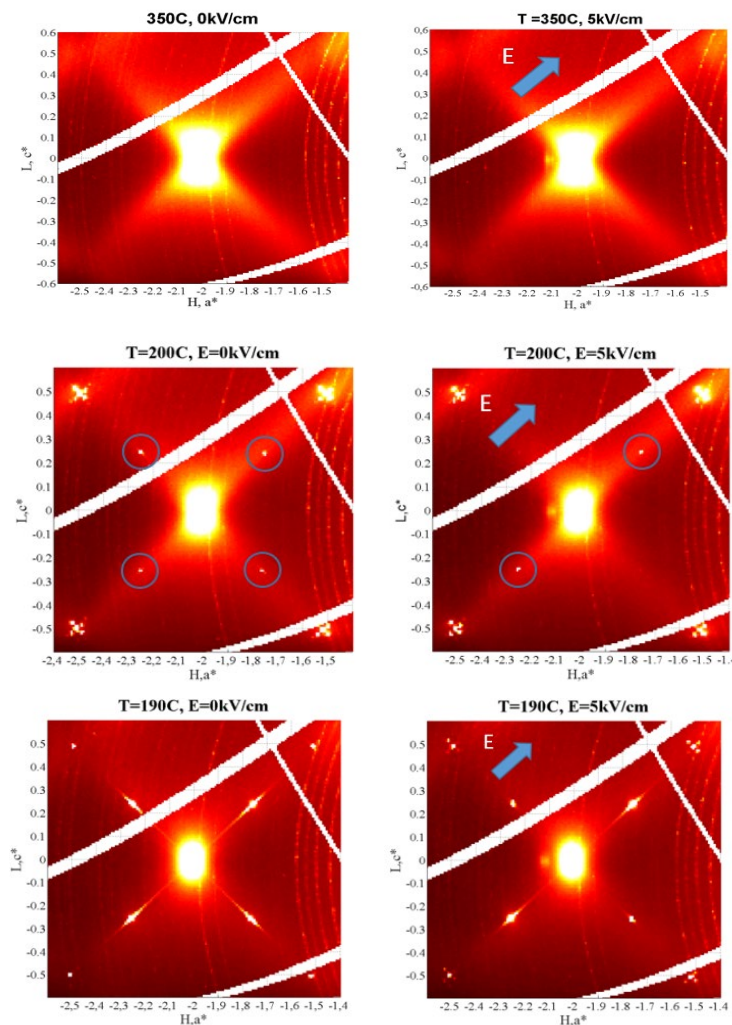


Fig.3 Slices of reciprocal space with H0L surface at 350, 200 and 190 °C in zero field (left column), at 5kV/cm (right column)

It is seen that at a temperature of 350 ° C, in the paraelectric phase, the electric field does not make a visible change in the intensity distribution of the diffraction pattern. With decreasing temperature, the sample enters an intermediate phase, as evidenced by the emerging M-type superstructural reflections. When the sample is cooled to 200 ° C, superstructural Σ -type reflections appear, corresponding to the antiferroelectric displacements of lead ions. In the presence of a Σ -type reflection field, they appear only in the direction of the electric field, which corresponds to the displacement of lead ions

perpendicular to the field. When the sample is cooled further to 190 ° C, narrow diffuse scattering bands appear in the vicinity of Σ -type reflections. It is seen that the application of the field also leads to the formation of stripes in the direction perpendicular to the direction of the field. To determine the spatial form of the intensity distribution, a small volume of the return space was reconstructed in the vicinity of one of the Bragg reflections at a temperature of 190 ° C (Fig. 4) with no field (left), with an applied field of 5 kV / cm. in the direction of the blue arrow (right).

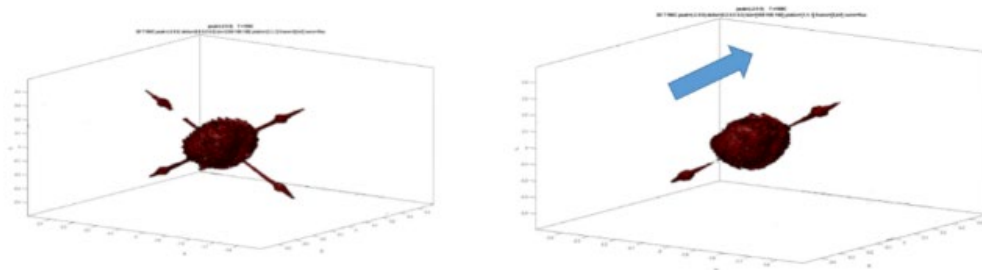


Fig.4 reconstructed 3-dimentional volume of reciprocal space around Bragg $(-2\ 0\ 0)$ peak at 190 °C in zero field (left column), at 5kV/cm(right column)

From figure 5 it can be seen that:

1) The spatial distribution of diffuse scattering has the shape of a narrow rod,

2) In the absence of a field, the intensity distribution of the rods is almost the same in both directions

3) The application of the field leads to the disappearance of the rod in the direction perpendicular to the field direction, which indicates the suppression of the antiferroelectric displacements of lead ions in the direction coinciding with the direction of application of the field.

In view of the conjugacy of the reciprocal and direct space, the narrow rods in the inverse space correspond to extended objects in the direct space. We assume that this scattering is associated with scattering on antiphase domain walls. As shown in reference [8], domain walls are antiphase and polar.

CONCLUSION

We have shown the effect of a weak electric field on the formation of antiphase polar domain walls in the antiferroelectric phase in PZT single crystals with a titanium concentration of 1.1%. This effect can be used to create electronic memory with a high recording density.

REFERENCES

1. J. M. Berak and M. Sienko, *E*_ect of oxygen-

de_iciency on electrical transport properties of tungsten trioxide crystals, *Journal of Solid State Chemistry*, vol. 2, no. 1, pp. 109_133, 1970.

2. K. Roleder, I. Jankowska-Sumara, G. E. Kugel, M. Maglione, M. D. Fontana, and J. Dec, *Antiferroelectric and ferroelectric phase transitions of the displacive and order-disorder type in pbzro3 and pbzr1-xti x o3 single crystals*, *Phase Transitions*, vol. 71, no. 4, pp. 287_306, 2000.

3. G. Shirane, E. Sawaguchi, and Y. Takagi, *Dielectric properties of lead zirconate*, *Journal of the Physical Society of Japan*, vol. 6, no. 3, pp. 208_209, 1951.

4. A. Chauhan, S. Patel, R. Vaish, and C. Bowen, *Anti-ferroelectric ceramics for high energy density capacitors*, *Materials*, vol. 8, pp. 8009_8031, 12 2015.

5. W. R. C. B. Jaffe and H. Jaffe, *Piezoelectric ceramics I*, *Piezoelectric Ceramics*, p. 136, 1971.

6. Andrew J. Bell, Factors, influencing, the piezoelectric behavior of PZT and other "morphotropic phase boundary" ferroelectrics, *J. Mater. Sci.*, vol41,pp.13-25,2006.

7. Bronwald Yu. A., св-во о гос регистрации программы для ЭВМ №2017617111.

8. X.-K. Wei, A. K. Tagantsev, A. Kvasov, K. Roleder, C. lin Jia, and N. Setter, *Ferroelectric translational antiphase boundaries in nonpolar materials*, in *Nature communications*, 2014.

HYBRID STAND FOR MODELING EXTREME CONTROL SYSTEMS

E. Vataeva

Saint-Petersburg University of Aerospace Instrumentation,
Saint – Petersburg, Russia
evataevv@inbox.ru

Annotation

The paper discusses the construction of a hybrid test bench, which allows you to simulate various nonlinear automatic control systems (ACS) with extreme characteristics in terms of their parametric nonstationarity. The NI ELVIS-II platform is used as the hardware, and the simulation results are also provided as the software LabVIEW.

The combination of physical and mathematical modeling provides great opportunities in hybrid modeling of complex automatic control systems (ACS). Such an approach makes it possible to investigate nonlinear control systems at modeling complexes that include elements of real equipment.

The use of hybrid modeling is possible both at the design stage and at the stage of testing the performance of individual components and the finished product. In this case, the crowding out method can be used when the use of real hardware expands as new nodes are implemented. It is important to note that an interesting feature of the method is the possibility of a relatively arbitrary combination of real and simulated parts of the system [1].

Hybrid modeling is widely used in the development of aircraft control systems and the creation of training complexes. Along with the real equipment, the closed model includes simulators of effects and interference, mathematical models of the environment and processes.

One of the main tasks of the development of control systems for unmanned aerial vehicles is the creation of devices that have the ability to operate in a passive mode. Often, such devices are based on correlation extremal systems (KES), in other words, extremum seeking control (ESC), whose task is to maintain the extreme values of the output signal of the correlator — the cross-correlation function of some signals applied to its input.

A rather complicated task is the modeling of the dynamics of the ESC in the conditions of parametric

nonstationarity of the extremal characteristic [2, 3].

The structure of the stand that implements the ECS is shown in Figure 1 and includes two functionally identical channels – software and hardware, combined by means of a switch [4]. In the figure, the following notation is used: HMO – hardware model of the object; HR – hardware regulator; SI and C are, respectively, software implementations of the facility and the controller. The block diagram of the control object is shown in Fig. 2. The object includes the actuator (1), the block forming the variable extremal characteristic (2) and the linear part (3). The switch allows you to get all the possible combinations of software and hardware nodes, as well as combine both parts of the stand to build a two-dimensional extreme system.

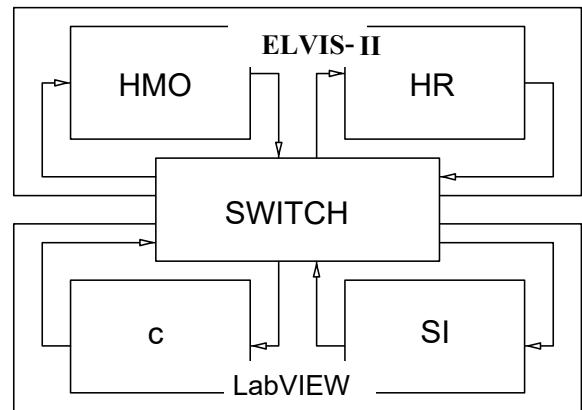


Figure 1 – The structure of the stand that implements the ESC

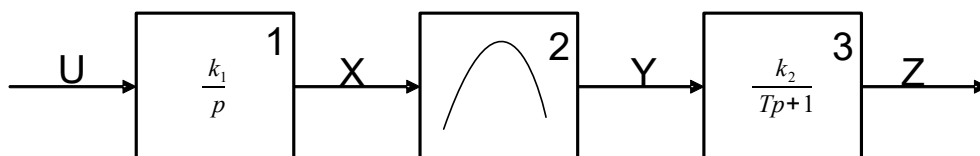


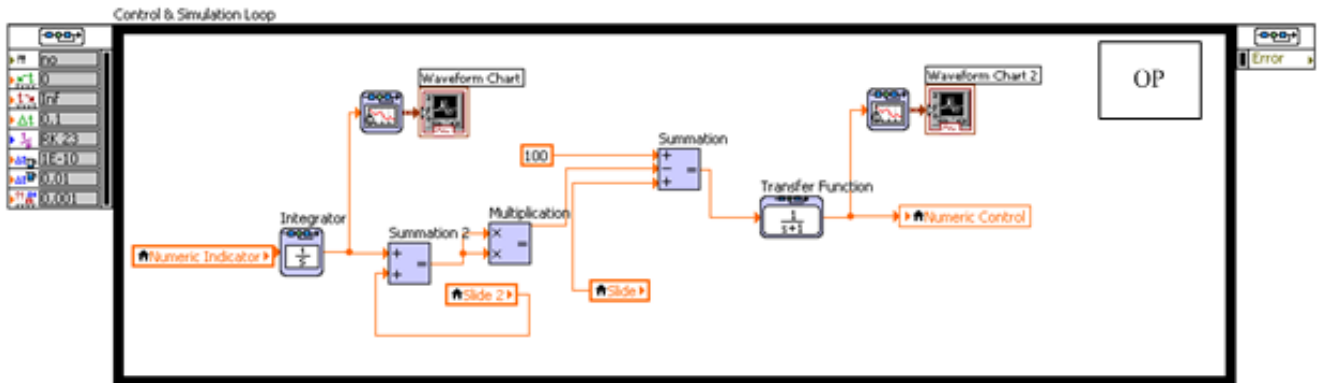
Figure 2 – Structural diagram of the control object

The presented structural diagram of the implementation of the ESC model is universal and has ample opportunities for solving modeling problems. The analog part of the model, without simplifications and assumptions, reproduces the non-stationary extremal characteristic, the hardware controller has a fixed structure and limited options for setting parameters, and the software controller allows you to

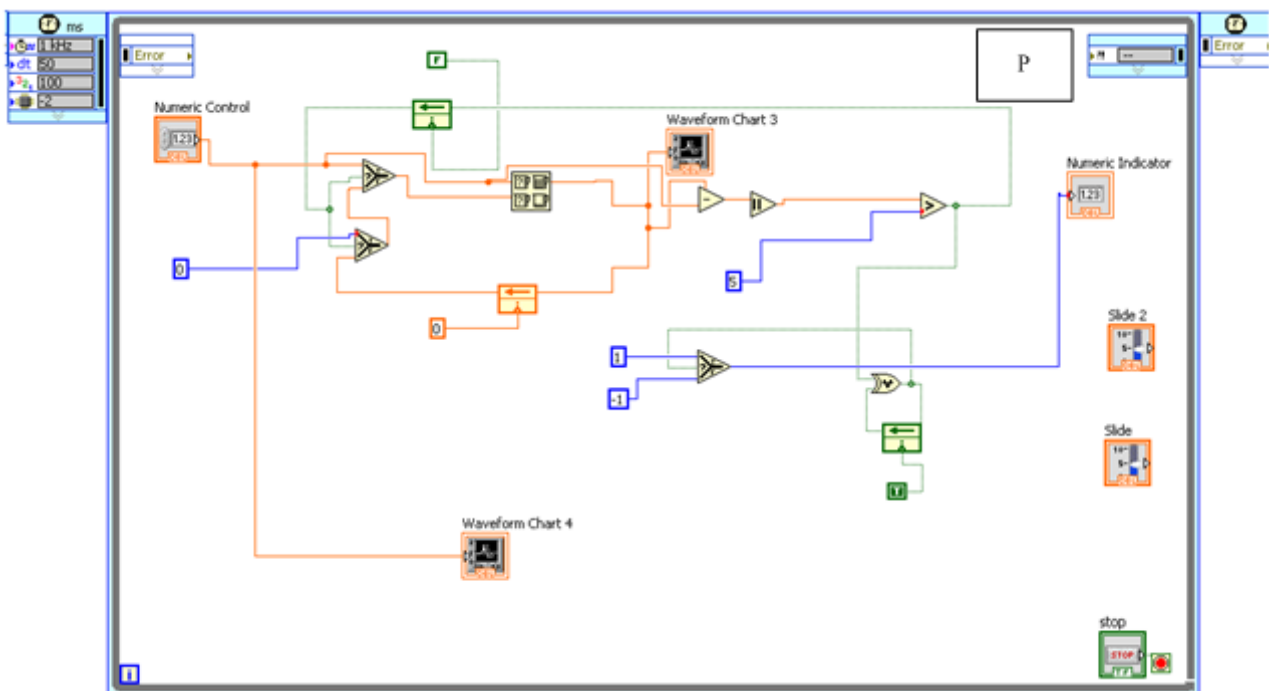
simulate the control laws of the ACS brake wheel of any degree of complexity [5,6].

Figure 3 shows the functional diagram of the software controller, which includes the model of the control object and the controller. The extremum seeking control with a delay is chosen as the object of regulation.

Figure 4 shows the phase portrait and the process taking place in the hardware model of the object.



a) Model of the object of regulation



b) Model of the object of regulation

Figure 3 – Structural diagram of the control object

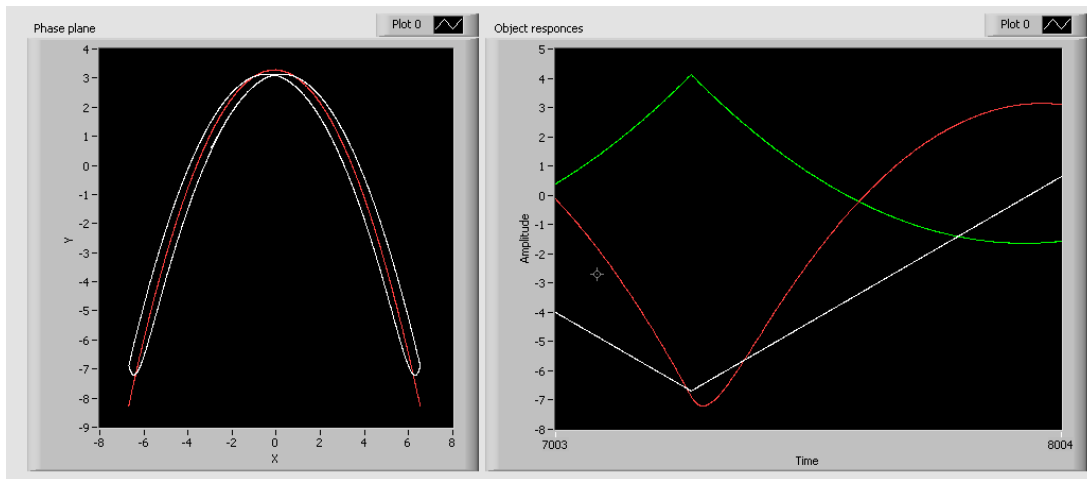


Figure 4 – Phase portrait and process in the hardware model of the object

The interface of the program part of the model is shown in Fig. 5, where it is indicated:

Symmetry – the symmetry of the extreme characteristics; Xoffset – offset of the characteristic along the x coordinate; Yoffset – offset of the characteristic along the y coordinate; Slope – the

steepness of the characteristic; – gain; – mistake; T_{c2} is the time constant of the aperiodic link. Using the Xoffset and Yoffset, it is possible to change the parameters of the parabola along the x and y coordinates, to introduce non-stationarity of the extremal characteristic.

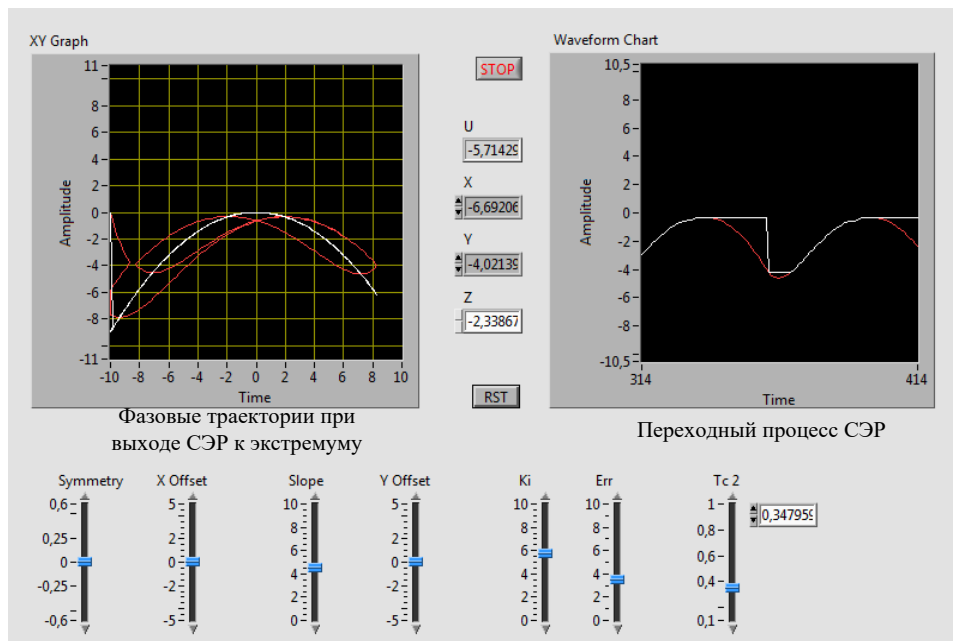


Figure 5 – Interface control program layout

The analog part of the system is implemented on the NI ELVIS – II debug board and is presented in Figure 6, where the following notation is used: 1 – a slider that allows the parabola to be moved along the x axis; 2 – multiplier; 3 – device sampling / storage (writes / extracts values in block 5); 4 – system storage capacitor; 5 – comparator; 6 – the linear part of the object (aperiodic link); 7, 8 – operational amplifiers

(op-amp); 9 – the engine that changes the direction of the eight; 10 – OU, which receives the coefficient of inclination of the branches of a parabola; 11 is a slider allowing to move the parabola along the y axis; 12 – multiplier that implements the change in the slopes of the branches; 13 is a slider that regulates the slope of the branch.

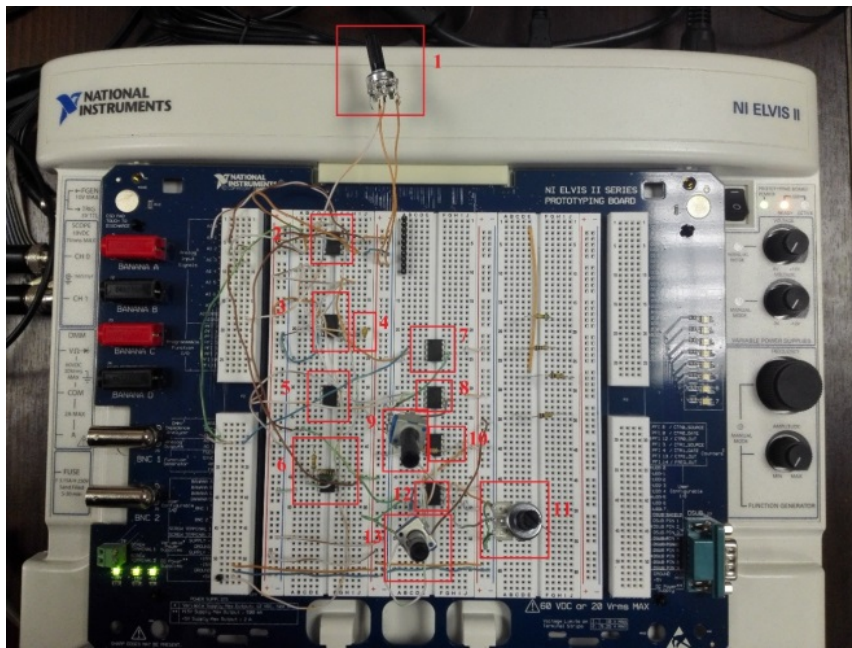
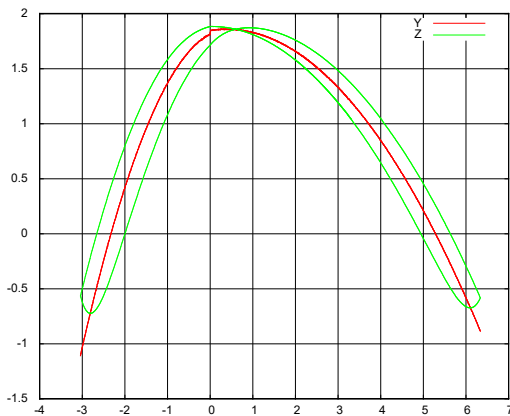
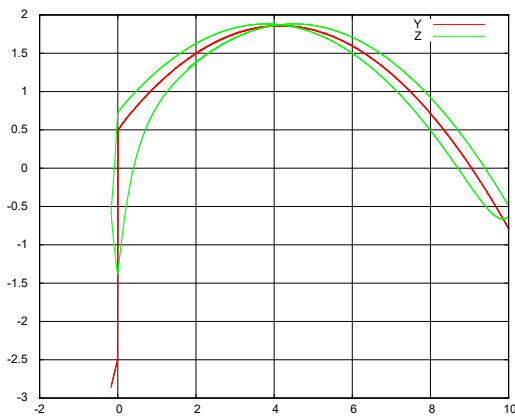


Figure 6 – System layout on the NI ELVIS debug board – II

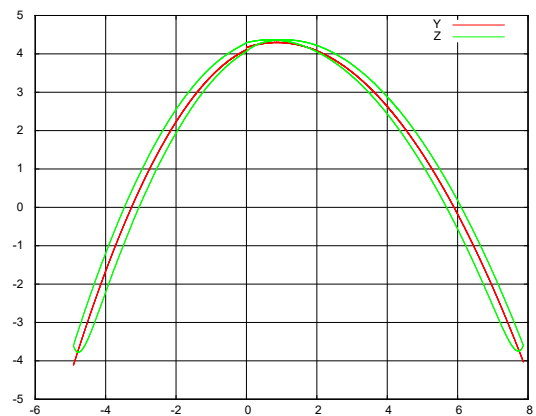
Figure 7 (a, b, c, d) shows the oscillograms of the analog model with different parameters of the object an different settings of the controller.



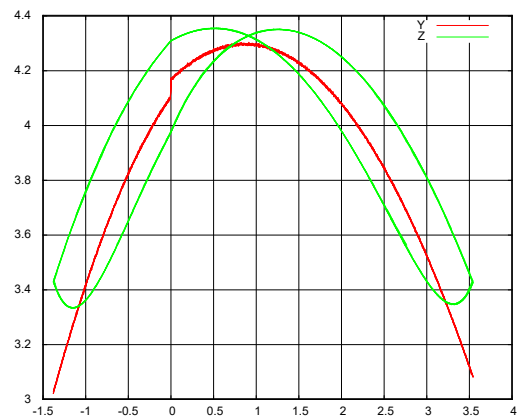
a) Symmetry distortion characteristics



b) x and y offset value change



c) The effect of the object time constant on the system operation at $T_p = 0.1c$



d) The effect of the object time constant on the system operation at $T_p = 0.5c$

Figure 7 – Phase trajectories at the exit of the ESC to the extremum

During this work the hybrid stand is developed for modeling of extreme characteristics, the received results show that for a solution of problems of modeling of nonlinear systems of automatic control with parametrically non-stationary extreme characteristics it is reasonable to solve by a combination of analog and computer simulation. As computer allows to investigate different laws of management, and analog allows to simplify modifications and researches of a system, eliminating defects of use of mathematical methods.

References

1. Shishlakov, V.F. , Krivolapchuk I.G., Vataeva E.Yu. Modeling the dynamics of the work of extremum seeking control (ESC) // Mechatronics, automation and robotics: Materials of the international scientific – practical conference. – Novokuznetsk: SIC MS, – 2017. – №1.C.130 – 132
2. NI ELVIS II Series Quick StartGuide, December 2015.
3. Nikitin A.V., Shishlakov V.F. Parametric synthesis of nonlinear automatic control systems: Monograph / Under. Ed. V.F. Shishlakov, SPbGUAP. St. Petersburg, 2003. 358c.
4. Shishlakov V.F., Shishlakov A.V., Timofeev S.S. Synthesis of ACS for various types of approximation of nonlinear characteristics: theory and practice: monograph / Under. ed. V.F. Shishlakov. SPb .: SUAI, 2017
5. Shishlakov V.F., Tsvetkov S.A., Shishlakov D.V. Synthesis of parameters of continuous and pulsed multiply-connected automatic control systems: monograph / Under. ed. VF Shishlakov. SPb .: SPbGUAP, 2009
6. Vataeva E.Yu., Krivolapchuk I.G., Shishlakov, V.F. Hybrid modeling of ESC on the ELVIS – II platform // Computer-aided design in mechanical engineering: Materials of the V international scientific and practical conference by correspondence. – Novokuznetsk: SIC MS, – 2017. No. 5.C.90 – 96

SMART TRAFFIC LIGHT

M. Messina, C. Vecchio

Computer Engineering and Networks Laboratory – Kore University of Enna – Italy

Email: {corrado.vecchio, michele.messina}@unikorestudent.it

Abstract

Sometimes travelling around people go through many intersections equipped with traffic lights that regulate the traffic flow in a “static” way. The proposed approach wants to get the traffic flow more dynamic and more intelligent:

- Dynamic: the aim is to regulate the traffic giving the right priority to the street also having regard of the time they are busy.
- Intelligent: there are some special vehicles, such as ambulance, having high priority and must cross immediately the intersection.

The problem is been studied and simulated with Matlab & Simulink through the library TrueTime 2.0.

INTRODUCTION

“Smart Traffic Light” shows up as an innovation in Smart City context and its aim is to extend the Surtrac Project already published by “Rapid Flow Technologies of Pittsburg”. Our project follows these sections:

- Section II shows Surtac Project features with a following review;
- Section III shows Smart Traffic Light presentation starting from the proposed approach until the used architectures in a meticulous way.
- Section IV describe the simulated scenery through Matlab/Simulink/TrueTime 2.0.
- Section V deals with the performance metrics need to establish the QoS.

RELATED WORKS

Surtrac is an innovative approach to real-time traffic signal control, combining research from artificial intelligence and traffic theory. Surtrac optimizes the performance of signals for the traffic that is actually on the road, improving traffic flow for both urban grids and corridors and leading to less waiting, reduced congestion, shorter trips, less pollution, and happier drivers. The first thing Surtrac does, like any good robotic system, is it senses its surroundings, or what is going on, in real-time, at the intersection. It gets this information from a software integration/API with the existing sensing infrastructure, which can include cameras, radar, or even induction loops.

Surtrac processes this information and then,

every second, via its patented scheduling software, creates an optimization plan for how to move multi-modal traffic through the intersection as efficiently as possible. Next, via a second software integration/API, Surtrac acts on this plan by sending commands to the controller to coordinate the signals in support of its optimization plan. Finally, Surtrac communicates information about its plan and the traffic that will flow from the intersection.

How does Surtrac result in an emergency? For this reason, “Smart Traffic Light” commits itself to get priority to emergency requests. When an emergency is recognized in a street, traffic light’s actuator lock the other roads allowing the emergency up to 60 seconds.

THE PROPOSED APPROACH

An isolated intersection with four streets has been implemented (streets are called Street1, Street2, Street3, Street4, respectively): streets have 10 Wireless Sensor Network (WSN) for traffic detection connected each other with IEEE 802.15.4.

Every street stand for a wireless network, connected with a Gateway device.

Some other devices, like a controller and an actuator, are connected each other with a wired network.

Overall, there are six networks in “Smart traffic Light” project: four are wireless networks and two wired (an auxiliary network has introduced to calculate response-time). All the networks in our project are shown in figure (1).

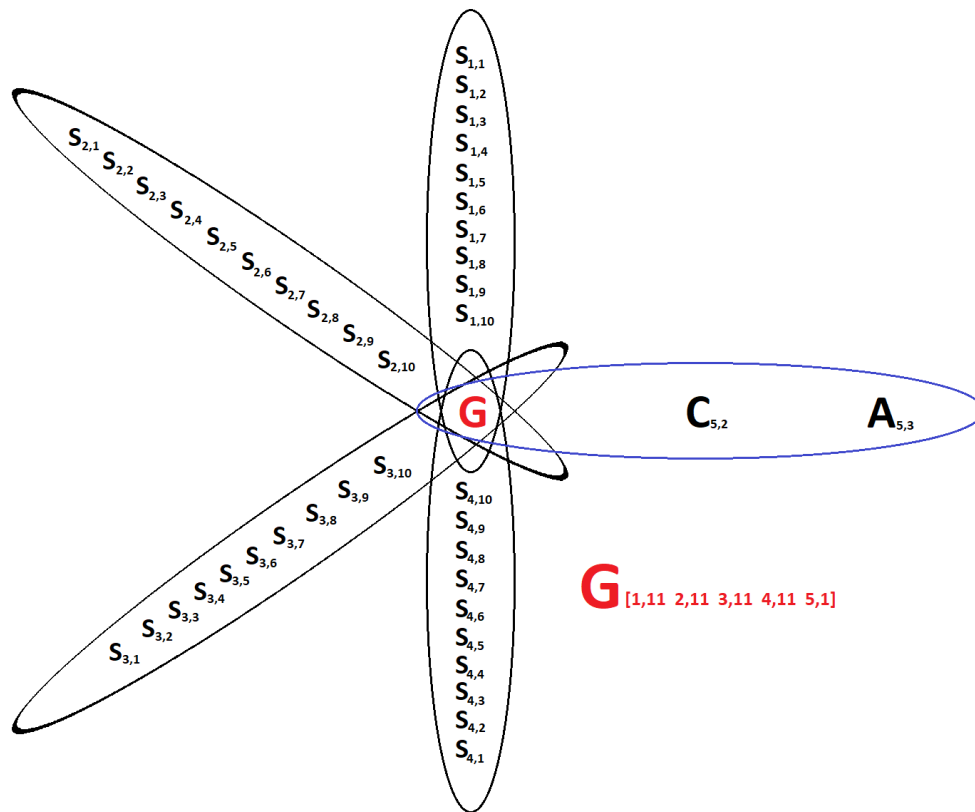


Figure1: Smart Traffic Light Network

WSN

Wireless Sensor Network, made up with TrueTime Kernel, are equipped of battery and they can be divided in:

- Periodic Task;
- Aperiodic Task;

Periodic tasks are the furthest from the intersection and they have to transmit the possible presence of vehicles to the next WSN, through an integer variable between 0 and 10. These devices are connected in feedback with the tenth WSN of the same network: so, the periodic task always is able to know the traffic condition in the next cycle.

Aperiodic tasks, from the second to the tenth have, as input variable, the WSN's identifier to send the message to. If the traffic level become higher (beyond a certain threshold), the WSN will save once the current time in the package of the message; otherwise, time will be initialized to zero.

The aforementioned WSN are aperiodic tasks because they must wait the message of the previous WSN, and then, they will find out the traffic situation. This choice has been made because WSNs are arranged in a row and the communication is hop-by-hop. Through this choice, high power level in transmission is unuseful.

The tenth detector (of every network) sets the type of the message after receiving it ("street_num.strada_signal") and forwards the

message to the Gateway.

- Gateway: It is the wireless networks' eleventh device and the wired network's first device. Its aim is to acquire all streets' data and forwards these to controller through the fifth networks. This transmission start only when gateway receives traffic levels from the roads. Gateway is shown in figure (2).

- Controller: It is the wired network's second node. It is aim is to produce a new variable called alarm through a fuzzy logical controller (one for each roads). This variable depends from traffic and time values received from gateway. If time values are not equal to zero, WSNs detected a high traffic value, controller will make a subtraction among the current time and the received time, giving the range in which a huge number of vehicles persists; if time values are equal to zero, WSNs didn't detected a high traffic value, controller won't make any algebraic operations. Controller is equipped of eight outputs including four traffic levels and four time ranges (more or less elaborated). Controller is shown in figure (3).

- Actuator: It is the fifth network's third node. Its aim is setting green traffic light (level zero) to the street with the highest alarm value; in the same way it sets red traffic light (level one) to the remaining ones. Before setting green and red traffic lights, actuator sets yellow traffic lights (level 0.5) for 2 seconds. Actuator is shown in figure (4).

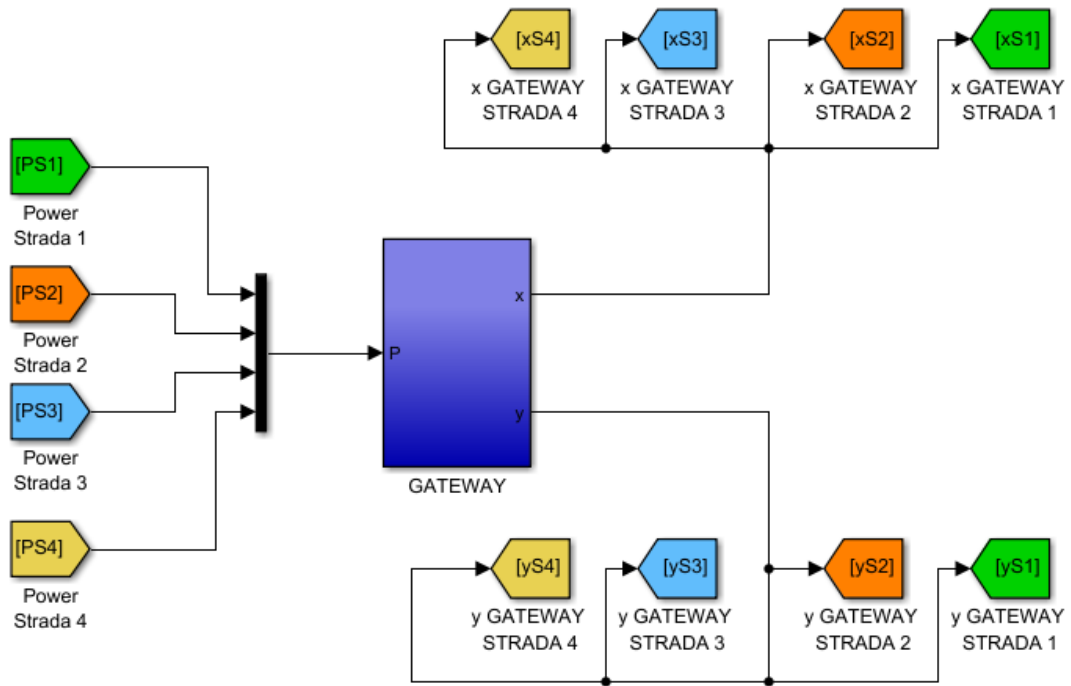


Figure 2: Smart Traffic Light Gateway

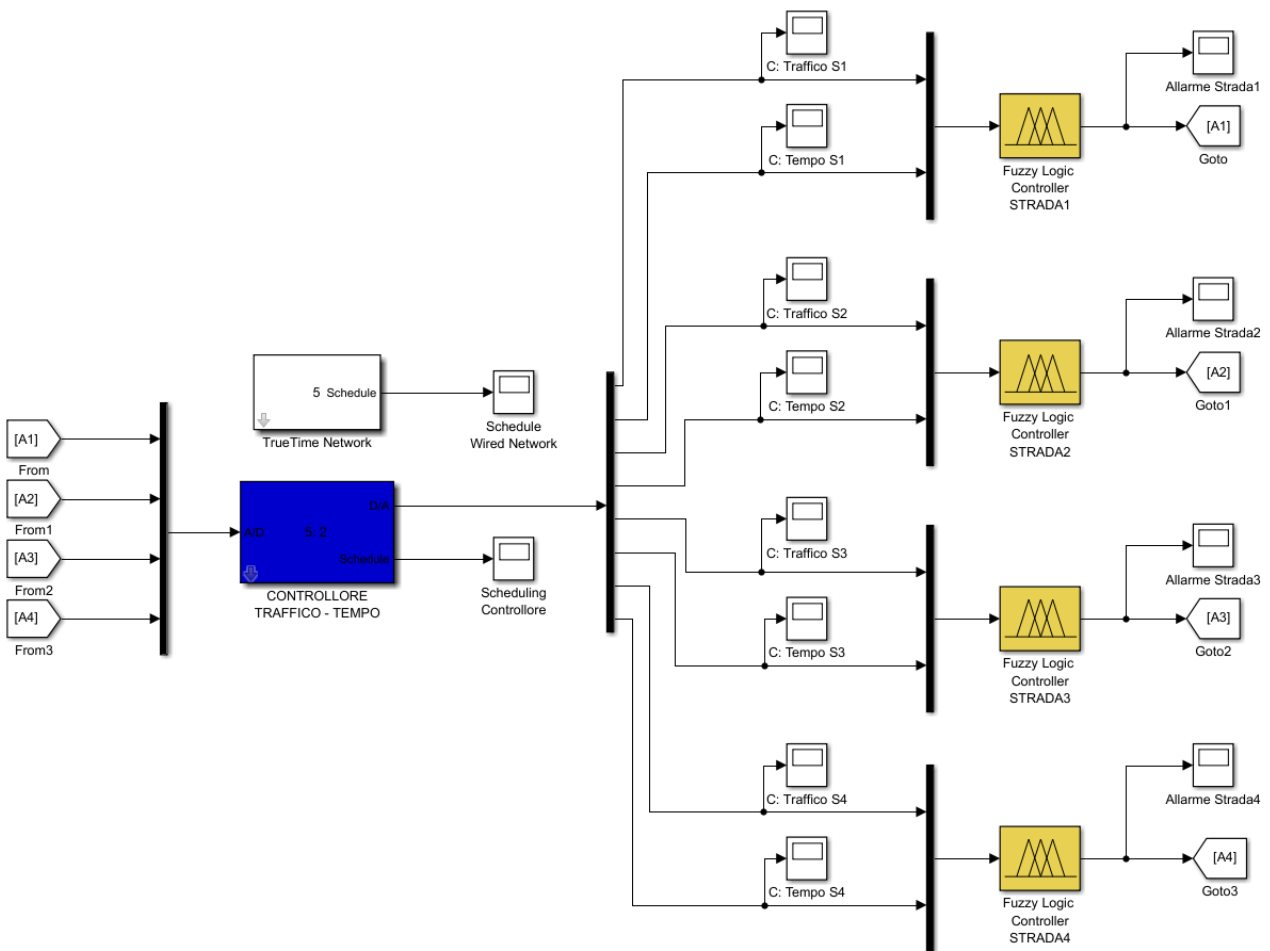


Figure 3: Smart Traffic Light Controller

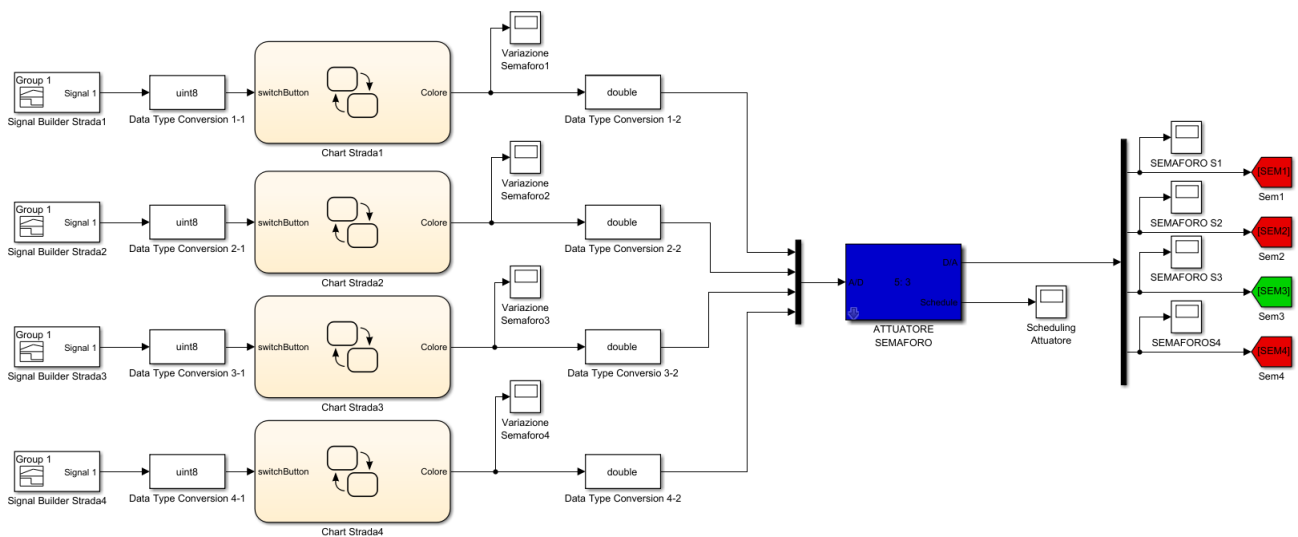


Figure 4: Smart Traffic Light Actuator

- Use of Soft Computing: fuzzy logical controller are equipped of two inputs including time range and traffic level (from the same street). They

have to produce alarm level taking care of input data. Alarm levels are inputs of controller, which forwards these to actuator. Fuzzy’s surface is shown in figure (5).

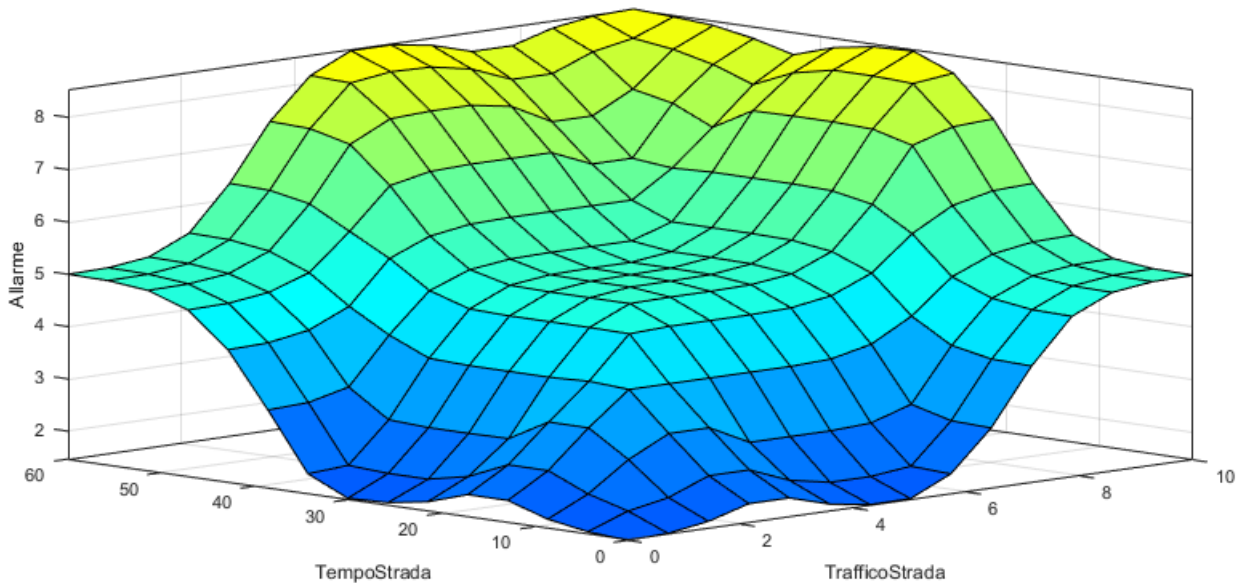


Figure 5: Fuzzy’s surface

- MBSD: In the project, there are four MBSDs, each one for a different road. Their aim is setting green traffic light (level zero), through a remote signal, giving an high priority to the current street for sixty seconds (starting from the next period) and setting red traffic light (level one) to the

remaining streets due to a less priority. MBSD’s input is a signal builder while MBSD’s output is traffic light’s color (0 Green – 1 Red). Inside there are two states stand for traffic light’s colors and a debounce control which checks how long the button has been pressed (time pressing > 0.1s). MBSD’s structure is shown in figure (6).

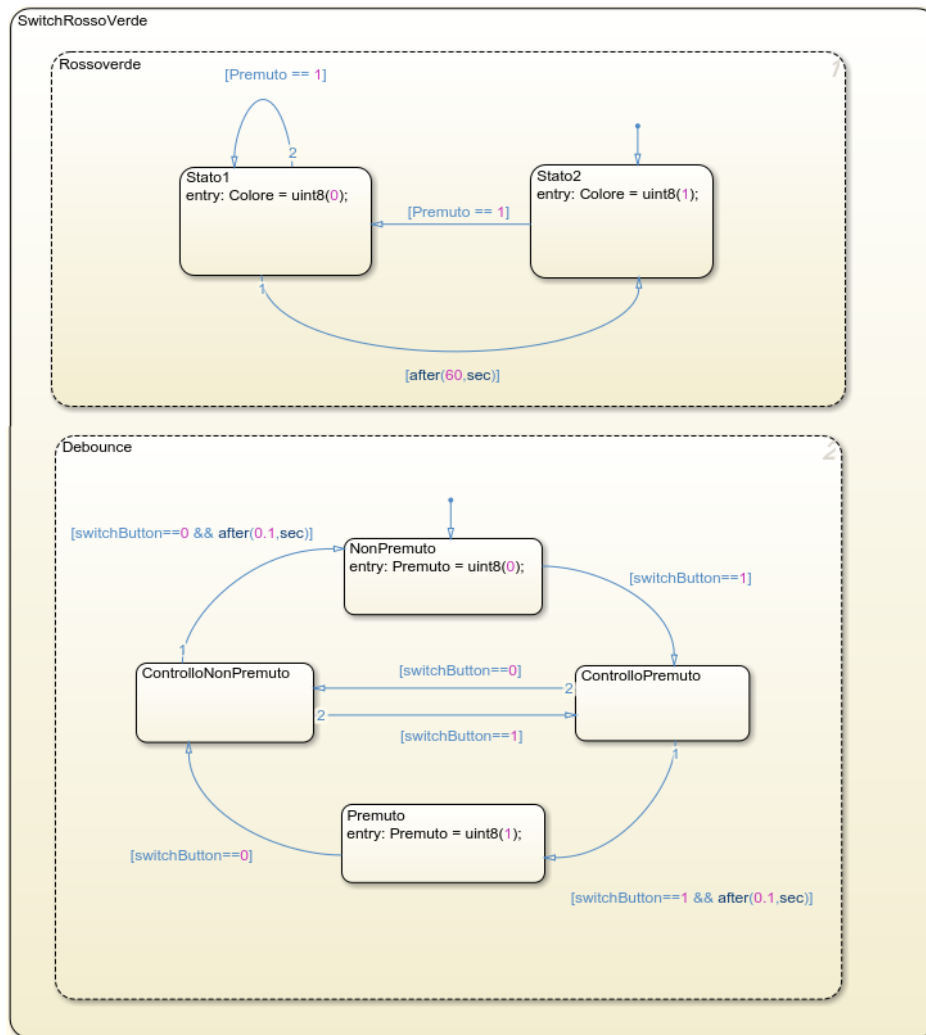


Figure 6: MBSD's structure

SCENARIO

This scenario has been simulated with Matlab / Simulink using TrueTime for 25 minutes. First, the traffic level of each roads has been detected (figure (7, 8, 9, and 10)). Then, their alarm level has been generated as shown in figure (11, 12, 13 and 14) and finally traffic lights have been settled (level 0, 0.5, 1 corresponds respectively at green, yellow and red light) as shown in figure (15, 16, 17 and 18). The study's aim is showing how, when an emergency comes out, traffic lights will be settled giving high priority to the road with emergency.

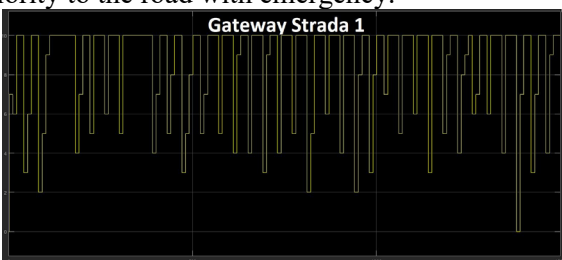


Figure 7: Street 1 traffic level

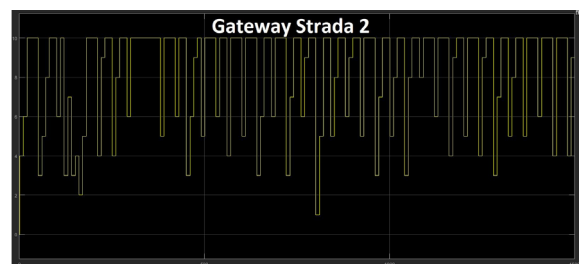


Figure 8: Street 2 traffic level

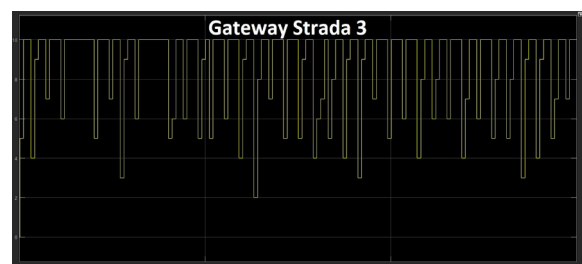


Figure 9: Street 3 traffic level

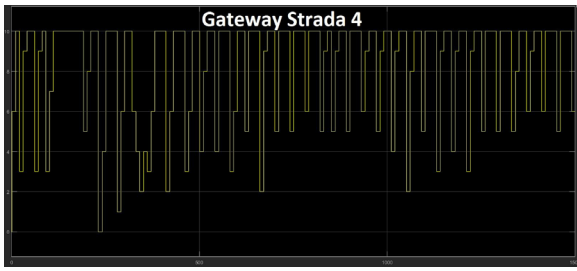


Figure 10: Street 4 traffic level



Figure 11: Street 1 alarm level



Figure 12: Street 2 alarm level



Figure 13: Street 3 traffic level

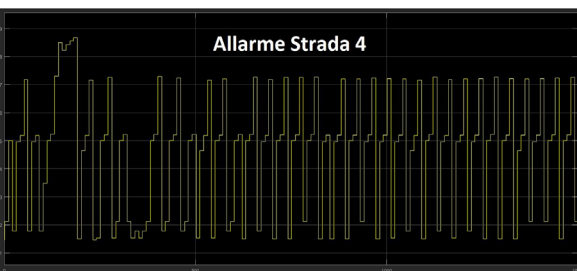


Figure 14: Street 4 alarm level

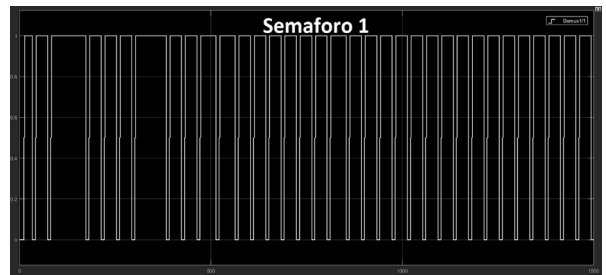


Figure 15: Street 1 traffic light

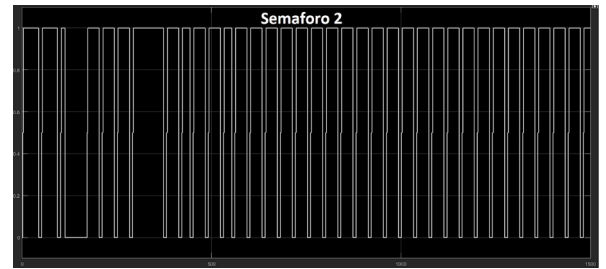


Figure 16: Street 2 traffic light

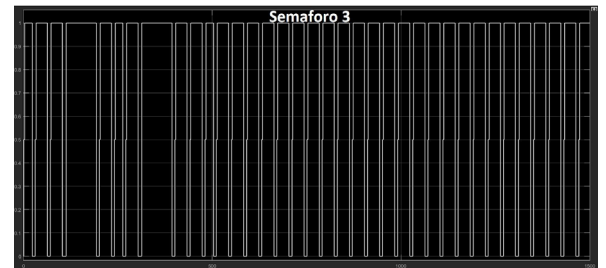


Figure 17: Street 3 traffic light

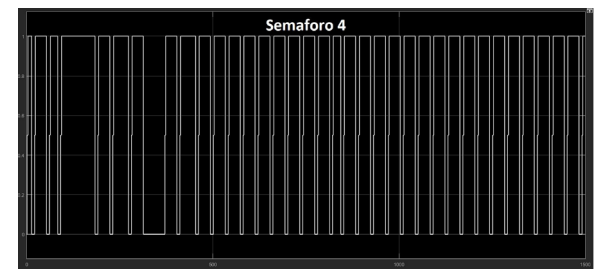


Figure 18: Street 4 traffic light

CONCLUSIONS

“Smart traffic light” means a concrete step forward in a smart world, and it can surely be part of already existent projects such as Surtrac, because of its combination of existent technologies with its innovative ideas. The result will be a new intelligent traffic light that incorporate Surtrac’s multi modal network with Smart Traffic Light’s control emergency.

REFERENCES

1. <https://www.rapidflowtech.com/Yunseop>

DEVELOPMENT OF INVARIANT MODELS OF THE NOMENCLATURE QUALITY INDICATORS OF COMPLEX TECHNICAL SYSTEM

A. Vinnichenko

Saint-Petersburg State University of Aerospace Instrumentation,
Saint-Petersburg, Russia

E-mail: alex23rain@gmail.com

Abstract

The modern development of technology does not stand still; therefore, to achieve a high level, demand and interest and to enter the market, it is necessary constantly improve the range of quality indicators of products. The object of the study was selected civil aviation technology (GAT) – an aircraft without a crew aboard. GAT may have varying degrees of autonomy – from remotely controlled to fully automatic ones, as well as vary in design, purpose, and many other parameters. GAT may be held by episodic command or continuously — in the latter case, GAT is called remotely piloted aircraft unit [1].

The problem area is quite widely manifested in the consumer sector: first, the lack of design flexibility and perfect fuselage shape compared to traditional aviation and second, the redundancy and protection of control channels of a complex technical system (CTS) during operation. Thirdly, the level of reliability of drones is still inferior to traditional aircraft; fourthly, the system survival protocols under extreme conditions and returning to the operator in case of partial loss of performance characteristics are an important part of the reliability indicators. It is also worth bearing in mind that drones flying in peacetime in many areas are limited for various reasons. The development of GAT is one of the most promising directions for the development of modern aviation. The progress of unmanned aerial vehicles is probably the most important achievement of aviation over the past decades. The scope of GAT is quite wide and multifaceted: the functional characteristics of GAT actively used in the civilian sector of the economy so successfully that some social services use them for aerial photography, patrolling, geodetic surveys, monitoring facilities and even for home delivery. To begin with, several GAT models were chosen for the study and comparison of flight performance (Fig.1).

The activities of Russian companies operating in the GAT market are very extensive, starting from the usual aerial survey and ending with the protection of objects. In fig. 2 shows the fields of activity using GAT [2].

The buyer acquires the product, based on the need for it, given its newness, economy, reliability and other equally important indicators. Satisfying needs and operational properties from the consumer's point of view determined by individual consumer characteristics, which are a certain set of quality indicators, which in turn constitute the nomenclature of product quality indicators established by the state standard (GOST) [3].

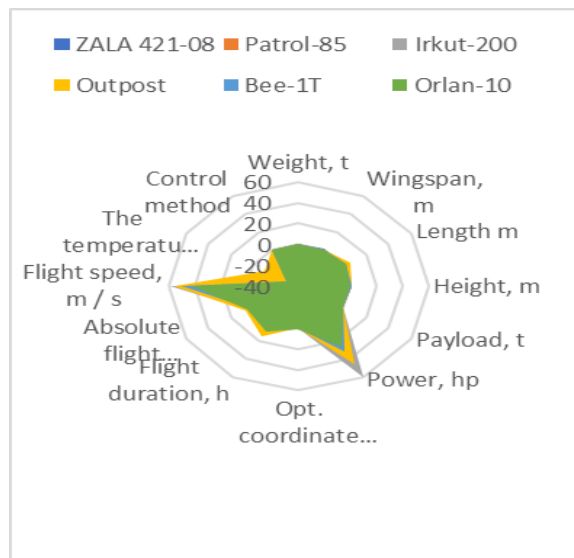


Figure 1 – GAT flight performance

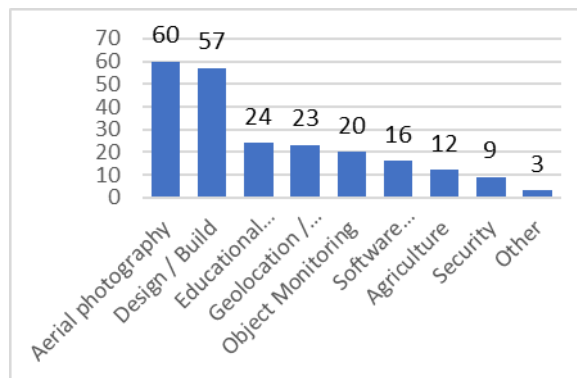


Figure 2 – Areas of use of GAT

Consequently, there is an incomplete systematization of the nomenclature of quality indicators in the standards and the presence of outdated values of product quality indicators. As well as an abundance of technological indicators, that do

not provide information about the quality of the product. In GOST R 51303-99, the following definition given: the consumer quality indicator is a quantitative characteristic of one or several consumer properties of a product, considered in relation to the conditions of its consumption. The nomenclature of quality indicators depends on the destination of the goods [4].

Exit of system elements fails to proceed at any stages (Fig. 3). For example, suppliers deliver counterfeit materials, manufacturers work with outdated or inaccurately calibrated equipment, and manufacturers, not taking into account the regulatory and technical documentation in the production process, as a result, the quality of such products is much lower [5].

Thus, taking into account the main problem areas of GAT, consumer characteristics of GAT were formed (Fig. 4).

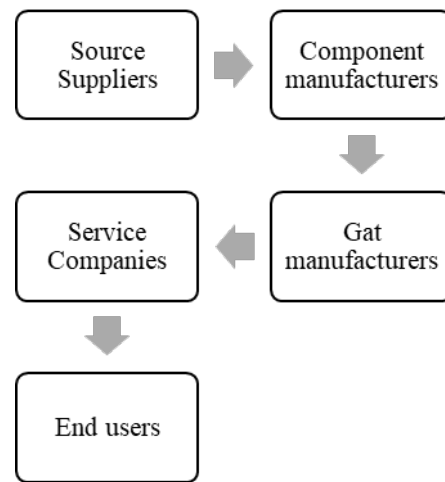


Figure 3 – GAT Market Value Chain

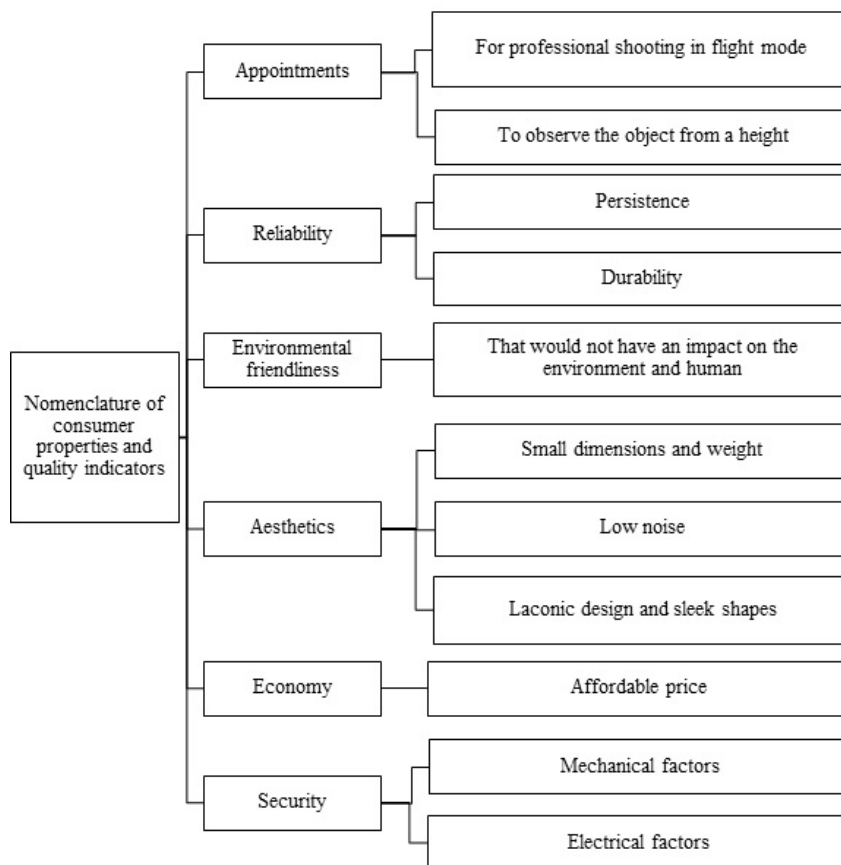


Figure 4 – GTA Consumer Characteristics

The choice of a quality indicators nomenclature for complex technical systems is a rather complicated and time-consuming process. This process is basic on the potential of a complex technical system associated with the value of its functional characteristics, the development of which should be predicted in the planning horizon of 10-15 years.

The main objective of the development of the technical potential of unmanned aerial vehicles is to

create, to the maximum extent possible, such a system of indicators of consumer characteristics, which would change together with the technical characteristics during the life cycle of the product. The basic concept of grouping the quality indicators of the product under study is the formation of clusters, including similar technical characteristics, selected according to functional and value criteria [6].

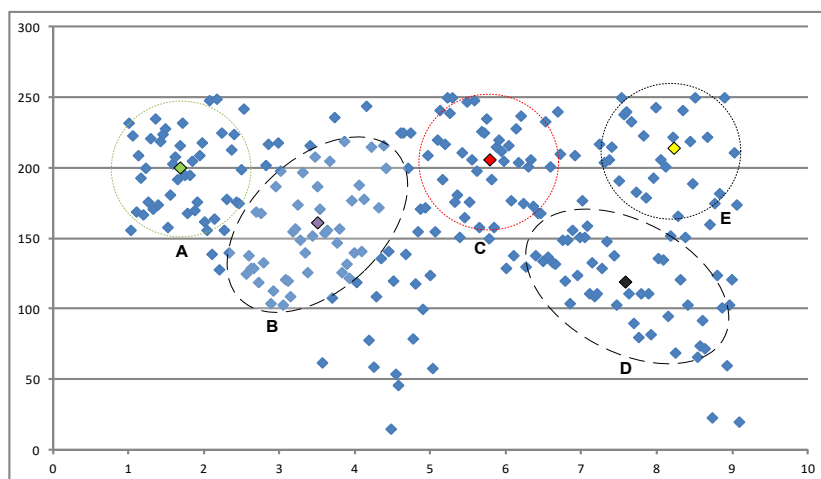


Figure 5 – Scatter Chart

Table 1 – a fragment of the product innovation table

Names of changes in product characteristics	Technical specifications
Amount of advanced technical specifications (I ₁₁)	Weight, kg
	Wingspan, mm
	Height, m
	Payload kg
	Power, hp
	Determination of object coordinates, km
	Flight duration, min
	Flight speed, km / h
	The temperature at the ground at which work is possible, ° C
Amount of advanced consumer characteristics (I ₁₂)	Clear shooting
	Simple operation
	Impact resistance
	Dust and moisture resistant
	Ease
	Small dimensions
	Fast
	Viewing range
Long operation	

On the basis of the problem areas formulated, a comparative analysis will be carried out using the described flight-technical characteristics of the models under study (Fig. 1), the current range of quality indicators specified in GOST R 56079-2014 [7] and consumer characteristics (Fig. 4). In the course of the work, five clusters were identified (Fig. 5), the basic structures of the CTS models were modeled and a decision was made to upgrade a number of quality indicators to ensure stable operation of the CTS with external factors affecting it, in the planning horizon

ten years. Using the assessment of the innovativeness of the product (Table 1), we determine the level of modernization of the CTS model. [8,9].

Evaluation of product innovation is determined the formula:

$$I_{1n} = \frac{P_{\text{improved}}}{P_{\text{common}}}$$

где P_{improved} – improved indicators, P_{common} – total number of indicators.

$$I_{11} = \frac{P_{\text{improved}}}{P_{\text{common}}} = 0,7,$$

$$I_{12} = \frac{P_{\text{improved}}}{P_{\text{common}}} = 0,7$$

According to the results of the conducted approaches on the scale of interpretation, it can be seen that the degree of progressiveness of the innovation belongs to the category of significant improvement of the main characteristics of the object, as well as the social effect created. Thus, when modernizing the selected indicators, due to the replacement of the system elements and the improvements already installed, the complex technical system will take an invariant form, which will allow it to ensure stable operation of the GTA regardless of the influence of external factors on it. But, it must be understood that this technique requires a high level of technical support and after-sales service.

References:

1. Авиация: Энциклопедия / гл. ред. Г. П. Свищёв. — М.: Большая Российская энциклопедия, 1994. — 736 с.
2. А.С. Сунгуров, С.С. Гарманов, Обзор беспилотных летательных аппаратов // Современные научные исследования и инновации. 2017. № 5

3. В.М. Балашов, Подготовка кадров для инновационной экономики / В.М. Балашов, Е.С. Малинушкина, Е.Г. Семенова // Инноватика. М.: — 2011. С. 2011

4. Б.Г. Литвак, Стратегический менеджмент: учебник для бакалавров / Б.Г. Литвак. — М.: Издательство Юрайт, 2013. — 507 с.

5. Семенов, С.С. Основные положения системного анализа при оценке технического уровня сложных систем с применением экспертного метода / С. С. Семенов // Надежность и качество сложных систем. – 2013. -№ 4. — С. 45-53.

6. Г.И. Коршунов, А.М. Дозмаров, Методика первичной оценки инновационных проектов для последующей реализации на промышленном

предприятии. Вопросы радиоэлектроники. 2017. № 10. С. 60-64.

7. ГОСТ Р 56079-2014 «Изделия авиационной техники. Безопасность полета, надежность, контролепригодность, эксплуатационная и ремонтная технологичность. Номенклатура показателей»

8. С.А. Назаревич, Методика оценки технического уровня новшества. – М.: Изд-во: ООО «РИА «Стандарты и качество», 2014. – № 6. (924). – С. 95.

9. Г.И. Коршунов Оценка эффективности технологической модернизации сборочно-монтажного производства РЭА / Г.И. Коршунов, В.М. Балашов, С.Л. Поляков // Вопросы радиоэлектроники. 2013. Т. 2. № 2. С. 100-109.

DIGITAL SIMULATION OF MAGNETIC PHONOGRAM SOUND

A. Vinogradov, S. Gerasimov

Saint-Petersburg State University of Aerospace Instrumentation
Saint-Petersburg, Russia
E-mail: gall2000av@gmail.com, gerasimov310796@gmail.com

Abstract

The article describes the process of modeling the operation of digital simulators of magnetic tape sound in MathCAD environment. As a demonstration of the device operation, figures of various static characteristics of the digital device and spectra of operating signals are presented.

INTRODUCTION

The perception of the timbre of sound is largely due to the nonlinearity of human hearing, in particular the nonlinearity of the transfer function of the tympanic membrane and the middle ear. Each human ear is unique. But most people can easily distinguish between the sounds produced by digital instruments, as well as specialized programs, and the sounds produced by the violin, piano, cello and other musical instruments.

First of all, the "live" sound differs from the synthesized one by the presence of distortions, as a rule, high-frequency ones. Therefore, modern digital software products are faced with the task of simulating these very distortions to give computer sounds the effect of live, "warm" music, as well as simulating the operation of devices that allow you to save the entire spectrum of "analog" sound. As an example, we can consider the problem of simulating the playback of a recording from a magnetic phonogram – a sound sample recorded on a tape recorder [1].

EFFECTS IMPLEMENTATION

When using high-frequency magnetization, the static characteristic of magnetic tapes, which determines the relationship between the magnetic field strength (H) and the residual magnetization (M_r), due to the saturation effect of magnetic tapes is completely symmetrical with respect to the axis of the magnetic field strength. Another important feature is that with both positive and negative magnetization, as the magnetic field strength approaches the value close to saturation, the steepness of magnetization decreases very smoothly. Due to this, when recording with a high level of already compressed audio signal, additional compression occurs due to the saturation effect, due to which the peak factor of the phonogram is reduced. As a result, a phonogram recorded on an analog magnetic tape has a much higher volume level than a similar phonogram on a digital tape. When magnetic recording due to the significant nonlinearity

of the transfer function at high levels of recording there are quite strong nonlinear distortions (up to 3%), which give the sound a very pleasant timbral color, and it is very like sound producers. That is why until now in the Studio recording still widely used analog multi-channel Studio tape recorders. In most cases, compact discs were also made with analog magnetic master tapes. When the transfer function is symmetric with respect to the time axis, only odd harmonics arise because of its nonlinearity, and they decay very quickly. The signal from the magnetic phonogram of a sinusoidal oscillation can be described by equality:

$$U(t) = \frac{4}{\pi} \cdot \frac{U_{\max}}{a} \cdot (\sin \alpha \cdot \sin \omega t + \frac{1}{3^2} \sin 3\alpha \cdot \sin 3\omega t + \frac{1}{5^2} \sin 5\alpha \cdot \sin 5\omega t + \dots), \quad (1)$$

where the parameter α is determined by the ratio of the cut-off time to the period of the audio signal.

It follows from this that harmonics decrease very quickly according to the quadratic law, inversely proportional to their number. By changing the parameter α , you can set a different degree of saturation. Depending on it, harmonic levels and waveform are automatically changed. The values of all these parameters are specified by the nature of the sound – like or not. Figure 1 illustrates the static characteristic graph:

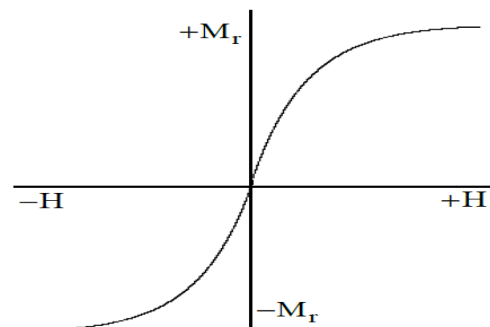


Figure 1. Static characteristic

Digital simulators of magnetic tape saturation are based on the simulation of static characteristics [1]. For example, let us first consider the test single-tone harmonic signal, applying to it the selected mathematical model of processing (figure 2):

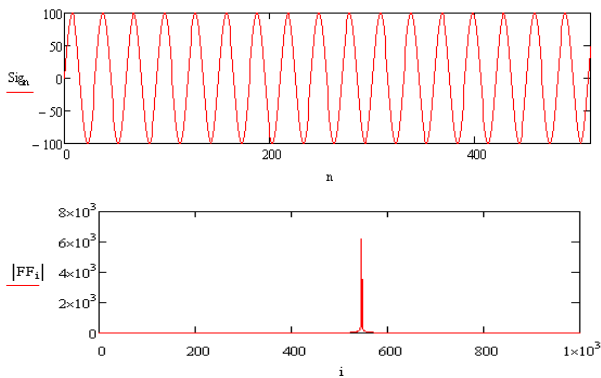


Figure 2. Test single-tone harmonic signal and its spectrum

It can be shown [1] that as such a mathematical model corresponding to the formula (1) it is appropriate to use a half-period of a sine wave with a saturation region (Fig. 3):

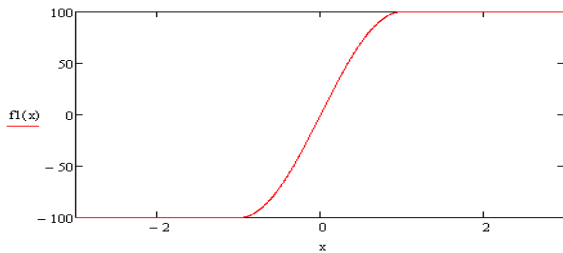


Figure 3. Model of static characteristics

The converted signal and its spectrum are shown in figure 4. As can be seen from the figure, only odd harmonics are present in the spectrum, and their amplitude quickly fades.

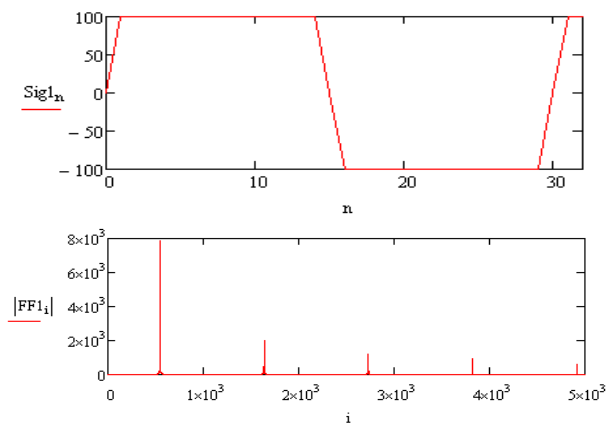


Figure 4. Output signal and its spectrum

After making sure that the algorithm works on a simple example, apply it to an audio file recorded

using a computer program. To do this, we decompose the stereo track into two channels – left and right, respectively. The result is shown in Fig. 5.

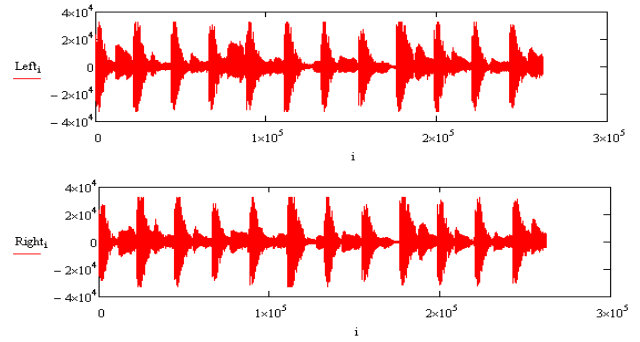


Figure 5. Decomposition of the stereo signal into the left and right channels

The signal spectra for the left and right channels are shown in Fig. 6.

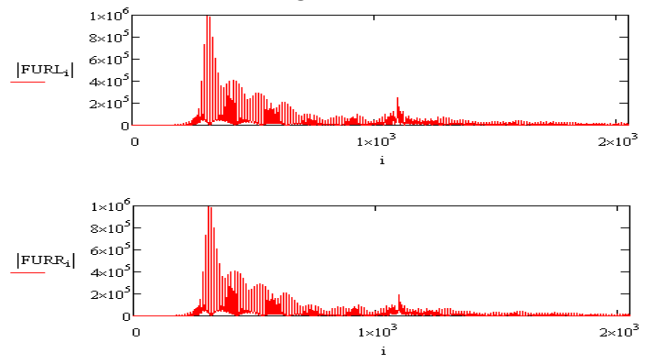


Figure 6. Stereo Spectra of the left and right channels respectively

The model of the static characteristic of a magnetic tape is illustrated in Fig. 7.

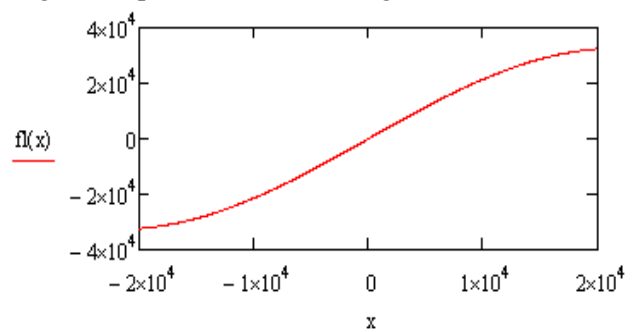


Figure 7. Static characteristic of magnetic tape

The algorithm of per-channel data processing is applicable to the considered signals. In fig. 8 shows an example for the left channel.

$$d := \frac{\pi \cdot 4}{1.764 \times 10^5}$$

$$N1 := \text{last}(\text{Left})$$

$$\text{maximum1} := \max(\text{Left})$$

$$f(x) := \begin{cases} \text{maximum1} \sin(d \cdot x) & \text{if } |d \cdot x| \leq \frac{\pi}{2} \\ -\text{maximum1} & \text{if } d \cdot x < -\frac{\pi}{2} \\ \text{maximum1} & \text{otherwise} \end{cases}$$

$$n := 0 \dots N1$$

$$\text{Left1}_n := f(\text{Left}_n)$$

Figure 8. Example of execution in MathCAD of the algorithm of per-channel signal processing for the left channel

The result of processing the left and right channel is shown in Fig. 9.

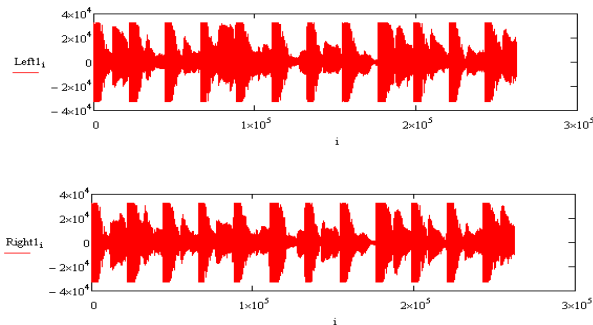


Figure 9. Converted signal (left and right channel respectively)

The spectra of the input and output signals for each of the channels are shown in Fig. 10.

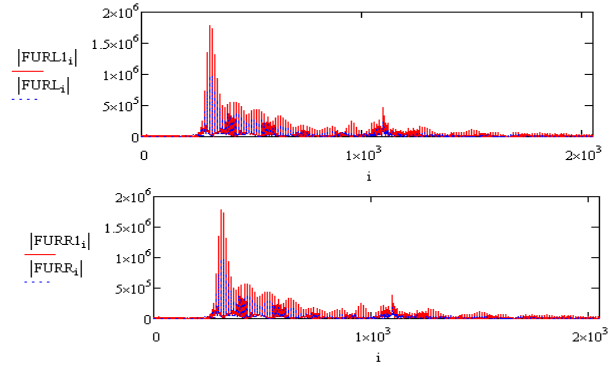


Figure 10. Signal spectra before and after conversion

CONCLUSION

Simulation in MathCAD[2] allows to mathematically describe the work of digital simulators of magnetic tape sound – saturators. The convenience of working with audio files makes it possible to illustrate the results of such devices. Changing the parameters of the mathematical model (in particular, the parameter d) allows you to change the magnitude and nature of nonlinear distortions, making the sound more pleasant for auditory perception.

REFERENCES

1. *Vologdin, E.I. (Вологдин, Э.И.) Методы и алгоритмы обработки звуковых сигналов / Э.И. Вологдин СПб: КОРОНА, 2012. 96 с.*
2. *Makarov, E.G. (Макаров, Е.Г.) Инженерные расчеты в Mathcad / Е.Г. Макаров СПб: Питер, 2015. 448 с.*

DEVELOPMENT OF SYSTEM FOR DETECTION EXTERNAL PARTS DEFECTS IN PRODUCTION

O. Zaplatin

Saint-Petersburg University of Aerospace Instrumentation,
Saint-Petersburg, Russia
E-mail: oleg.zaplatin@mail.ru

Annotation

The article presents an example of building a system for detecting external defects of parts in production using computer vision and deep learning methods. Recognition of defective objects is considered on the example of paper sheets, with using binarization of their images and contours selection. This material gives an idea of the possibilities of using computer vision and deep learning in production. The technology stack used to implement the system is described.

Keywords: computer vision, binarization, contour selection, deep learning, neural networks, classification.

Introduction

In recent decades, the world's new application area is booming — deep learning, which specializes in artificial neural networks. Artificial neural networks – mathematical models, also their software or hardware implementations, built on the principle of organization and functioning of biological neural networks from neural cells of a living organism. Neural networks have the opportunity to learn, which is one of their main advantages over traditional algorithms.

Technically, neural networks training is to finding the coefficients of connections between neurons. In the process of training, the neural network is able to detect complex dependencies between input and output data, and perform a generalization. In the case of successful training, the network can return the correct result based on the input data that was missing in the training set.

The relevance of research in this direction is confirmed by the widespread use of neural networks in automating image recognition processes, adaptive management, forecasting, organization of associative memory, etc. [1] [2] [3]. With the help of neural networks, one can predict the indicators of the exchange market, perform the recognition of optical or sound signals, create self-learning systems capable of driving cars while parking, or synthesize speech through the text.

But, although neural networks shows a much better result compared to the classical recognition methods, there remains a huge number of spheres of human activity in which automation is carried out using outdated methods or not implemented in principle.

The trend and ways of using neural networks in industry

One of the promising areas of application of

artificial neural networks is industrial production [4]. In this area, there is a noticeable tendency of transition to production modules with a high level of automation, which requires an increase in the number of intelligent, self-regulating and self-adjusting machines.

Traditional analytical models can often be built only with a significant simplification, and they are mainly evaluative.

In production, the use of neural networks is the recognition of internal or external defects in a part. When detecting defects by traditional methods, a number of difficulties arise, because the practical application of all detection methods imposes great inquiries to operators on the physical side, and at the same time requires special knowledge. This concerns, first of all, the methods, where the presence of an error should be evaluated "indirectly" by indication (signal) on the monitor in real time. Proper evaluation of the X-ray frame and indication of the magnetic or capillary method is also difficult, requiring rich experience.

Neural networks do not have the disadvantages described above – no long-term analysis is needed of the data received from the device or video camera – the ins classifies the input data, even if they were not present in the training set during training;

It is only necessary to determine the type of neural network architecture suitable for the specific task and correctly select the training set (dataset) that can be built using the same instruments that will be used in production.

For example, a convolutional neural network (CNN) is a popular type of architecture. This neural networks type is good where you need to see a piece or the whole sequence and draw some conclusion from this. Thus, they can be used not only for the classification of images, but also for the classification of other input data. And the architecture of such a neural network can be used to classify images

received from cameras, and to classify data received from an ultrasonic flaw detector. It turns out that you can check the quality of the part using almost one neural network – depending on the input data, only the set of weights will change. One will be received when training on images from the camera, the second – received when training on data from the flaw detector. Indeed, with proper development of the structure of the neural network and the preparation of input data, the architecture, in theory, can be left unchanged.

Defect Detection Algorithm Development

For successful defects detection, it is necessary to be able to solve such tasks as the selection of the object edges in the image, image binarization, and the assessment of the damage level of the object. This section describes the developed method for solving the listed problems.

1. The choice of image processing method

When choosing the image processing algorithm, preference was given to those algorithms that allow not only to binarize the image, to clear from noise, but also to isolate potential defects as much as possible. After comparing the existing algorithms, the algorithm proposed by John F. Canny; 1953 [8] was selected. John Canny studied the mathematical problem of filter developing that is optimal in terms of selecting, localizing and minimizing several responses of one edge. This means that the detector reacts to the edges, but at the same time it ignores false ones, accurately determines the edge line (without fragmenting it) and reacts to each edge only once, thus avoiding the perception of wide bands of brightness as a combination of edges.

The operation of the selected algorithm was tested on A4 sheets (Figure 1-2). Initially it was supposed to look for defects on the boxes, but because of the lack of the necessary number of boxes, it was decided to use a more common and cheaper material.

The choice of the method of determining the presence of defects in the image

After the image has been correctly processed and cleared of noise, it is necessary to start defects detection – it was decided to choose a neural network as a detector.

For solving problems of image classification and pattern recognition, convolutional neural networks are best suited. The basis was taken scheme neural network VGG-16. (The scheme is shown in Figure 3.1) VGG-16. – The scheme proposed by K. Simonyan and A. Zisserman from the University of Oxford in the article “Very Deep Convolutional Networks for Large-Scale Image Recognition”. The model achieved an accuracy of 92.7% – top-5, when tested on ImageNet in the task of recognizing objects in an image. To speed up the learning

process and image recognition speed, it was decided to reduce the number of convolutional layers to 4.



Figure 1 – Image binarization using the Otsu criterion [7] (a is the original image, b is binarized)



Figure 2 – Image processing by the Canny edge Detector (a is the original image, b is the application of the Canny edge Detector to the original image)

At the same time, the quality of recognition does not decrease because after the initial image processing, the defects imprinted on the image become pronounced.

As the activation function [5], the function ReLU (“rectifier”) was chosen – it contains all hidden layers, as well as in the original VGG-16 scheme.

ReLU is described by the formula

$$f(x) = \max(0, x)$$

and implements a simple threshold transition at zero.

The implementation in Python [6] is as follows:

def ReLu (x):

*return ((x > 0) * 1.0) * x*

The neural network diagram is shown in Figure 3. As a result of its work, it is possible not only to classify an object, but also to determine the degree of damage. To demonstrate the work, a dataset of 200 shots of sheets of paper was prepared: 100 shots of crumpled sheets and 100 – smooth sheets. The use of such an affordable and cheap material allows you to correctly make a training sample, as well as reduces the time to create a training sample.

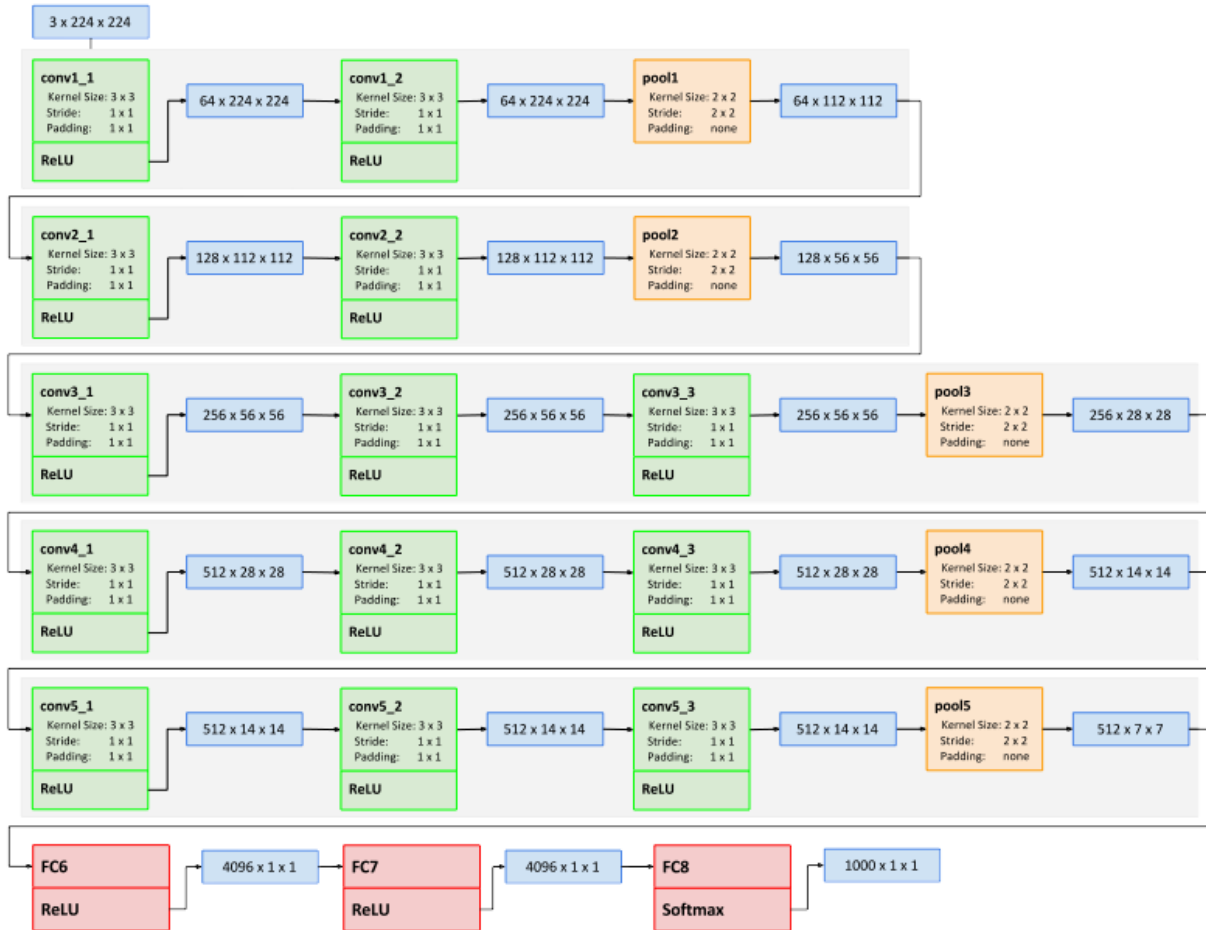


Figure 3.1 – Diagram of a neural network for a defect detection system

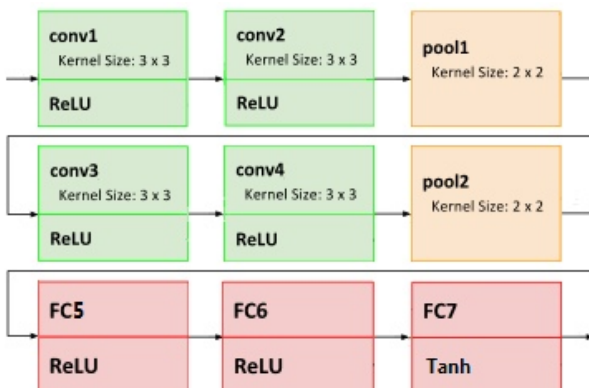


Figure 3.2 – Neural network diagram for the defect detection system

Figure 4 shows an example of a trained neural network :

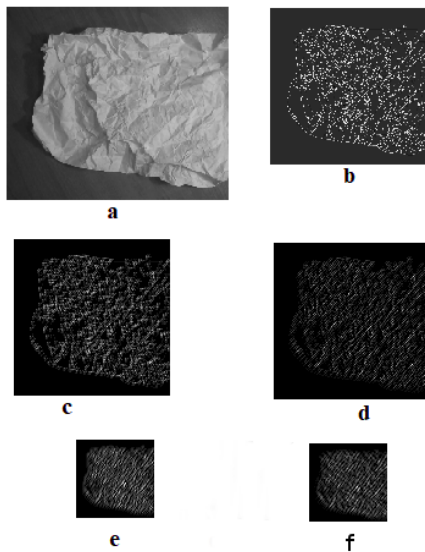


Figure 4 – neural networks working visualization – convolutional layers. (a is the original image, b is the image processed by the Canny edge detector, c is the result of image processing by the first convolution layer, d is the result of image processing by the second convolution layer, e is the result of image processing by the third convolution layer, f is the result of image processing by the fourth convolution layer)

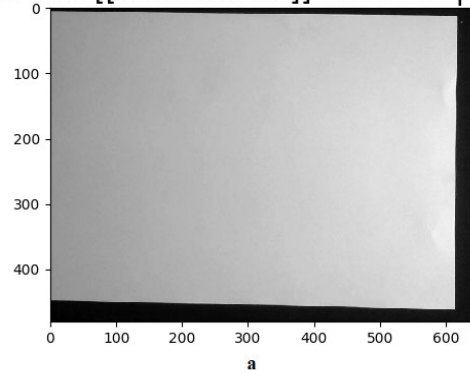
Figure 5 shows the trained neural networks working result .

In order to demonstrate the advantage of convolutional neural networks in the classification of patterns compared to other types of neural networks, we compare the results of the developed system with the results of the system using the multilayer perceptron as a defect detector. The multilayer perceptron was trained on the same dataset as the convolutional neural network (dataset of 100 images of crumpled sheets and 100 smooth sheets).

When you try to train a perceptron with the same number of layers as in a convolutional network, retraining occurs – networks with a large number of parameters have an additional tendency to retrain. After solving this problem, we can compare the results:

When comparing the results of the work, it is clear that both architectures classify simple images equally well, but perceptron does not classify more complex images correctly.

nn out: $[[0.02300789]]$ - smooth paper



nn out: $[[0.98791468]]$ - crumpled paper

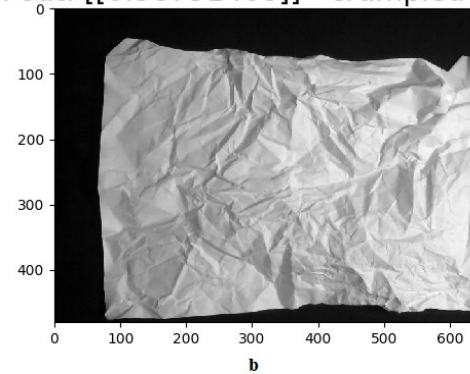
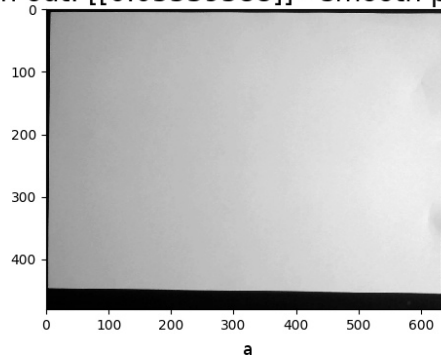


Figure 5 — neural networks working results (a – the object is classified as a defect – defects percentage is less than zero, b – the object is classified as a defect – 98% of the object is damaged)

nn out: $[[0.05539588]]$ - smooth paper



nn out: $[[0.09010805]]$ - smooth paper

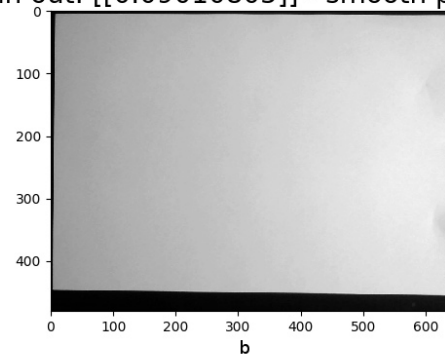
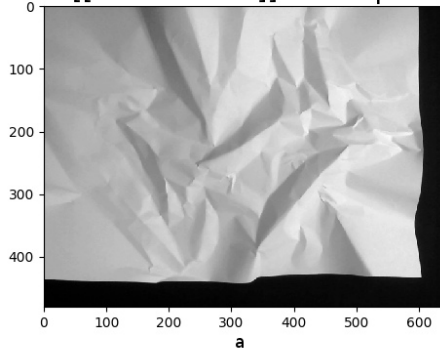


Figure 6 – Neural networks working results comparison (a – an object classified by a convolutional neural network, b – an object classified by a perceptron)

nn out: [[0.79530448]] - crumpled paper



nn out: [[0.38196749]] - smooth paper

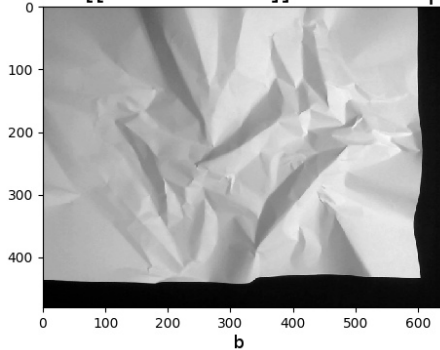


Figure 7 – neural networks working results comparison (a – an object classified by a convolutional neural network, b – an object classified by a perceptron)

Indeed, compared to a fully connected neural network, the convolutional neural network has a much smaller number of adjustable scales, since one core of the scales is used entirely for the entire image, instead of doing its own personal weights for each pixel of the input image. This pushes the neural network, when learning, to generalize the displayed information, and not to memorize each shown picture by pixel, as the perceptron does. That allows her to correctly classify an image that is different from those that were used during the training.

Technology stack used when developing the system.

The following technology stack is used to develop the application:

1. Programming language – Python.
2. Code editor – Sublime text 3.
3. NumPy library
4. Matplotlib library
5. Scipy library

Python – an interpreted object-oriented programming language that includes modules, dynamic data types, and classes.

Sublime text 3 – a proprietary text editor that supports a large number of programming languages and has the ability to highlight syntax for a large

number of languages. In addition to those programming languages that are enabled by default, users have the option to download plugins to support other languages.

NumPy – an open source library for Python that provides implementations of computational algorithms in the form of functions and operators optimized to work with multidimensional arrays.

Matplotlib – library in the programming language Python, designed to visualize the data of two-dimensional graphics.

Scipy – a library for the open source Python programming language designed to perform scientific and engineering calculations.

CONCLUSION

The described system for detecting external defects of parts in production gives an idea of the modern possibilities of using computer vision in the automation of production. With its simplicity and rather small training set, the system is able to accurately determine the defective object, which proves the possibility of its use.

The use of the developed system allows to solve a number of difficulties associated with the practical application of detection methods in production, and the ease of implementation and the lack of expensive equipment will allow the system to be used even in small-scale production.

BIBLIOGRAPHY

1. Ronay Ak, Max Ferguson, Yung-Tsun T. Lee, Kincho H. Law. Article. Capital Defects with Convolutional Neural Networks, 2017 IEEE, Boston, MA, USA, December 11, 2017, DOI: 10.1109 / BigData.2017.8258115;
2. Soukup D, Huber-Murk R. Convolutional Neural Networks for Steel Surface Defect Detection from Photometric Stereo Images. In: Advances in Visual Computing – 10th International Symposium, ISVC 2014, Las Vegas, NV, USA, December 8-10, 2014, Proceedings, Part I; 2014. p. 668–677;
3. Jian C, Gao J, Ao Y. vol. 52; 2017. p. 348–358.
4. Kuzichkin A.A. Neural networks in industry and information technologies, Collection of scientific papers on the basis of the international scientific-practical conference, the development of technical sciences in the modern world, Voronezh, December 8, 2015, p. 18-20.
5. Sagar Sharma, Activation functions in neural networks, URL: <https://towardsdatascience.com/activation-functions-neural-networks-1cbd9f8d91d6>
6. Python Software Foundation URL: – <https://www.python.org/> (date of access: 02.20.2019)
7. Object detection using the Ots method – URL: <https://habr.com/en/en/post/112079/> (date of access: 03.02.2019)

8. Kanni edge Detector – URL: <https://habr.com/ru/en/post/114589/> (access date: 02.25.2019)
9. Xinghui Dong, Chris J. Taylor, and Tim F. Fayerekleimozovar Neural Networks and Forests, 2018 European Conference on Computer Vision Workshops, Computer Vision – ECCV 2018 Workshops, p. 398-412
10. Sublime Text 3 Software URL: <https://www.sublimetext.com/3> (date of access: 02.26.2019)
11. NumPy-the fundamental package for scientific computing with Python. URL: <http://www.numpy.org/> (date of access: 02.21.2019)
12. Matplotlib – Python 2D plotting library URL: <https://matplotlib.org/> (date of access: 02.22.2019)
13. SciPy Python-based ecosystem URL: <https://www.scipy.org/> (date of access: 02.23.2019)

СОДЕРЖАНИЕ

GREETINGS

Paul Gruhn	3
Brian J. Curtis	5
Gerald W. Cockrell.....	7

PROFESSIONAL SPEAKING

<i>Kryachko A., Kryachko M.</i> ACCOUNTING FOR ELECTROMAGNETIC WAVES SCATTERING IN THE ANGULAR AREAS DURING FORMATION OF THE MULTIPATH COMMUNICATION CHANNEL FREQUENCY CHARACTERISTICS	9
<i>Chabanenko A.</i> MODELING OF AUTOMATED PROCESSES OF BUILDING A PHYSICAL MODEL OF AN OBJECT ON A 3D PRINTER	15

THE FIFTEENTH ISA EUROPEAN STUDENTS PAPER COMPETITION (ESPC-2019) WINNERS

<i>Afanasev M.</i> AN EFFICIENCY ESTIMATION OF THE TRANSPORT CODING FOR PACKETS WITH AN EXPONENTIALLY DISTRIBUTED DELAY.....	18
<i>Akopyan B.</i> DEVELOPMENT OF A MULTICHANNEL WIRELESS OPTICAL DIGITAL COMMUNICATION SYSTEM BASED ON FREQUENCY-DIVISION MULTIPLEXING	23
<i>Bogatov N.</i> MODERN AUTOMATIC WAYS OF AIRCRAFT PRE-FLIGHT MANAGEMENT	26
<i>Dobrovolskaya A.</i> PRACTICAL EXPERIENCE IN THE USE OF SIMULATION MODELING FOR PASSENGER TRANSPORTATION BY TAXI.....	29
<i>Emelyanov G.</i> PIPELINE OF MOBILE SERVICE FOR GENERATING IMAGE DESCRIPTIONS	32
<i>Fedorov I.</i> RESEARCH OF METHODS FORMATION SAW TAGS FOR IDENTIFICATION SYSTEMS.....	37
<i>Forestiere W., Turco M. F.</i> AUTOMATIC HEADLIGHT DIMMING THROUGH SOFT COMPUTING TECHNIQUES	42
<i>Gerasimov S.</i> COMPARATIVE ANALYSIS OF READY-MADE SOLUTIONS FOR IMPLEMENTATION OF VOICE CONTROL ON MICROCONTROLLERS	46
<i>Grigoriev E.</i> MODELING OF THE PROCESS OF ASSESSMENT OF COORDINATES OF OBJECTS IN THE TWO-POSITION RADAR SYSTEM	49
<i>Karataev A.</i> DEVELOPMENT OF MOBILE APPLICATION BASED ON MACHINE LEARNING METHODS FOR SKIN CANCER SCREENING	54
<i>Kniazeva M.</i> THE EFFECT OF OXYGEN INSTABILITY ON THE FORMATION OF AN INCOMMENSURATE PHASE IN LEAD HAFNATE.....	59
<i>Kuzmenko V.</i> SUSTENTION OF THE LIGHT FLOW FOR LED LIGHT SOURCES	63
<i>Lityagin G.</i> STRAIN-DRIVEN MODIFICATION OF PHASE TRANSITION SEQUENCE IN EPITAXIAL ANTIFERROELECTRIC THIN FILMS	66
<i>Shaniiazov R.</i> AN OPTIMAL SHAPING FOR QAM MODULATION AND NON-UNIFORM DISTRIBUTION OF SOURCE DATA SYMBOLS.....	71

Shchukina D. DEVELOPMENT OF AUTOMATED SYSTEM OF SITE SELECTION FOR EVENTS CONSIDERING QUALITY INDICATORS	76
Skorniakova E. DEVELOPMENT OF AUTOMATED PRODUCTION PLANNING SYSTEM BASED ON LEAN PRINCIPLES.....	79
Yu. Sokolova ANALYSIS OF COMPLEX FILTERS BASED ON TRANSITION CHARACTERISTICS	82
Svinina A. ROLE OF AUTOMATION IN SAFE FUNCTIONING CROSSROADS	85
Tornabene A. SMART GARDEN: AUTOMATION APPLIED TO BOTANY.....	88
Tvardovsky G. DEVELOPMENT OF RECOGNITION SYSTEM OF HAND GESTURES	91
Udovenko S. METHODS OF VISUALIZATION OF ANTIPHASE POLAR DOMAIN WALLS IN A SOLID SOLUTION OF LEAD ZIRCONATE-TITANATE BY MEANS OF SYNCHROTRON RADIATION SCATTERING	95
Vataeva E. HYBRID STAND FOR MODELING EXTREME CONTROL SYSTEMS	98
Messina M., Vecchio C. SMART TRAFFIC LIGHT	103
Vinnichenko A. DEVELOPMENT OF INVARIANT MODELS OF THE NOMENCLATURE QUALITY INDICATORS OF COMPLEX TECHNICAL SYSTEM.....	109
Vinogradov A., Gerasimov S. DIGITAL SIMULATION OF MAGNETIC PHONOGRAM SOUND.....	113
Zaplatin O. DEVELOPMENT OF SYSTEM FOR DETECTION EXTERNAL PARTS DEFECTS IN PRODUCTION	116

The scientific edition

ИЗВЕСТИЯ КАФЕДРЫ UNESCO ГУАП
«ДИСТАНЦИОННОЕ ИНЖЕНЕРНОЕ ОБРАЗОВАНИЕ»

Сборник статей

Выпуск 4

BULLETIN OF THE UNESCO DEPARTMENT
«DISTANCE EDUCATION IN ENGINEERING» OF THE SUAI

Collection of the papers

Issue 4

Computer imposition

Papers are publish in author's edition

Подписано в печать 15.04.2019. Формат 60x84 1\8.
Усл. печ. л. 7,3. Тираж 150 экз. Заказ № 135.

Редакционно-издательский центр ГУАП
190000, Санкт-Петербург, Б. Морская ул., 67
Department of operative polygraphy SUAI
190000, St. Petersburg, st. B. Morskaya, 67